Conformational Bidentate Fluorescent Sensors for Small Halide Anions

Galbraith, Ewan

Award date:
2010

Awarding institution:
University of Bath

Conformational Bidentate Fluorescent Sensors for Small Halide Anions

Ewan Kit Galbraith

A thesis submitted for the degree of Doctor of Philosophy

University of Bath

Department of Chemistry

January 2010

Signature Date

Acknowledgments

Team TDJ: Thatcher (for the gossip and for putting in a good word for me), Andi Kelly (WELL… for his generosity, for being El Smuggo and for both ends of his mood swings), スチヴ Flower (for incredible patience, humour, Scrabulous and wide-ranging knowledge), Magdaloonie Poowell (for calling me a Loser so many times and lots of entertainment), Lloyd and Damien Rogalle. Non-Team TDJ Bath chemists: Silvanus (for attempting to have a social life in Bath), Hargave, Chen Wenbo, Penrose, Axeman, Franky D Huge. Japanese labmates: Kumicho Nangou, Aiko, Ishii-san, Kenichi Kataoka and their prof Kubo-sensei. Fujita-kun, Tani-san *et al.* under the leadership of Sada-sensei and Shinkai-sensei. The Yoon lab at Ewha Woman's University in Seoul, particularly Dr Sook-Kyung Kim, Ha Na Kim and Prof Ju-Young Yoon for Hite/Shoju bombs. Mom and Pops for patience and ridiculous financial support. Stéphanie for her tolerance, always putting a positive slant on things and being a beautiful inspiration. Dr Steve Bull for the occasional chemistry/pub chat and support. Dr John Fossey, Prof Matt Davidson. TDJ for a whole host of things.

Abbreviations

Å	Ångström
app	apparent
Ar	aryl
ATP	adenosine-5'-triphosphate
ATPase	class of enzymes that catalyse decomposition of ATP
bp	boiling point
br	broad
°C	degree Celsius
$CDCl_3$	deuterated chloroform
cm^3	cubic centimetre
cm^{-1}	wavenumbers
COSY	correlated spectroscopy
[2.2.2]-cryptand	4,7,13,16,21,24-hexaoxa-1,10-diazabicyclo[8.8.8]-hexacosane
CTP	cytidine-5'-triphosphate
δ	chemical shift in parts per million
Δ	heat
2D	two dimensional
D	deuterium (^2H)
D	dextrotatory
d	doublet
Da	Dalton
dan	1,8-diaminonaphthalene
D-A	donor-acceptor
D-B-A	donor-bridge-acceptor
dd	doublet of doublets
diff.	diffraction
dt	doublet of triplets
dec	decomposition
DCM	dichloromethane
dm^3	cubic decimetre
DMSO	dimethyl sulfoxide
e^-	electron
E. coli	*Escherichia coli*
ESI^+	positive phase electrospray ionisation

ESI^-	negative phase electrospray ionisation
Et	ethyl
EtOAc	ethyl acetate
EtOH	ethanol
ET	electron transfer
eq.	equivalent
FAB	fast atom bombardment
g	gram
GTP	guanosine-5'-triphosphate
h	hours
$h\nu$	incident light
HPLC	high performance liquid chromatography
HRMS	high resolution mass spectrometry
I	fluorescence intensity
I/I_0	relative fluorescence intensity
ICT	internal charge transfer
J	coupling constant
k	rate constant
K	stability constant
K_a	acidity constant
K_a'	acidity constant of complexed boronic acid
K_{obs}	observed stability constant
K_{tet}	ligand – tetrahedral boronate anion stability constant
K_{trig}	ligand – trigonal boronic acid stability constant
kJ	kilojoules
λ	wavelength
λ_{em}	emission wavelength
λ_{ex}	excitation wavelength
L	Litre
L	levrotatory
LE	locally excited
lit	literature
LRMS	low resolution mass spectrometry
μM	micromolar
μm	micrometre
μmol	micromole

µL	microlitre
m	*meta*
m	unresolved multiplet / minutes
M	molar (moles per cubic decimetre) / mega
M^{-1}	cubic decimetres per mole
$[M]^+$	parent molecular ion
Me	methyl
MeOD	deuterated D4 methanol
MeOH	methanol
mg	milligram
MHz	megahertz
mm	millimetre
mM	millimolar
mmol	millimole
mol	mole
mp	melting point
mV	millivolt
m/z	mass-to-charge ratio
ν	infrared
nm	nanometre
nmol	nanomole
NMR	nuclear magnetic resonance
ns	nanosecond
o	*ortho*
p	*para*
PET	photoinduced electron transfer
pK_a	- log K_a
pK_{aH}	pK_a of the conjugate acid
ppm	parts per million
q	quartet
r^2	coefficient of determination
R_f	retardance factor
rt	room temperature
s	singlet / second
S_0	singlet electronic ground state
S_1	first singlet electronic excited state

S_2	second singlet electronic excited state
t	triplet
T_1	first triplet electronic excited state
TBAB	tetra-*N*-butylammonium bromide
TBAC	tetra-*N*-butylammonium chloride
TBAF	tetra-*N*-butylammonium fluoride
TBAI	tetra-*N*-butylammonium iodide
THF	tetrahydrofuran
TICT	twisted internal charge transfer
TLC	thin layer chromatography
TMS	tetramethylsilane
p-TSA	*p*-toluenesulfonic acid
tt	triplet of triplets
TTP	tyrosine-5'-triphosphate
UV	ultraviolet
wt%	weight percent

Abstract

Anions are involved in fundamental processes in all living things. Recognition, transport and concentration control of anions such as chloride, phosphate and sulfate is carried out by biological systems on a perpetual basis. Fluoride, nitrate and pertechnetate are potentially dangerous contaminants that can gain access to our water systems by various means. Fluorosis, toxicity due to high levels of fluoride in drinking water, is a serious human health concern in many parts of the world Synthetic chemists seek to mimic nature's level of sophistication in designing and making chemosensors capable of determining the concentration of a target anion in any medium.

Beginning with a review of anion sensor chemistry with a particular focus on developments over the past 15 years, this thesis documents research into novel molecular sensors that target the differential sensing of fluoride and chloride anions. The design of these sensors has focussed on an optical signalling event based on electronic changes on binding but in addition, by virtue of a significant change in structural conformation. Fluorescent molecules have been utilised and as such, fluorescence emission changes investigated in the presence of a variety of anions.

Results and Discussion I outlines our conformational model and discusses the design, synthesis and sensory behaviour of phenyl(boronates). UV, electrochemical, fluorescence and NMR techniques are brought together to elucidate the response of this class of molecule to various anions. One example designed to fit our proposed model shows interesting and unusual fluorescence quenching response to chloride anion. In addition, the synthesis of a related carbamate species and a range of oxygen bridged boron macrocycles are reported.

Results and Discussion II discloses our approaches to more synthetically demanding constructs, obeying the model but trying to overcome the challenges met previously. An interesting, highly selective ratiomeric response to fluoride is observed with an isolated target molecule. Fluoride binding behaviour of a previously unexamined sp^2 boron centre is examined.

Contents

1 INTRODUCTION

1.1 Overview

This Chapter is intended to give a brief introduction to the field of anion sensors, with a particular focus on the small halide ions. Following an explanation of the common signalling mechanisms employed in fluorescent chemosensing, a review of the literature is conducted, highlighting examples relevant to the work detailed later in this thesis.

1.2 Anion Sensing

1.2.1 Recognition

Molecular recognition describes the selective interaction of two substances typically denoted as the host and guest respectively. Selectivity is attained through complementary molecular or ionic properties, considering the geometry, electronics and polarity of the species. Attempting to reproduce the selectivity shown by biological receptors, supramolecular chemists have to design suitable structural and functional group features into synthetic host molecules.

1.2.2 Sensors

Following the definition given by IUPAC, a chemical sensor is a device that transforms chemical information, ranging from the concentration of a specific sample component to total composition analysis, into an analytically useful signal.[1] This highlights the critical difference between a receptor and a sensor, that is, the communication event. The system must incorporate a mechanism which can report the binding event to the macroscopic world.

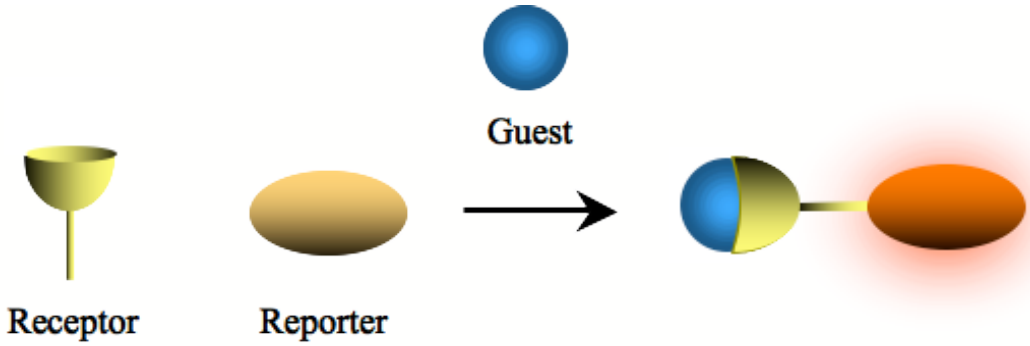

Scheme 1 Schematic of the action of a sensor.

There are several analytical techniques for reporting, be it qualitatively or quantitatively, the molecular recognition event. NMR techniques can provide useful information but offer a limited concentration window, with sensitivity restricted to millimolar concentrations. CD spectroscopy can be used to monitor optical rotation in systems that respond structurally to binding. Chemosensors that incorporate a redox active component allow electrochemical signals to be measured, with excellent sensitivity. Perhaps the most powerful are optical systems, potentially combining UV-vis, phosphorescence and fluorescence properties. Colour changes visible by naked eye are possible, and can allow an immediate indication of the presence of a target analyte. UV-vis spectroscopy can be used in tandem with naked-eye observations to quantitatively determine the concentration of a species. Phosphorescence is uncommon but has seen some use[2]. Fluorescence possesses many advantages which have seen its use rise to the forefront of most sensor research. Fluorescence has great potential for in-vivo analyte monitoring and is an extremely sensitive technique, having been shown to detect single molecules in solution.

1.3 The Importance of the Small Halide Anions

1.3.1 Chemical and Biological Impact

Fluoride is the smallest anion and due to its extreme hardness, often displays differing properties to the rest of the halides. The real-time monitoring of fluoride ion concentration in aqueous and physiological media is of vital importance. Quantitative determination is highly desirable across a large concentration range, due to the various environments fluoride is thought to have detrimental effects. The nerve toxin Sarin (isopropyl methylphosphonofluoridate), notorious for being the poison of choice of the Aum Shinrikyu Clan in the Tokyo Subway attack of 1995, which killed a dozen people and injured over fifty, generates fluoride on hydrolysis. A rapid method for determining whether Sarin has been utilised in a terrorist attack could save lives. A chemosensor device is an appealing solution to this problem. The role of fluoride in dental health appears to be one of balance, with fluoride crucial in forming and preserving tooth enamel and yet higher levels cause dental caries. Fluorosis, the term given to over-exposure of fluoride can cause kidney failure[3] and severe skeletal defects. Crippling skeletal fluorosis is a significant cause of morbidity in a number of regions of the world, in fact, UNICEF has estimated 60-70 million people in India are at risk.[4] Figure 1 below shows the increased density is clearly visible in the X-ray of a fluorosis sufferer's forearm (left) compared to a normal forearm (right). Acute systemic fluoride poisoning can result in systemic hypocalcaemia, cardiac dysrhythmias, and cardiovascular collapse.[5]

Figure 1 X-rays showing effects of fluorosis on human forearm. The image on the left shows increased density between the ulna and radius of a patient suffering from fluorosis. The image on the right is of a healthy forearm.

Chloride (usually from sodium chloride) is essential for human health, regulating blood pressure, maintaining metabolism and the acid-base balance within the body. Typical levels are at around 0.1 M in blood serum. Chloride anion transport processes within the human body (and therefore chloride recognition) are linked to a number of conditions including cystic fibrosis,[6] Bartter's syndrome,[7] Dent's disease,[8] developmental pain[9], Pendred's syndrome,[10, 11] and osteopetrosis.[12]

Following a look at the role various anions play in biological systems, this Chapter is intended to provide a overview of the different molecular motifs utilised in designing anion receptors. The examples discussed will demonstrate the variety of molecular properties utilised in achieving host-guest complexes that supramolecular chemists have observed in nature.

1.3.2 The Role of Anions in Biological Systems

Biological systems are underpinned by anion recognition and transfer processes, with anions present in the majority of enzymatic active sites and controlling the conformation of a number of proteins. Variation or misregulation in cellular flux of anions including ATP, sulfate, phosphate and halides can be a useful indicator for a range of diseases.[13]

The haloalkane dehalogenase *Xanthobacter autotrophicus* GJ10 has been proposed as a possible aid in the decomposition of prevalent and harmful halogenated species. During mechanistic investigations, Verschueren *et al.* isolated crystals of this nitrogen fixing bacterium at various stages of the catalytic pathway of dehalogenation of 1,2-dichloroethane, isolating crystals showing chloride ions bound in the active site of the enzyme (Figure 2), [14, 15]

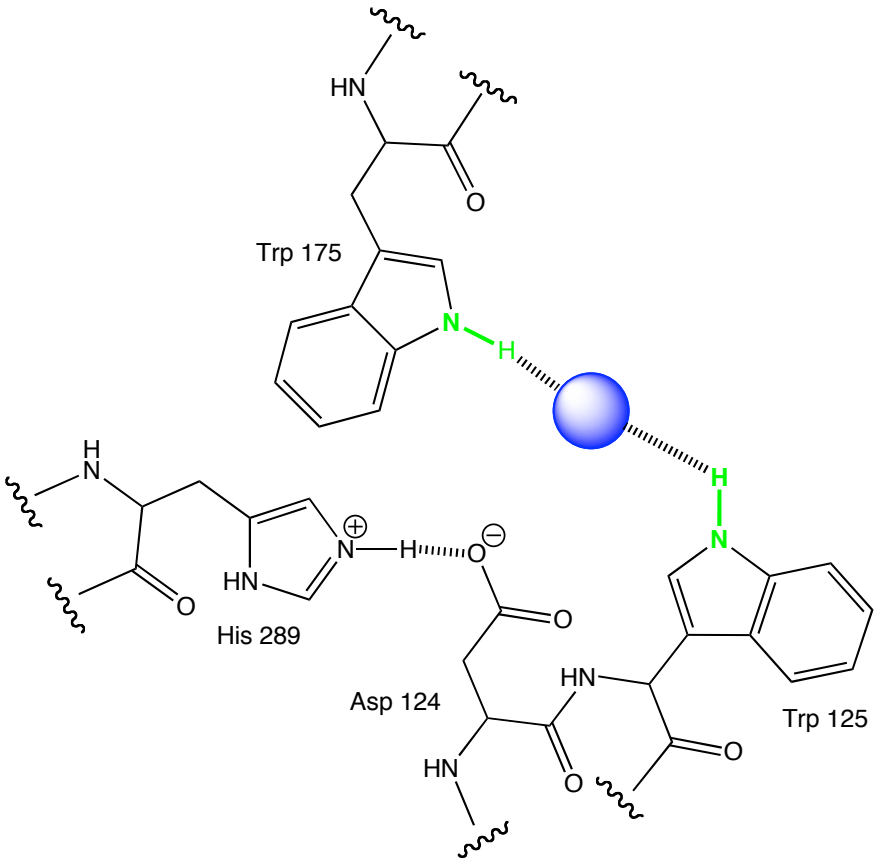

Figure 2 Schematic diagram showing a chloride ion (blue sphere) bound in the active site of *Xanthobacter autotrophicus* GJ10.

Chloride is also capable of influencing protein conformation and hence inhibition *via* coordination to an allosteric site. *O*-acetylserine sulfhydrylase enzyme plays a crucial role in the final step of the biosynthesis of *L*-cysteine. Although sulfide is the physiological inhibitor of this process, Burkhard *et al.* reported that *O*-acetylserine sulfhydrylase manifests in an inactive conformation due to the presence of a bound chloride anion in an allosteric site, with a sulfate anion bound to the active site. This illustrates how chloride can inhibit or regulate enzymatic action.[16]

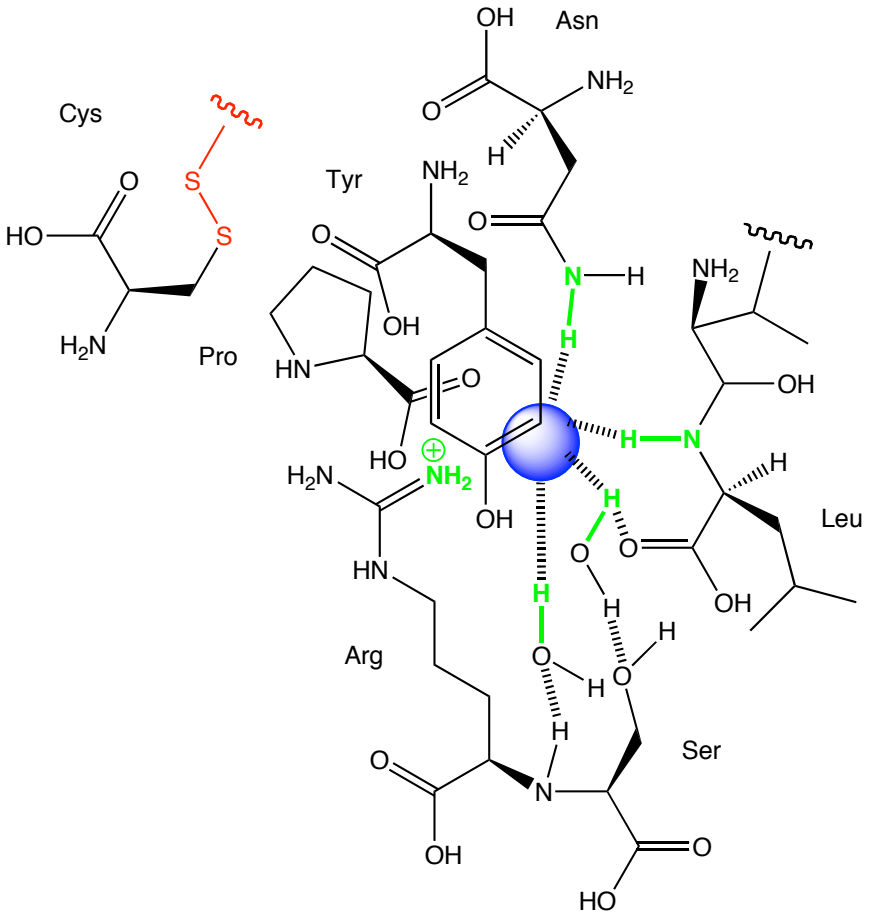

Figure 3 Simplified diagram representing the crystal structure of inhibited O-acetylserine sulfhydrylase with a chloride ion (depicted as a blue sphere) bound in an allosteric site.

The chloride anion is bound to the amide of an asparagine residue and the peptide nitrogen of a leucine on the adjacent monomer (the chloride is located at the dimeric interface) *via* hydrogen bonding interactions. Other short interatomic distances indicate the positively charged guanidine of a arginine residue plays a role and two water molecules are engaged in systematic hydrogen bonding processes with a serine functionality. It is worth noting at this point that both of these examples show NH

hydrogen bonding to chloride, as this chapter will later show many supramolecular chemists have attempted to mimic nature and adopt similar recognition motifs.

A report by Eustáquio and co-workers illustrates an interesting example of the potential for anion recognition chemistry to have an impact on synthesis or possibly even catalytic design. 5'-CIDA (compound **1**) is a precursor in the biosynthesis of Salinosporamide A (**2**); a natural product extracted from a marine bacterium *Salinispora tropica*. Chlorinase SalL is the enzyme responsible for introducing the chlorine substituent, known to increase the activity of Salinosporamide A by a factor of 500 compared to a nonchlorinated analogue.[17]

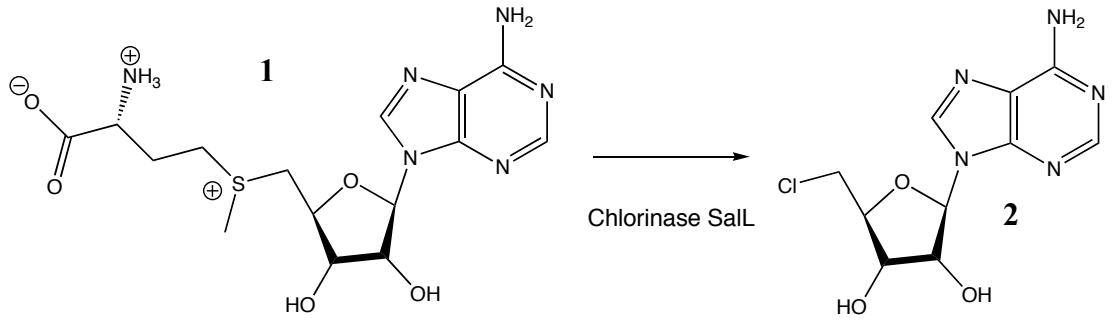

Scheme 2 Reaction catalysed by Chlorinase SalL.

The group succeeded in isolating a crystal indicating chloride was bound to the amino group of a glycine residue within the interior of a ChlorinaseSalL mutant, orientated perfectly to undergo an S_N2-type nucleophilic substitution reaction with the bound SAM reactant at the active site.

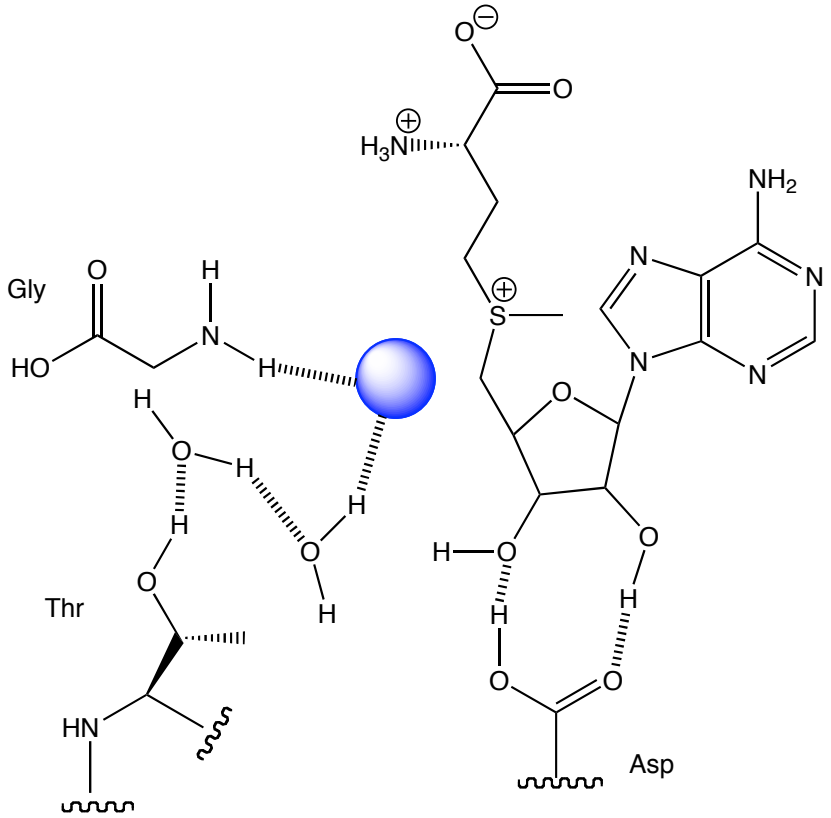

Figure 4 Chloride ion (depicted as a blue sphere) bound by Chlorinase SalL. Other amino acid moieties orientate SAM in correct position to undergo reaction.

Dutzler *et al.* presented the X-ray structure of the StClC chloride ion channel, an hour-glass shaped channel with an interesting feature of a charged glutamate side chain which is thought to be acting as a gate regulating the passage of chloride anions.[18] Atom-ion distances imply CH, NH and OH hydrogen bonding interactions, including the phenoxyl proton of a tyrosine, the amino group on an isoleucine and the oxygen on the side chain of a serine substituent.

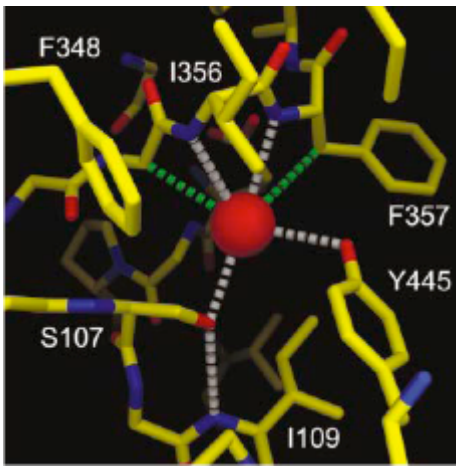

Figure 5 Adapted from Nature article, green dashed lines represent hydrophobic contacts and white dashed lines represent polar interactions of less than 3.6 Å.

In a later publication Dutzler compared wild-type ad mutant ClC channels, finding three distinct chloride binding environments in the 'neck' of the hourglass structure and confirming the glutamate side chain was responsible for closing the pore.[19]

Fluoride has received less attention in the biochemical literature when compared with chloride but NaF has been shown to function as a potent G protein activator and Sr/Thr phosphatase inhibitor and affects an array of essential cell signalling processes.[20] Calcium ATPase in sarcoplasmic reticulum membranes function as an ion pump in muscle cells, relaxation being produced by calcium transport out of the cytoplasm and into the SR^1 lumen. Studies have shown fluoride anion to act as a slow, tight-binding inhibitor of ATPase.[21]

1.3.4 The Challenges of Anion Recognition

Synthetic anion receptor chemistry is in its infancy in comparison with the more established field of cation recognition. This difference can be attributed to two factors: lower charge to radius ratio (so larger, softer, more diffuse) and the variation in geometry presented by anionic species, making selective recognition more demanding. To illustrate this latter factor, the conceivable range in anion geometry ranges from spherical (eg bromide, iodide) to tetrahedral (eg phosphate, sulfate), octahedral (eg $[PF_6]^-$, $[Co(CN_6)_3]^-$) or even complex biological anions such as the helical DNA polyanion. Particularly relevant to this body of work is the fact that the halide anions

are significantly larger than their isoelectronic cations, indicative of their lower charge to size ratio.[22]

There are further complications in that anions tend to be vulnerable to protonation at low pH and even if the receptor is neutral or operating in non-protic solvent, competition with the solvent molecules has to be considered in all anion-binding situations. The anion source counter cation plays a role, and ion-pairing is affected by the nature of the cation as well as the solvent (particular non-polar solvents) in which recognition is occurring.[23]

If a receptor is designed with biphasic extraction from water in mind, the Hofmeister series[24] becomes highly pertinent. This series, indicating the increasing degree of anion solubility and is usually presented in the form of decreasing hydrophobicity: organic anions > chlorate > thiocyanate > iodide > salicylate > nitrate > bromide > chloride > hydrogen carbonate > dihydrogen phosphate > fluoride > sulfate > hydrogen phosphate. If a localised molecular sensing environment can be designed that interrupts this sequence it is possible to extract a particular anion selectively. The most important outcome of these competitive factors is that it is imperative that binding constants and recognition events be considered with respect to the solvent, binding motif and measurement conditions.

1.4 Fluorescence Sensor Concepts

1.4.1 The Principles of Fluorescence

Luminescence, the emission of light produced by electronic excited states within a substance, is defined into two categories, namely phosphorescence and fluorescence. Fluorescence results from a relaxation of a singlet state and phosphorescence is an emission arising from decay at the triplet state. A Jabłoński diagram is the classic way to illustrate the various energetic and optical processes that can occur in a molecular system.

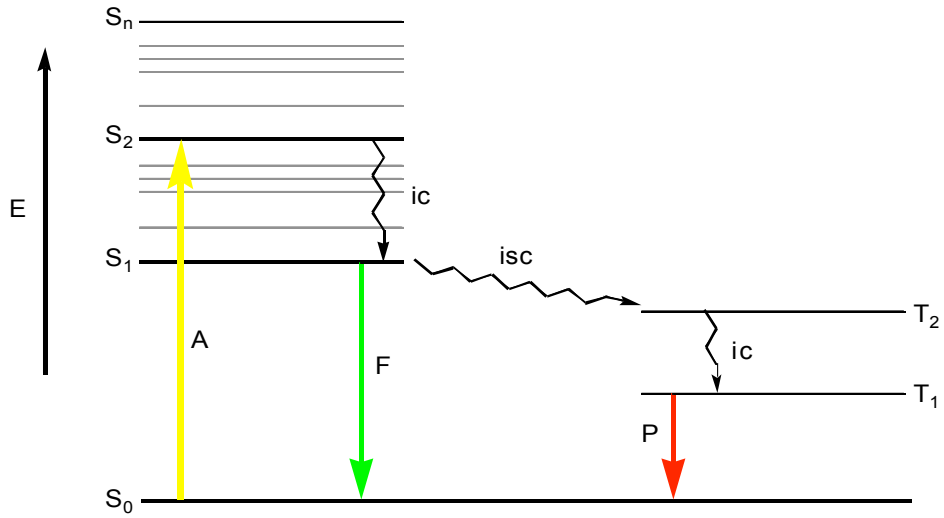

Figure 6 Jabłoński diagram showing various energy transitions in common optical events. A = photon absorption, F = fluorescence emission, P = phosphorescence emission, S = singlet state, T = triplet state, ic = internal conversion, isc = inter-system crossing. The E axis is energy relative to the ground state, S_0.

1.4.2 The Application of Fluorescence

Researchers are always trying to gather information about events occurring at the molecular level. Light as a means to transfer information via the phenomenon of molecular fluorescence offers many advantages. Optical signals travel through, and therefore transfer information through space, allowing fluorescent sensors to provide information inside living tissue remotely. Information can be communicated in near real-time and it is possible to locate fluorophores within tissue with sub-nanometre accuracy.[25] In terms of sensitivity, fluorescence excels, with the developments of methods to detect single fluorescent species (and simultaneously their movement over micrometer distances) and the presence of single guest molecules.[26-30] Although not all fluorescent sensors are this sensitive, micromolar concentrations are typical and a significant amount of physical information can be retrieved with minimum interference with the system. From both an analytical and commercial standpoints these characteristics are appealing.

Fluorescent sensors can be found in many recent analytical advances, such as the TNT vapour sensor in the Fido system employed by the U.S army which achieves ultrasensitivity by utilising self-amplifying fluorescent conjugated polymers.[31]

Confocal microscopy is developing rapidly in microbiology arenas intracellular monitoring of fluorescent-tagged biomolecules expected to be an area of huge impact.[32] Recently Edgington *et al.* used the non-invasive optical imaging of apoptosis to show the potential of fluorescence for monitoring and hence evaluating cancer treatments.[33] Aptamer units have been incorporated into fluorescent sensor systems allowing specific drug molecule detection.[34] The development of commercial equipment, particularly in the healthcare market, that incorporate fluorescence is ongoing. This variation in application highlights the robustness and versatility of fluorescence based sensing.

This thesis discusses the design and synthesis of fluorescent sensors for anions, primarily utilising boronic acid derivatives as the receptor site. Sensors combining these two features have received a lot of research effort since James and Shinkai's original publication in 1998.[35] Across the diverse range of boronic acid-based fluorescent sensors developed, two distinct design principles predominate in the scientific literature: internal charge transfer (ICT) and PET. In both cases, successful signalling of the binding event arises from alternative low-energy pathways being discretely offered to either the bound or unbound sensors, these processes affecting defined spectral changes in the emission band. The following part of this thesis details some of the aspects of these optical phenomena.

1.4.3 Photoexcitation and Subsequent Relaxation

When an electron in the singlet ground state (denoted S_0) of a fluorophore (a substance which exhibits fluorescence) is bombarded by an incident photon of sufficient energy it is promoted or excited to a higher energy level (Scheme 3). Typically, this initial excited state is a higher vibrational level within a excited singlet state (S_1, S_2, S_3 etc).[36]

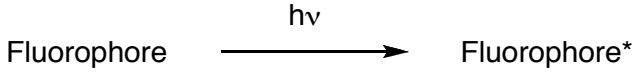

Scheme 3 Fluorophores can be excited to an excited state by light of a given energy.

Vibrational energy is easily lost in solution courtesy of molecular collision, meaning internal conversion to the lowest available excited state S_1 usually occurs very rapidly,

with the concurrent reduction in energy.

From this S_1 state, fluorophores are capable of dissipating their residual energy in the form of light waves. The energy – and the emissive wavelength – of the resulting photon corresponds to the difference in energy between the final and initial occupied energy states. Excitation occurs on the femtosecond time scale, followed by internal conversion processes, which typically occur in the picosecond range.[36] However, significantly, S_1 excited-states exhibit fluorescence lifetimes of approximately 10 nanoseconds, allowing the utilisation of optical processes for transduction of recognition events.

1.4.3 Internal Charge Transfer

Sensor Systems Utilising Internal Charge Transfer

Considering the ICT mechanism, any sensor design must incorporate a receptor and a fluorophore unit integrated into the molecule in a manner which allows direct electronic communication between the two components. This feature allows guest binding to influence the electronic properties of donor or acceptor groups within the sensor species, or in the case of TICT molecules, invoke conformational restraint.[37]

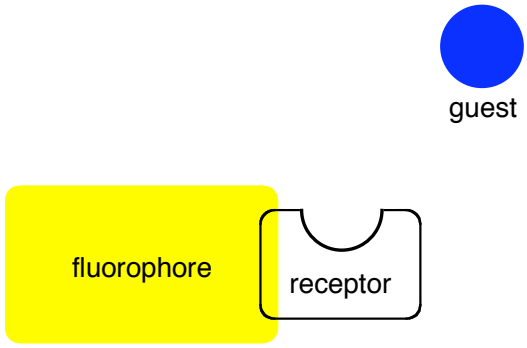

Figure 7 Schematic of an ICT sensor.

Sensors which exclusively employ ICT as a signalling mechanism are less common in recent years but an example of a simple ICT type anion sensor **3** can be found in James' 1998 paper (as seen below in Figure 8) discussed in further detail later in the Chapter.[35]

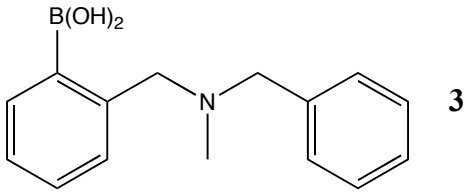

3

Figure 8 A classic ICT system.

1.4.4 Excited State Photoinduced Electron Transfer

Differing slightly but significantly from an ICT sensor, a PET system design must incorporate a linker or spacer group between the ubiquitous receptor and fluorophore units.

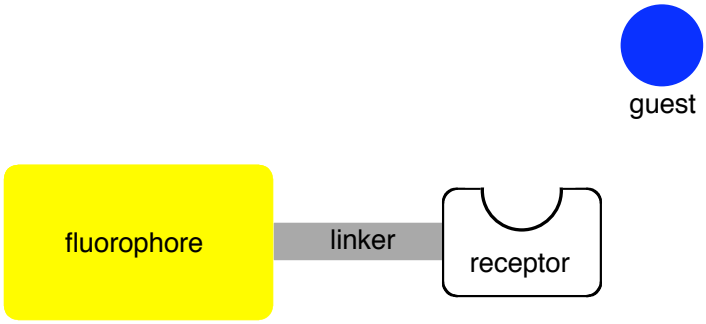

Figure 9 Schematic of a PET sensor.

Considering the mechanistic aspects of such a system, following electronic excitation of the fluorophore by a photon of sufficient energy, the system then undergoes the normal relaxation processes to the lowest vibrational level of the S_1 excited state. At this point, molecules which contain a bridging linker group (B) between the donor (D) and acceptor (A) regions can rapidly perform an intramolecular electron transfer process, lowering the energy of the system. Thus, D-B-A* motif becomes D^+-B-$A^-$and in the case of PET sensor systems, the D^+-B-A^- state lies, energetically speaking, between the D-B-A ground state and D-B-A* states (as in Figure 10 below).

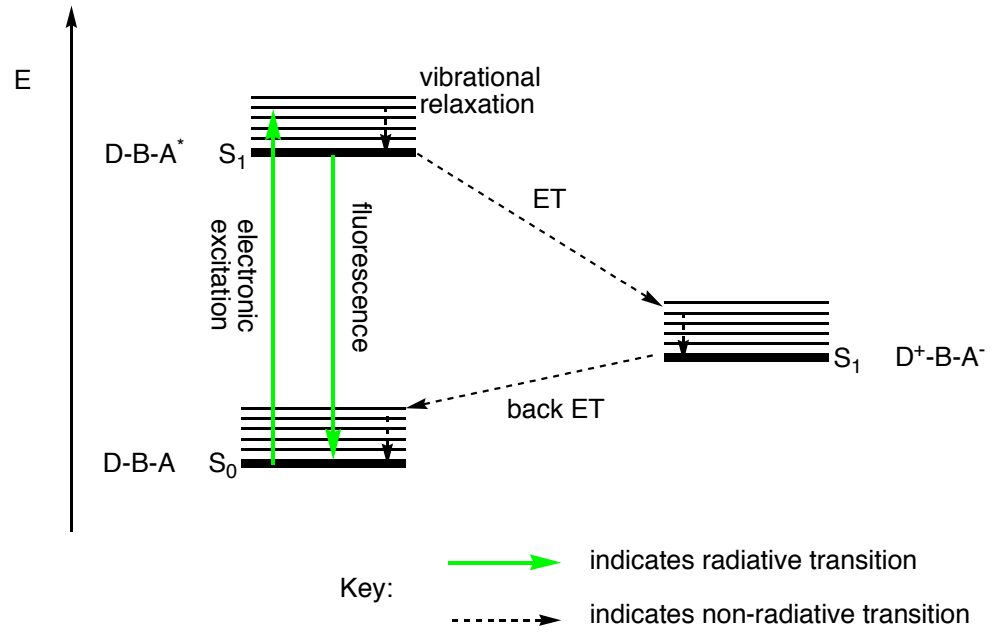

Figure 10 Jabłoński diagram depicting the non-radiative pathway available to compounds that undergo internal PET.

This lowering of energy is attributed to the rearrangement of the surrounding solvent shell and internal rearrangement of bond angles and lengths. The resultant internal conversion process of back ET as the geminate recombination occurs from the S_1 state of the D^+-B-A^- to a vibrational state of the S_o D-B-A state. This allows highly efficient fluorescence quenching to occur.[38-40]

In a recent illustrative example, the components of donor, acceptor and bridging linker (methylene group) can be clearly identified in the family of compounds **4a-4d**, reported by Gunnlaugsson and coworkers.[41]

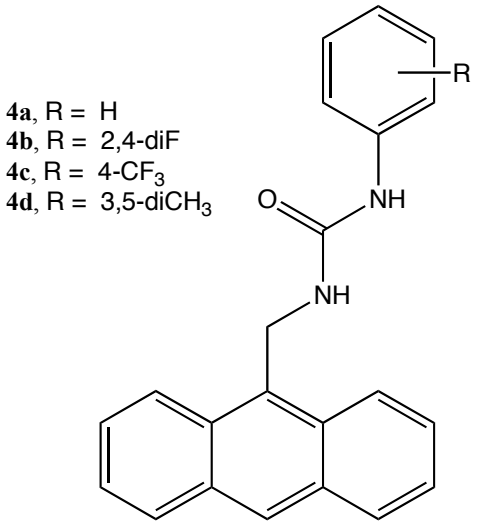

Figure 11 Recent family of sensors displaying typical PET fluorescence behaviour and structural characteristics.

Anion recognition *via* strong hydrogen bonding interactions with the aryl urea groups prompted enhanced quenching response of the excited state of the anthracene by electron transfer from the receptor. The limited changes to the ground state and the fluorescence emission 'switch off' response are characteristic of an ideal anion PET sensor.

1.4.5 Alternative Signalling Methods

Metal-ligand charge transfer (MLCT) is another emissive phenomenon utilised in synthetic anion receptors. Following absorption, MLCT complexes undergo intersystem crossing to triplet state (femtosecond timescale) and decay occurs by radiative and non radiative processes. MLCT absorptions typically occur in the 450 nm region. Advantages include a large Stoke's shift so compounds do not self-quench and often emission occurs at useful longer wavelengths, around 650 nm is typical.[42-44]

The various electronic states in any metal-ligand complex are shown in Figure 12.

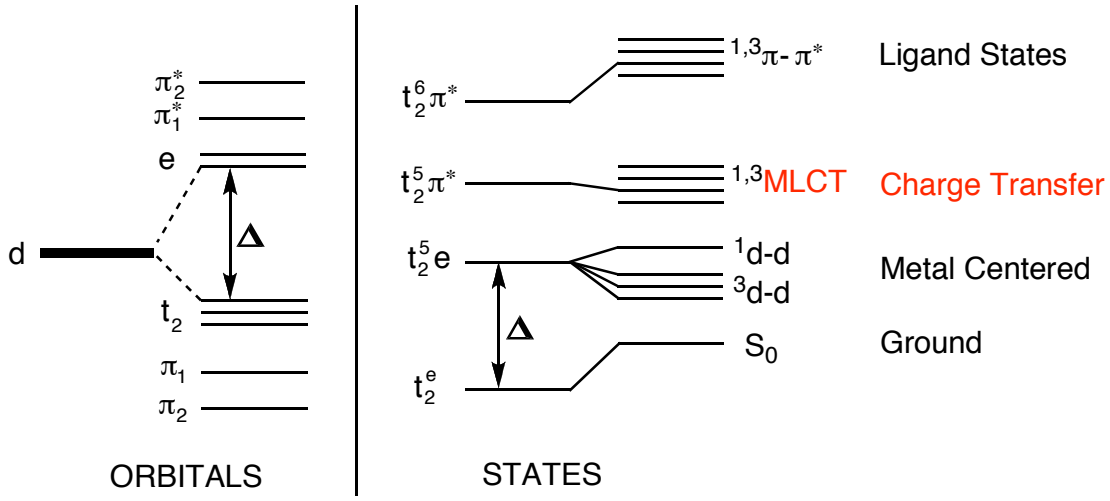

Figure 12 Orbital and electronic states of metal-ligand complexes. The *d* orbitals are associated with the metal and are split according to crystal field created by the ligands. The π orbitals are associated with the ligand.

Considering a typical metal centre capable of forming a MLCT species, Ruthenium, the t_{2g} states are fully occupied by 6 d electrons. On photon absorption, transitions from the t_{2g} to the e_g^* state are formally forbidden. Also, electrons in the e orbitals are antibonding with respect to the metal-ligand bonds, so excited *d-d* states are unstable. The resulting combination actually results in a new transition involving charge transfer between the metal and ligands, called the MLCT band. This transition causes the broad emission phenomena observed in these type of species.

1.4.6 Measurement Limitations

When calculating the binding constant or selectivity of a host-guest system, titrations are performed and monitored by NMR, UV, fluorescence spectroscopy or isothermal calorimetry. Many processes are analysed with multiple techniques, due to concentration limitations and the variety of the information provided by the data. NMR spectroscopy operates in the 10^{-3} M range, whereas optical spectroscopy techniques function at concentrations in the range of 10^{-5} to 10^{-6} M.

When performing sensitive titration experiments it is imperative to maintain constant measurement conditions and to consider any data reported with respective to the counter ion and solvent in question. Solvents directly affect the strength of any binding events and the degree of ion-pairing in solution between the anion and the counter ion.[23]

1.5 Synthetic Anion Receptor Chemistry

Although not a complete review of the field, the remainder of this Chapter provides insight into the foundations of anion recognition chemistry and highlights some particularly relevant and exciting new developments that have emerged in the last decade.

1.5.1 Pioneers and Early Research

Three highly significant pieces of work mark the earliest foundations of synthetic anion receptor chemistry. Tanford was the first chemist to examine the anion binding behaviour of synthetic molecules, as he observed changes in pK_a values for guanidinium complexes with the conjugate base of acetic acid and went on to report association constants with anions such as phosphate and acetate, although these were fairly weakly binding (0.32-1.37 M^{-1}).[45]

The next small but significant contribution to anion recognition chemistry - particularly pertinent to the chemistry disclosed in this thesis - came in 1967 with Shriver and Ballas, who identified the complex formed between the bidentate Lewis acid **5** and a methoxide anion as being the opposite of the better described situation between a central metal ion accepting electron density from a difunctional base.[46]

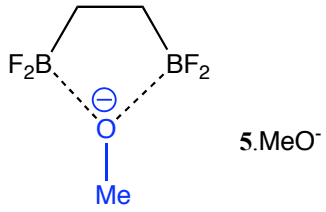

Figure 13 First known example of a bisboron compound binding an anion.

This paper was pioneering, as over 40 years later, molecules with single, dual or multiple Lewis acidic sites (including those with mercury,[47-49] tin,[50-55] germanium[56-58] and silicon[59] centres in addition to the more commonly employed boron) remain attractive recognition units.

In a more directed approach, Simmons and Park reported the synthesis and binding

behaviour of macrobicyclic host molecules in 1968, work which paved the way for a large amount of research into this type of molecular scaffold. Proton NMR experiments confirmed two different conformations could be observed for the macrobicyclics, with the ammonium hydrogen orientated either internally or externally with respect to the cavity. An association constant of 4.0 M^{-1} was measured for compound **6** in 50 % aqueous TFA solution, with concurrent ^{1}H NMR showing the presence of the single (protons internally directed) conformer. The proposal of an internally bound anion was later confirmed by Marsh *et al*.[60]

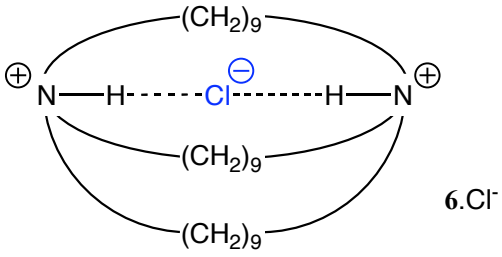

Figure 14 An early chloride receptor.

Nobel-Prize winner Jean-Marie Lehn, awarded the honour for his contribution to supramolecular chemistry, used a series of macrocyclic ammonium based receptors to show the influence of optimum fit on anion binding. The tetraprotonated forms of **7** and **8** were found to be highly selective by size, compound **7** binding chloride with a binding constant of log $K_s > 4.0$ for chloride and log $K_s < 1.0$ with respect to bromide. The larger iodide did not appear to enter the cavity.[61, 62]

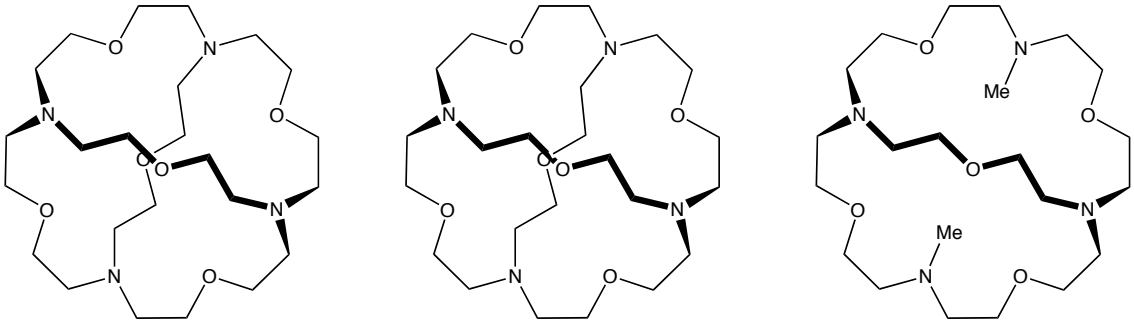

7 **8** **9**

Figure 15 Anion receptors based on cryptands.

Compound **9** was used to illustrate the importance of employing the cryptate effect to achieve strong anion binding. Compound **8** was found to bind chloride with a significantly higher binding constant than the bicyclic **9** (log K_s > 4.5 compared to log K_s 1.7), owing to its enclosed recognition environment and rigid nature. The systems were investigated in water (pH 1.5), so the degree of hydration of the ammonium binding sites was also put forward as significant. Soon after, Weiss *et al.* confirmed the chloride anion is centrally bound within the cryptand, as proposed by Lehn.[63]

Another significant contribution showed that synthetic anion receptors can operate using electrostatic interactions. Schmidtchen utilised quaternary ammonium groups orientated in a tetrahedral arrangement and by altering the size of the cage showed it was possible to tune selectivity of the receptors for iodide. Iodide has a radius of 4.12 Å, and the cavity of **10** was measured as 4.6 Å. The larger receptor **11** was able to bind *p*-nitrophenolate which is too large to be encapsulated by **10**.[64]

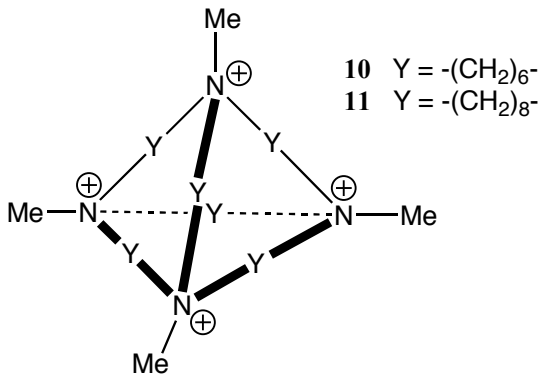

Figure 16 Receptors can be tailored by the dimensions of the binding cavity.

To overcome the limitation of competition with a counter anion, zwitterionic receptors **12** and **13** were prepared.[65, 66] Indeed proton NMR studies showed that competition was highly likely to be occurring in solutions of **10** as **13** complexed chloride, bromide and iodide more strongly.

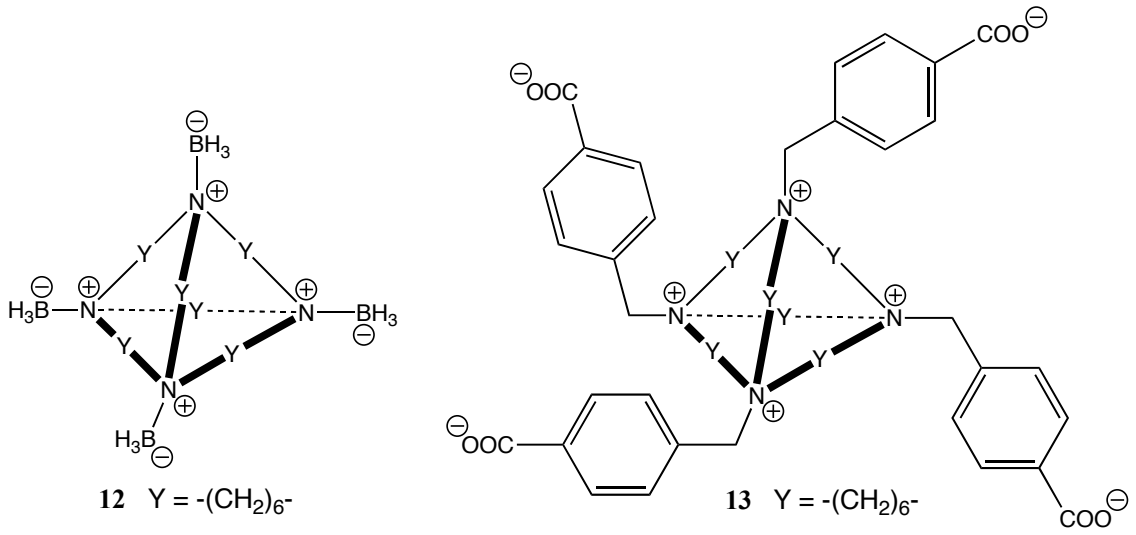

Figure 17 Zwitterionic receptors demonstrating tuneable electrostatic halide ion binding.

Unlike systems relying on electrostatics, synthetic anion receptors that utilise hydrogen bonding are common and diverse. The neutral anion receptor **14** was the earliest of a large number of sensors developed based on N-H···anion interactions.[67] Despite the fact that the NH groups are directed out of the cavity in the solid state, proton and fluorine NMR indicated that fluoride binding was occurring in DMSO solution.

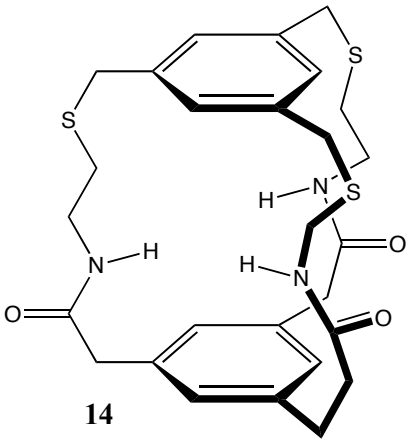

Figure 18 Cyclophane anion receptor.

The first example of using Lewis acidic boron to bind the fluoride ion was published in 1985 by Katz[68] (compound **15** pictured in Scheme 4). The adduct **15**.F^- was characterised successfully by ^{19}F-^{1}H and ^{19}F-^{13}C coupling in its NMR spectra, with large ^{19}F-$^{1}H_{Me}$ coupling verified on a 60 MHz spectrometer. A later publication by the same author found the two B centres to be sp^2 hybridized. On binding, the B-B distance

was found to be significantly shorter and sp^3 character at the boron centres was indicated by ^{11}B NMR.[69]

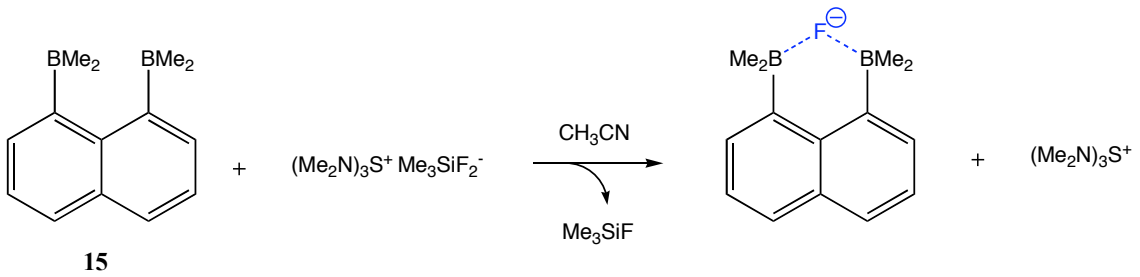

15

Scheme 4 The first Lewis acid based bidentate fluoride receptor **15**.

Derivatives of this 1,8-diboronaphthalene skeleton are still explored as effective fluoride sensors today, and the ability of fluoride to bridge between two boron atoms is a driving factor behind some of the experimental design discussed in Chapter 2.

One of the family of compounds which have received a lot of attention over the last 20 years are cyclic and acyclic receptors engineered from pyrrole subunits. Early on, the group headed by Sessler identified a mixed anion salt of Sapphyrin **16**, including the observation of a fluoride bound complex.[70] Unlike porphyrin which is composed of four pyrrole units, pentapyrrolic Sapphyrin is easily protonated.

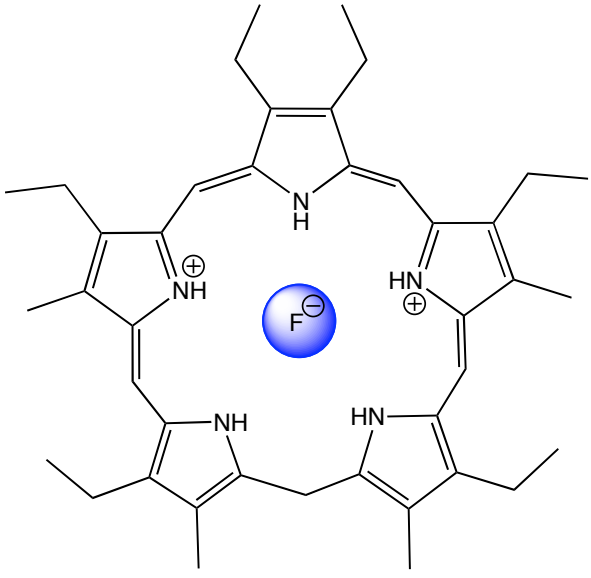

16.F^-

Figure 19 Sapphyrin has been shown to bind fluoride in solution.

Ibers went on to disclose the crystal structure of the doubly protonated sapphyrin complex with fluoride.[71] A complex array of five hydrogen bonds and electrostatics combine to promote fluoride binding. Fluoride was measured as binding more strongly than the larger and softer halides by at least 2 orders of magnitude.[72] This strong and selective mode of binding ignited a wealth of research into this type of molecular scaffold.

All of these examples highlight the emergence of influential areas of anion recognition chemistry, current developments will be discussed shortly, all underpinned by the observations made in these pioneering reports.

1.5.2 Existing Methods of Fluoride Detection

Fluoride concentrations can be determined by ^{19}F analysis or the specific ion electrode method.[73, 74] These systems, although well established, possess some disadvantages. The latter is a membrane electrode containing single crystals of LaF_3, a method which is accurate but fragile and time consuming.[75] ^{19}Fluorine NMR can only be used reliably on the micromolar scale typical to most NMR studies. Neither system can be used to study biological processes *in vivo*, and an alternative system allowing intra cellular monitoring would be infinitely preferable to researchers.

1.5.3 Boronic Acids and Derivatives as Binding Sites

The boron atom of trisubstituted boron species possesses an sp^2 trigonal planar geometry with an empty *p* orbital perpendicular to the plane of the molecule. This feature dominates both the synthetic and receptor chemistry of boron compounds. The various common boron derivatives are discussed from a synthetic perspective in Chapter 2. Nucleophiles are able to interact with or donate into this vacant site, causing a subsequent change in geometry and hybridisation. The phenylboronate anion was first confirmed to be tetrahedral by Lorand and Edwards in 1959.[76]

Scheme 5 Diagram showing the change in geometry undergone at the boron centre when the vacant *p* orbital is filled by an attacking nucleophile.

This relatively weak Lewis acidity at the boron centre opens up a wealth of synthetic chemistry but also allows boron to act as a receptor for hard anions, particularly cyanide, hydroxide and fluoride. The Brønsted acidity of boron species becomes more important when considering covalent interactions, for example with vicinal diols. The pK_a of phenylboronic acid is 8.70 in water at 25°C[77]. It is known that boronic acids react rapidly and reversibly with diols to afford cyclic boronate esters in non-aqueous or basic aqueous conditions.[78, 79] It has also been widely reported that boronic acids show good binding affinity with other nucleophiles such as dicarboxylic acids[78, 80] and α-hydroxy-carboxylic acids.[81, 82] The use of boron as a Lewis acid extends to formation of coordinate bonds with a wide variety of hetero-atoms including oxygen, sulfur,[83] phosphorus[84] and nitrogen.[85] Such compounds have widespread use in organic synthesis.[86]

The earliest example of a dative nitrogen boron interaction is the complex formed between ammonia and trimethylborane, first documented in 1862.[87] One of the earliest examples of a compound containing an intramolecular N→B bond was reported in 1968 by Dunn *et al.*[88]

A Note on Boron Centres

The change in geometry described above can be monitored by ^{11}B NMR, as sp^2 boron resonances appear at 25 – 30 ppm (relative to boron trifluoride diethyl etherate internal standard) and tetrahedral boron can be visualised as a peak at around 0 ppm. Resonances between 5 and 15 ppm are due to boron centres accepting some electron density, typically from an oxygen or nitrogen atom. This can be *via* both intermolecular or intramolecular coordination. In 1992 Oki *et al.* introduced tetrahedral character (THC) as a means of evaluating the geometry of boron complexes containing an intramolecular N-B interaction.[89] Further to this, Hopfl proposed an improved equation,

scaling the THC between 0 and 100 % and including the bond angle with the donor atom, to compensate for steric effects between substituents on the boron atom that may affect geometry.[90]

1.6 Developing Receptors into Chemosensors

The examples discussed previously in this thesis were the pioneering developments that led to the emergence of anion sensor chemistry. However, they almost exclusively rely on NMR techniques to elucidate binding events, a method limited by concentration (millimolar concentrations), very expensive equipment and certainly no potential for *in vivo* studies. Essentially they can be considered only as receptors, incapable of chemosensing. In this next section the more recent developments in the field of anion sensing are explored, detailing researchers' attempts to transform the binding event at a molecular level into a response which can be measured qualitatively or quantitatively by the end user.

1.6.1 Organoboron Derivatives

Reetz observed in 1991 that a crown ether, the archetypal cation binding skeleton, appended with a Lewis acidic boron centre, served to solubilise a stoichiometric amount of a suspension of KF in dichloromethane.[91] A simple crown ether only binds catalytic amounts of KF. The proposed dual host-guest system **17** was examined by ^{11}B and ^{13}C NMR spectroscopy. The crown ether showed low-field shifts in the ether carbon atoms expected due to cationic binding. More noteworthy, the complex showed an upfield shift in ^{11}B NMR from characteristic sp^2 30 ppm to 10 ppm, indicating a pseudo tetrahedral sp^3 environment at the boron centre. KCl and KBr did not bind monotopically or heterotopically even after 2 weeks. Competitive selectivity was also displayed wherein in the presence of potassium salts of fluoride, chloride, bromide and iodide, solely the fluoride adduct was observed.

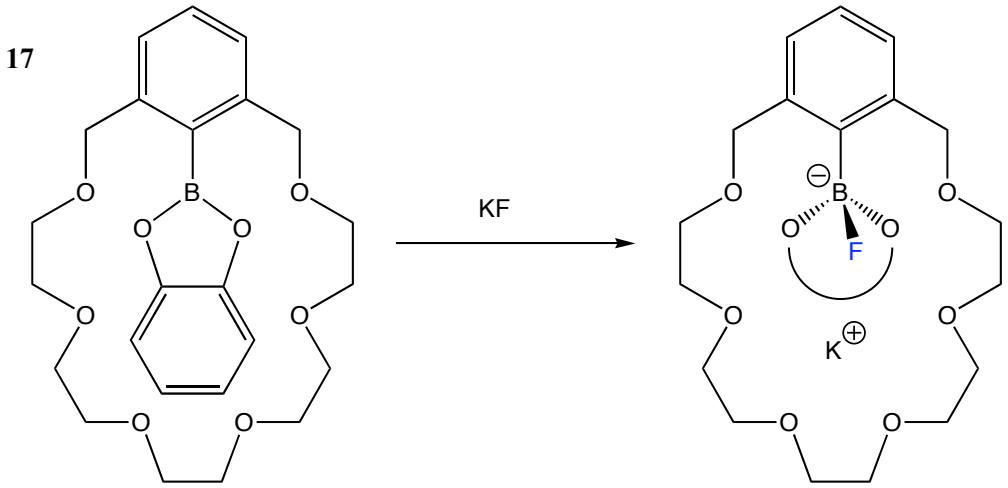

Scheme 6 A ditopic receptor for potassium fluoride based on a crown ether.

Jacobsen reported the results of a theoretical study of organoboron macrocycles indicating it was possible to design different Lewis acid macrocycle hosts for optimum binding with specific anions.[92] Molecular orbital (AM 1) calculations were performed on trimethylboron, two classes of boron-containing macrocycles, and their anion complexes with H^-, F^-, Cl^- and O^{2-}. These calculations indicated that ion binding occurs with a change in boron hybridization from sp^2 to sp^3. The nature of the anion-boron interaction was found to be more like a covalent bond than a purely ionic interaction. A significant amount of charge is transferred from the anion to the host upon complexation. An important consequence of this is that anions can fit into cavities which are smaller than their ionic diameters. Size exclusion, μ-anionic bridge formation, and cage flexibility are all key factors for anion complex formation. Formation of a μ-anion bridge was found to improve ion binding; one key outcome was the tendency of fluoride to bind exclusively in a μ-F bridge formation, that is, bound to only 2 boron atoms even in the presence of 4 Lewis acidic sites. However, chloride recognition appeared to be favoured by the inclusion of 4 boronic acid moieties. Another finding was that host flexibility facilitates μ-F type binding at the expense of selectivity, a particularly pertinent point regarding the molecular design discussed in this thesis.

Shinkai showed the relationship between the Lewis acidic boron and strongly basic fluoride could be exploited to create a means of determining the concentration of fluoride present in aqueous solution, even in the presence of other anions including

halides.[93] This landmark paper was the first example of transforming a receptor unit for fluoride anion into a sensory reporting system. The electron-withdrawing nature of the ferrocenyl group in compound **18** increases the affinity of the boron-fluoride interaction whilst simultaneously providing the redox active centre. Assuming thermodynamic equilibrium, the proposed redox cycle with the electrochemically active intermediates is shown below (Scheme 7).

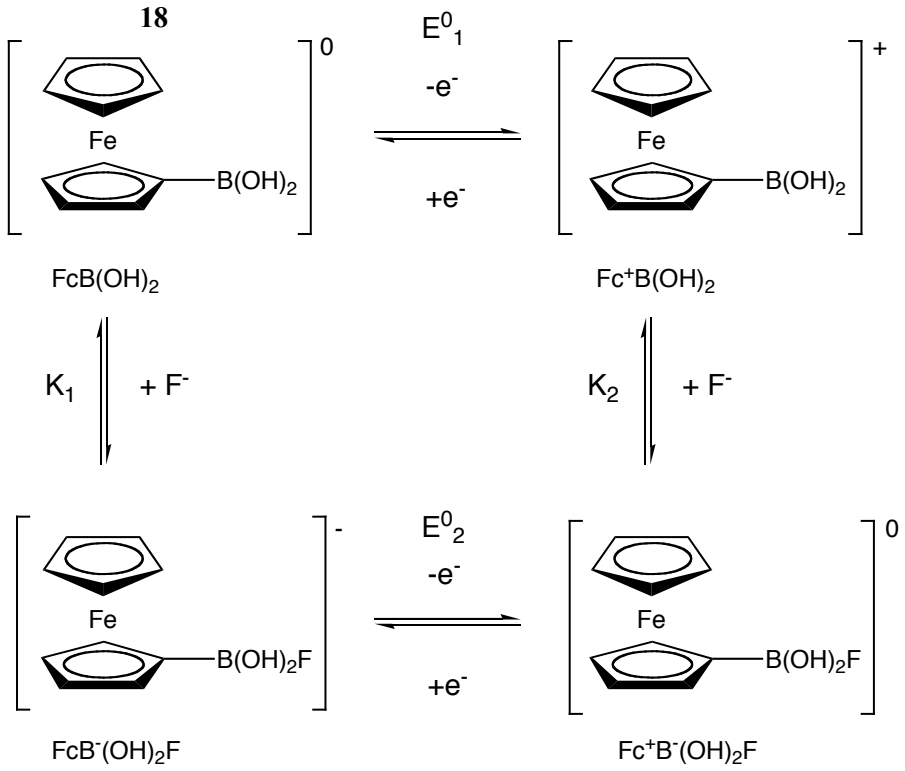

Scheme 7 Proposed redox cycle of interaction of **18** with fluoride anions.

Increasing the concentration of fluoride ions incurs a decreasing polarographic half wave potential which is linear over a range of 200 mM. Using Equation 1, it is possible to calculate the concentration of fluoride.

$$E = E^{O}_{1} + RT/F \text{ In } ([Fc^{+}B^{-}F(OH)_2]/[FCB(OH)_2]) \; RT/F \text{ In } (K_2[F^{-}])$$

Equation 1

In 9:1 H_2O-MeOH, selectivity for fluoride over chloride was 500-fold and even sulphate anions by a 50:1 ratio. Hydroxide interacts in similar fashion to fluoride but this only occurs at high pH.

Shinkai[94] enhanced the ferrocenyl system and created a molecular system capable of a visually detectable event, by naked eye, on binding to fluoride, thus devising the first optical sensor for fluoride. Taking advantage of a redox reaction between a suitable dye molecule (Methylene Blue **19**) and ferrocenyl boronic acid, it becomes possible to visually determine the fluoride concentration. Decolourisation begins to occur at 4 x 10^{-3} mM (monitored by UV-Vis spectroscopy as a decreasing absorbance at 665nm) and reaches zero at 3 x 10^{-2} mM.

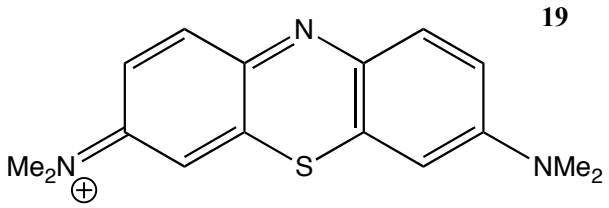

Figure 20 Methylene Blue.

James published the first fluorescent sensor selective for fluoride[35]. Fluorescence quenching of simple aromatic boronic acids (**20**-**22**, Figure 21) was observed in buffered aqueous methanol solution at pH 5.5 upon addition of KF. Tetrahedral boronate anions had already been shown to quench the fluorescence of directly covalent fluorophores in work investigating saccharide sensors and this same ICT mechanism was shown to proceed upon fluoride binding (in the paper it was discussed in terms of PET, later work found a different pathway). In a short study into the ^{11}B NMR behaviour of **20** and **22**, shifts consistent with a change from an sp^2 to sp^3 boron centre as the concentration of fluoride was increased from 1 to 5 equivalents were observed.

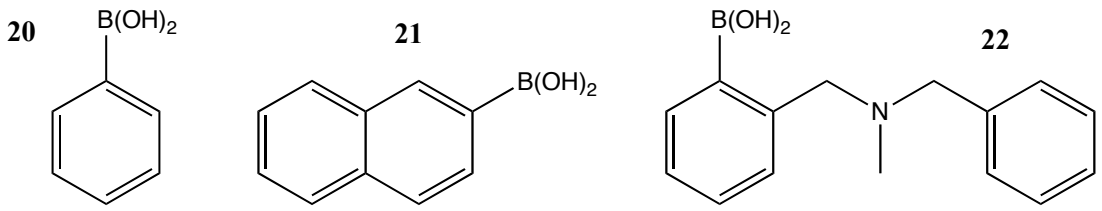

Figure 21 The first examples of fluorescent sensors for fluoride.

The group added a tertiary amine component to the molecule to provide an additional hydrogen bonding site, permitting determination of fluoride at lower concentrations (5-30 mM). The amine proton of **22** has a $_p$Ka of 5.5 so at under the conditions described

the nitrogen is considered to be half protonated, allowing a hydrogen bonding interaction with the fluoride on the boron. Compounds **20-21** allow concentration determination over 50-70 mM fluoride range but amine **22** allows for greater sensitivity. This introduces another aspect of the concept of 'tuneability', that is, making simple alterations to the molecule without interfering with the mode of action but altering binding strength, an essential feature for sensors for commercial application, as different environments require monitoring across varying concentration ranges. The fluorescence curve was best fitted assuming a reversible formation of a trifluoro tetrahedral boronate as in Scheme 8 below.

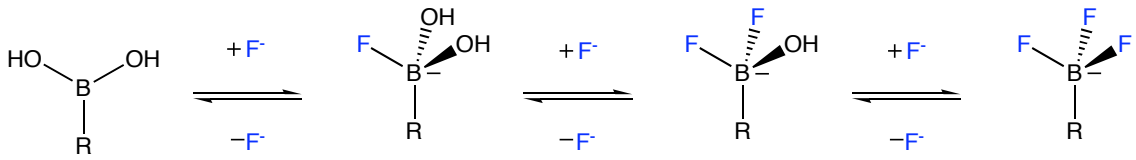

Scheme 8 Shows the proposed stepwise formation of the trifluoroborate anion.

In 2001, Yamaguchi *et al.* reported a range of boron-containing species **23a-c** and **24** that showed a visible colour change upon binding in THF media.[95] The highly conjugated system is interrupted by the boron-fluoride interaction and the concurrent change from sp^2 to sp^3.

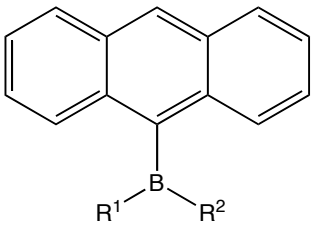

23a $R^1 = R^2$ = 9-anthryl
23b R^1 = 9-anthryl, R^2 = mesityl
23c $R^1 = R^2$ = mesityl

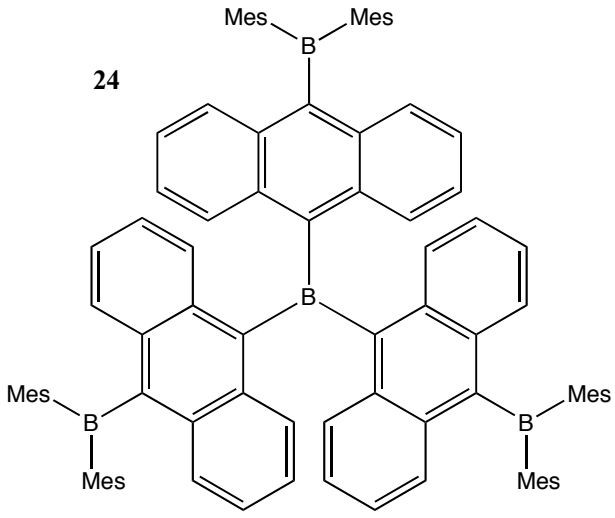

Figure 22 Triaryl borane species can act as colorimetric fluoride sensors.

Shinkai contributed further with a colorimetric and ratiomeric fluorescence chemosensor **25** that displayed three emission responses at 356, 670 and 692 nm to

fluoride ions.[96] The system was comprised of a porphyrin and a triarylborane centre connected *via* a conjugated linker (Figure 23). Changing the conjugation of a laterally expanded porphyrin results in a significant hypsochromic shift of the Soret band and a bathochromic shift of the Q band.[97] Fluoride coordination to the boron centre generates an anionic charge on the boron causing a change in the linker conjugation and a change in the energy pathway. Evidence for the latter finding was provided by measuring the fluorescence decay of the emission band. The fluorescence lifetime at 515nm of free **25** corresponds to less than 100 ps, extended to 0.53 ns in the fluoride bound species. Compound **26** does not contain a porphyrin linked component, and has a longer lifetime than that of **25**, at 4.52 ns. The shorter lifetime of **25** can be rationalised by Dexter-type energy transfer from the triaryl borane to the porphyrin ring system. Across the host-guest complex **25**.F^- however, only limited energy transfer can occur.

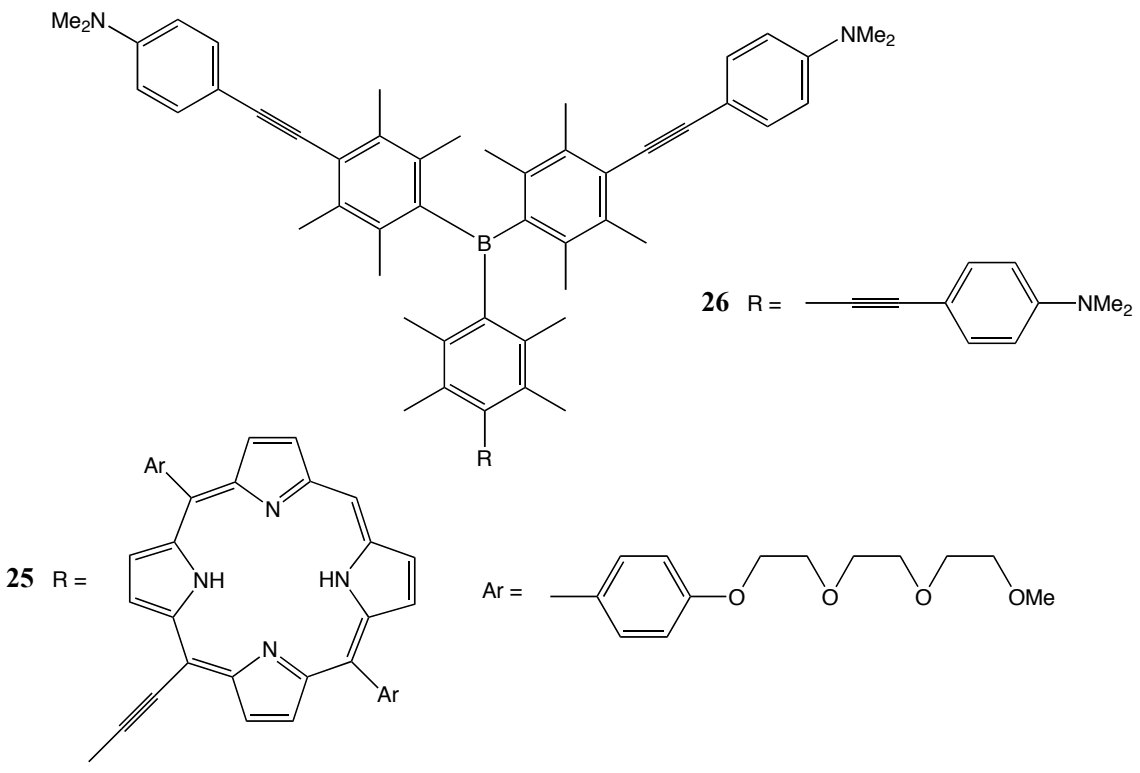

Figure 23 Ratiomeric sensors **25** and **26**.

This publication is particularly noteworthy in that the authors employ a ratiomeric sensor. For the majority of reported fluorescent sensors for fluoride, the binding of the anion causes a quenching of the fluorescence emission.[98] Only a few sensors in which the binding of a fluoride ion causes an increase in the fluorescence have been reported.[99] However, in most practical applications, changes in fluorescence intensity (fluorescence

quenching or enhancement) can also be caused by many other poorly quantified or variable factors such as photobleaching, sensor concentration, the environment around the sensor molecule (polarity, temperature, and so forth) and the stability of sensory system under illumination. To increase the selectivity and sensitivity, ratiometric measurements are utilised, which involve the observation of changes in the ratio of the intensities of the absorption or the emission at two wavelengths. Ratiometric fluorescent probes have the important feature in that they permit signal rationing and thus increase the dynamic range and provide built-in correction for environmental effects.[96, 100-103]

Gabbaï is at the forefront of the challenging prospect of anion recognition in aqueous media and his first foray into this area came in 2004 when his group used a neutral bidentate diborane species to bind fluoride and create a colorimetric sensor **27** which is not affected by the presence of water. At the foundation of much of the group's research is the use of a rigid 1,8-naphthalene backbone with two proximal Lewis acidic sites promoting fluoride anion chelation. The association constant of **27** (Scheme 9) with fluoride, measured as 5 x 10^9 M^{-1} in THF, was higher than that observed with any previously documented monofunctional borane receptor. Addition of $B(C_6H_5)_3$ permits conversion back to the unbound sensor, confirming reversible binding.[104] The visual cue to the binding event is the dissipation of the vivid yellow colour, recordable as a decreasing absorption at 340-390nm by UV spectroscopy.

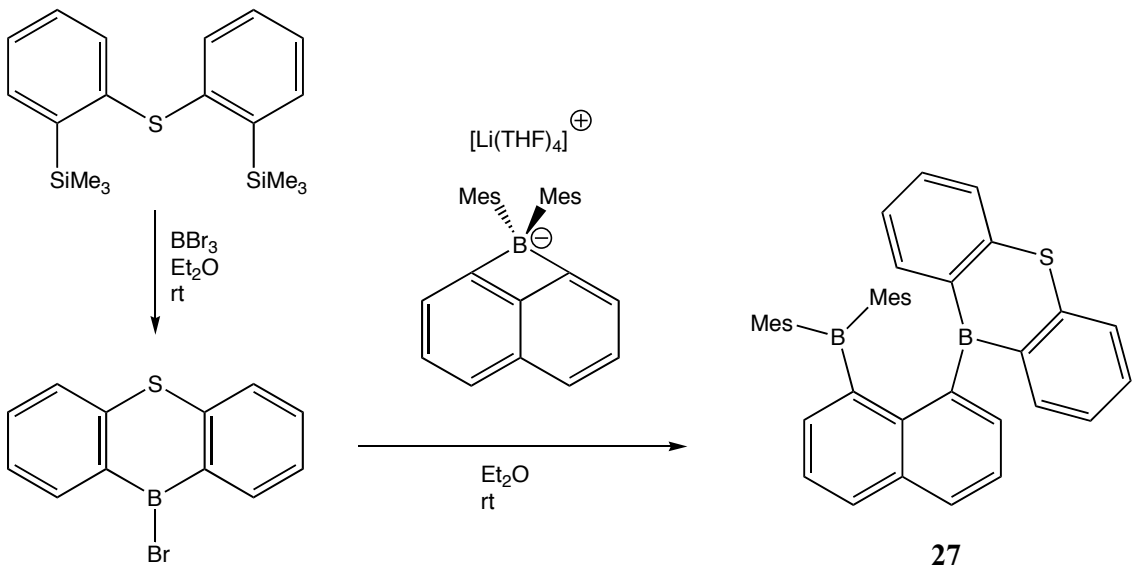

Scheme 9 Facile synthesis of Gabbaï's first bidentate system targeting fluoride.

The bridged fluoride species [**27**μ_2-F]$^-$ was successfully isolated and characterised, confirming the bidentate binding by shifts in the ^{11}B NMR, expected -188ppm ^{19}F NMR signal and X-ray analysis showed B-F bonds and pyramidal B centres.

Kubo *et al.* reported a novel sensor system in which anions induce self-organisation of 3-nitrophenylboronic acid and alizarin.[105] In the presence of fluoride or acetate ions, the two components bind, 'switching on' the fluorescence. In the absence of a strongly basic anion the reporter and receptor barely interact but once the boronic acid is converted into the phenylfluoroboronate the change from sp^2 to sp^3 and the increased electron density on the boron stabilises the ensemble **28** (pictured below in Figure 24). Obviously the system is not completely selective but successfully showed an interesting way to bring unbound components of a sensor together in the presence of a target analyte.

28

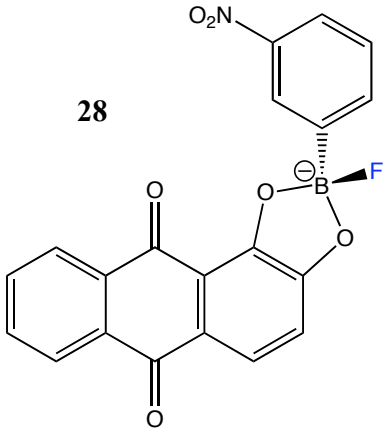

Figure 24 3-nitrophenylboronic acid and alizarin self-organise in the presence of various anions.

Another group, headed by Liu, reported a highly sensitive and selective sensor for fluoride based on an organic borane (**29**, Figure 25).[106] A colour change of bright green to colourless accompanies the fluorescence quenching on fluoride binding. The dimesityl tri-coordinated boron species showed interesting two-photon excited fluorescence (TPEF) and single-photon excited fluorescence (SPEF) activity on binding with fluoride. The trigonal planar boron is shown to be well shielded by the dimesityl groups, possibly increasing the selectivity towards fluoride ion due to its small size. TPEF chemosensors have been used in conjunction with laser scanning microscopy in the imaging of ions in cellular processes with greater 3D spatial selectivity then SPEF techniques.

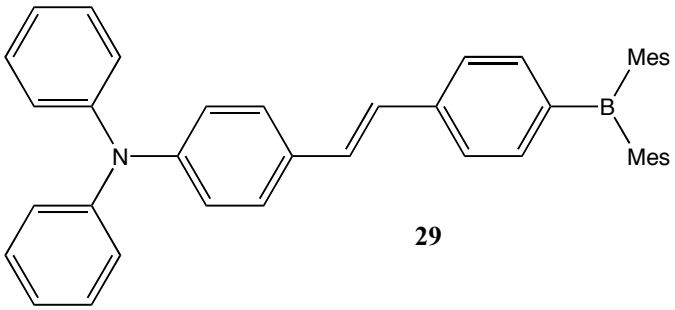

29

Figure 25 Fluoride sensor incorporating bulky mesityl substituents intended to increase fluoride selectivity.

Most monodentate boron based chemosensors show a fluorescence quenching on binding, termed 'switch-off' sensors. Practical applications however, would benefit from a 'switch-on' type response, particularly if accompanied by a visible colour change. The same group reported the synthesis of fluorescent sensors **30-31** virtue of some palladium catalysed organozinc couplings and observed fluorescent enhancement in the case of **30** in the presence of fluoride selectively over other halides in dichloromethane.[107]

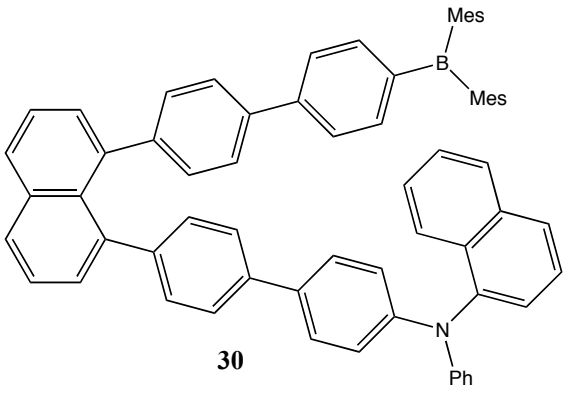

30

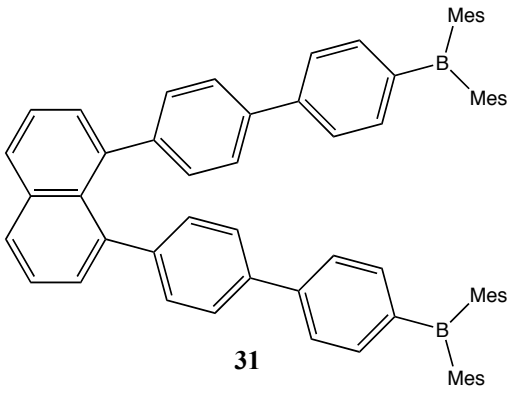

31

Figure 26 Two related molecules that serve as examples of a "switch on" fluorescence sensor **30** and a "switch off" fluorescence sensor **31** for fluoride.

Molecular modelling predicts that the two biphenyl 'arms' of compound **30** sit orthogonally to the naphthalene ring system, implying charge transfer through space from the 'donor' nitrogen to the dimesitylboron 'acceptor'. Compounds 4,4'-bis[(1-naphthyl)(phenyl)amino]biphenyl and 1,8-bis{4-[(1-naphthyl)(phenyl)amino]biphenyl-4'-yl}naphthalene, molecules closely related to the donor motif, exhibit a strong emission in the blue region of light. In solution, compound **31** emits in the green spectrum but on binding to fluoride the charge transfer is interrupted and a change to the

characteristic blue colour is observed. Compound **31** showed a typical fluorescence quenching behaviour, indicating the amine functionality and its interaction with the neighbouring boron centre was critical to the desired enhancement effect.

In perhaps the most compelling example of a fluoride sensor system to date, Gabbaï synthesised an impressively simple series of sensors that incorporated a charged phosphonium unit (see Figure 27) and a triarylborane. Binding constants were calculated at optimum pH (pH 4.6 to 4.9) in 9:1 H_2O-MeOH giving a maximum value of 10.5 x 10^3 M^{-1} for species **32d**.[108] The increased Lewis acidity required to overcome the large hydration enthalpy (504 $kJmol^{-1}$) of fluoride anion in water had been proposed by the authors to be provided by the Coulombic effect of the cationic substituent.[109]

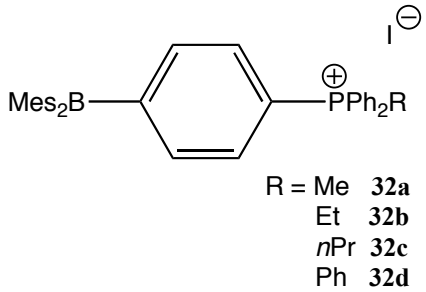

Figure 27 A cationic borane capable of sensing fluoride in 90% aqueous media.

Across the series **32a-d** it was found that as the hydrophobic character increases, there is a corresponding increase in the Lewis acidity of at the boron centre. To highlight the success of this body of work, compound **32d** is capable of binding fluoride in pure water at pH 4.9[108], at concentration levels below the US Environmental Protection Agency's recommended level for drinking water of 4 ppm.

1.6.1 Mixed or Assisted Lewis Acid Systems

Sensors containing boronic acids (or derivatives thereof) as binding sites have not been limited to bearing this type of binding moiety exclusively. Several groups have attempted to introduce different features in parallel to the boron centre to either complement the binding or to explore different methods of signalling the complexation event.

In parallel to their work intro neutral bisboron bidentate frameworks for anion sensing the Gabbaï laboratory have looked at mixed Lewis acid centres and charged receptors for fluoride, aimed at working in aqueous media. In 2005, Gabbaï developed a highly selective phosphorescent sensor **33** for fluoride anion similar to sensor **27** but containing a mercury centre.[2] Again, a μ_2-F^- bridged species (Scheme 10) was isolated and characterised fully be X-ray diffraction study. The distinct green solid state phosphorescence changed to red on binding. With a binding constant higher than that measurable by direct titration in THF ($K_a > 10^8$ M^{-1}) this system also showed, albeit reduced, respectable binding in partially aqueous media ($K_a = 3.3 \times 10^5$ M^{-1}). Even the highly competitive acetate anion showed no binding, possibly due to the propensity for acetate not to form a μ_2- bridging binding mode.

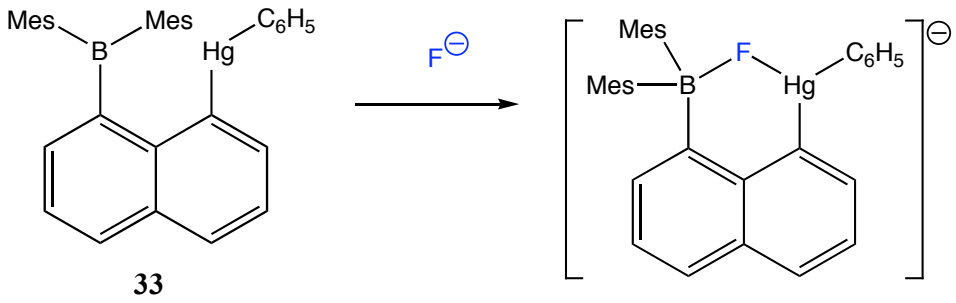

33

Scheme 10 Fluoride capture by a mixed Lewis acid system.

Phosphorescence is rarely utilised as an optical property for anion sensors in comparison to fluorescence. However, in this example, the authors took advantage of mercury's ability to induce phosphorescence of hydrocarbon chromophores *via* spin-orbit coupling at room temperature. These values are much higher in comparison to the Mes_3B species, adding to the cooperative binding argument. In a related communication the group outlined the synthesis of two very closely related cationic bidentate Lewis acids. This was done in an attempt to assess whether Coulombic attractions improved the binding constant. Stronger binding was indeed shown by the cationic version in partially aqueous - THF/H_2O (9:1) - media.[110] However, this system does suffer somewhat from a weak response to acetate ions, so some degree of selectivity is lost.

Continuing their exploration into Coulombic factors, in a significant receptor development they showed cationic borane **34** to capture fluoride ion across a phase barrier, extracting fluoride from water in a chloroform/water biphasic system.[111]

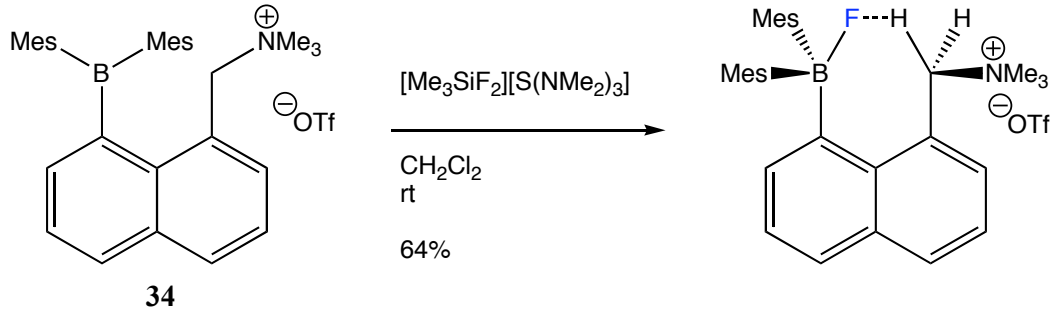

34

Scheme 11 Compound **34** combines Lewis acidic boron interaction with a neighbouring hydrogen bonding interaction to selectively extract fluoride across a biphasic barrier.

X-ray diffraction studies confirmed the presence of a C-H···F-B hydrogen bond arrangement contributing to the binding motif. A striking piece of evidence for this behaviour persisting in solution came from ^{1}H and ^{19}F NMR, paying particular attention to the diastereotopic methylene protons on the nitrogen-containing substituents. Regarding species **34**.F^{-}, one of the resonances showed coupling to the fluorine nucleus ($^{1}J_{H\text{-}F}$ = 9.2 Hz) and was resolved as a doublet of doublets ($^{2}J_{H\text{-}H}$ = 12.9 Hz).

One recent mixed Lewis acid system, looking at an area surprisingly neglected considering the obvious relationship to Katz's system, containing both boron and silicon centres in geometry favourable to encourage fluoride bridging, has been synthesized.[112] Katz showed the 1,8-naphthyl arrangement to be relatively weakly binding but **35a-b**, based on a *o*-phylene backbone, have shown stronger binding than the comparative monodentate boron analogues. Fluoride-bound species **35a-b** have been studied by X-ray crystallography and Si-F coupling in the ^{19}F NMR showed evidence of the silicon adopting a pseudo-pentacoordinate geometry and ^{11}B NMR indicated strong tetrahedral character. At time of writing this affinity for fluoride has not been utilised in making a useful chemosensor and competition studies with other anions have not been published.

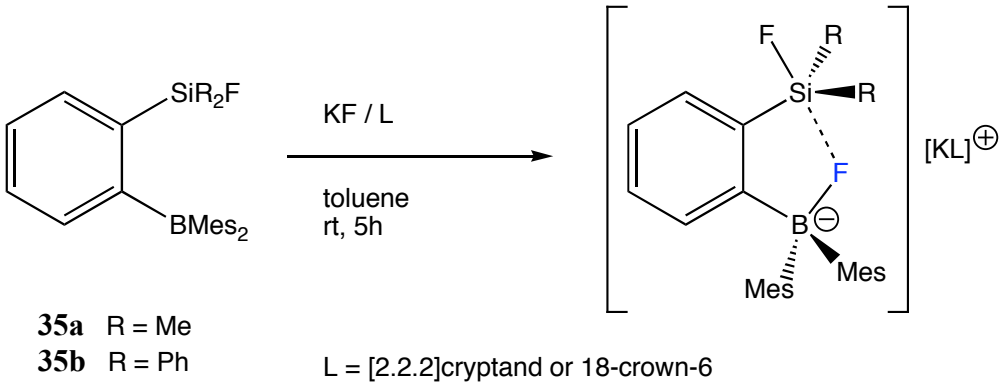

35a R = Me
35b R = Ph

L = [2.2.2]cryptand or 18-crown-6

Scheme 12 A mixed silicon-boron bidentate receptor for fluoride.

In 2009, James and Yoon collaborated in the design and synthesis of a bidentate receptor **36** for fluoride anions that employs a boronic acid site and an imidazolium group.[113] In a competitive aqueous solvent system (95:5 CH_3CN-HEPES) selectivity was achieved over challenging acetate and phosphate anions and a ratiomeric fluorescent response was observed. The orientation of the boronic acid group was critical, with only the *ortho* derivative (shown) showing selectivity, the *para* and *meta* derivatives failed to show comparative binding selectivity.

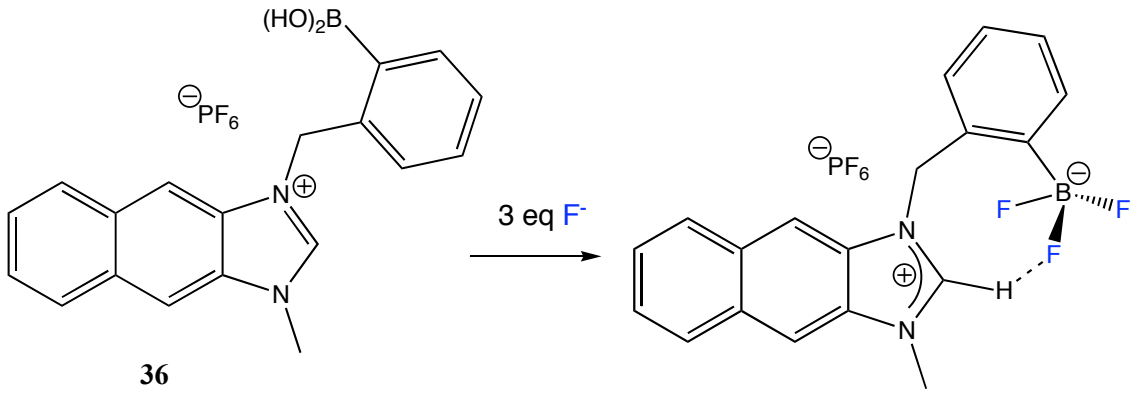

36

Scheme 13 A sensor that combines a boronic acid receptor with a CH-anion interaction.

The C-H hydrogen bond donor is proposed to stabilise the binding, allowing recognition to occur in the competitive media. ^{19}F NMR spectroscopy studies showed the hydrogen bonded fluorine was resolved from its neighbours.

1.6.3 Chemosensing *via* Hydrogen Bonding

A Lewis base-Lewis acid interaction is not the only possible means of binding halide ions. Binding solely through hydrogen bonding has been utilised in a large range of sensors, predominately N-H donor sites.

Sessler and Gale are two chemists who have contributed immensely to the field of anion receptor chemistry. Initial work into polypyrrole and similar N-H donor constructs as anion receptors came about in the late 1980s with highlights including calix[4]pyrroles[114], bipyrrole based [2]catenanes[115] and bridged pyrrolic ansa-ferrocenes[116]. However, it wasn't until 1999 that N-H donor molecules started to be reported as showing useful chemosensor behaviour.

Sessler first revealed dipyrrolylquinoxalines as a framework for anion sensing.[117] Although the group had previously reported many examples of anion recognition, they had lacked the ability to conveniently report the binding event. A range of analogues (**37**-**39**, Figure 28) are simple to access from pyrrole and various 1,2-diaminobenzenes. 2,3-dipyrrol-2`-ylquinoxaline **37** shows a dramatic colour change from yellow to dark purple in the presence of fluoride in dichloromethane and dimethylsulfoxide. A conformational change on fluoride recognition was proposed as perturbing the orbital overlap between the pyrrole and quinoxaline sub-units thus altering the optical properties of the species.

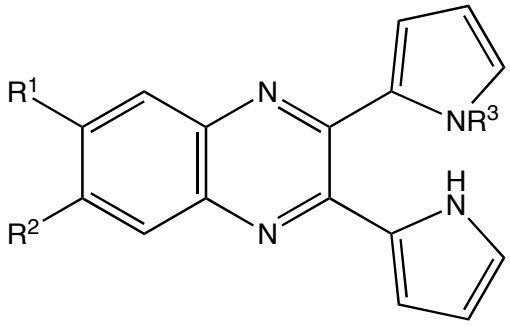

37 $R^1 = R^2 = R^3 = H$

38 $R^1 = R^3$; $R^2 = NO_2$

39 $R^1 = R^2$; $R^3 = SEM$

Figure 28 Pyrrole-based sensor for fluoride thought to change conformation in the presence of the target anion.

The performance of quinoxaline **38** relative to quinoxaline **37** is worthy of note. Introducing the electron withdrawing nitroso group enhances the hydrogen bond donor

character of the amine group and hence increases the fluoride binding constant by an entire order of magnitude. Phenanthroline complexes bearing fused dipyrrolylquinoxalines incorporating transition metal centres were an expansion of the work.[118] Although the UV response was complex, qualitative selectivity was achieved to an extent with a colour change from pale red-pink to purple. This was only observed in DMSO however, and addition of water reversed the change.

Gale collaborated with Sessler on utilising the calix[4]pyrrole system as a colorimetric sensor for fluoride. An early compound **40** involved the binding of a coloured species, 4-nitrophenolate **41** *via* the 4 N-H donor groups which, when bound, lost its characteristic colour in solution. Subsequent substitution by a target anion would then cause the solution to release the 4-nitrophenolate back into solution, giving a colorimetric response.[119] However, selectivity for fluoride over chloride, phosphate and even the much softer bromide ion was poor. The structural motif has been appended with various substituents in an attempt to increase binding constants, improve selectivity for either fluoride or phosphate and also to find a system that works in conditions approaching that of the physiological. Species **42** (Figure 29), incorporating a thiourea introduced at a designed distance from the primary binding site to provide an additional hydrogen bonding site, was the first system to bind anions strongly with water present at physiological pH.[120]

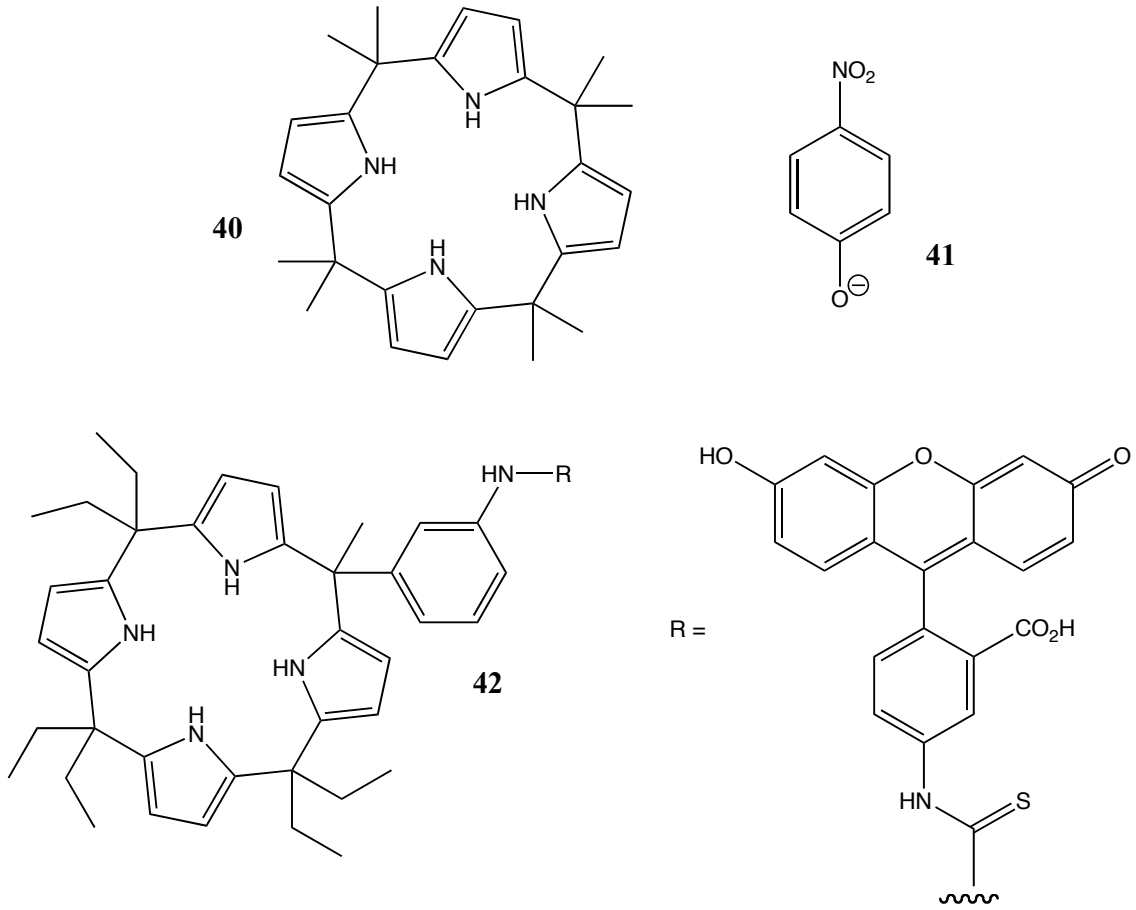

Figure 29 Anion binding behaviour of calixpyrroles is dependant on the substituents and the resulting cavity formed.

Sessler coined the term 'Off –the-Shelf' in reference to using commercially available, often classic dye molecules for achieving colorimetric responses to anions in DCM or DMSO media.[121] Selectivity was extremely limited, although 'acid blue 45' **43** showed a blue to colourless change in DMSO exclusively on addition of fluoride. DMSO, although water miscible, is a far from ideal solvent for any practical sensor system, due to its high boiling point and ability to penetrate skin.

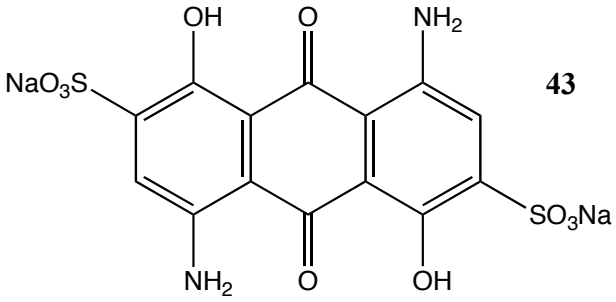

Figure 30 Acid Blue 45.

Improved selectivity for fluoride was achieved by Gale *et al.* who used a clever deep cavity molecular design strategy to devise calix[4]pyrrole **44**.[122, 123] However, only ^{1}H NMR techniques could be used to observe the recognition event and again solubility proved to be a problem, with studies undertaken in DMSO.

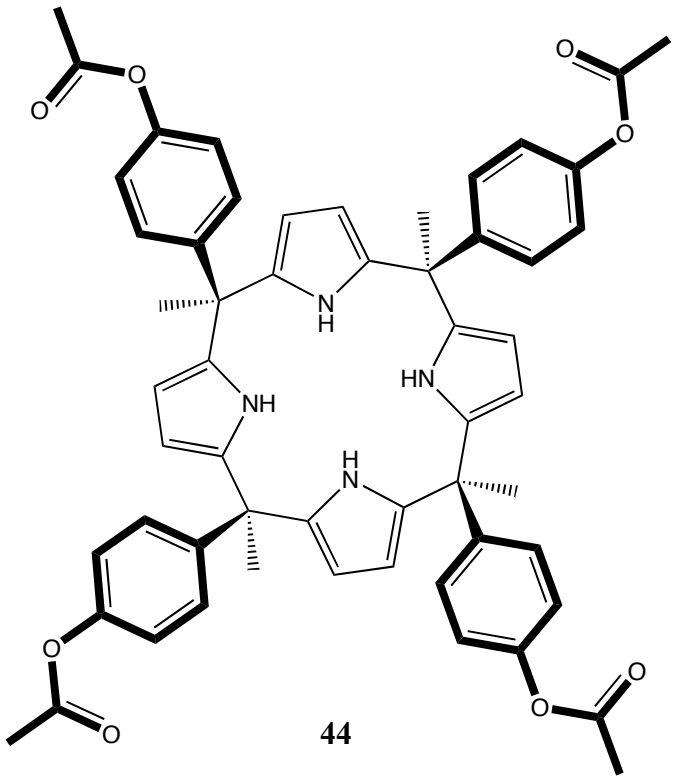

44

Figure 31 A deep cavity sensor designed to be selective for fluoride.

In one recent adaptation of the calix[4]pyrrole motif, Sessler incorporated a chromogenic dipyrrolylquinoxaline strap in **45** to show selective sensing of fluoride and phosphate and improved binding in comparison to a calix[4]pyrrole lacking the strapping unit. Strong colorimetric responses were observed for both fluoride and phosphate ions.[124]

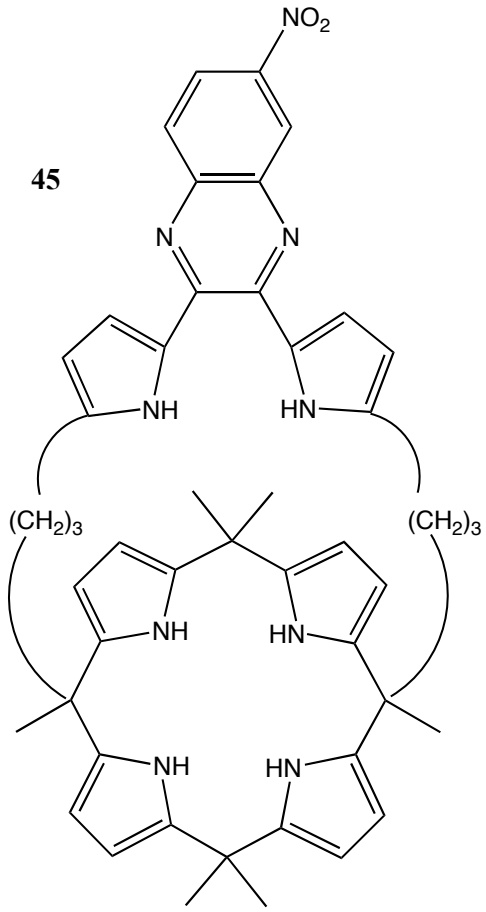

Figure 32 Strapped calix[4]pyrrole that binds anions in its cavity *via* hydrogen bonds and π-anion interactions.

Taking advantage of N-H hydrogen bonding donors has not been restricted to polypyrrole chemistry. An anthracene derivative **46** bearing two phenylurea groups at the 1,8-positions was proposed to act *via* a PET mechanism in acting as a chemosensor for fluoride (Scheme 16).[125] The anthracene acts simultaneously as a fluorophore and a template for creating a selectivity enhancing binding pocket. The binding constant for this species with fluoride was calculated as 71270 M^{-1} in 90:10 CH_3CN-DMSO, with selectivity over chloride 120:1.

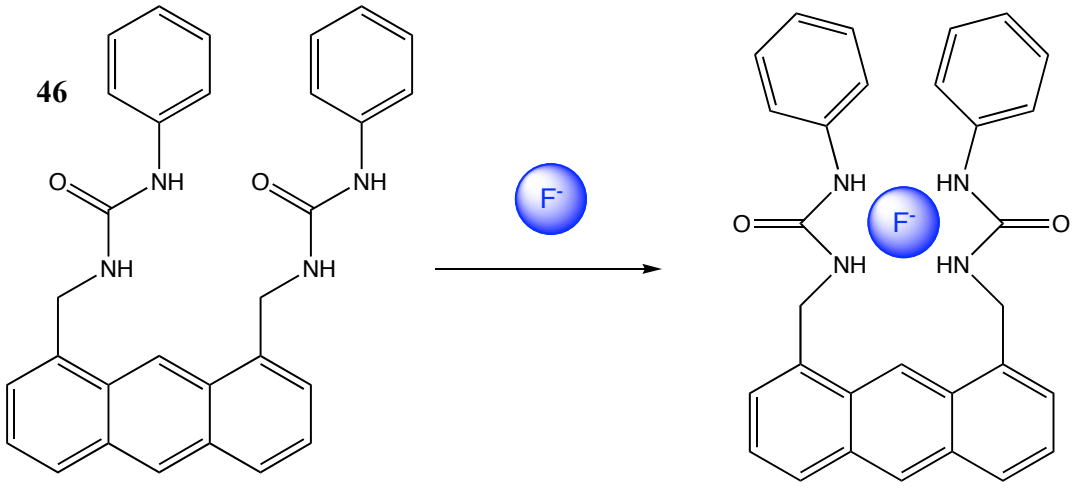

Scheme 14 Urea groups have been utilised in fluoride sensors.

This proposed scheme of binding (Scheme 14) is not the only possibility. The group proposed a PET mechanism, by which on excitation the anthracene effectively becomes the donor portion of a PET D-B-A arrangement. The acceptor in this case is the urea functionality. Once the NH protons are involved in hydrogen bonding, the energy of the acceptor system is raised, preventing charge separation. In fact, fluoride induced deprotonation may be occurring rather than the suggested hydrogen bonding complex. After deprotonation the nitrogen would possess a lone pair of electrons, becoming capable of acting as an electron donor and hence 'switching off' the fluorescence. The ^{1}H NMR spectra published in the article clearly indicate the disappearance of the urea protons in the presence of 2 equivalents of fluoride. The electron rich system is then capable of quenching the fluorescence emission by a PET mechanism.

Cho *et al.* have published closely related work in the synthesis of several fluorescent and chromogenic sensor compounds for fluoride ions based upon a naphthalene urea derivative.[126] A selective visible colour change (pale yellow to red) occurred on addition of TBAF in DMSO (Scheme 15), with compound **47** showing no red colour response in the presence of chloride, bromide, iodide, dihydrogen phosphate, hydrogen sulfate, acetate and benzoate ions.

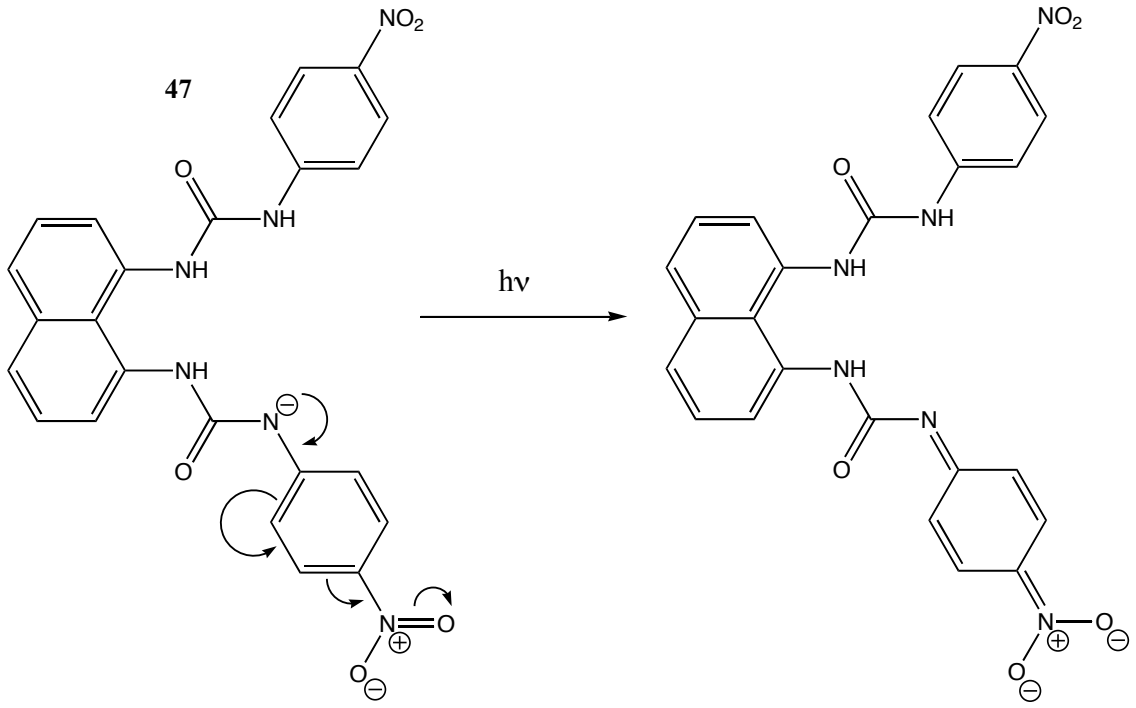

Scheme 15 Proposed charge transfer transition upon deprotonation in the presence of fluoride.

It was proposed that the colour change arose from charge-transfer between electron rich donor units and electron deficient *p*-nitrophenyl and azo phenol moieties. Fluoride binding increases the electron density of the system enhancing charge transfer. No fluorescence data is given in the report but deprotonation is directly mentioned, with a mechanism proposed for the generation of a charge separated species responsible for the observed red colour (absorbance peak in UV-Vis spectrum at 490 – 520 nm).

Curiel *et al.* detailed another novel example of a preorganised framework, in this case indolo[2, 3-a]carbazoles **48a-d** (Scheme 16).[127] Although selectivity for fluoride anion over phosphate was not achieved with a simple example, a crystal structure of a 1:1 complex with TBAC was reported, illustrating the ability to bind chloride by two N-H hydrogen bonds. Interestingly, it was possible to look at the fluoride binding in the solid state also, with an unusual 1:2 receptor-anion crystal structure involving two adjacent fluoride anions about which four bound indolocarbazole ligands display a helical nature with an almost square planar geometry at the fluoride centres.

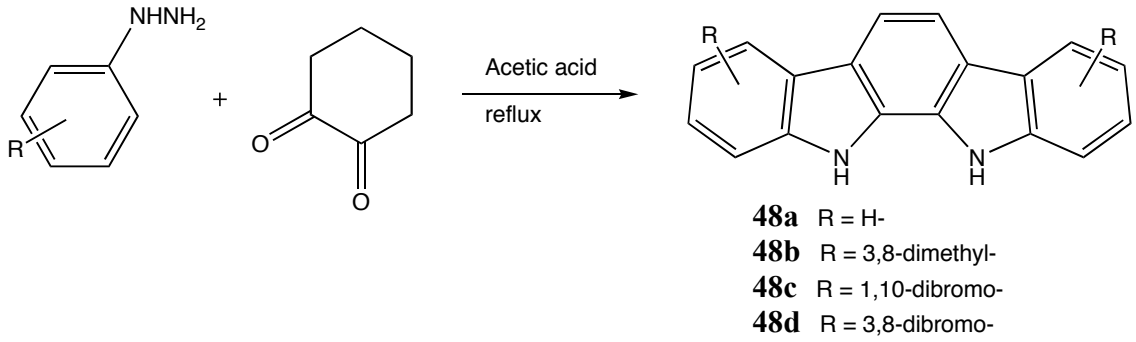

Scheme 16 A family of compounds capable of binding chloride *via* two NH hydrogen bonds.

Peng *et al.* showed (2005) it is possible to control the binding characteristics of NH hydrogen bond donor sensors by studying a family of ratiomeric fluorescence sensors for various anions.[128] Selectivity is not achieved to a desirable level but interesting insight is given into the binding behaviour of N-H hydrogen bond donors with fluoride. Compounds **49-51** (Figure 33) share characteristic intramolecular hydrogen bonding between the N-H of the imidazole ring and the carbonyl group on the neighbouring quinone.

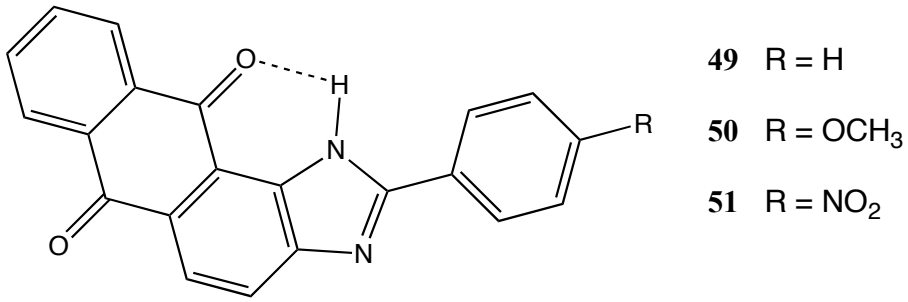

Figure 33 Controlling hydrogen bonding is possible by changing the *para* substituent.

The acidity of the NH proton is key to the strength and selectivity of binding and even the mechanism of sensing, be it by hydrogen bonding or complete fluoride induced deprotonation. In fact, compound **49** showed the best selectivity for fluoride over hydrogen phosphate and acetate, attributed to the complementarity of the NH.

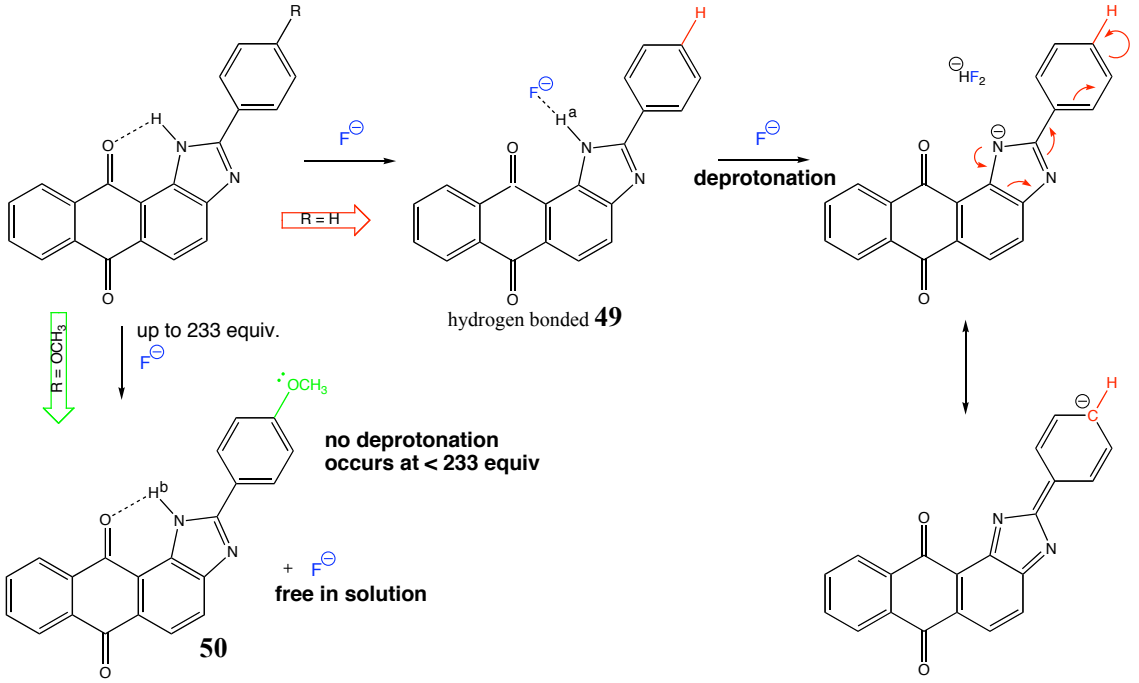

Figure 34 A diagram showing the response of **49** and **50** to fluoride ions (ignoring counter cations).

A resonance structure of the deprotonated form of **49** (R = H) (pictured in Figure 34) shows how the electron density of the phenyl *para* position is enhanced upon deprotonation. This indicates the potential for tuning the acidity of the NH donor by changing the *para* substituent. The authors synthesized **50** (*p*-OCH3 electron-donating substituent) and **51** (*p*-NO_2 electron-withdrawing substituent) to investigate the effect of electronic properties of *p*-substituents on fluoride selectivity. The UV-vis fluoride titration spectra of **50** exhibited stepwise changes. Firstly, the λ_{max} absorbance at 416 nm of **50** was barely affected until the addition of a very large amount (up to 233 molar equiv) of fluoride ions; this step corresponds to **50**-fluoride hydrogen-bond formation. Further addition of fluoride was required to generate the deprotonated species. Only addition of acetate resulted in similar stepwise response in the absorbance spectra. This shows that the introduction of the electron-donating group enhances the electron density of the imidazole ring and consequently increases the basicity of the hydrogen-bind donors, hence deactivating the sensor to deprotonation. The nitroso derivative **51** also experiences spectral changes (from 380 to 497 nm) upon interaction with fluoride. However, unlike **49** (R = H) and **50** (R = OCH_3) the fluoride spectra of **51** displayed a significant CT band with addition of only 1 equiv. of fluoride. This result indicates the strongly electron-withdrawing *p*-NO_2 substituent boosts charge delocalization upon

interaction with fluoride thus deprotonation is facile.

In 2008, an interesting study of the binding interactions of **52** was reported, in which it was observed that the more basic anions (F^-, OAc^-) caused a colour change of purple to dark purple but the less basic anions titred (Cl^-, Br^-) resulted in a yellow solution. This was reasoned as owing to the nature of the hydrogen bonding occurring at the same proton but binding to the sensor in a different tautomeric form. Proton NMR and UV-vis spectroscopic evidence was used to elucidate what was occurring. Based on previous observations of the tautomerism by Kaupp, an absorption band at 370 nm can be assigned to the hydrazone tautomer and the band centred at 545 nm is characteristic of the azo form. NMR analysis revealed that the NH resonance of the hydrazone disappears in the presence of fluoride and the OH peak (azo signature) is shifted significantly upfield indicative of hydrogen bonding occurring. However, in the presence of chloride anions, the NH peak remained clearly visible, in fact showing a downfield shift indicative of hydrogen bonding.[129, 130]

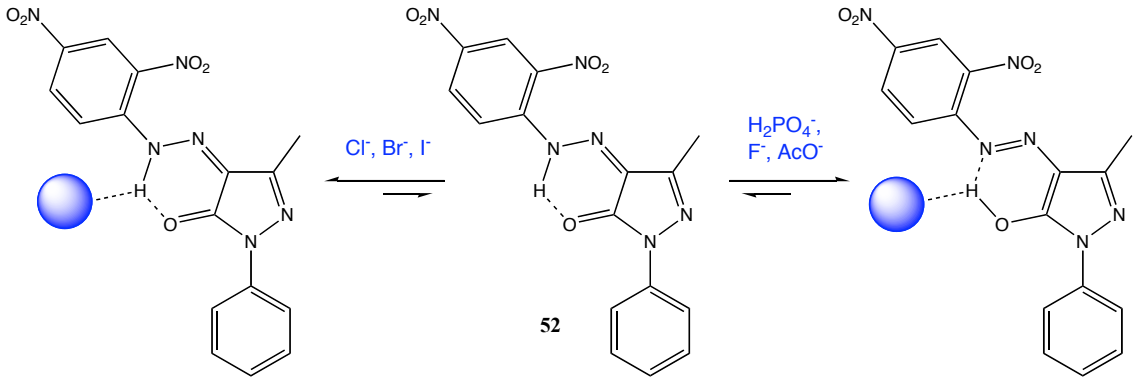

Scheme 17 Alternative tautomers of **52** are prevalent in the presence of different anions (depicted as a blue sphere).

Calixarenes offer great potential as sensory frameworks, providing a preorganised backbone with upper and lower rims available for modification aimed at creating one or two binding cavities. Diamond *et al.* reported the synthesis of tetrasubstituted calix[4]arene **53** (Scheme 18), which exists in a 1,3-alternate conformation.[131] Employing a pyrene excimer/monomer system, the ratio of two fluorescence emissions measurements is used to quantify binding. Remarkably, the excimer system was only interrupted to any extent by chloride anions in 95:5 acetonitrile/chloroform. The urea

protons were shifted downfield in the presence of 300 equiv. of chloride but fluoride induced no change in the triplet resonances.

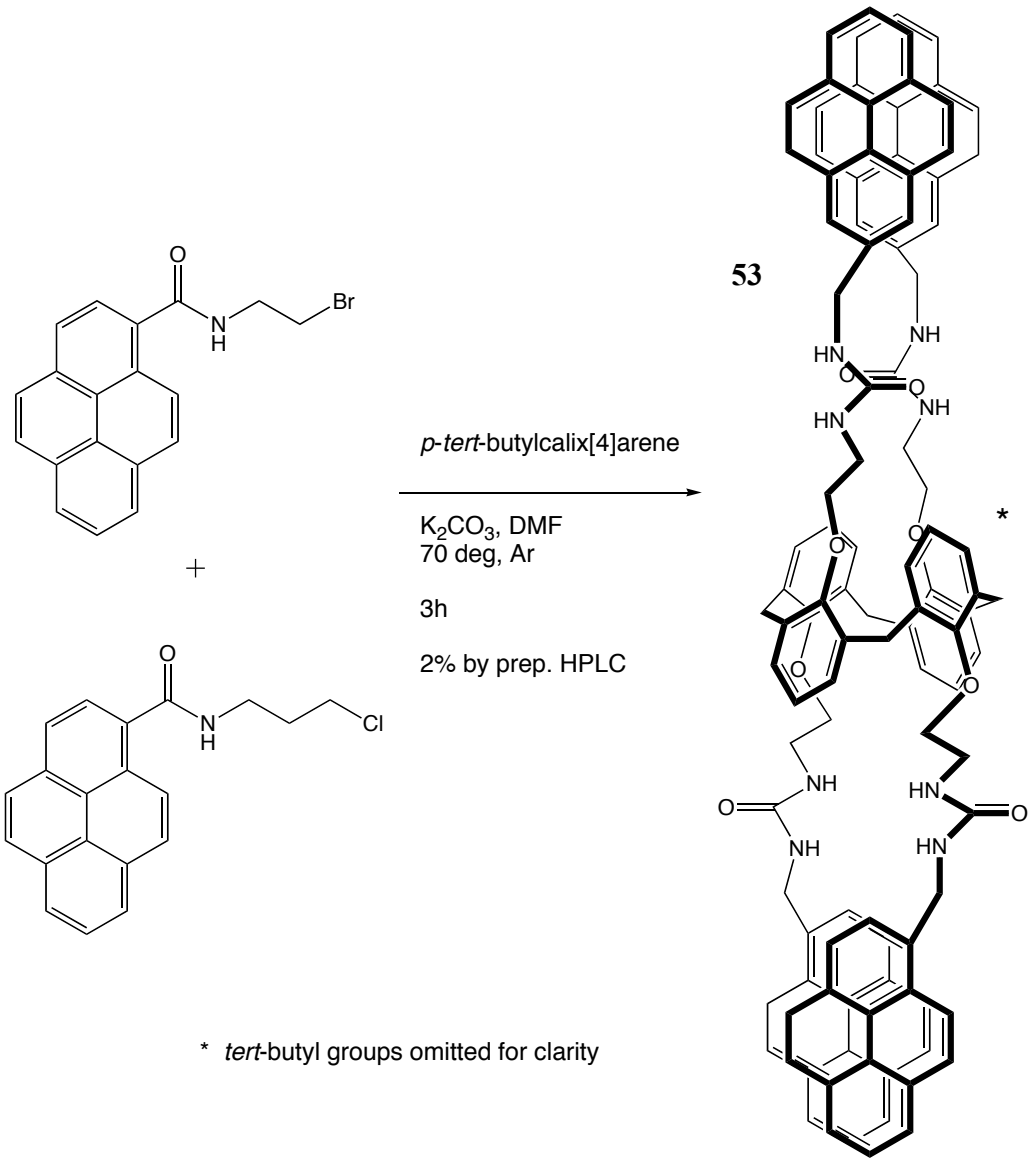

Scheme 18 Synthesis of a calixarene sensor **53** selective for chloride ions.

In 2008, Flood *et al*. reported the anion binding behaviour of a triazolophane **54**, a molecule that exploited only C-H···Cl^- hydrogen bonding interactions to selectively bind chloride over fluoride in dichloromethane solution.[132] Composed of four 1,2,3-triazole rings, the system is designed to be preorganised for anion recognition with CH groups orientated in a pseudo-planar arrangement directed towards the centre of the central cavity. These features - coupled with the complementary size of the cavity - engineer the impressive selectivity for chloride anions.

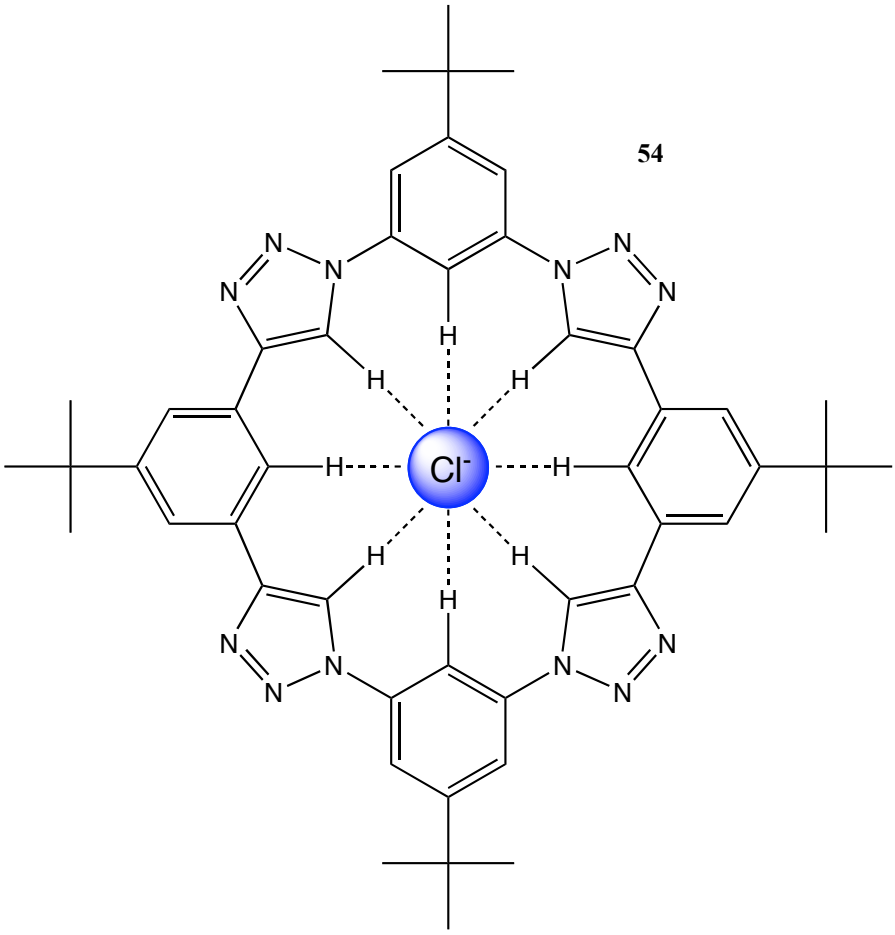

Figure 35 A sketch of compound **54**, showing the position of a bound chloride anion, and the unusual CH-anion hydrogen bonding array.

A later publication by the same author highlighted the high binding affinity of **54** and similar compounds to chloride (11 x 10^6 M^{-1}) but also showed bromide was captured to a large degree (7.5 x 10^6 M^{-1}).[133] The hydrogen bonding was also studied in further detail, highlighting the secondary but significant role of the hydrogens on the phenylene linker and that altering the electron donating properties of groups on the phenylene linkers dictated the anion binding capabilities. Recently, the group have shown that the hydrogen-bonding properties of CH groups are comparable to pyrrolic NH groups, and suggest the concept of CH hydrogen bonds being weak may be flawed.[134]

An interesting recent example employs a platinum metal centre; not as an anion binding site, but to induce structural pre-organisation by locking the conformation of **55** in the system **56**.[135] This is found to increase anion binding affinities, with the most dramatic improvement being displayed for phosphate, which showed a 40-fold increase in binding constant when the compound was bound to the metal centre.

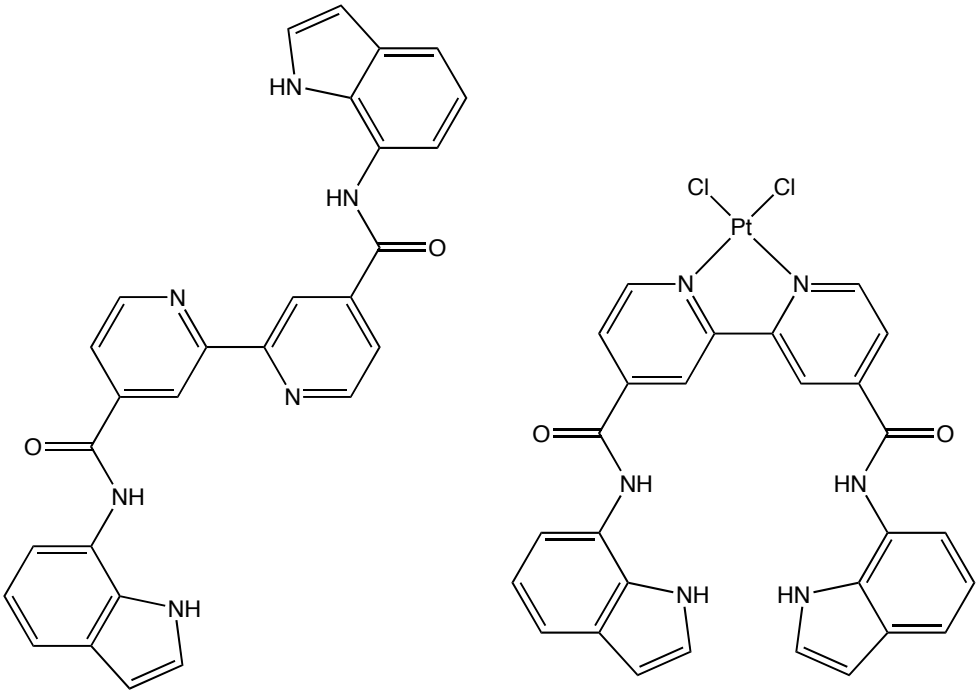

Figure 36 Fluoride sensor **56** is formed *via* coordination of a platinum centre to lock the conformation of **55** by the addition of a simple platinum salt.

An unusual method of discrimination between fluoride and the other halides and nitrate and acetate anions has been reported by Arunachalam *et al.*[136] Triamide **57** binds to all the anions studied but a dimeric capsule only forms in the presence of fluoride. X-ray diffraction data revealed that in fact, two fluoride anions reside in the centre of the capsule, accompanied by six water molecules, in an arrangement depicted in Figure 37 below.

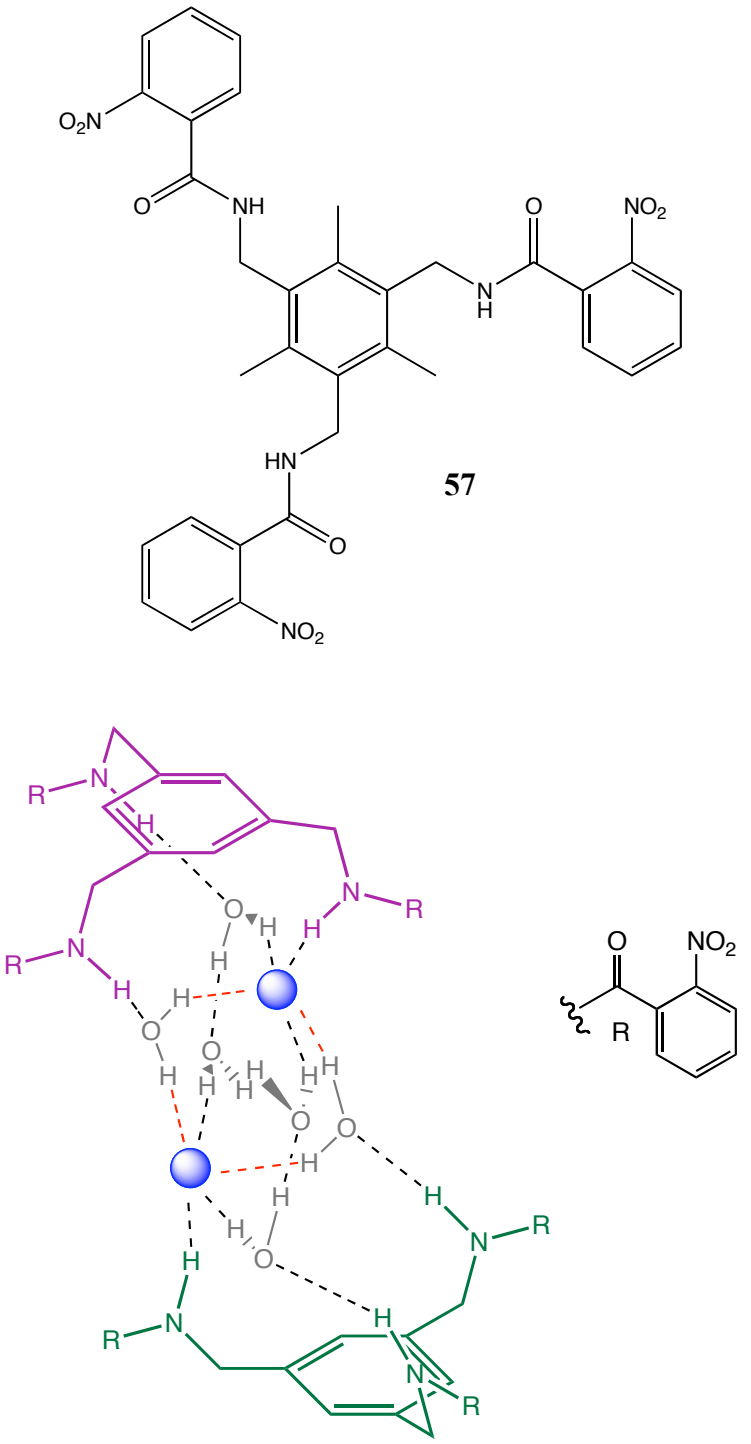

Figure 37 Tripodal receptor **57** (top) encapsulates two fluoride anions (depicted as blue spheres) in a dimeric capsule as shown (bottom – note methyl groups have been omitted for clarity).

1.6.5 Other Sensors for Anions

Beer has been a pioneer of research into the design and synthesis of inorganic anion recognition since he introduced a new class of polycobalticinium macrocyclic receptor molecules.[137]. Beer showed bipyridinyls bind to chloride anion in solution as early as

1992[138] but typically earlier work focussed on binding and not reporting the binding event. However, electrochemical readout was possible for compound **58**-**60** (Figure 38) and they were found to be phosphate (dihydrogen phosphate, $H_2PO_4^-$) selective even in the presence of a ten-fold excess of chloride and sulphate ions.[139] The cathodic shift relative to the ferrocene/ferricinium redox couple (270 mV) was 100 mV in the presence of phosphate alone and < 5 mV in the presence of chloride.

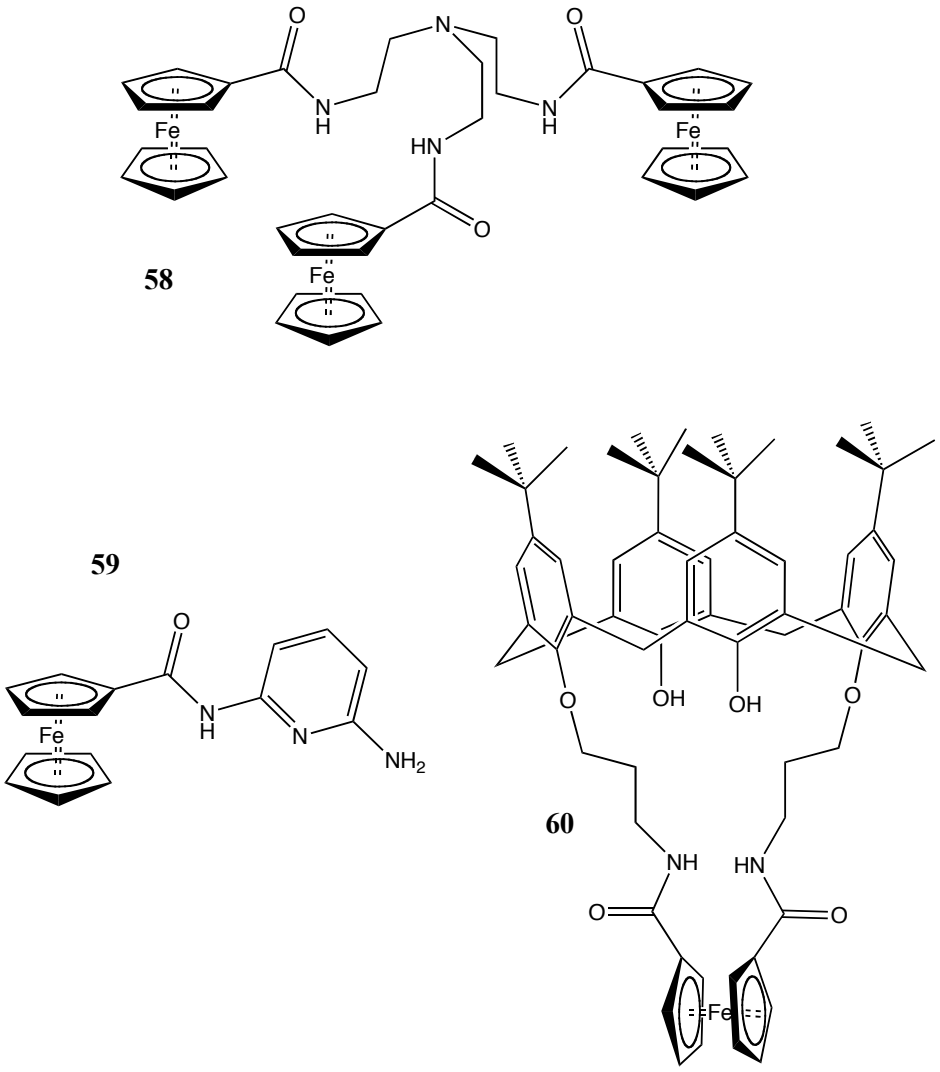

Figure 38 Anion sensors incorporating ferrocenyl units reported by Beer *et al*.

In comparison, Beer also used a ruthenium based system that showed remarkable selectivity for chloride over phosphate ions (Figure 39).[140]

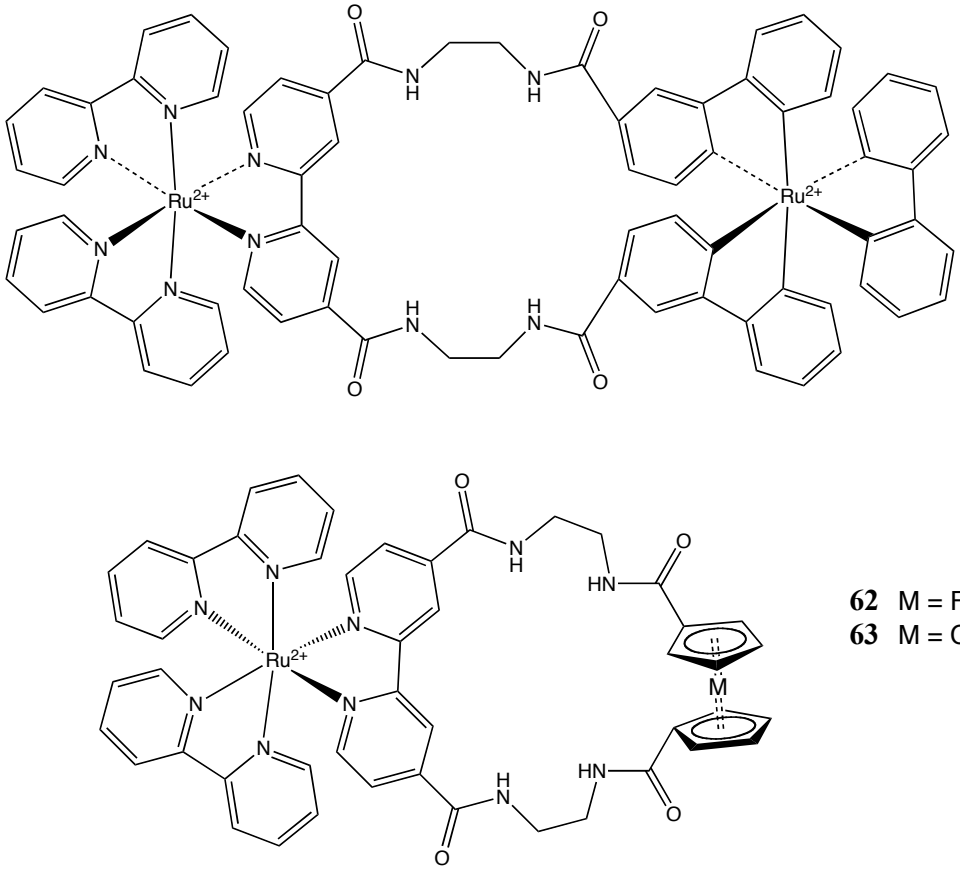

Figure 39 Ruthenium based sensors show some anion selectivity.

The respective rigidity of **61-63** is thought to be responsible for this selectivity, with rearrangement to accommodate the tetrahedral phosphate ion energetically unfavourable. Additionally, fluorescence quenching was observed in the presence of chloride over phosphate selectively. No results for fluoride were shown, or are indeed shown in the vast majority of publications discussing chloride or phosphate sensors, presumably on the basis that fluoride is typically rarely present in their target physiological environments. However, it seems likely that fluoride and also potentially acetate would have an impact on these systems. The Ru(II) system has also been appended to a calix[4]arene that was shown to bind anions.[141]

Hong and Kim reported a chromogenic and fluorescent chemodosimeter **64** that operates in aqueous (50:50 acetonitrile/water) media.[142] A chemodosimeter has the significant disadvantage compared to a chemosensor in that the binding event incurs a

irreversible chemical change on the receptor system. A likely mechanism behind the fluorescence enhancement caused by fluoride is shown in Scheme 19. The resorufin anion **65** is released into the solution and this species is responsible for the emission recorded, confirmed by examining the absorption spectra of the sodium salt of resorufin. An accompanying colour change from pale yellow to bright pink is observed.

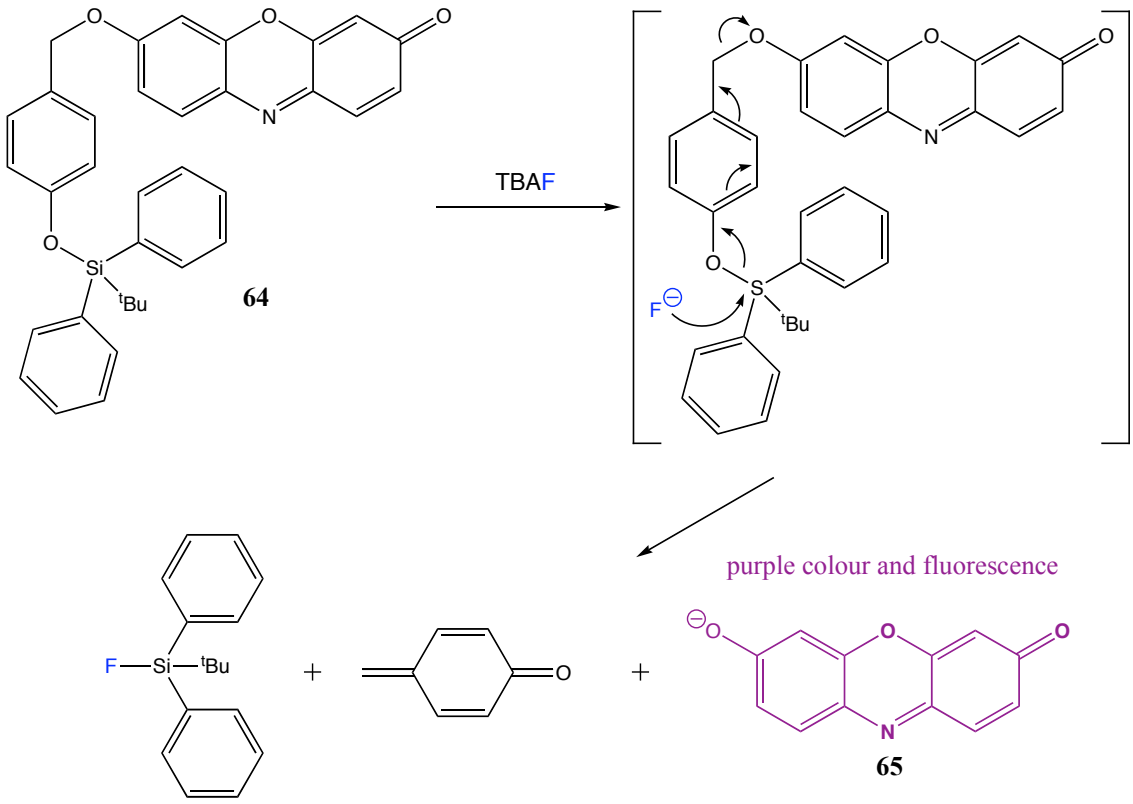

Scheme 19 Response of chemodosimeter **64** to fluoride ion in solution.

A group in China have reported another example of a chemodosimeter.[143] The boron in the axially substituted subphthalocyanine (SubPc) **66** favourably interacts with the fluoride ion to give a dramatic chromogenic change (Scheme 20). However, at lower concentrations of fluoride the sample can require 6 hours to fully bleach and an immediate response would be preferable.

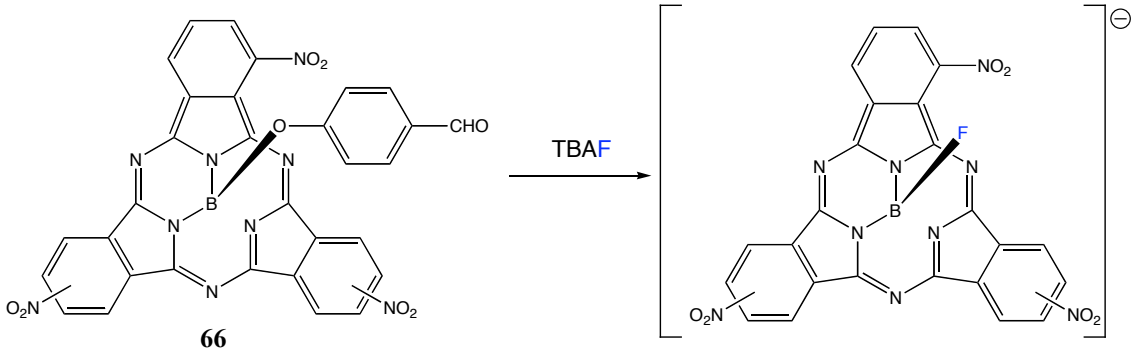

66

Scheme 20 Chemodosimeter **66** containing a boron centre.

Mascal has showed the use of a fluoride selective, specifically designed macrocyclic host that simultaneously utilises hydrogen bonding, anion-pi interactions and ion pairing (Figure 40).[144] A protonated form of cylindrophane **67** binds fluoride in an inclusion complex H_3**67**.F^{2+}, a finding confirmed by X-ray diffraction, with π-F^-···π distances of 2.68 and 2.69 Å and $^+$NH···F^- distances of 2.79 and 2.80 Å. This correlates well with the comparative distances in comparison compounds trimethylcyanuric acid-halide sandwich and tris(trimethylammonium)-halide complexes.

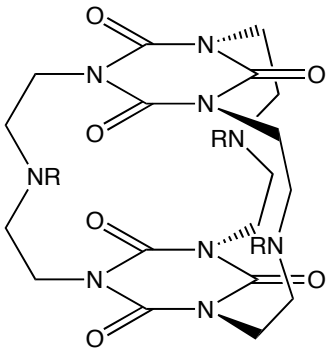

67

Figure 40 Cylindrophane **67**.

Oton and co-workers successfully combined electrochemical and fluorescence signalling in the design of a range of ferrocene-naphthalene dyads selective for fluoride (see Figure 41).[145, 146] In an elegant design, any binding events at the NH donor positions affects the electronic properties of the redox active component and the pi-electron rich naphthyl system. Molecules **68** and **69** are particularly noteworthy in that they contain 1,8-diaminonaphthyl units (see Chapter 3). Sensor **68** shows excellent selectivity against dihydrogen phosphate. In DMF, a dramatic enhancement in the

fluorescence emission was observed and a large cathodic shift from E = -0.270 V vs Fe/Fe^+ to -0.460 V vs Fe/Fe^+ was seen in the ferrocene oxidation wave.

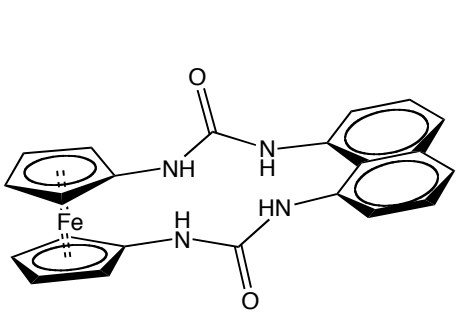

68

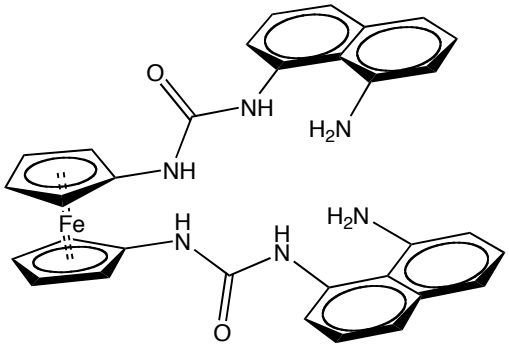

69

Figure 41 The development of sensors **68** and **69** combined electrochemical and fluorescent detection methods.

Calculated structures based on energy minimisation estimate all 4 NHs of **68** are involved in fluoride binding in an asymmetric fashion as **68**.$2F^-$. No ^1H NMR data is given in the publication to support this proposed binding.

There is some precedent for fluoride sensors that use silicon exclusively as the Lewis acidic binding site. One particularly impressive example, pictured in Scheme 21, showed a large enhancement in fluorescence emission on hypercoordination of the silicon centre .[147] The electronic changes at the silicon centre of **70** were proposed to be less important than the through-space interaction of the anthracyl units as the geometry changes from tetrahedral to trigonal bipyramidal. This was backed up by negligible change in the quantum yield. This is a rare example of a genuine 'switch on' fluorescence sensor and no spectral changes are observed with other halides. However, hydroxide evidently competes with fluoride at the Lewis acid site, as washing with water reverses the fluorescence enhancement.

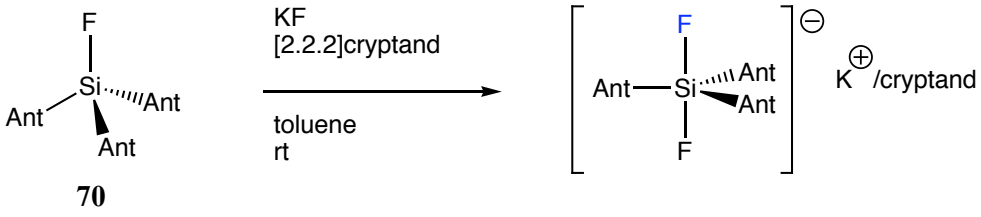

Scheme 21 A silicon based Lewis acid sensor for fluoride.

Callan and co-workers were the first to report the use of Quantum Dots as the fluorophore in a classic PET sensor system.[148] Employing CdSe-ZnS quantum dots and functionalising their surface with a simple thiourea, they were able to show that it is possible to utilise the beneficial properties of quantum dots, namely narrow emission and resistance to photobleaching in synthetic anion receptors.

Although the selective detection of biologically important anions such as ATP is still a challenging prospect, new insight has been garnered by the researchers at the University of Firenze in Italy.[149] They successfully showed the phenanthroline-based polyammonium receptor **71** binds ATP in the presence of a number of nucleotides. Hydrogen bonding interactions combined with π stacking of the phenanthroline unit. Although over a limited pH range (pH 4.5 - 7), this shows the potential for selectively binding more complex anionic species of biological importance.

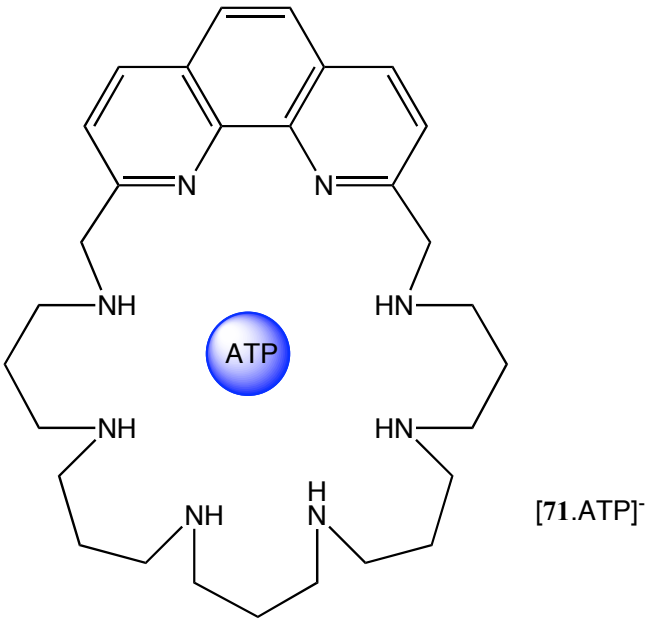

Figure 42 Receptor **71** selectively binds ATP over CTP, GTP and TTP

1.6.1 Non-Solution Based Anion Sensors

An approach to greater sensitivity in fluorescence detection schemes is to use the exciton-transporting properties of semiconducting polymers to amplify perturbations (transduction events) produced by analyte binding. These methods were originally demonstrated using electron-transfer quenching[150] and variations on this scheme have been used to create a number of chemical and biological sensory methods, most of which involve changes in the emission intensities.[151-153]

Binding a chemosensor to a surface is very desirable, as it would allow that sensor to be potentially be used for a wider range of practical applications, like in-*situ* monitoring or built-in sensors which are only triggered at a certain concentration threshold. A thin polymeric film has been doped with a highly selective optical fluoride sensor based on aluminium (III) octaethylporphyrin and shows very encouraging results[154], with selectivities rivalling the current established electrode methods described previously in the chapter. The film operates in a concentration range suitable for monitoring fluoride concentration in drinking water. Although good selectivity is observed with respect to chloride, sulfate, nitrite and bromide, a low pH buffer must be used to avoid interference from hydroxide ions.

An alternative to polymeric systems are modified electrodes for anion detection. A ferrocene-substituted calix[4]pyrrole has been shown to recognise various anions in aqueous media using a carbon paste electrode.[155] Selectivity is not achieved but the advantage of this type of electrochemically-active receptor is that the redox signal can be used as an internal readout. Umezawa *et al.* highlighted that the difference in selectivity of ion selective electrodes and ion-channel mimetic sensors suggests that the total dehydration of anions is not necessary for detection. This highlights this method of immobilisation as highly desirable for the sensing of very hydrophilic (eg fluoride, chloride) or highly charged anions.[156]

Nicolas *et al.* published a fluoride-sensing electroactive polymer film (based on **72** as a monomeric dopant at 0.20 – 0.30 in polypyrrole) based on the anodic oxidation of a boronate-substituted pyrrole in the presence of fluoride anions in an acetonitrile-water system.[157] Other polymer based anion recognition systems have been published[158, 159]

but the utilisation of a boron centre is more relevant to the body of work outlined in this thesis. A non-functionalised polymer film showed no change in the voltammetric response upon the addition of fluoride anions. The sensitivity to fluoride was found to be higher for thin films, a finding already observed for other sensory materials.[160, 161]

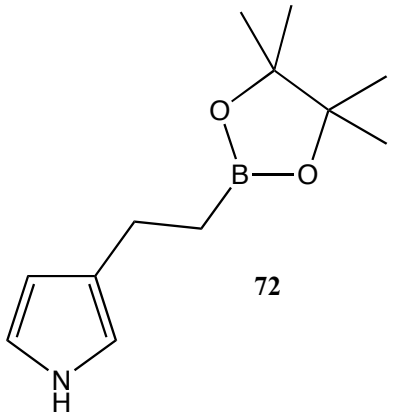

72

Figure 43 Boron functionalised monomer in polymer coated electrochemical fluoride sensor.

Kim & Swager[162] used a semiconducting organic polymer (monomeric unit **73** shown in Figure 44) to amplify the response of the bound fluorescent chemosensor unit to the fluoride binding event. Unusually, the change was not merely a modification of the existing peak intensity but the emergence of a new peak at a different wavelength. If a fluorescence sensory signal involves a new emission at a different wavelength rather than a modulation of an existing signal it is inherently easier to detect than an intensity change. Furthermore, non-specific chemical interactions are more likely to produce intensity changes than new signals, hence specificity gains are possible in properly designed sensors that create new emissions. In addition, this is a useful characteristic for a practically useful sensor, particularly if the shift is bathochromic (to a longer wavelength) as potentially, at higher wavelengths, the autofluorescence of blood can be avoided.

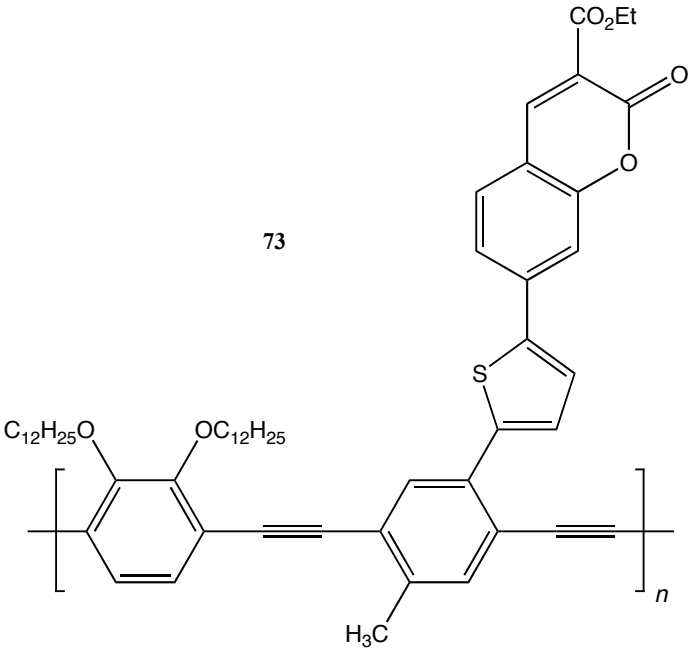

73

Figure 44 Monomeric unit of a self-amplifying polymer that detects fluoride.

1.7 Summary

Anion recognition chemistry is a recent and rapidly developing area of chemistry that is varied in its approach to a challenging analyte. With a particular focus on the small halide ions, this chapter has described why anion recognition and sensing is important and detailed several biological and abiological examples.

Chemosensors employ several types of intermolecular interactions in anion chelation, with some examples attempting to take advantage of multiple attractive forces. Lewis acid-Lewis base interactions, in particular boronic acids and triaryl boron have shown great success but other Lewis acid centres have found some use.

Neutral sensors that operate *via* hydrogen bonding interactions, mostly NH donors and more recently a few compelling examples of CH donors, have perhaps received the most attention. Fluoride-induced deprotonation is a process to consider in sensor design.

A variety of analytical techniques have been employed by chemists to monitor the binding event, including CD spectrometry, electrochemistry, UV-vis and NMR. However, fluorescence spectroscopy remains the most widely used because of its high

sensitivity, potential for *in vivo* monitoring and the simplicity of the method. Enhancements in fluorescence emission on binding is thought to be more desirable than a quenching effect, which may be caused by a range of stimuli. Ratiomeric responses about a single isoemissive wavelength are desirable and also, due to the autofluorescence of blood, higher wavelength emitting sensors have been targeted.

Receptors with more than one binding site have repeatedly shown themselves to be attractive in increasing binding constants and multipoint binding is often essential to the mode of signalling. Preorganised sensing frameworks are often used to induce selectivity and to increase the strength of binding.

Although some inroads into working in fully aqueous or physiological pH media have been made but an 'ideal' system has not been disclosed to date.

2 RESULTS AND DISCUSSION I

Phenyl Boronates as Optical Halide Sensors and Synthetic Investigations into Related Luminescent Macrocycles.

2.1 Overview of R&D I

Following our initial communication showing simple boronic acids and their derivatives to be capable of acting as fluorescent and electrochemical fluoride sensors[35] we have focussed primarily on the molecular design of novel saccharide sensors, in particular the use of two boronic acid units to achieve selectivity for *D*-glucose. Sensors for fluoride incorporating two boron centres have recently received a lot of attention in the literature and we decided to look at applying our knowledge in seeking anion selective species.

The main challenge in halide recognition (indeed in all recognition science) is selectivity. Selectivity for chloride is extremely rare and for the even softer bromide there are no examples at the time of writing. Small, hard, strongly Lewis basic hydroxide competes with fluoride in most, if not all sensor systems. One way to get around this may be searching for different modes of sensor action. Conformational changes or reorganisation only in favourable binding situations is a concept already employed in a limited number of sensor systems for anions.[117] This type of molecular reorganisation on binding may also provide insight into anion templated synthesis or anion operated molecular devices in the future. This chapter outlines the design and synthesis of molecules intended to examine an interesting structural sensor model. The anion binding properties of these molecules will be looked at in a variety of ways in an attempt to assess their potential as anion sensors.

2.2 Synthetic Scope of Boronic Acid Derivatives

2.2.1 Boronic acid synthesis

Boronic acids - either in the free form or as cyclic esters - can be synthesised in a myriad of ways, typically starting from alkyl or aryl halides, although a large range of

substrates - such as alkenes[163] and alkynes[164] - have been shown to be suitable parents for preparing boronic acid derivatives. More relevant to this body of work are the aryl compounds, for which preparation *via* lithiation or formation of a Grignard reagent[165] is common. The aryllithium or arylmagnesiumhalide species is trapped with an electrophilic trialkoxyborate and hydrolysed at low pH to liberate the free boronic acid. More recently, palladium catalysed reactions using pinacol diborane have been widely utilised to access a wider range of boronic acid derivatives.[166, 167]

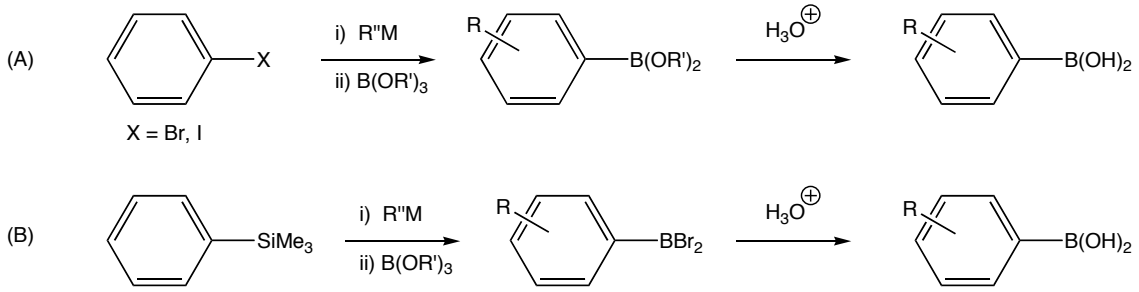

Scheme 22 Scheme showing two common methods of boronic acid synthesis; electrophilic trapping of an arylmetal intermediate with borates (A) and transmetallation of aryl silanes (B).

Boronic acids can also be prepared by transmetallation of arylsilanes with boron tribromide - typically in chlorinated solvent - and subsequent hydrolysis.[168, 169] There is a huge variety of methods used to access alkenyl boronic acid derivatives and other non-aromatic boron-containing species; for a more detailed review, see the comprehensive book entitled Boronic Acids.[170]

2.2.2 Boronic Acids and Diols

Although diol-boronic acid interactions are used more extensively in a different field of chemosensing (saccharides), their reversible reactivity is integral to protecting group strategy critical in almost all syntheses involving boronic acids. Depending on the solvent, boronic acids are able to dimerise or trimerise to form boronic anhydrides, interfering with reactivity and analysis. Polar protic solvents tend to inhibit this formation.

The formation of a cyclic boronate ring has a large impact on the hybridisation at the boron centre. The free boronic acid adopts a trigonal planar, sp^2 hybridised, geometry

(with a bond angle of 120°). When the boronic acid condenses with a 1,2- diol the bond angle reduces to approximately 113° which is closer to the ideal bond angle of 109° for sp^3 hybridised systems.

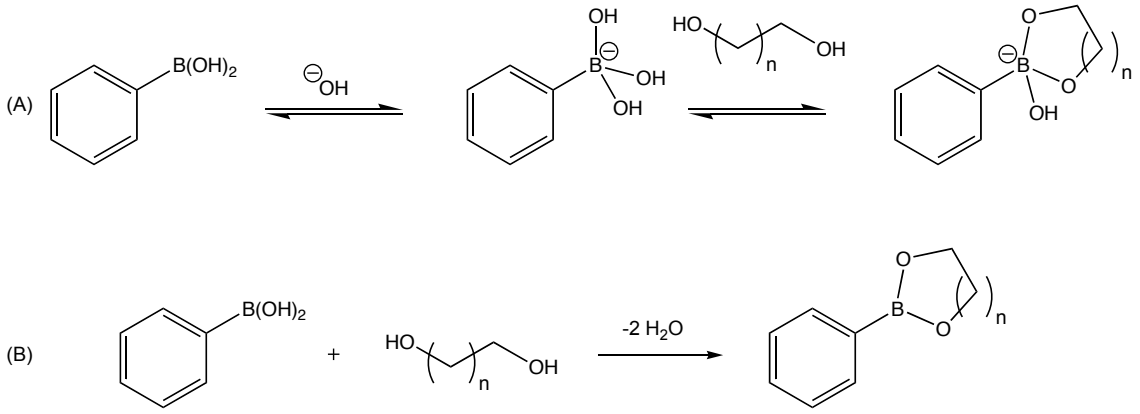

Scheme 23 Reversible formation of cyclic boronates in basic aqueous media (A) and irreversible formation in aprotic solvent (B).

Addition of a diol also increases the Lewis acidity of the boron atom. This change in acidity is often ascribed to the contraction of the oxygen-boron-oxygen (O-B-O) bond angle on complexation. Thus controlling the geometry around the boron centre through diol condensation can assist addition of a nucleophile such as a water molecule.

Typical diols used to protect boronic acids include 1,3-propanediol **74**, 2,2'-dimethylpropanediol (neopentyl glycol) **75**, 1,2-dihydroxybenzene **76** (catechol) and 1,1'-dimethyl-2,2'dimethylethane-1,2-diol **77** (pinacol).

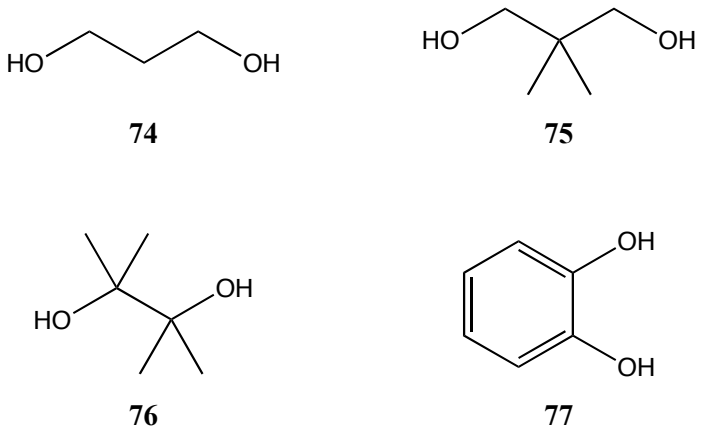

Figure 45 Some common protecting groups for boronic acids.

In most protocols reported herein, neopentyl glycol **75** is used because it remains intact under most reaction conditions encountered and yet can be easily removed by using silica gel column chromatography. The two signature ^{1}H NMR singlets also aid characterisation. Pinacol **77**, being more strongly binding, is used when operating under harsher reaction conditions.

Mesityl boron

Mesityl groups in di- or tri-aryl boron species are often implemented in fluoride sensor chemistry due to their extra steric bulk compared to phenyl substituents.[95, 104, 171] In addition, their electron-donating methyl groups make them electron-rich, potentially improving the selectivity of a boron-fluoride interaction. However, we decided not to use mesityl boron in our investigations, as our steric demands are quite different.

Triol Borates

Cyclic triol borates have recently been synthesised by Yamamoto *et al.*[172] Air and water stable, they are accessed by condensation reaction with a triol and subsequent treatment with inorganic base to access the triolborate as a K, Li or ammonium salt (Scheme 24). These stable ate complexes have been shown to be useful for a range of carbon-carbon and carbon-nitrogen bond forming processes, including Pd-catalysed Suzuki couplings and Cu-catalysed arylation.

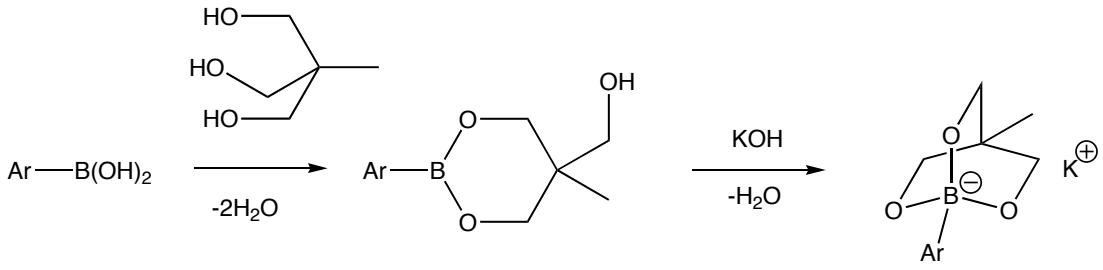

Scheme 24 Triol borate formation.

Five coordinate boron can also be achieved, with the first crystal structure of a pentavalent boron centre being isolated and fully characterised in 2000.[173]

2.3 Previous Work Within the TDJ Group

2.3.1 Fluorescent Sensors for Fluoride

Some of the earliest research into the design, synthesis and application of useful chemosensors for fluoride was reported by the James group. The interaction of a boronic acid moiety with a fluoride anion had been shown to be an incredibly selective recognition event previously but our group published the first example of a fluorescent sensor for fluoride.[35]

In 2005, a ditopic sensor **78** for potassium fluoride was developed within the group, consisting of a fluorophore, a boronic acid and a crown ether unit, all linked through a tertiary amine *via* insulating methylene groups (Scheme 25).[174] No fluorescence enhancement was observed in the presence of potassium chloride or potassium bromide. Sodium fluoride also resulted in no change in the emission spectrum. Only potassium fluoride provides two complementary guest ions, prompting a fluorescence enhancement, *via* a PET mechanism, as the potassium cation is the correct size to fit the crown ether and the boronic acid centre is selective for fluoride. [2.2.2]Cryptand can be used to scavenge the potassium ion, switching off the fluorescence.

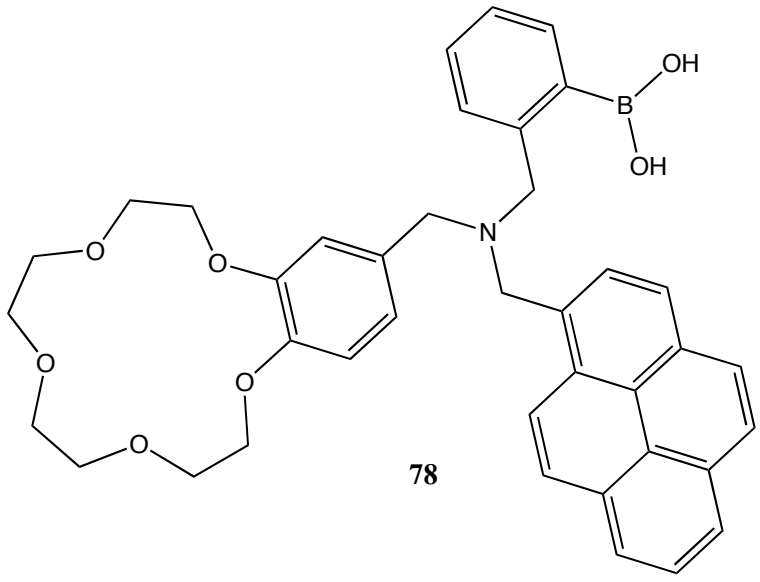

78

Scheme 25 Ditopic sensor for potassium fluoride.

More recently, bis(bora)calixarene **79** was reported, the first example of a lower-rim boron derivatised calixarene to be structurally characterised (Figure 46).[175] The characteristically rigid cone-shaped calixarene which provided a preorganised binding site with an affinity for 2-point binding to fluoride[92, 176] was the driving force behind the molecular design. In addition, calixarenes possess inherent potential for ditopic sensing, as the upper rim can also be derivatised. Early fluorescence studies indicated a fluorescence quenching in the presence of fluoride, thought to be due to bidentate binding, resulting in an interruption of the π-π interactions between co-planar phenyl rings bound to the boron centres.

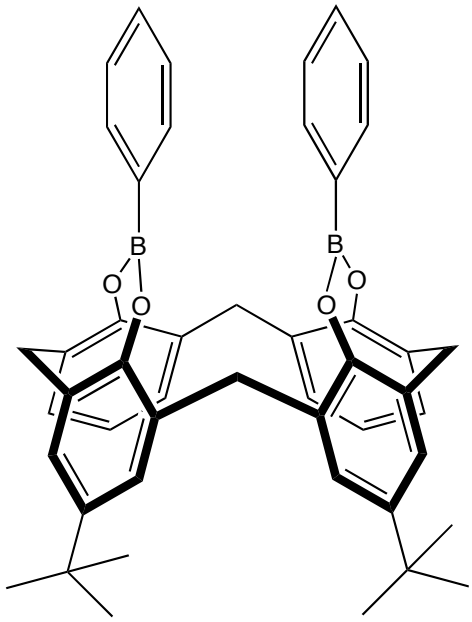

79

Figure 46 Two *tert*-butyl groups omitted for clarity.

We therefore wanted to look at synthesising fragments based on this original construct and examine any possible binding. During the course of the work described in the following pages, Aldridge *et al.* looked at this calixarene framework in greater detail during investigations into the influence of the chelate backbone of ferrocene functionalised boronic acids[177] and found that **79** (and a ferrocene substituted derivative) decomposed in the presence of 0.5 equivalents of TBAF. ^{1}H NMR showed that the characteristic set of four doublets of **79** disappeared on addition of TBAF in $CDCl_3$ and the two doublets indicative of the more symmetric precursor calixarene were visible. Further ^{11}B (δ_B 27.0 changed to two peaks at δ_B 28.5 and 4.5 respectively) and

^{19}F (δ_F -144.3, -136.1, -131.7; owing to the three forms of $[RB(OH)_nF_{3-n}]^-$) NMR studies provided further evidence indicating phenylboronic acid and - at higher concentrations of TBAF - its fluoride derivatives were being generated. These observations confirm what we later observed in the electrochemistry of **90** (see **Section 2.5.6**).

2.3.2 Consequences for Sensor Design

The naphthalene backbone has been explored extensively as a framework for fluoride sensing, along with other rigid aromatic frameworks, as described in Chapter 1.[104] Such Gabbaï-type naphthalene systems interact preferentially in a bidentate fashion over a 1:1 motif, even in the presence of excess fluoride. Steric factors are particularly important in dimesityl boron examples but even in the diboronic acid species both boron centres are sp^3 hybridised in the presence of 1 equivalent of fluoride.

We therefore decided to begin our investigation by synthesising molecules that shared some structural features of bisboracalixarene **79** with the intention of looking at the fluoride binding behaviour of boron phenolates.

2.4 Boron Phenolates

2.4.1 Synthesis

Typically, a boronic acid, boronate ester or triarylborane is used as the Lewis acidic site for fluoride binding in chemosensors. However, in light of the aforementioned commercially availability of an array of phenols and bisphenols (a simple search of SciFinder yields over 34,000 compounds with at least one related reference), we envisaged a simple protocol for obtaining a range of molecules with poorly investigated potential binding motifs *via* treatment with base and subsequent reaction with dichlorophenylborane, in a similar route to that used in the generation of **79**.

This one-pot synthesis could be used to access a selection of boron phenolates which can be used to investigate potential fluoride binding. Analogously, bisphenols with closely-orientated hydroxy groups can be used to generate complete boronate esters (Scheme 26).

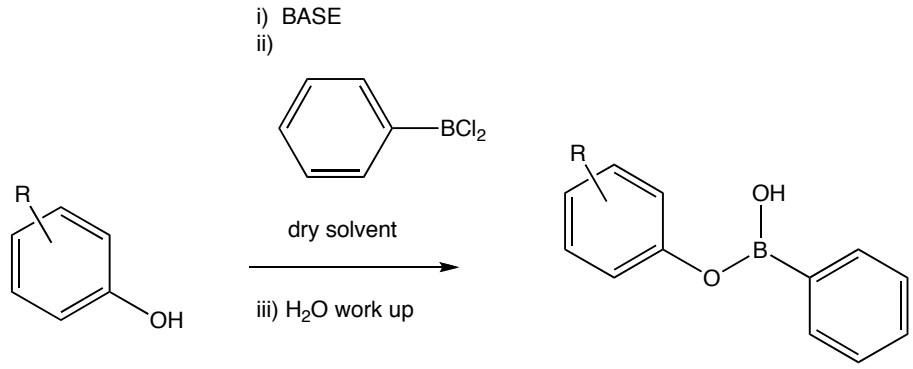

Scheme 26 General procedure for the preparation of boron phenolates.

During the course of the work performed as part of the development of calixarene **79**, phenoxyboronates **80-83** (Figure 47) were also synthesised within the group[178] using the general methodology described above (Scheme 26) in reasonable yields (72-89 %).

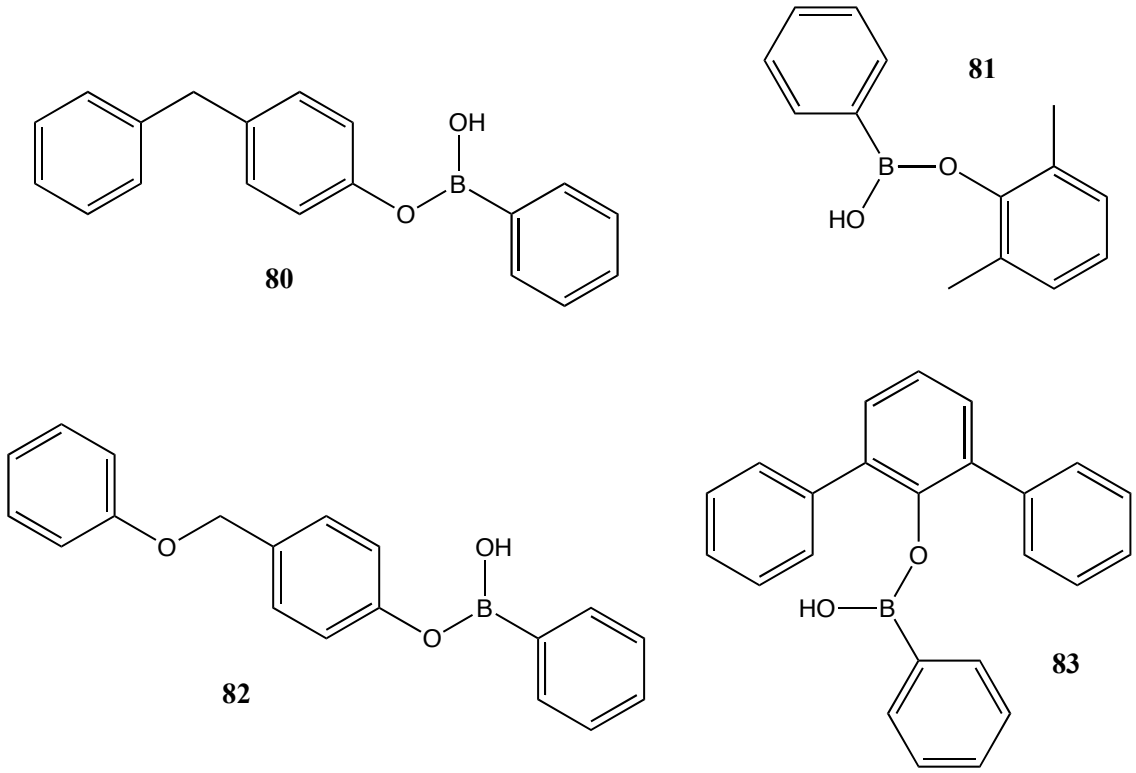

Figure 47 Boron phenolates synthesised previously in the James group.

The facile synthesis of these compounds is encouraging since they present a range of steric demands. The products were typically air-stable, non-hygroscopic recrystallisable solids. As phenylboronates possess only a single OH functionality, competing

formation of stable dimers or boroxine trimers in non-polar solvents observed for boronic acids is avoided.

2.4.2 Sensor Design Focus

Although many sensors are built around a rigidly constrained framework - thereby maximising binding constants - this is not always ideal. In molecular machines or anion templated synthesis, reversing a binding event or having a different type of control could be advantageous. Some naphthalene based systems require the addition of Al(III) to reverse the binding. Controlling the binding event with ease and without aggressive, highly reactive species is desirable.

Many bisboron systems are designed to be preorganised for a guest fluoride anion by placing the two boron centres in close proximity to one another. If the binding event changes the structural or conformational characteristics of the system, this is a very different response to a fixed system changing to accommodate the guest. The ditopic potential would be lost if we move away from the calixarene backbone, but a new system could also be based on bidentate binding causing conformational, electronic or structural change. It is of interest to investigate whether the tendency for anions to bind to multiple receptors holds under a system that is not rigidly preorganised.

With fluoride as our target, several molecular design features emerged, both general to sensor chemistry and anion-specific. Firstly, the interaction of boron centres with fluoride is well described and understood.[35] Jacobsen and Gabbaï in particular have shown fluoride to preferentially bind in a bidentate fashion both theoretically and practically.[92, 110] Finally, any proposed conformational changes on binding should be in a limited sphere, that is, if the sensor can be designed so that changes are restricted to for example, one axis of rotation, then observed responses to binding can be more easily understood.

Thus, although the binding site is not rigidly preorganised, some degree of control and preorganisation is present. Upon binding, either an existing luminescent system is interrupted or two-or-more optically active substituents interact intramolecularly in a

different manner to intermolecular excimer signalling sensors, such as Yoon's pyrophosphate ion system.[179] The general postulated system is shown in Scheme 27.

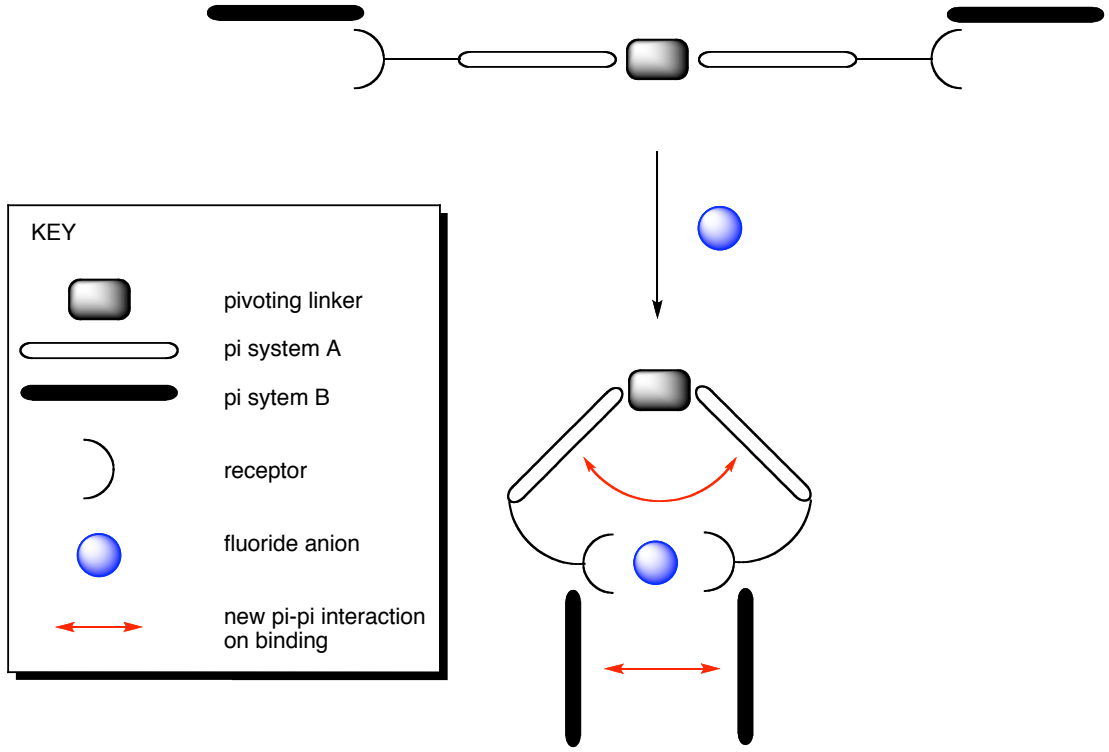

Scheme 27 Schematic of the proposed bidentate conformational sensor model.

This sensor has several key design aspects:

1. **linker** – an insulating linker, acting as a pivot provides some flexibility and rotation and inhibits conjugation between the pi systems
2. **conjugation** - twin aromatic systems with luminescence properties
3. **steric hindrance** - steric bulk in suitable geometry to restrict the free rotation in the free and bound states, forcing pi systems (A, above) into a complementary arrangement and creating a potential binding pocket of a suitable size and orientation
4. **modular design** - opposing terminal positions available for functionalisation to allow introduction of two suitable binding sites and additional pi systems (B, Scheme 27) capable of signalling conformational change

Linker

From the viewpoint of designing intramolecular ET into supramolecular compounds, the relative distances between the donor and acceptor fragments is particularly important, with an sp^3 hybridised methylene bridge ideal for ET; the bridge being suitably small, yet capable of effectively insulating the charge separated species. However, the proposed sensor model is not organised into a D-B-A arrangement. In our model the linker is not present to insulate donor and acceptor groups. Most crucially a methylene group can be seen as a hinge, a single carbon atom about which the two 'arms' of the bidentate ligand are able to move or rotate. Considering the size of the target anions a longer linker was unlikely to be advantageous.

An alternative would be to arrange a fixed optically active unit as the linker and then allow the two arms of the molecule to act as the signalling components, as in compound **46** (see Chapter 1, Scheme 14). Adapting a system of this nature so as to incorporate two boronic acid or boron phenolate functionalities was thought to be interesting but the naphthyl systems pioneered by Katz and furthered by Gabbaï are the most simple expression of this form.

Pi System A

The twin aromatic systems could be any optically active system but the size of the target analytes (and hence the desired cavity size) and the extra complexity in synthesis of larger or longer wavelength fluorophores led us towards twin phenyl groups being a likely starting point. Any twist or further deviation from a pseudo co-planar geometry would interfere with orbital overlap and electron transfer and hence affect the fluorescence behaviour. If more specialised fluorophores are desirable in the future, methodology performed on the more easily synthesised and relatively inexpensive biphenyl compounds is likely to be transferable.

Substituents, likely at the *ortho* positions, are intended to play a key structural role in the steric properties of the structure, with the bulkiness of the group particularly likely to effect any conformational changes on binding. Methyl, ethyl, *iso*-propyl, *tert*-butyl, cyclohexyl, phenyl and adamantyl encompass a conceivable range in size. In the absence of steric hindrance the two aromatic systems would be free to rotate, meaning the compound would not act like a tweezer or pincer but just envelop the target ion if

binding occurs. The use of bulky substituents should limit the conformational change on binding to pseudo-2D movement, thought to give more finite, discernable emission responses.

The Receptor and Pi system B

The terminal position does not have to be occupied by merely a simple binding site. The motif gives scope to tailor the solubility of the compound, the environment around the binding sites and also provides the opportunity to introduce another fluorophore or other reporting system. For example, if a substituted phenyl ring is utilised, there is scope for attaching a fluorophore, a water-solubilising moiety and a binding site simultaneously. The synthesis of this fragment could be done prior to addition to the bidentate sensor backbone. Varying the substitution pattern allows for further selectivity tuning and conveniently a phenyl ring is likely to sit almost perpendicular to the rings of the backbone because of the sterically hindered *ortho* positions, creating an obvious binding pocket. Excimer formation, accompanied by a useful, relatively long-wavelength fluorescence signal are formed between pyrenes and several other pi systems in some molecular sensors.[131, 180] This then provides a second mode of signalling action in the same molecule, both potentially affected by conformational change on binding, which may lead to ratiometric multi-signal monitoring, potentially advantageous over recording single intensity changes at one fixed wavelength.

2.4.3 Narrowing the Search

At this early stage, aiming primarily to test the model, we were keen to employ commercially available starting materials. Figure 48 shows some examples of commercially available bisphenol substrates with suitable linkers.

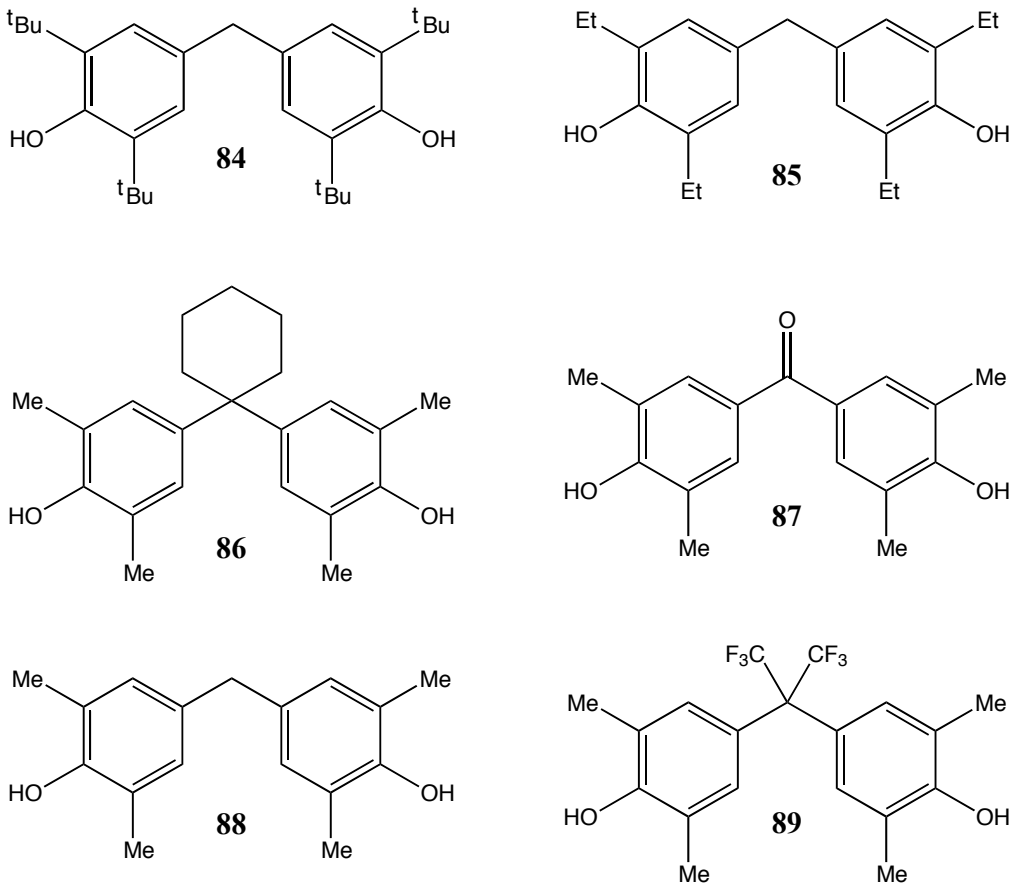

Figure 48 A range of commercially available starting materials.

4,4'-methylenebis(2,6-di-*tert*-butylphenol) **84** appeared to offer a useful starting point both due to its commercial availability and its structural features. Compound **84** is low-cost, possesses the desired methylene linker and offers a very high level of steric hindrance.

In the preparation of bisphenolate **90** (Figure 49), during the dropwise addition of *n*-butyllithium, a glass-like solid is formed and a vibrant purple colour is observed. Dissipation of the purple colour and the presence of a white precipitate can be observed around 30 min after the addition is complete. The system was allowed to warm to 0°C before the dichlorophenylborane was introduced in one steady injection - as opposed to a dropwise addition - to avoid the reactive dichlorophenylborane reacting with two molecular equivalents of the deprotonated phenol. After reaching room temperature, the reaction mixture was heated at 100°C for 12 h. Following an aqueous work-up, **90** was purified by recrystallisation from hexane and isolated as an off-white crystalline solid in 81 % yield.

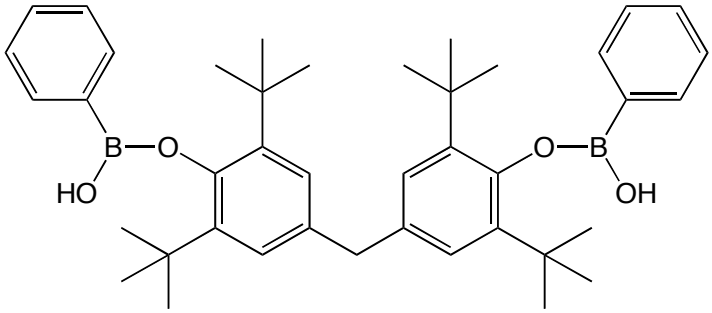

Figure 49 Boron (bis)phenolate **90**.

The related monodentate molecule **91** was synthesised *via* the same general protocol described in Scheme 26 to compare a single binding site with bidentate binding for direct comparison with **90**.

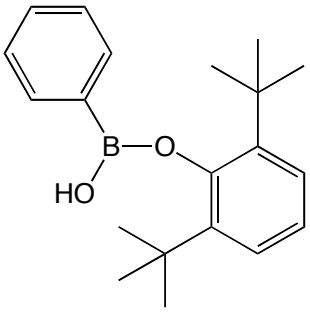

Figure 50 Boron phenolate **91**.

To extend the binding motif further the tripodal and potential tridentate molecule **92** was also synthesised (Figure 51). Whilst this species does not follow the model outlined in Scheme 27 it has potential to provide further information about the nature of the fluoride binding, if it occurs, and prove the predisposition of fluoride to prefer a μ-bridging binding mode.

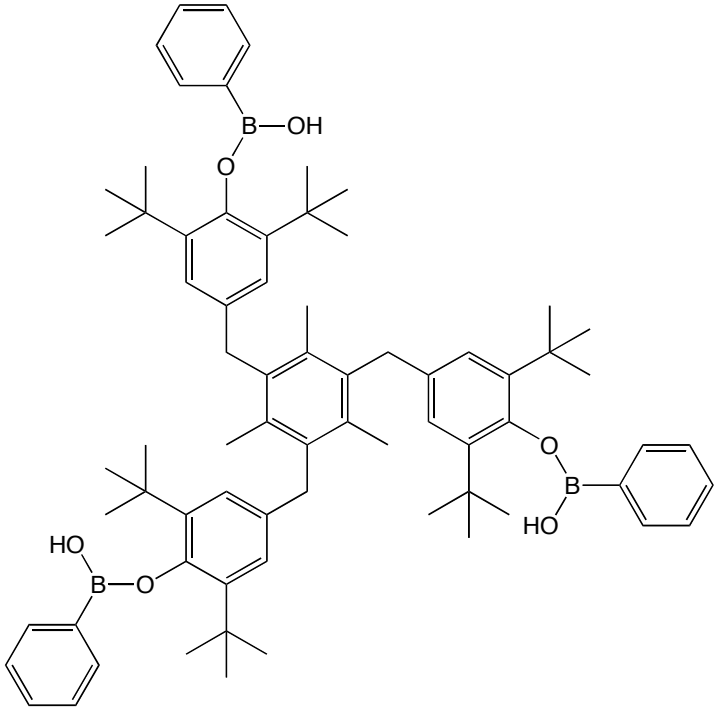

Figure 51 Tris(boronphenolate) **92**.

We had also fortuitously prepared phenolate **83** (Figure 47) which provided an opportunity to directly compare the *tert*-butyl appended **91** to its phenyl analogue, albeit in the monodentate motif (the bisphenol equivalent was not commercially available and as such the synthesis was not immediately a priority).

2.5 Anion Interactions of Phenyl(boronates)

2.5.1 Solvent Considerations

All binding studies were performed in organic solvent, typically dichloromethane though acetonitrile and deuterated chloroform were also utilised for various applications. The boronphenolates were not water soluble, although pH buffered solutions were not trialled. Hydroxide was thought to be likely to be extremely competitive with fluoride, restricting our work to organic media. All optical spectroscopy measurements were performed at 298 K.

2.5.2 Qualitative Visual Analysis

Fluoride anion, as the tetra-*n*-butylammonium salt was added in excess to solutions of all the boron(phenolates) in dichloromethane under atmospheric conditions. Several species showed a dramatic colorimetric response within a few seconds. All the boron phenolates which changed colour shared the 2,6-disubstituted pattern (**83**, **90-92**) implemented to induce rigidity. Species with one, two and three boron centres all showed colour changes in response to fluoride. No other anions (including acetate, hydroxide, phosphate and chloride anions) tested prompted colour changes visible to the naked eye.

Although a dramatic colour change specifically in the presence of fluoride is a highly desirable response for a sensor, as it allows immediate qualitative analysis, this result was unexpected. No immediate electronic process, assuming one or more fluoride anions are interacting at the boron centres, was envisaged as being responsible for such dramatic colour changes. The bidentate model proposed was not responsible for the colour change in **90**, as boron(phenolates) with 1-3 boron centres also showed colorimetric responses to fluoride. The previously synthesised bisboracalixarene **79** showed fluorescence quenching in the presence of fluoride but no colour changes were observed. Therefore, more detailed spectroscopic analysis was required to elucidate what was occurring at the boron centre.

^{11}B NMR spectroscopic study of **90** alone showed the expected broad peak at δ_B = 28.3 ppm in $CDCl_3$, indicative of the expected sp^2 hybridized nucleus. ^{11}B NMR of 1:1 **90**-TBAF in $CDCl_3$ showed a single peak at δ_B = 4.1 ppm indicating significant tetrahedral character at the boron centres, suggesting that the fluoride anion is interacting with the boron centre in an equilibrium.

To determine whether the boronate fragments were required to facilitate the colour change, dichloromethane solutions of the parent phenols of compounds **83**, **90-92** were prepared and their colorimetric response to fluoride was monitored by naked eye.

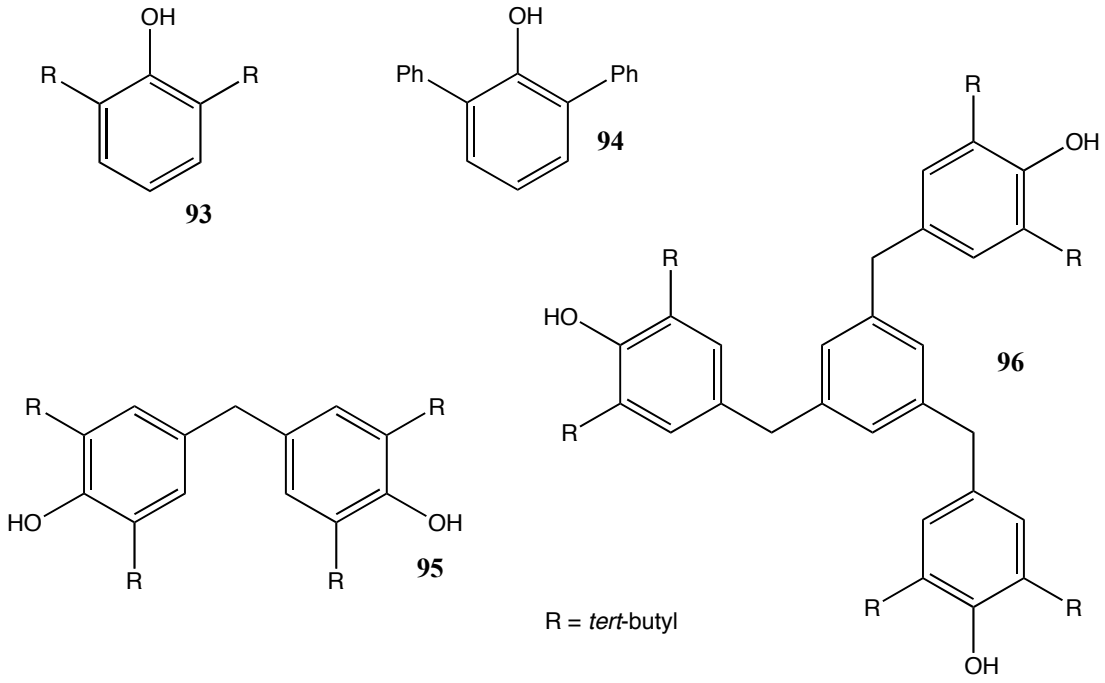

Figure 52 Phenols **93-96**.

In approximately a 10-fold excess of anion, almost instantaneous colourisation occurred with phenols **93-96**. These phenomena show the boron-containing substituents are not necessarily required for the formation of the coloured species. Addition of water reversed the colorimetric response.

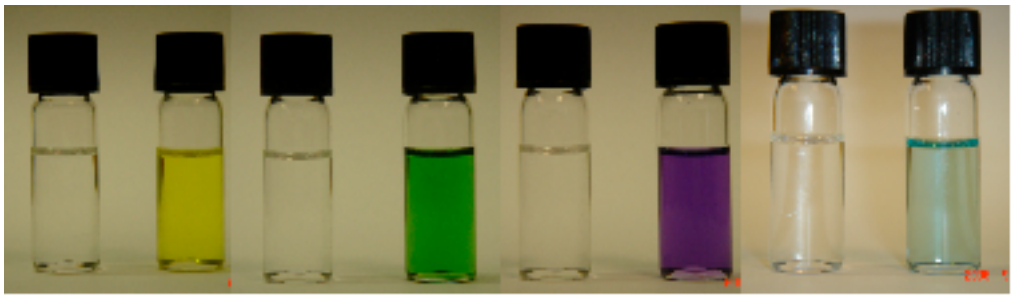

93+F^- **94**+F^- **95**+F^- **96**+F^-

Figure 53 Naked-eye colorimetric changes in the presence of fluoride (phenol 1.0 mM, TBAF 10.0 mM in dichloromethane).

Although not direct precedent, the system described in Chapter 1 (Scheme 20) includes a boron-aryloxide linkage which proves vulnerable to fluoride anions resulting in a chemodosimetric mode of action.[143]

2.5.3 Luminescent Spectroscopy

We then performed UV-vis spectroscopy in dichloromethane solution using tetra-*N*-butylammonium salts of various anions. Figure 54 shows the UV-vis spectrum of 0.1 mM 4,4'-methylenebis(2,6-di-*tert*-butylphenol) **95** in dichloromethane overlaid by the spectra of the compound in the presence of an excess of fluoride, chloride, bromide and phosphate ions respectively. Only fluoride evoked a significant change in the absorption spectrum, with a broad and intense peak across the 525-610 nm range, visualised as a vibrant purple colour. Phosphate anions did induce a very small absorption peak response but the intensity was extremely small in comparison with the absorption in the presence of fluoride (< 0.1 %). No colour change due to phosphate anion is visible by the naked eye.

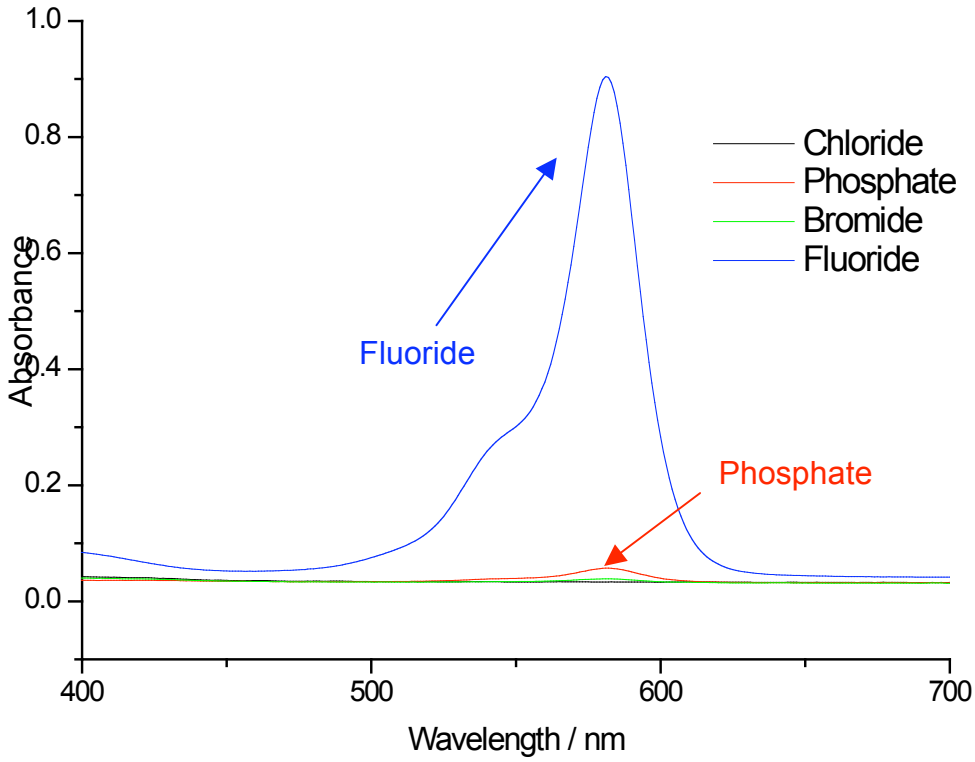

Figure 54 Overlaid spectra of bisphenol **95** in dichloromethane in the presence of the anions shown. Measurement conditions: 0.1 mM **95**, phosphate, bromide and chloride 1.0 M and fluoride 10.0 mM respectively.

The other 2,6-dialkylsubstituted phenols **93**, **94** and **96** showed similarly selective responses to the fluoride anion by UV-vis spectrometry. Figure 55 shows the corresponding overlaid spectra for 2,6-diphenylphenol **94** titrated against the same selection of anions, fluoride again provoking dramatic changes in the absorption spectrum, evidenced by a visible colour change from colourless to green.

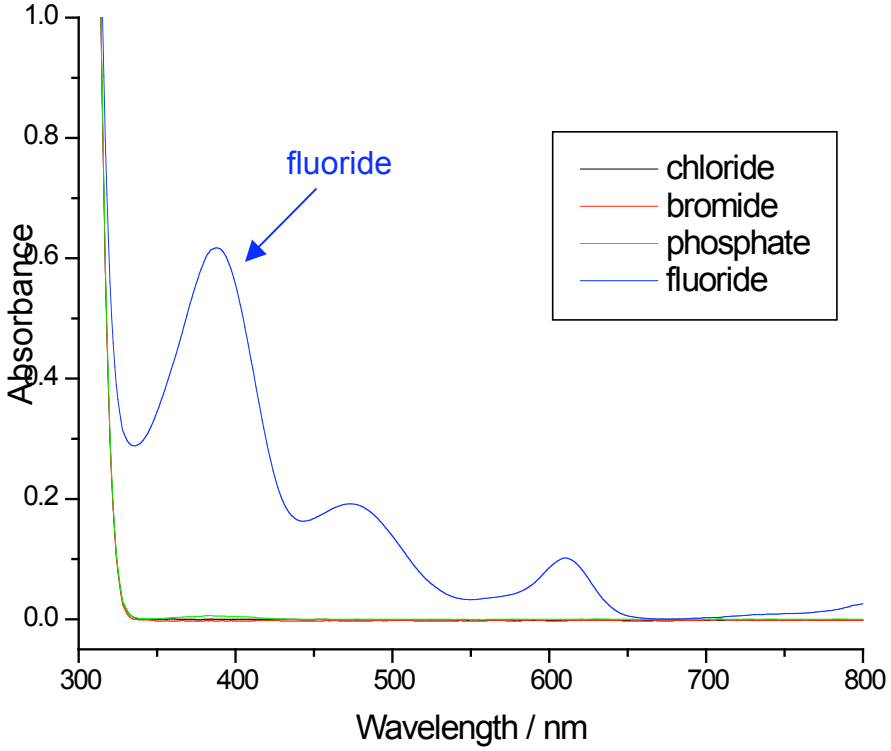

Figure 55 Overlaid spectra of phenol **94** in dichloromethane in the presence of the anions shown. Measurement conditions: 0.1 mM **94**, phosphate, bromide and chloride 1.0 M and fluoride 10.0 mM respectively.

Scheme 28 shows the proposed response to fluoride at the molecular level in solution. In the case of the naked phenols, fluoride mediated deprotonation occurs. The phenoxyl anion is easily oxidised in air to form the coloured stable, coloured, phenoxyl radical species. The formation of the anion is also driven by generation of the stable hydrogen bifluoride or HF_2^- ion and the phenoxyl radical is stabilised by the electron donating alkyl or phenyl groups which play no steric role in the mode of action. NH-containing fluoride sensors have shown formation of HF_2^- after the initial hydrogen bonding recognition event and ensuing deprotonation.[128] HF_2^- is resolved as a triple centred at 16.3 ppm relative to TMS.[181] No colour changes were observed in the presence of fluoride for phenols without electron donating substituents examined.

Following the observed shift from 28.3 ppm to 4.10 ppm in the ^{11}B NMR of **90** in the presence of 1 eq of TBAF, we postulated that the phenyl(boronate) species undergo an additional step in the formation of the same phenoxide radical. Fluoride is thought to bind to the boron centre and in the presence of additional fluoride anion, the phenoxy

substituent on the boron could be liberated and then rapidly oxidised. Cyclic voltammetry experiments were performed to confirm this, as detailed later in this Chapter.

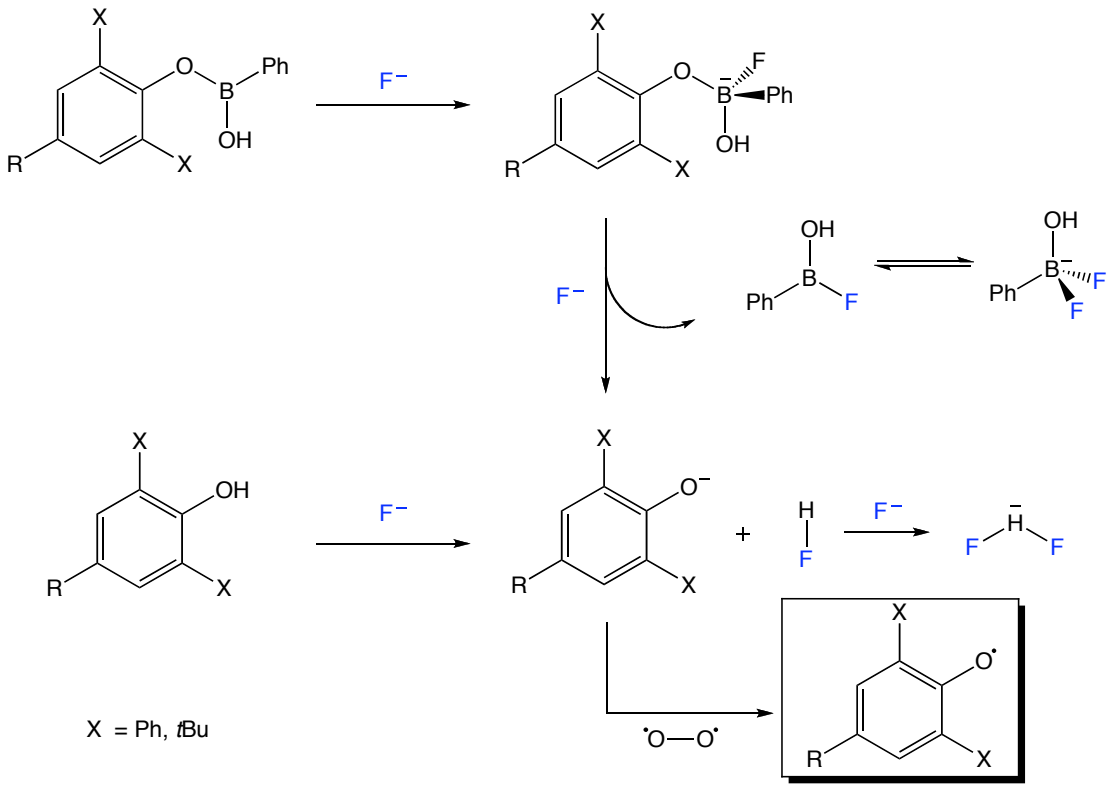

Scheme 28 Proposed mechanism of the formation of the stable coloured species in the presence of fluoride anions.

One advantage of the boronate system is that no extremely harmful HF is liberated, as the boron species effectively scavenges the fluoride.

Boron phenolates **83**, **91-92** were exposed to a range of anions (chloride, bromide, iodide, phosphate, hydroxide and acetate, all as their respective tetra-*n*-butyl ammonium salts) to check for similar colorimetric response. As no visible colour changes were observed for any of the boron phenolates for any anion other than fluoride, it can be assumed that the boron(phenolate) species do not dissociate in the presence of these anions.

Precedent of Phenols as Anion Sensors

The precedent of simple phenols acting as selective colorimetric indicators of fluoride

anion is limited. Some early examples of co-crystallised phenols and chloride were documented in the 1980s. [182, 183] There are several examples of phenolic sensors acting as anion sensors in the literature but most examples show poor, if any selectivity.[184-186] However, Winstanley has utilised catechols as anion sensors, comparing their relative halide binding behaviour.[187] Of particular relevance is simple catechol itself, which showed a dramatic colour change from colourless to blue in acetonitrile solution. After some detailed mass spectrometry studies of a mixture of catechol **97** and TBAF, this colour was attributed to oxidative degradation products (including polymerisation products), as *cis*, *cis*-muconic acid **98** was identified at *m/z* 142. This species had previously been observed in Cu^{2+} catalysed aerobic oxidation of catechol and is a further oxidation product of *ortho*-quinone **99**. The group did notice colour changes in the presence of acetate over a period of 1 hour however, something we did not observe with the 2,6-disubstituted phenols.

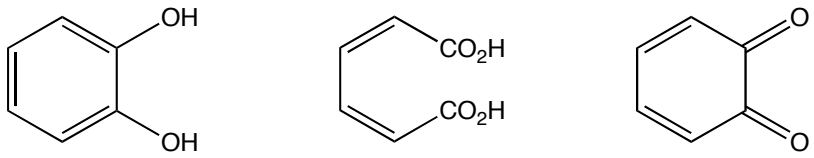

97 **98** **99**

Figure 56 There is only very limited precedent of phenols being utilised in attempts to design sensors for fluoride.

Sessler's 'off-the-shelf' colorimetric sensors generally did not show good selectivity but acid blue 45 (see Chapter 1, Figure 30) displayed selectivity for fluoride with a colour change from blue to colourless in DMSO.[121] This species contains two hydroxyl groups and two amino groups and no proposals are made in regard to the mechanism of binding.

2.5.4 Fluorescence Study

Despite the findings which showed compound **90** did not bind to fluoride in a bidentate fashion as proposed in the sensor design, the fluorescence behaviour was investigated, in order to examine any useful emission changes. All measurements were recorded at 298 K.

Exciting at a wavelength of 289 nm, compound **90** showed an emission maxima at 375 nm. A rapid and total quenching effect was observed for **90** in the presence of fluoride anion, which fits the proposed chemodosimetric process. Boronic acids or their derivatives have not been used as sensors for other anions, the unusual B-F interaction being due to the extremely hard Lewis acidic nature of the fluoride anion, so any hydrogen bonding processes occurring were thought to be weak, and unlikely to cause spectral emission changes. However, a titration of **90** in dichloromethane against TBAC showed a quenching effect markedly different from the complete and immediate (~1eq) quenching observed due to fluoride cleavage of the boron-oxygen bond previously observed (Figure 57).

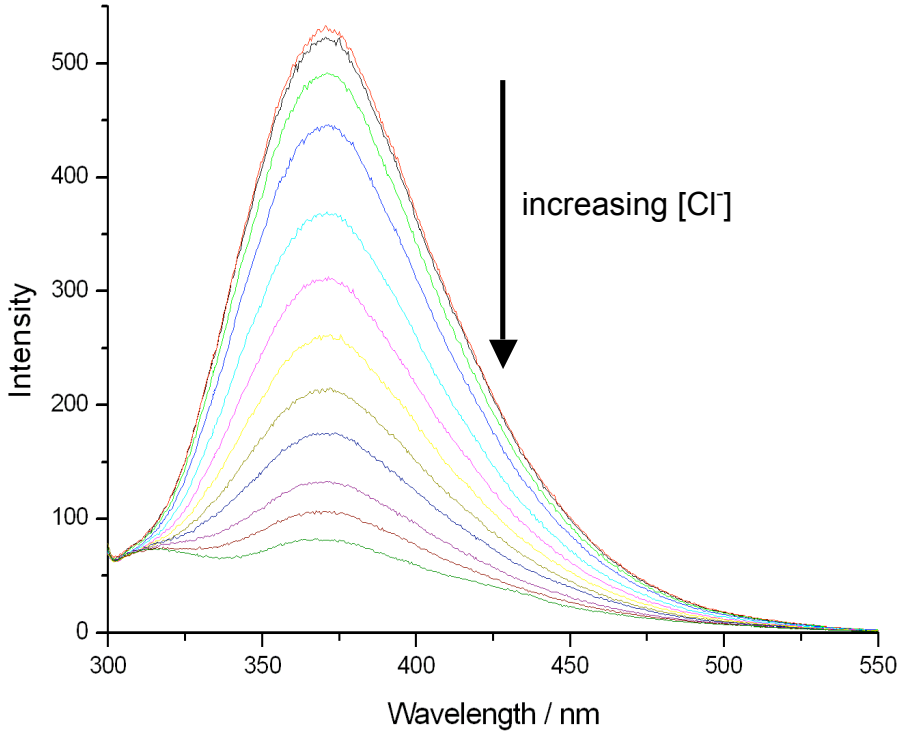

Figure 57 Overlaid spectra of bisboron(phenolate) **90** showing quenching response to increasing TBAC. Measurement conditions: λ_{ex} 289 nm, 0.1 mM **90**, 0.1 – 1.4 mM TBAC.

Maxima emissions were measured at 375 nm and the curve attained was found to be non-linear, indicative of a 2:1 binding mode with a log K = 4.5 (Figure 58). Any 1:1 binding model did not fit the data, nor did a 1:1 or a 2:1 mixed binding model.

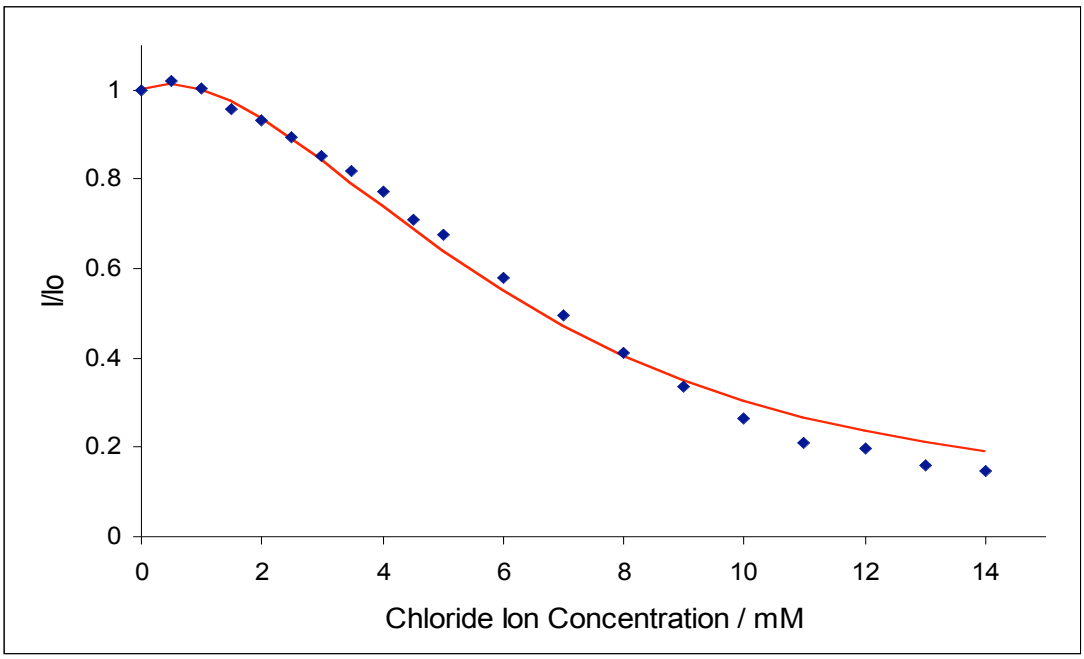

Figure 58 Plot of fluorescence emission maxima of bisboron(phenolate) **90** at 375 nm with increasing chloride concentration. λ_{ex} 289 nm, 0.1 mM **90**, 0.1 – 1.4 mM TBAC.

Tetra-*n*-butylammonium bromide (TBAB) and tetra-*n*-butylammonium iodide (TBAI) did not cause significant fluorescence quenching response beyond the expected small quenching caused by the external heavy atom effect[188], for which iodide is notorious.[189] At 10 mM anion concentration, the relative intensity of **90** at 375 nm is 0.21 in the presence of TBAC but 0.86 in the presence of TBAB.

2.5.5 Probing the Binding

We then decided to consider the potential binding of chloride to a single receptor site using monophenylboronate **91**. We wanted to test for a fluorescence response to see whether the response was exclusive to the bidentate receptor, although in the case of chloride we knew from theoretical and practical observations that chloride prefers to bind in a tetrahedral environment.[92, 131] Exciting at 251 nm afforded a maxima at 355 nm in the emission spectrum. Figure 59 shows a plot of the fluorescence titration of chloride against species **91**.

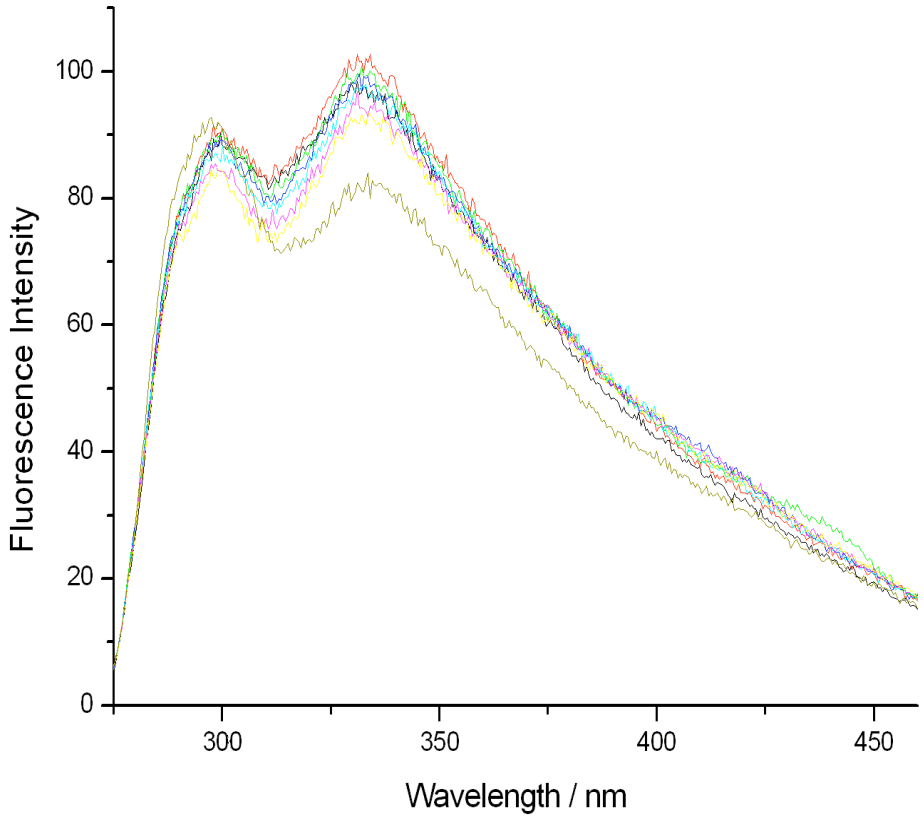

Figure 59 Overlaid emission spectra for compound **97** in the presence of increasing concentration of chloride ions. λ_{ex} 251 nm, 0.1 mM **91**, 0.1 – 1.0 mM TBAC. NB bottom curve in the presence of a large excess (> 100 equivalents) of TBAC.

Interestingly, boron(phenolate) **91**, which only has a single B-OH moiety showed a very slight decrease in its fluorescence emission at 355 nm in the presence of chloride, only being quenched by ~15% in the presence of a large excess (> 100 equivalents) of chloride. This result showed the bidentate nature of the compound is required for effective binding.

Fluorescence titrations with chloride were also recorded for bisphenol **95** ie with no boron functionality present. Exciting at 257 nm produced an emission maximum at 308 nm but no quenching was observed in the presence of TBAC. This confirmed that the chloride must interact with the boron-containing fragment of **90**.

2.5.6 Electrochemistry

The electrochemistry of the interaction of sensor system **90** with both anions was monitored in an effort to understand and confirm the aerobic oxidation mechanism. Cyclic voltammetry studies were performed with differential pulse voltammetry modes. A solution of 1.0 mM **90** in acetonitrile is colourless and exhibits an oxidation peak at 1.8 V vs. SCE (see Figure 60 A)i)).

Figure 60(A)ii) shows that 0.2 mM fluoride causes a decrease in the peak response at 1.8 V vs. SCE and the appearance of a new peak at 1.5 V vs. SCE. For fluoride concentrations of 0.4 mM and higher additional anodic currents at a potential of ca. 0.0 V vs. SCE are detected and two new peak responses at -0.3 V and +0.1 V vs. SCE are observed. In complementary cyclic voltammetry experiments both peak responses are observed to be chemically irreversible. For applied potentials positive of ca. 0.0 V vs. SCE the characteristic purple colour of the galvinoxyl radical is observed. Furthermore, additional experiments with the parent phenol **95** in the presence of base show that the peaks observed at -0.3 V and +0.1 V vs. SCE are associated with this precursor for the galvinoxyl radical. The fluoride anions have removed the boronic acid residues and liberated the readily oxidised phenolate. In the presence of dioxygen this phenolate quickly undergoes multi-electron oxidation to the galvinoxyl radical or further coloured products.

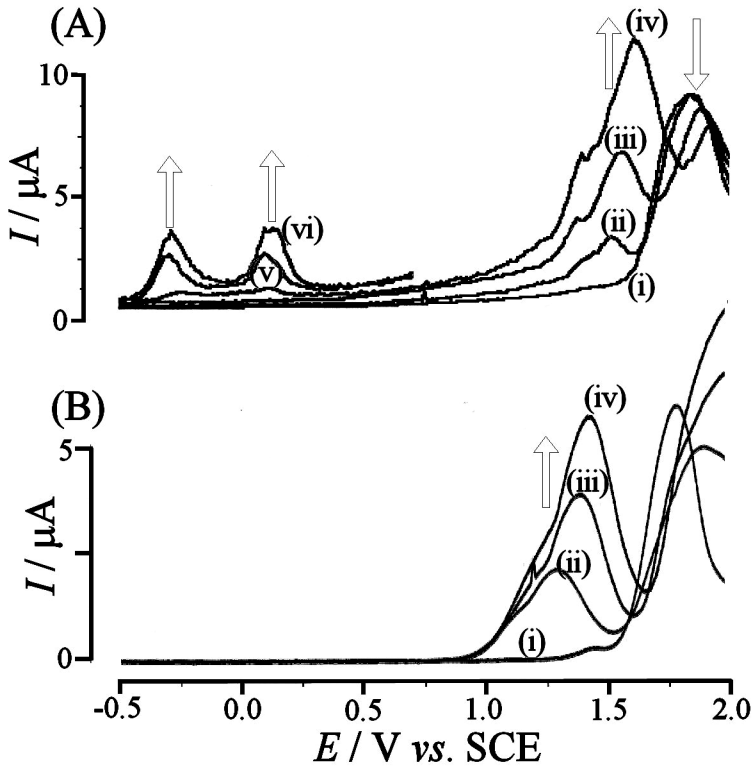

Figure 60 (A) Differential pulse voltammograms (modulation time 0.05 s, modulation amplitude 25 mV) for the oxidation of 1.0 mM **90** in acetonitrile (0.1 M NBu_4PF_6) at a 3 mm diameter boron-doped diamond electrode in the presence of (i) 0 mM, (ii) 0.2 mM, (iii) 0.4 mM, (iv) 0.6 mM, (v) 0.8 mM, and (vi) 1.0 mM TBAF. (B) Differential pulse voltammograms (modulation time 0.05 s, modulation amplitude 25 mV) for the oxidation of 1.0 mM **90** in acetonitrile (0.1 M NBu_4PF_6) at a 3 mm diameter boron-doped diamond electrode in the presence of (i) 0 mM, (ii) 1 mM, (iii) 2 mM, and (iv) 3 mM TBAC.

Figure 60B shows data for the same experiment with addition of tetra-*N*-butylammonium chloride is shown. In this case the easy to oxidise fragments are not formed and no colour change is observed. Upon addition of chloride a new signal at 1.3 V vs. SCE is detected and this signal can be identified as chloride oxidation.[190]

2.5.7 X-ray Crystallography Structural Evidence

Crystals of **90** were obtained from both rigorously anhydrous toluene (Figure 61) and reagent grade toluene (Figure 63 and Figure 64).

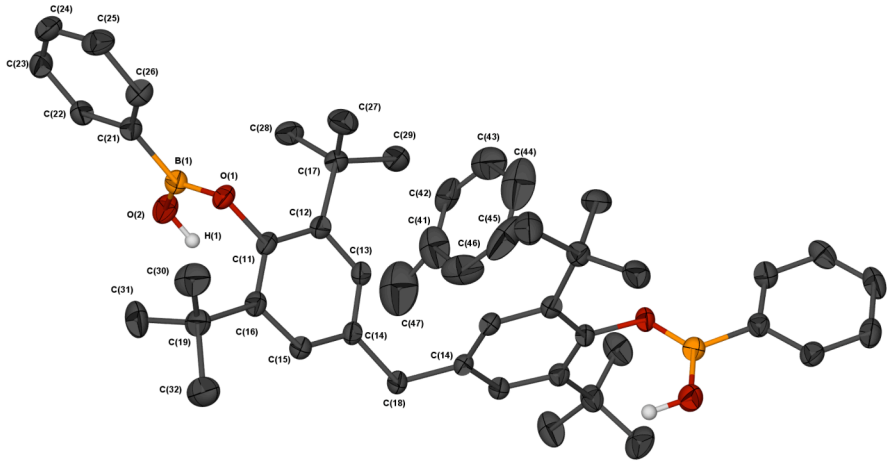

Figure 61 Structure of **90** as elucidated by X-ray crystallography.

In the absence of water, the structure of **90** elucidated from the X-ray diffraction pattern adopts a 'propeller' conformation (pseudo-C_2 symmetry) and associates into a 2D supramolecular array via a series of O-H · · · π interactions.

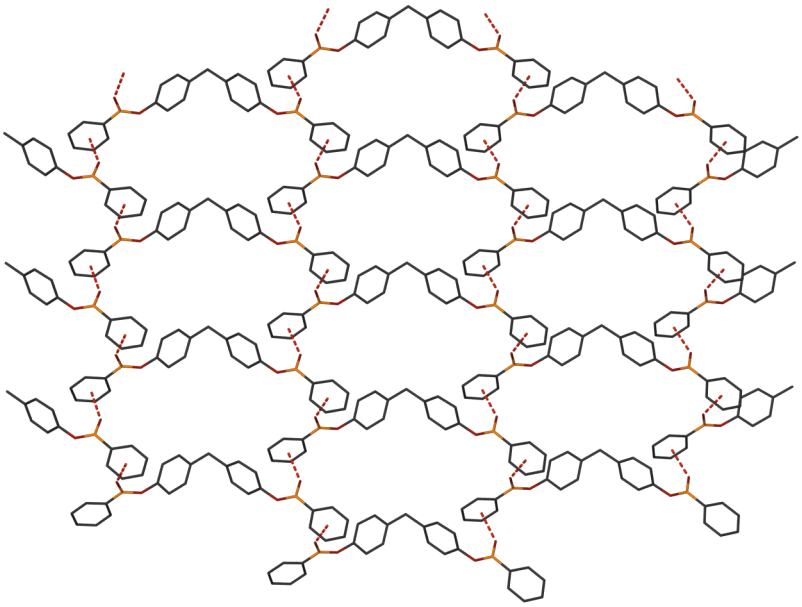

(A)

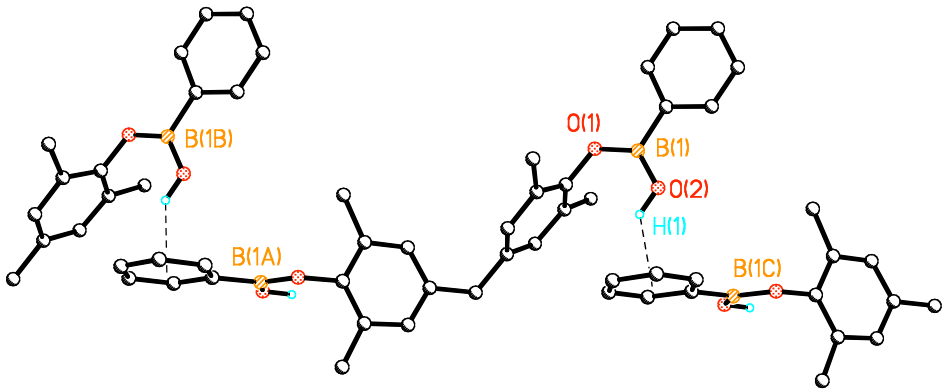

(B)

Figure 62 (A) 2D supramolecular sheet in *ab* plane of crystal lattice of **90** (B) detailed view of intermolecular interactions in crystal lattice of **90**. Dashed lines between H atoms and centroid (X) identify short (2.46 Å) H···π distances with an O-H-X angle of 127º.

However, as can be seen in Figure 63 and Figure 64, in the presence of water, the solid state structure adopts a very different arrangement.

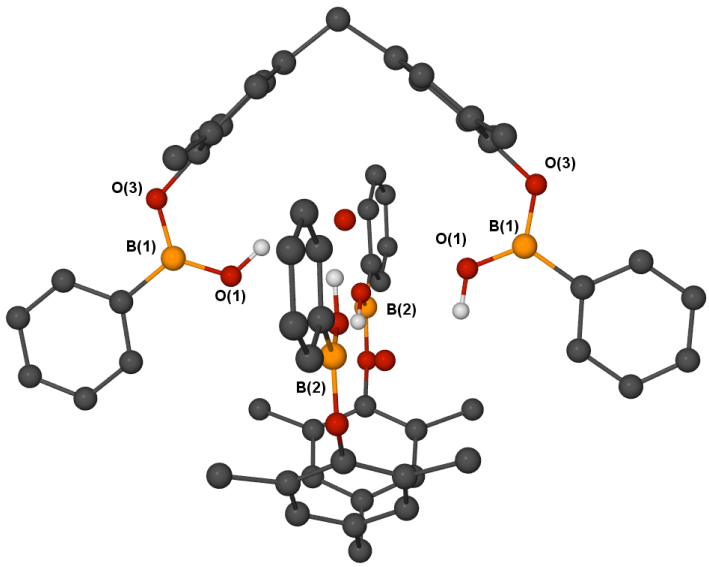

Figure 63 Structure of **90**·H_2O as elucidated from X-ray diffraction data. *Tert*-butyl groups partially omitted for clarity.

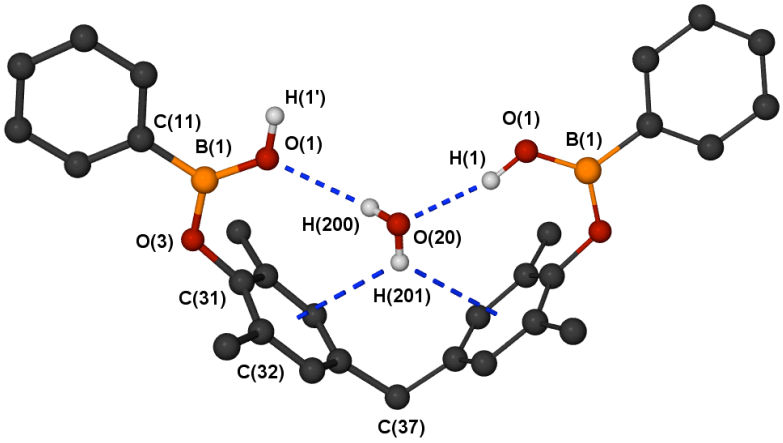

Figure 64 Half-dimer of **90**·H_2O. *Tert*-butyl groups partially omitted for clarity.

In **90**•H_2O, the aryl rings adopt a 'butterfly' conformation that has a pseudo C_{2v} symmetry and two orthogonal molecules of **90** are assembled around two water molecules. Unfortunately, significant disorder in this crowded cavity precluded detailed analysis of the hydrogen bonding interactions. Whilst this cannot be taken as direct evidence in disclosing the chloride binding mode in solution, it does show, at least in the solid state, that binding to a guest can occur and does induce a conformational change in the biaryl construct. Given the precedent of anion binding within a tetrahedral hydrogen bonding network[115] (Figure 65) the possibility of chloride binding in this cavity seems highly plausible.

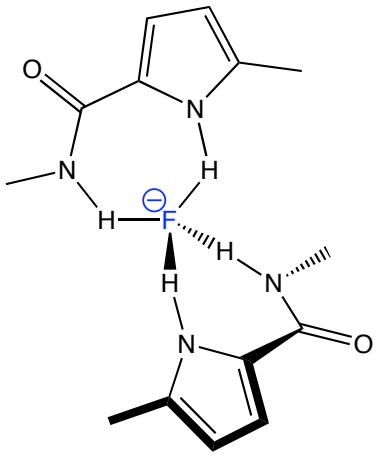

Figure 65 Fluoride bound in a tetrahedral environment.

The X-ray structure of boron(phenolate) **91** was also elucidated (see Figure 66).

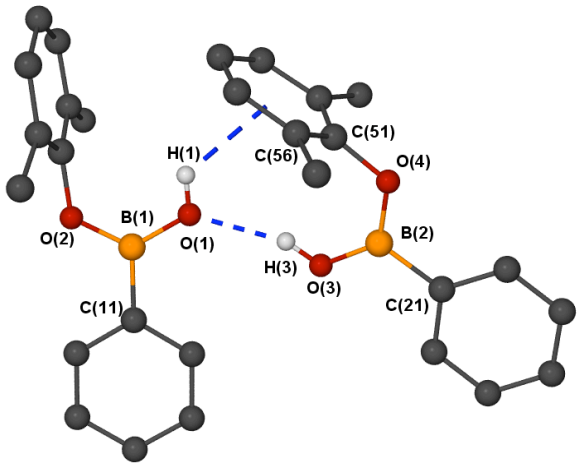

Figure 66 Crystal Structure of dimer of **91**.

Crystals of **91** were obtained by slow evaporation of a saturated hexane solution. On the supramolecular level, dimeric association occurs *via* intermolecular hydrogen bonding interactions between two molecules of **91**. A short O-H···O hydrogen bond [O(3)-H(3)···O(1); H···O distance, 2.03(3) Å, O···O distance, 2.864(2) Å, O-H···O angle, 160(2) °] is accompanied by an O-H···π interaction in which the O(1)-H(1) vector is directed toward the face of the aryl ring [O(1)-H(1)···X, where X = centroid of C(51)-C(56); H···X distance, 2.53(2), O···X distance, 3.190(1) Å].

Compound **91** crystallises as a dimer within the monoclinic space group $P2_{1/a}$. A hydrogen bonding interaction between H(3) and O(1) can be inferred from an intermolecular distance of 2.036 Å and heavy atom length (O(3)-O(1)) of 2.864 Å. The O(1)-H(1) vector is directed at the face of the π system with an intermolecular centroid-oxygen distance of 3.1-3.7 Å, with the π cloud of the ring acting as a hydrogen bond acceptor. A heavy atom distance of 3.191 Å was measured for **91** indicating the presence of an O-H···π interaction at an angle of 128.3º.

*Attempts to Isolate Crystals of **90**·Cl⁻*

Disappointingly, despite several batches of crystals being grown under slow evaporation and vapour diffusion conditions, no crystals of sufficient quality for X-ray analysis were obtained.

2.5.8 ^{1}H NMR Evidence of Chloride Binding

If hydrogen bonding between the chloride and the B-OH protons of **91** is occurring in solution, it may be possible to observe shifts in the proton resonances in the ^{1}H NMR spectrum. Chloride binding has been shown to occur by downfield shifts in aromatic protons in a recent publication by Flood *et al.*[191] The potential of observing signals due to the resonance of OH protons is often limited by exchange, and the chemical shift could change based on any alteration in water concentration. Therefore, consideration was afforded to the entire spectrum of **91**. Spectra were collected for **91** in $CDCl_3$ and in the presence of 0, 1 and 10 eq of TBAC on a 500 MHz Bruker Avance NMR spectrometer. In deuterated chloroform the B-OH proton of **91** appears at 4.22 ppm, 0.25 ppm downfield of the methylene proton (3.97 ppm). A downfield shift of 0.20 ppm was observed in the presence of 10 eq of chloride anion, measured relative to both the methylene signal and the aromatic singlet (7.19 ppm). The observation of extensive line broadening after the addition of one equivalent of the chloride ion is consistent with binding dynamics occurring on a similar timescale to the ^{1}H NMR experiment.

2.6 Preparation of a B-O-B Macrocycle

2.6.1 A Related Target Molecule Containing a N-B interaction

Previous work by Briggs *et al.* disclosed the synthesis of an aluminium compound **100** (Scheme 29) with a large Stoke's shift that has parallels to the boron phenolates we had prepared. We decided to prepare a boron analogue with the aim of investigating their binding and luminescent properties.[192]

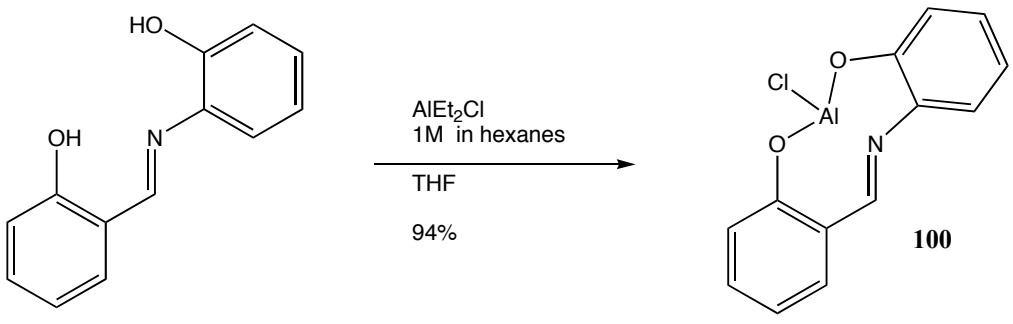

Scheme 29 Synthesis of a Schiff base compound **100**.

Examining the B-O bond lability was an attractive aspect of looking at an analogous boron species (simple retrosynthesis shown in Scheme 30 below) and the aluminium complex was fluorescent, indicating chemosensor or biotag potential.

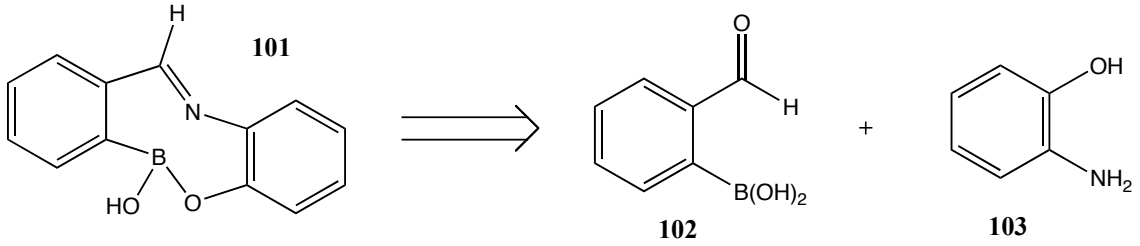

Scheme 30 Retrosynthetic disconnection of compound **101**.

Compound **101** was expected to feature a nitrogen-boron interaction, wherein the boron adopts a pseudo sp^3 hybridisation. This ability of boron to reversibly adopt a tetrahedral arrangement has been exploited by the group in the development of chiral derivatisation protocols for various chiral species capable of lone pair donation into the vacant p orbital on boron. It is of vital importance, particularly in the pharmaceutical industry to be able to accurately determine enantiomeric excess of a chiral compound. The most established method is to use plane polarised light and measuring the specific rotation. However, this technique is fallible[193, 194] and is sensitive to a number of factors including the solvent and the sample purity. Chiral derivatisation, chiral shift or chiral solvating agents can all allow provide simple and robust measurement of enantiomeric excess vital for monitoring asymmetric synthesis by NMR. The latter two methods make use of diastereomeric complexes formed *in situ* whereas chiral derivatisation involves covalent derivatisation of a substrate with an enantiopure reagent. Chiral derivatised agents are longer lived and despite the requirement for an expensive enantiomerically pure component and some kinetic resolution problems, the greater chemical shifts incurred with the derivatised protocols means there are widely used for determination of enantiomeric excess (for example Mosher's reagent, α-methoxy-α-trifluoromethylphenylacetic acid for determination of ee of chiral amines and alcohols).[195, 196]

The first substrates investigated were primary amines. As an illustrative example, combining equimolar quantities of 2-formylphenylboronic acid **102**, S-binol **104** and a racemic primary amine **105** results (after 5 min equilibration) in the formation of imino-

boronate esters **106a** (α-*R,S* diastereoisomer) and **106b** (α-*S,S* diastereoisomer). An ^{1}H NMR spectrum of an aliquot of the resultant mixture showed a 50:50 mixture of the two diastereomeric complexes, including well resolved peaks for the imine, α-methine, α -methyl and *p*-methoxy resonances. Although not the case in all examples, this multiple peak splitting feature is highly advantageous in terms of accuracy as it minimises baseline errors. The same three-component system allowed ee determination for a number of model chiral amines and in fact worked for species with remote chiral centres at positions up to five bonds away from the amino group.[197]

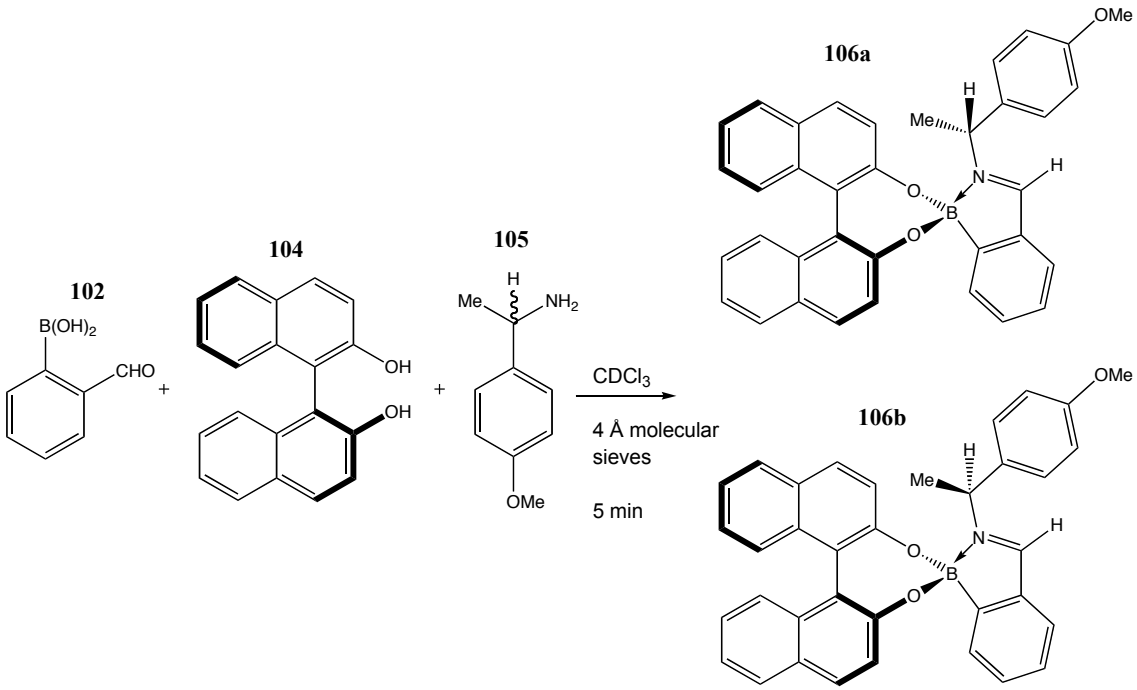

Scheme 31 The first of a series of three component chiral derivatisation methodologies employed by the group.

The group have studied various scope developments; the system was adapted via the use of *S*-α-methylbenzylamine **107** in the place of binol to determine enantiomeric excess for chiral 1,2-diols and the original scheme for primary amines can operate for mono-BOC protected diamines. Some simple diamines can be resolved using (1*S*,2*S*)-hydrobenzoin as the enantiopure component with no protecting group.[198]

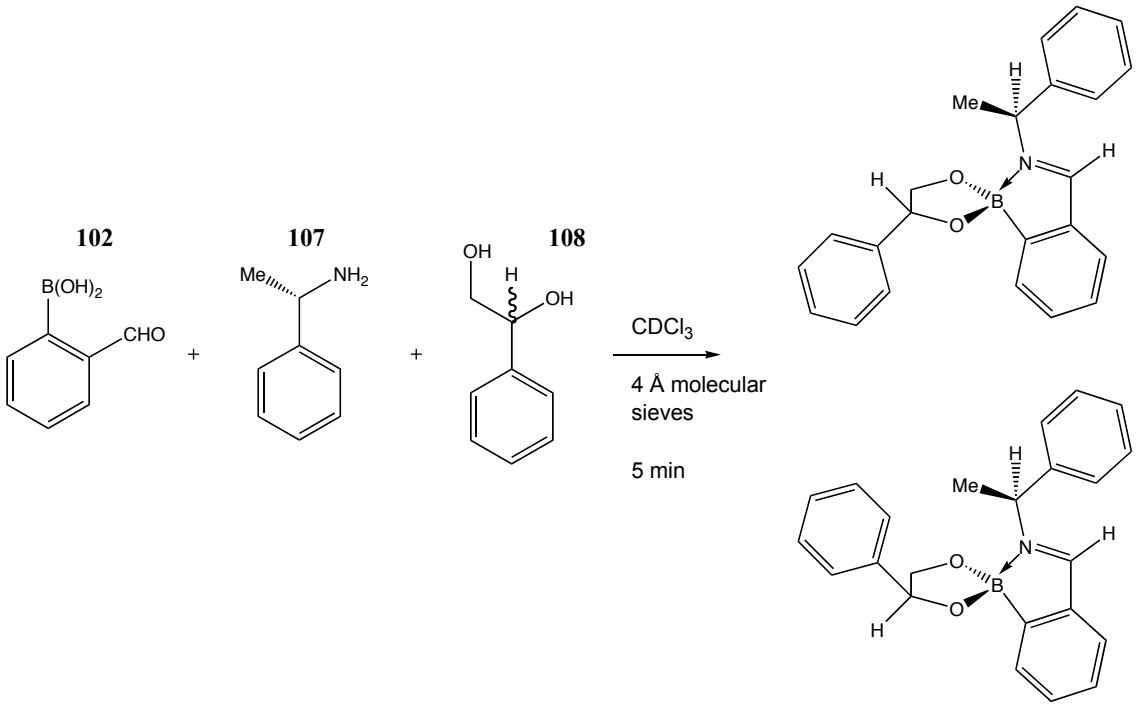

Scheme 32 Protocol developed in the group for determining the enantiomeric excess of a range of diols, illustrated with *rac*-1-phenyl-1,2-ethanediol **108** as an example.

Amino-alcohols also require a protection strategy prior to derivatisation but simple *o*-silyl protection allows a large number and variety of compounds to be analysed. In this instance the greatest resonance splitting was found using methyl-2,3-dihydroxy-3-phenylpropionate as the enantiopure chiral diol in the scheme in the place of *S*-BINOL.[199] Current work is looking at ^{19}F NMR methods.

2.6.2 Preparation of a Highly Fluorescent Macrocycle

Upon attempts to obtain **101**, when 5-methyl-2-aminophenol **109** (the methyl group is a useful analytical handle when compared to using 2-aminophenol **103**) and 2-formylphenylboronic acid **102** were reacted in refluxing ethanol-benzene (95:5) for 12h the expected product was not formed. Instead, the highly coloured, highly fluorescent (qualitative level) macrocycle **110** was formed in quantitative yield, precipitating as a dark orange solid on cooling (Scheme 33).

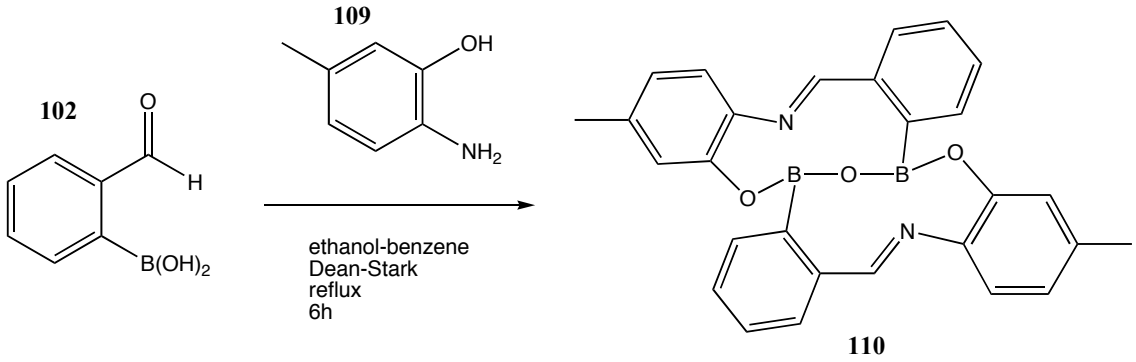

Scheme 33 Formation of a novel macrocyclic species.

Crystals suitable for X-ray diffraction were obtained (discussed below), leading to the discovery that Norman *et al.* had previously isolated a similar compound **111** during the synthesis of arylbenzoxazoles.[200] No anion binding studies were mentioned in the report and this macrocycle has not been investigated elsewhere in the literature. A further search showed that Farfàn *et al.* synthesised a calix[3]arene **112** *via* condensation of 3-aminophenylboronic acid and 3-salicylaldehyde.[201] These calix[3]arenes do not share the interesting feature of a bridging oxygen atom of **110**-**111** and binding studies were not undertaken as the work was aimed at examining self-assembly processes.

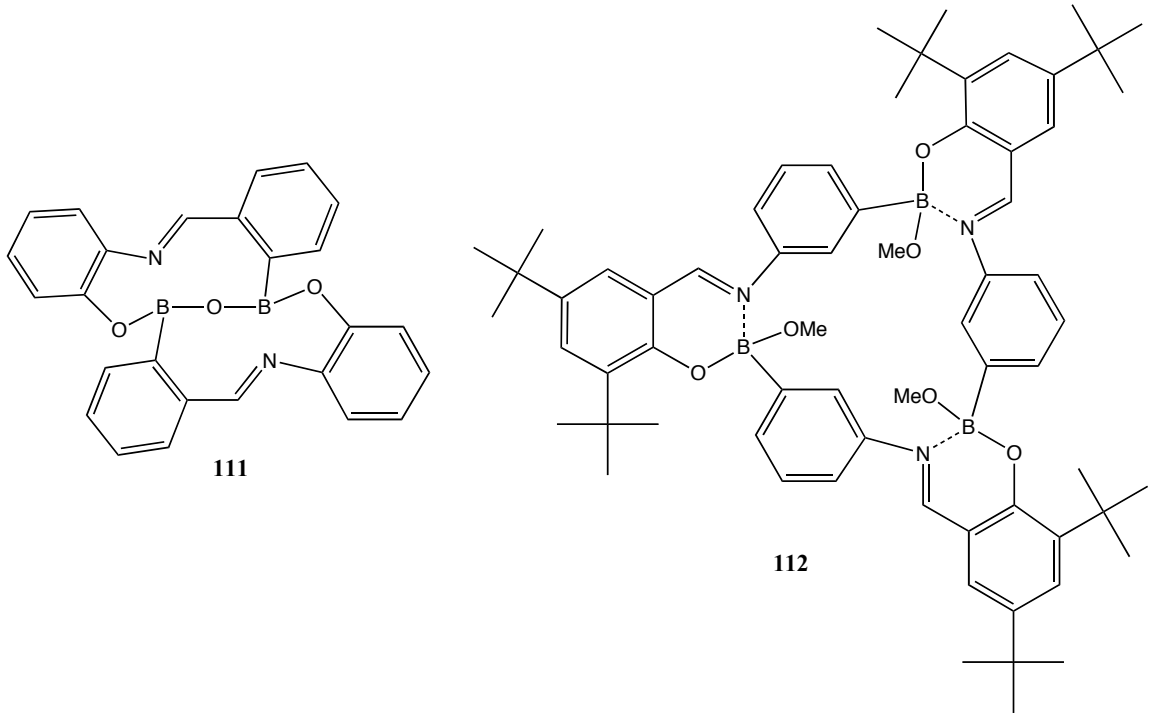

Figure 67 Previously isolated compounds related to macrocycle **110**.

Reaction Scope

Further to the synthesis of **110**, we wanted to examine the scope of this unusual macrocycle formation as well as investigate any anion binding phenomena. The highly coloured and fluorescent nature of **110** also led us to believe the framework showed potential as a biological tag or fluorophore, either binding *via* the boron centres to hydroxyl groups, or by direct covalent linkage *via* a convenient synthetic handle, for example carboxylic acid or amine groups.

With this in mind, a commercially available selection of aminophenols and boronic acids were screened, in order to briefly examine the scope of the macrocyclic formation.

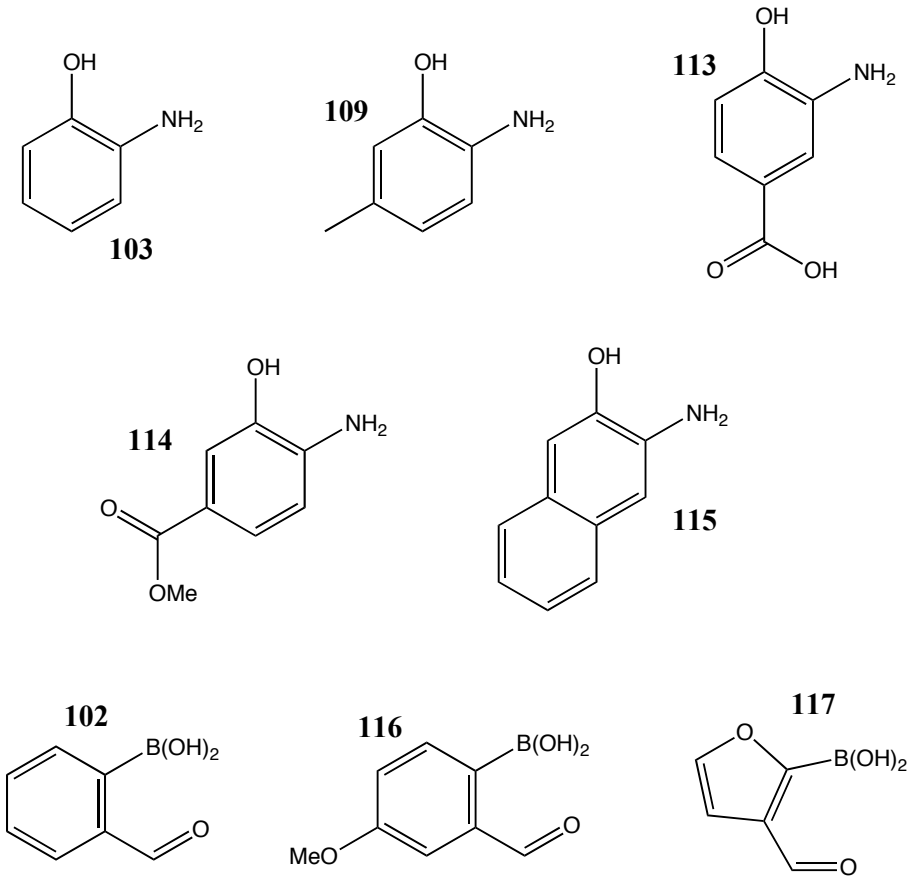

Figure 68 The range of substrates investigated.

Initially, synthesis of the previously reported **111** was repeated using our Dean-Stark method, which afforded the expected product in 90 % yield. Carboxylic acid, methyl ester and naphthyl derivatives **118-120** were successfully isolated using the same reaction conditions, albeit in significantly lower isolated yield (54-64 %).

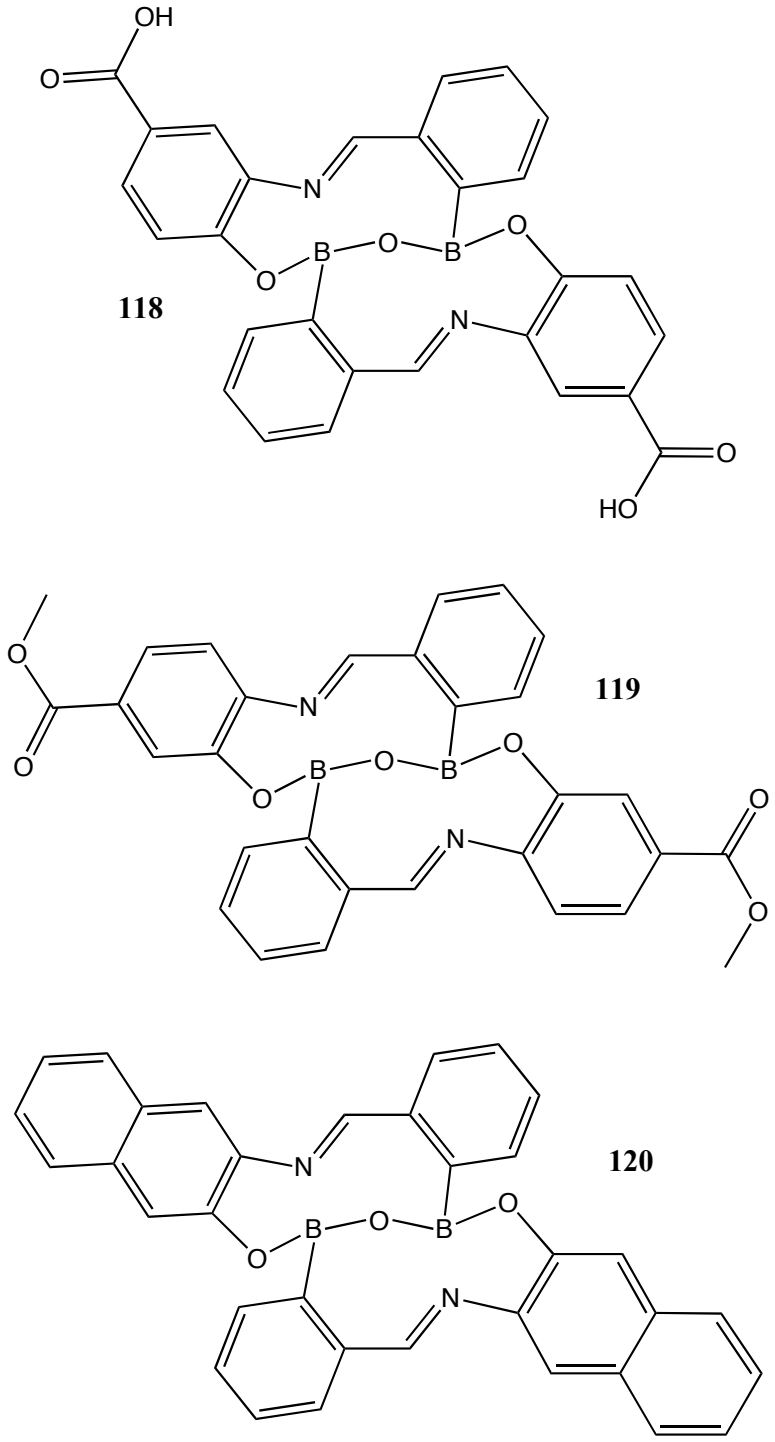

Figure 69 Macrocycles **118**-**120** formed from condensation reactions of 2-formylphenylboronic acid **102**.

Commercially available 2-formyl-4-methoxyphenylboronic acid **116** and 3-formylfuran-2-ylboronic acid **117** also formed respective macrocyclic products **121** and **122** with 2-aminophenol.

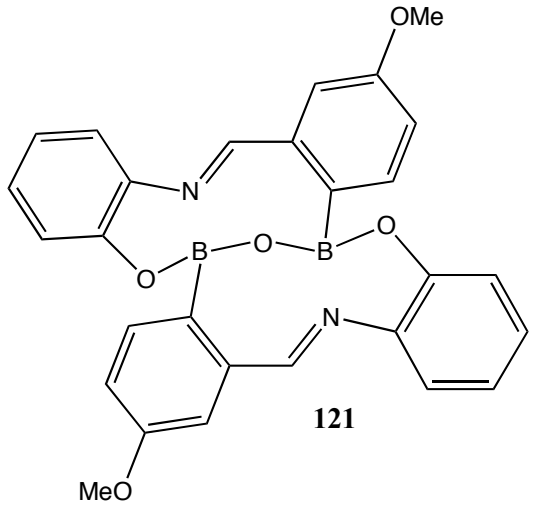

121

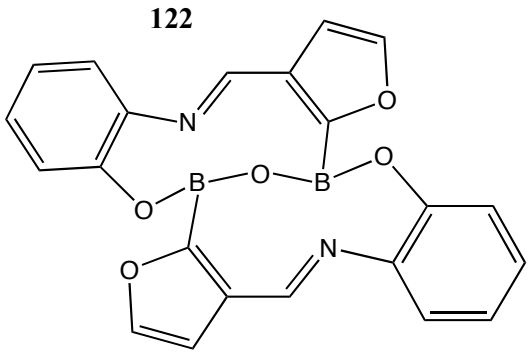

122

Figure 70 Macrocycles formed by varying the boronic acid component.

2-Hydroxy-5-methylaniline **109**, 3-amino-4-hydroxybenzoic acid **113**, methyl 4-amino-3-hydroxybenzoate **114**, and 3-aminonaphthalen-2-ol **115** all failed to cleanly form an isolable macrocycle with either of these boronic acid substrates (**116** and **117**). An issue in the successful but lower yielding reactions was solubility; macrocyclic compounds **110**-**111** are soluble in chloroform or methanol but the brightly coloured solids formed in the formation of **118**-**122** are almost insoluble, even in DMSO. In fact, the majority of the screened reactions prompted the isolation of a highly coloured solid precipitate product that were so insoluble ^{1}H NMR analysis proved impossible.

In an attempt to obtain a macrocyclic species with an amine functionality attached, a common alternative to carboxylic acid linkers in biotag molecules, the condensation of 2-formylphenyl boronic acid **102** and 2-amino-5-((methylamino)methyl)phenol **123** was performed. Compound **123** was prepared from the commercially available 3-hydroxy-4-nitrobenzaldehyde **124** in two steps. The imine generated upon reaction with dimethylamine was reduced *in situ* with sodium borohydride in methanol to form the isolated compound **125** followed by subsequent hydrogenation in the presence of a Pd/C catalyst in good yield.

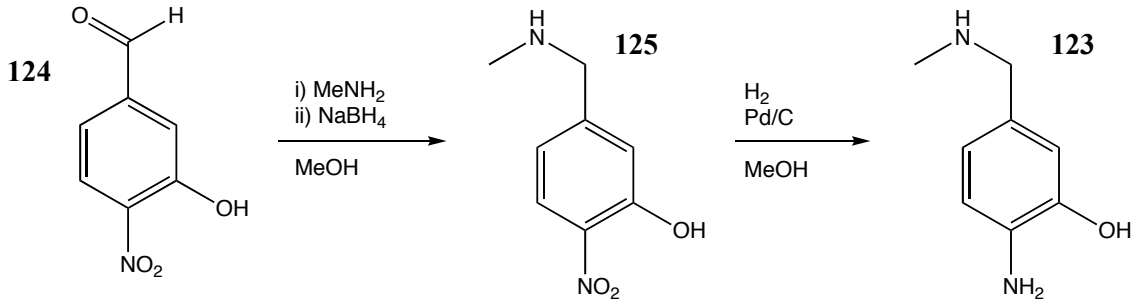

Scheme 34 Synthesis of an aminophenol precursor.

However, on reaction with 2-formylphenylboronic acid in ethanol-benzene, analysis of the crude mixture showed that clean conversion to the desired macrocycle was not observed, with multiple imine protons detected by ^{1}H NMR.

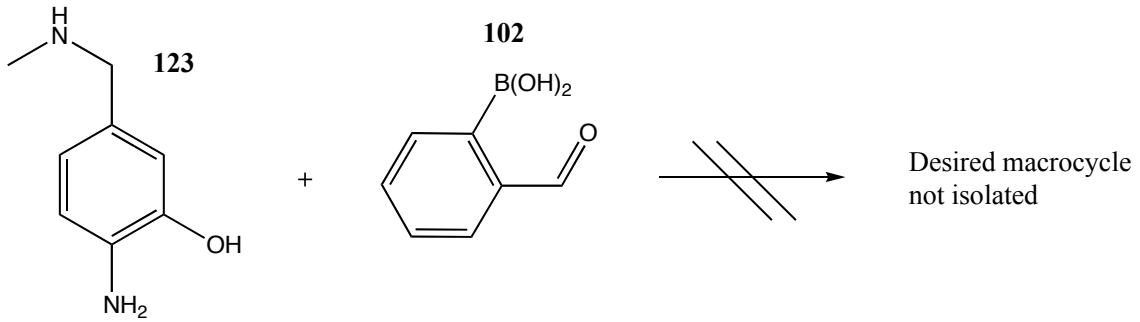

Figure 71 The attempted macrocycle formation of an amine-appended macrocycle proved unsuccessful under the same reaction conditions.

The highly insoluble nature of the crude material prevented any purification by column chromatography or recrystallisation methods. Hot trituration was also attempted but proved inadequate. This reaction may be optimisable but compound **118** does at least show there is potential of using the highly conjugated macrocyclic unit as a fluorophore, with further functionalisation possible at the carboxylic acid moieties.

In further scope and limitation studies performed within the group, a much larger range of aminoalcohols proved suitable substrates in the formation of similar oxygen-bridged macrocycles (for example compounds **126-127**, see Figure 72), proceeding successfully in $CDCl_3$ at room temperature in 5 minutes. Highlighted in a recent article,[202] this work is not discussed here, as the molecules possessed no luminescence properties for recognition studies.

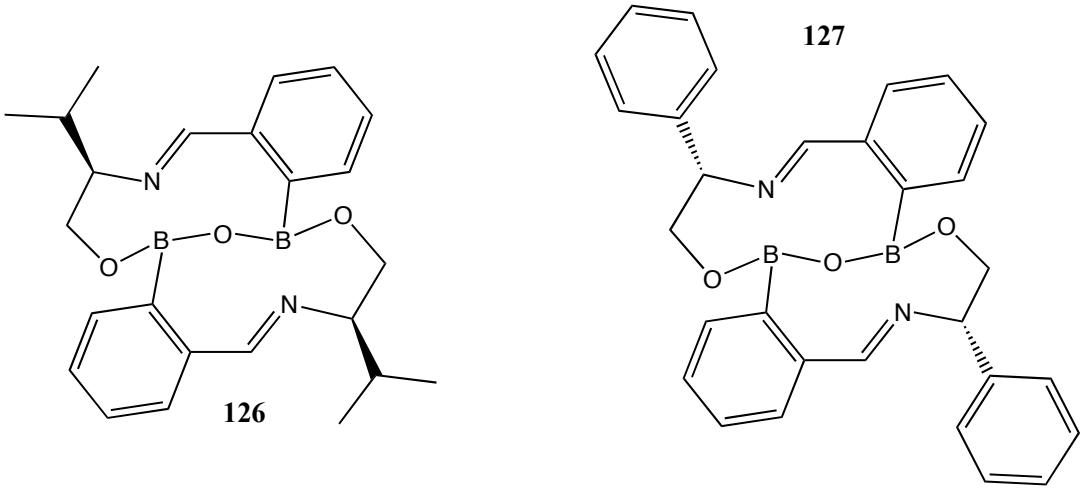

Figure 72 Macrocycles formed by condensation of 2-formylphenylboronic acid and aminoalcohols.

2.6.3 X-ray Crystallography Study.

Crystals of **110** and **111** suitable for X-ray diffraction studies were obtained by slow evaporation from chloroform.

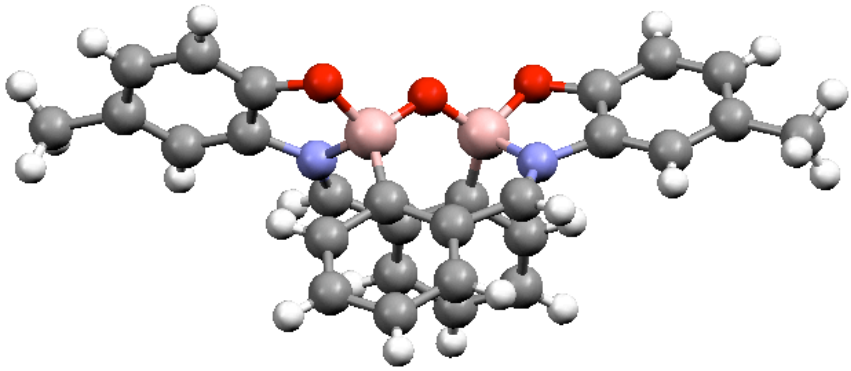

Figure 73 Crystal structure of **110**, as determined by X-ray diffraction studies.

Crystals of **110** were monoclinic, of space group $P2_1/c$ and have the interesting feature of presenting all three oxygens on the same face of the plane bisected by the two boron atoms, a feature which did not hold true for the macrocycles formed from non aromatic aminoalcohols (including compounds **126-127** in Figure 72). The X-ray analysis of crystals of macrocycle **111** confirmed the previous findings of Norman *et al.*[203] Unfortunately the poor solubility of the other macrocyclic species prevented any other crystals being obtained.

2.6.4 FAF Binding Studies

Operating in 4:3 MeOH-$CDCl_3$ (we have found non-deuterated chloroform adversely affects fluorescence behaviour) due to concerns about poor solubility, the fluorescence spectrum of **111** consists of 3 excitation maxima, at 270 nm, 357 nm and 462 nm with a single emission maximum at 515 nm. Fluorescence titrations of **111** with TBAF were performed, exciting at various excitation wavelengths but no significant changes in emission were observed. However, as **111** gave such a strong intensity at low concentrations (experiments were run at 1.0 μM) we were able to repeat the experiments operating in 100% $CDCl_3$. Exciting at 390 nm, the spectrum of **111** shows an enhancement in the peak at 518 nm in the presence of fluoride, but it is not a finite response. Repeat measurements recorded a continuous increase in the intensity over 30 minutes at the same concentration of fluoride. Furthermore, when the sample was left to interact over a longer time period of 8h in a sealed vial, after which the fluorescence emission spectrum was recorded, a general loss of optical activity was observed. This led us to believe the fluoride was not binding in a reversible manner, and ring-opening was likely to be occurring. Extensive investigation was not undertaken based on this observation and we decided to look at avoiding the problematic vulnerability of oxygen-boron bonds to fluoride.

2.7 NH donor equivalent

2.7.1 Rationale

The apparent susceptibility of the boron-oxygen bond in boron phenolates to fluoride mediated cleavage provides an interesting comparison of the nature of the two smallest halide anions. However, in seeking a fluoride sensor the functional group is inherently flawed and chloride binding does not occur preferentially in the presence of fluoride anions**.** One point to consider is that chloride sensors based on hydrogen bond donors that do not interact favourably with fluoride are extremely rare. Despite these limitations the potential of a bidentate sensor based on the biaryl skeleton remains and in fact some evidence, in the case of the proposed chloride binding motif, has enhanced this potential further. With fluoride as a target, the binding cavity would ideally be

smaller and rely on Lewis Acid boron interactions as opposed to weaker hydrogen bonding interactions.

Ease of synthesis is highly desirable when investigating any novel chemical sensing concept and a short synthetic route is highly desirable in any practical sensor system. For application purposes, obtaining a versatile, robust, sensor of perfect selectivity and sensitivity *via* lengthy, expensive synthesis is far inferior to developing a working system that can be easily accessed.

Incorporating a Lewis acidic boron binding site further from the proposed binding zone was felt likely to lead to a loss of sensor integrity. That is, if bidentate binding did occur, incurring defined conformational change in the biaryl system is far more difficult as the binding sites are situated in a vastly different environment, distantly associated with the signalling unit. Figure 74 shows the sensor immediately seen as accessible from bisphenol **95**.

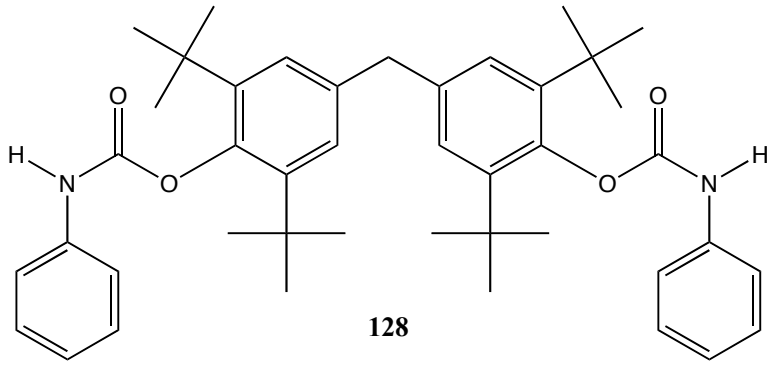

128

Figure 74 Target molecule not bearing F^- vulnerable B-O linkage.

Compound **128**, whilst it uses a different binding site, shares the same number of bonds between the oxygen and the hydrogen bond donor as bisphenolate **90**, albeit it *via* a NH as opposed to an OH group. The precedent for using NH donors is substantial, with examples for both fluoride and chloride. Of particular note is calixarene **53** synthesized by Diamond and co-workers (Scheme 18).[131] The chloride anion is thought to be binding in a tetrahedral geometry *via* 4 NH hydrogen bonds which induced interruption of a pyrene excimer emission. The compound shows selectivity for chloride even over fluoride showing if a suitable binding site is engineered it is possible to utilise NH donor groups successfully. However, the synthesis of this calixarene is not trivial and

the isolated yield after preparative HPLC is only 2 %. Our simple biaryl could serve to provide a more accessible chloride sensor based on a similar binding motif, albeit with a different mode of signalling. Although selectivity of chloride over fluoride is implausible, a differing interaction with the two halides is conceivable, as although both anions are capable of hydrogen bonding interactions, only fluoride is likely to induce deprotonation.

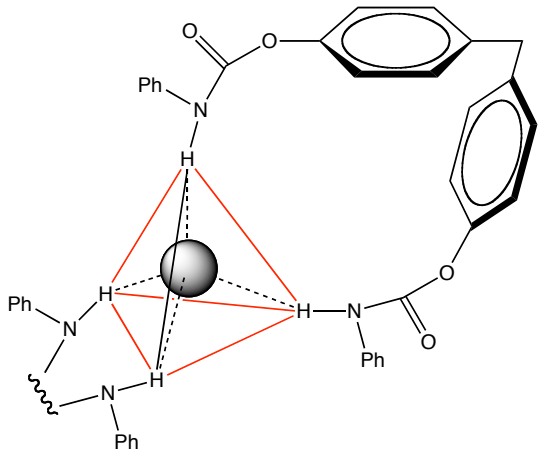

Figure 75 Proposed chloride binding between two molecules of **128**, *tert*-butyl groups omitted for clarity. Hydrogen bonding interactions are shown as dashed lines, the outline of the tetrahedral environment indicated by red solid lines.

Chloride sensors are so poorly represented in the literature that any insight gained into studying possible novel avenues of binding chloride is valuable. An ideal outcome of this work would be to isolate a sensor which shares a chloride binding response with bisboron(phenolate) **90** that displays a different optical response on reversible binding to fluoride.

2.7.2 Synthesis of Compound 128

Bisphenol **95** is by far the most convenient starting point for any subsequent functionalisation and immediately, in seeking to form the bis(carbamate) species **128** required, isocyanates appear to be the perfectly set-up reaction partner. Although literature precedence of such hindered substrates is limited, simpler phenols have been shown to react with phenylisocyanates to form the corresponding carbamates with and without the use of catalysis.[204, 205]

A variety of conditions were trialled in an attempt to isolate **128**. Initially, direct formation of the bis(phenylcarbamate) from **95** using phenylisocyanate with or without triethylamine as base in refluxing toluene was unsuccessful. A heterogeneous clay catalyst, K10 montmorillinite, exposed to microwave conditions, has been used to generate a range of carbamates[206] from the corresponding phenols and urea starting materials but no desired product was detected on work-up of the attempted reaction of the hindered **95**. A further preparation, using copper chloride as catalyst in dry dioxane also resulted in recovery of the starting materials.[205]

Generation of an acid chloride from the alcohol *in situ* and subsequent reaction with a suitable amine can lead to phenylcarbamate formation. Phosgene gas is a highly toxic and poisonous gas but triphosgene reagent is air-stable solid and if kept in the fridge and handled with care, a safer alternative. In DME, acetonitrile and THF solvents with various bases only starting materials were detectable by ^{1}H NMR analysis of the crude mixtures after 24 hours.

The synthesis finally proceeded successfully as expected *via* the use of a Tin (II) catalyst.[207] Purification by column chromatography afforded **128** in good yield (78 %, Scheme 35). The singly substituted product **129** was also isolated from the column, which would be useful if the bis(phenylcarbamate) showed useful binding to chloride, allowing us to compare the species with single or dual binding sites.

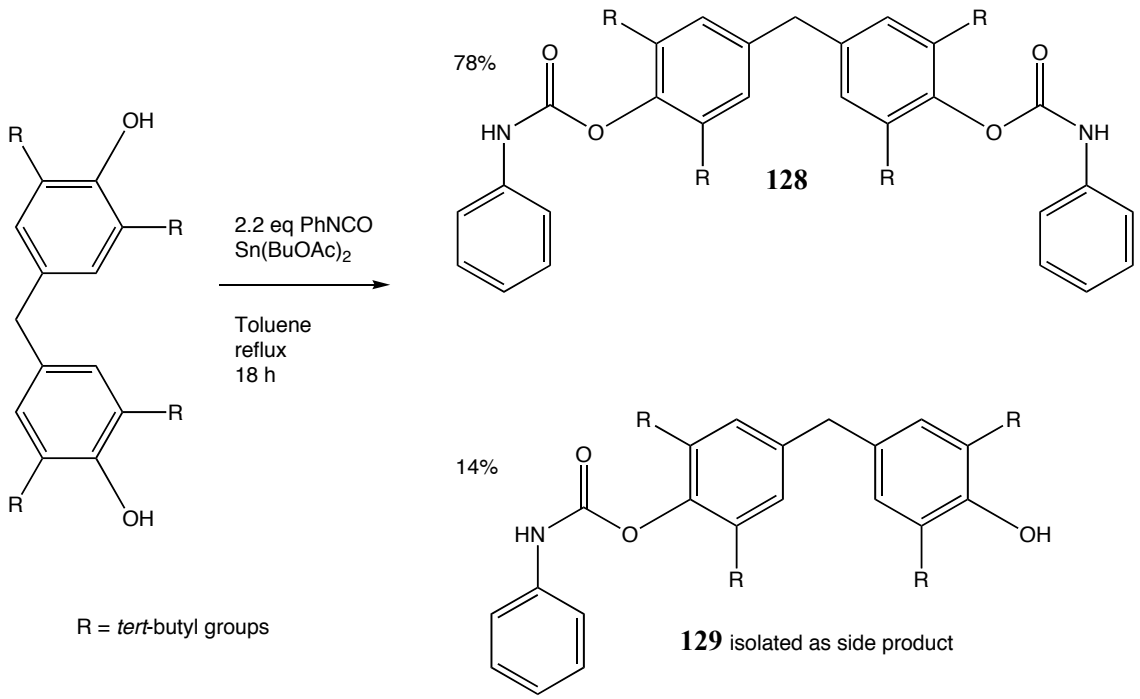

Scheme 35 Preparation of **128** was facilitated by use of a tin(II) catalyst.

2.7.3 X-Ray Crystal Structure

Crystals of **127** suitable for X-ray diffraction analysis were grown virtue of vapour diffusion between a chloroform-hexane system and found to adopt a similar 'propeller' or pseudo C_2 symmetric structure to that of anhydrous bisboronphenolate **90**.

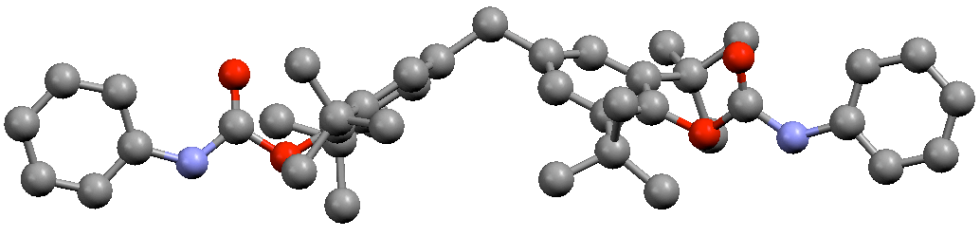

Figure 76 Structure of **128** as elucidated by X-ray diffraction studies.

2.7.4 Fluorescence Binding Studies

Exciting at 270 nm, compound **128** exhibits a maximum emission at 300 nm in dichloromethane solution. Fluorescence spectra were recorded for **128** in the presence of the target anion chloride and the same anions as sensor **90** (bromide, iodide, acetate,

phosphate and fluoride). Disappointingly, even in the presence of a large excess of chloride, no emission changes were observed in the spectrum of **128**. Only fluoride induced significant changes in the emission profile. A fluorescence titration was performed against fluoride to investigate the emission response fully.

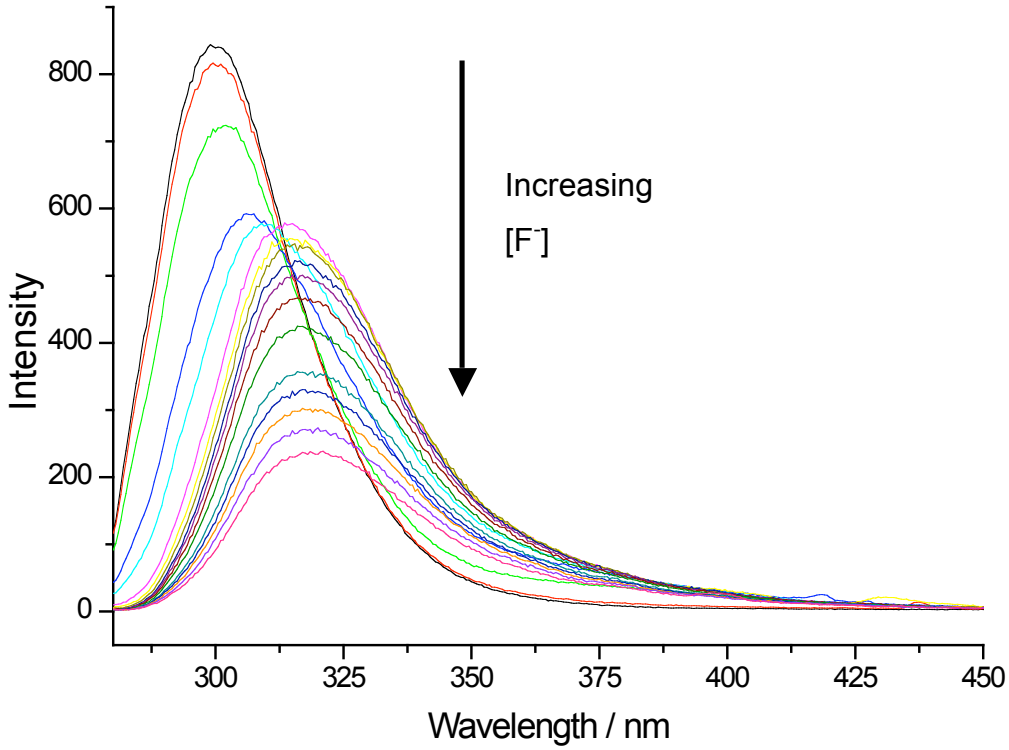

Figure 77 Plot showing overlaid spectra of **128** titrated against TBAF in DCM. λ_{ex} 270 nm, [**128**] 0.1 mM, [F^-] 0.1-1.7 mM.

The initial maximum at 300 nm shifted to 318 nm across the concentration range examined and a large quenching effect was observed. The emission profile is divided into three distinct phases, with dramatic intensity quenching observed between 0.0 – 0.3 mM fluoride and then a subsequent shift with diminished quenching between 0.3 – 0.6 mM. Above 0.6 mM the wavelength of the maxima remains at 318 nm, quenching in an approximately linear fashion.

2.7.5 ^{1}H NMR study of compound 128

^{1}H NMR spectroscopy was used to examine any hydrogen bonding or deprotonation events occurring in solution in the presence of both chloride and fluoride. All titrations

were recorded using a 500 MHz Bruker Avance operating in $CDCl_3$ media. All spectra can be observed in **Appendix**, **Section 6.2.1.**

Titration against TBAC

The NH signal of **128** appears at 6.98 ppm, upfield of the aromatic triplet peak at 7.11 ppm and the singlet of the biaryl aromatic protons at 7.18 ppm. At equimolar concentration of TBAC, the NH peak shifts slightly to 7.01 ppm and the other aromatic signals remain unchanged. However, at 10 equivalents of TBAC, the peak corresponding to the NH has shifted to 7.16 ppm, now appearing downfield relative to the triplet at 7.11 ppm and also to the slightly upfield shifted 4H singlet now appearing at 7.14 ppm.

The ^{1}H NMR data shows NH···Cl^- hydrogen bonding may be occurring but with no optical emission changes by UV or fluorescence methods, this molecule is thought not to bind in a bidentate fashion. This result also indicates hydrogen bonding does not necessarily translate into observable emission changes.

Titration against TBAF

The original NH signal at 6.98 ppm shifts to 7.02 ppm at equimolar concentration of TBAF and integrates slightly lower to 1.6 protons, disappearing completely at 2 equivalents of TBAF implying deprotonation is occurring. At 10 equivalents of TBAF, the aromatic peaks at 7.35, 7.18, 7.11 are shifted slightly upfield relative to the unchanged peak at 7.50 ppm, potentially reflecting the slight shielding effects caused by changing conjugation across the aromatic system upon complete deprotonation.

2.8 Summary

Previous work within the group on the synthesis of the first bisboracalixarene, and some initial robustness testing of phenyl(boronate) synthesis prompted the proposal of a model for a conformational sensor intended to take advantage of the tendency for fluoride anion to form a μ-bridging binding motif. The two arms of the sensor were designed to provide structural integrity in the form of a restricted range of rotation and allow modular synthetic modification. Several phenyl(boronates) were synthesised with the intention of testing the model. Unexpectedly, interaction with fluoride anion was

found to be dissociative, with elimination of a phenylfluoroboronate species. The resulting phenoxy anion, in the case of 2,6- dialkyl substituted examples, undergoes an oxidative process, thought to include the stable phenoxyl radical, to give a dramatic colorimetric response. Electrochemical measurements were carried out, confirming the proposed oxidative degradation. This observation shed light on the bisboracalixarene synthesized previously. The parent phenols are found to undergo similar processes *via* deprotonation and in fact several 2,6-disubstituted phenols show impressive selectivity. Of particular note is the lack of any visible colour change by naked eye in the presence of acetate, phosphate, chloride, bromide or hydroxide anions over a time period of 24h.

Compound **90** was synthesized specifically to fit the model and showed a rare associative binding response with chloride anion. A plot indicative of 2:1 receptor-anion binding was obtained, with fluorescence emission changes recorded at 375 nm. Good selectivity over bromide anion was observed. The model was tested with compound **91** - possessing only a single receptor site - which showed only a small quench of the emission in the presence of a vast excess of chloride anion indicating the presence of two binding sites were required to achieve binding. ^{1}H NMR showed some evidence of hydrogen bonding occurring *via* hydroxyls on boron. Although attempts to isolate a chloride bound species were unsuccessful, X-ray diffraction studies provided some possible insight, with the comparison of **90** and **90**·H_2O species showing one possible mode of host-guest complexation.

Nitrogen-boron interactions play an important role in saccharide sensors and this was investigated in terms of the fluoride labile oxygen-boron bond leading to the serendipitous discovery of a highly conjugated macrocycle **111**. A similar compound had been synthesized by Norman *et al*. but no analyte binding studies had been documented. A small investigation of the scope of this reaction was investigated, with several analogues successfully isolated including a carboxylic acid derivative, a useful synthetic handle, highlighting the potential of this class of molecule as a biotag or fluorophore. 2-formylfuranboronic acid also generating a macrocycle with a strongly tetrahedral boron. Unfortunately, no useful fluoride binding response was observed with this class of compounds.

A biscarbamate **128** was prepared in an attempt to prepare a simple species which shared as many features as possible as sensor **96** but was unlikely to decompose in the presence of fluoride. A response to fluoride was expected but it was thought that the sensor would demonstrate a different response relative to chloride. The carbamate NH groups were incorporated to act as the hydrogen bond donors in this case. Despite significant downfield shifts of the NH protons in ^{1}H NMR in the presence of chloride, no optical changes were observed. Compound **128** showed interesting quenching and bathochromic shifted emission responses with increasing concentrations of fluoride, thought to translate to hydrogen bonding and subsequent deprotonation processes.

3 RESULTS AND DISCUSSION II

Design and Synthesis of Fluoride Stable Boron-Based Sensor Framework and Study of the Anion Binding Properties of a Novel Receptor Motif.

3.1 Overview of R&D II

Chapter 3 describes the design and synthesis of novel molecular sensor frameworks aimed at taking advantage of the bidentate behaviour of **90** with chloride anion but targeting the fluoride anion discussed in Chapter 2. Chemosensors that are likely to have commercial applications should be synthetically simple but the synthesis of a sensor that avoids the inherent incompatibility with the aggressively Lewis basic fluoride of the phenyl boronate compounds described in Chapter 2 was thought to be quite challenging, particularly in light of the sterically hindered substrate. However, significant progress was made despite the demanding substrates involved. Derivatised boronic acids were the focus, as they were deemed superior to the hydrogen bonding type sensors, due to the non-dissociative nature of the interaction and their high selectivity for fluoride anions.

Although unlikely to be binding fluoride in a manner fitting the model described in Chapter 2, a novel compound **153** is isolated which shows interesting potential as a fluoride sensor in organic media, with all evidence indicating a non-dissociative molecule-anion interaction. This led to the binding behaviour of a previously unexamined sp^2 boron centre being investigated *via* the preparation of a model compound.

3.2 Improving the Biaryl Motif

3.2.1 Refining the Model

With the focus on aromatic boronic acid receptor units, there are a few possible methods of introducing them into the biaryl framework. The nature of the bonds formed in the resulting species must maintain the structural integrity of the model detailed in Chapter 2, that is not become entirely flexible in three dimensions and ideally complement the

signalling mechanism. Assuming our two or four point binding mode was accurate, we did not want to increase the size of the potential binding pocket. As fluoride is significantly smaller than chloride, and it would interact with the boron centres preferentially over hydrogen bonding with the hydroxyls, a smaller cavity was desired. Counter-intuitively this may mean the molecule would be larger, with the two 'arms' longer to create a tighter two-point binding. If achieved, any binding should also be stronger, as it would be a Lewis acid - Lewis base interaction compared to a series of $OH\cdots Cl^-$ hydrogen bonding interactions. Figure 78 below shows a range of molecules that were given consideration as new targets.

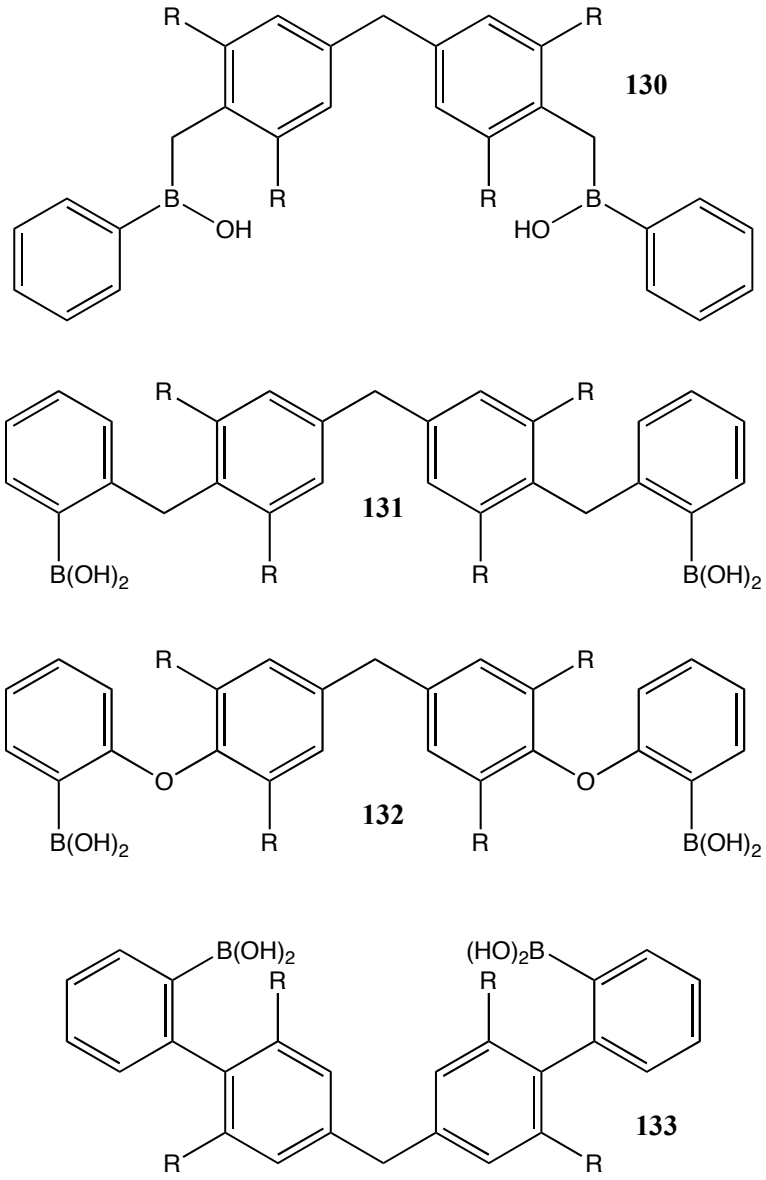

Figure 78 Some possible sensor targets that fit the model in Chapter 2 but are less likely to degrade in the presence of fluoride anion. R = bulky substituent.

As boronate bonds need to be avoided due to their susceptibility to cleavage in the presence of fluoride anions, it may be possible to replace the linking oxygen in sensor **90** directly with a carbon atom (general structure **130**). However, there is no synthetic precedent for dealing with this unusual motif or benzyl boronic acid derivatives such as **131**.

One of the simplest in terms of the number of synthetic steps is a bis(diarylether) type construct (general structure **132**). The parallel to compound **90** discussed in Chapter 2 is apparent, with a flexible C-O-R link and two proximal receptor sites. Although there is some precedent for Cu-catalysed[208], Ullmann type reactions[209] or Pd-catalysed[210] formation of sterically hindered biaryl ethers, it is fairly limited. In addition to the limited number of highly active catalysts for this type of transformation, we wished to avoid any C-O bonds, which we regarded as potentially vulnerable to fluoride.

Another alternative is incorporating the binding site using a linking moiety that introduces further conjugation, for example a triazole ring. This may lead to beneficial spectroscopic properties, for example longer wavelength responses to any binding events.

The biaryl type species **133** appeared to offer the most robust framework. Whilst synthetically challenging, connecting a phenyl ring directly to the terminal positions of the biaryl motif *via* a carbon-carbon bond offers some interesting potential advantages. The introduced phenyl rings would sit almost perpendicular to the bulky alkyl group appended diphenyl methylene system limiting conformational flexibility and potentially pre-organising the receptors into a bidentate binding orientation. However, conversely, the same feature could result in a high energetic barrier to bond rotation, potentially promoting 1:2 sensor-guest interaction. Carbon coupling reactions of sterically hindered substrates, whilst not trivial, have received a huge amount of attention in the literature and so more catalyst systems have been examined compared with the biaryl ether case.[211] Crucially, this compound is extremely unlikely to degrade in the presence of fluoride making.

3.2.2 Targets and Retrosynthetic Analysis

From a retrosynthetic point of view, the species we wanted to prepare essentially consisted of two unsymmetrical biaryls, linked by a methylene group. Unsymmetrical biaryls can be synthesized in a variety of ways but the most commonly used are transition metal catalysed cross-coupling reactions. Figure 79 shows the primary retrosynthetic disconnection and the opposing coupling partners realised.

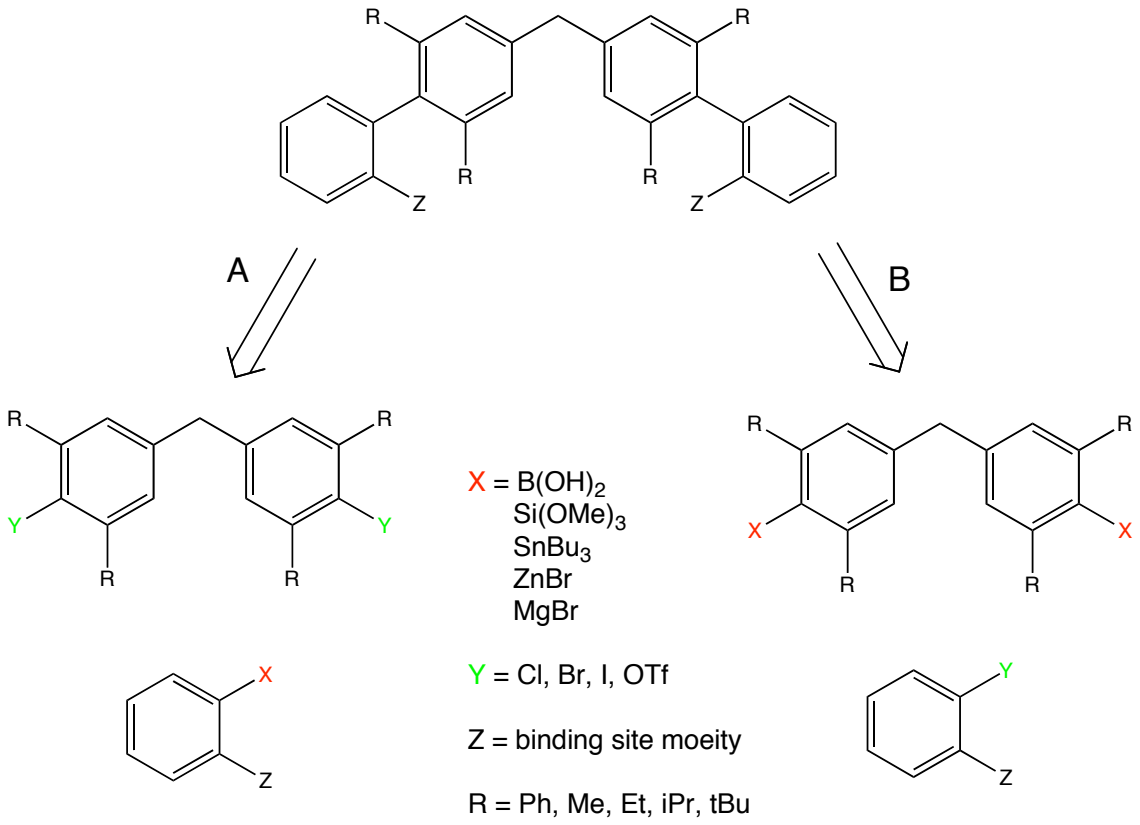

Figure 79 Retrosynthetic analysis of the general target motif.

There is a huge range of transition metal catalysed carbon-carbon coupling reactions to consider. Palladium catalysed Suzuki, Stille, Hiyama coupling reactions, and also Kumada (also Ni catalysed) and Negishi couplings (Ni, Al). Suzuki-Miyaura reaction has several advantages which is why the transformation has seen so much use in industry and received so much research interest. A Suzuki-Miyaura coupling consists of reacting an aryl halide or triflate with a boronic acid or boronic ester (Scheme 36).

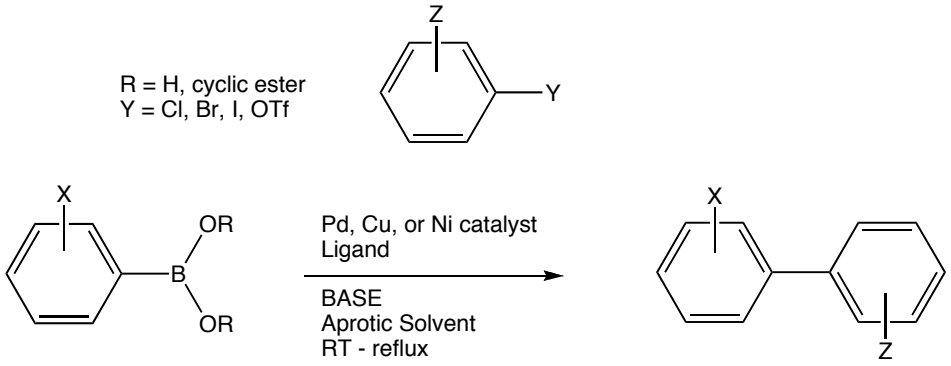

Scheme 36 The Suzuki-Miyaura Cross-Coupling Reaction.

A base, typically inorganic (eg sodium sulfate, potassium carbonate) is required to achieve conversion to product. There are two proposed reaction pathways explaining the role of base in the Suzuki-Miyaura reaction. The first is that the base serves to activate the boronic acid derivative to transmetallation, the second is that the anionic component of the base replaces the halide in the coordination sphere of the palladium complex. Either possibility, and it may be that the base performs both roles simultaneously, facilitates the transmetallation step.

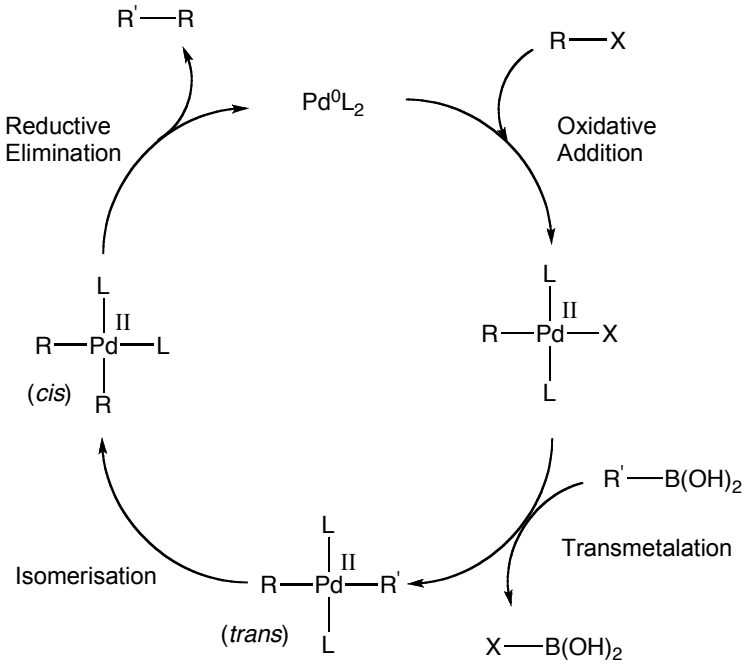

Scheme 37 Proposed catalytic cycle for the Suzuki-Miyaura Cross-Coupling reaction.

Generally, boronic acids, particularly when compared with the equivalent alternative coupling partners (eg tin species in Stille couplings are highly toxic), are easy to handle,

low toxicity, air-stable compounds. Suzuki chemistry is possibly the most versatile, with deactivated substrates such as aryl chlorides being shown to be suitable, in the presence of a designed active catalyst, for coupling even at room temperature. A wide-range of functional groups and steric hindrance can be tolerated and removal of the metal post-reaction is typically performed by simple filtration through Celite.

Steric hindrance was the main problem to overcome in the planned synthesis and although early Suzuki protocols with $Pd(PPh_3)_4$ (palladium tetrakis) fail to couple sterically hindered, demanding substrates, more recently developed catalyst systems show much greater scope. Ligand design has been an area of huge focus in the recent literature, with sterically crowded phosphines and *N*-heterocyclic carbenes facilitating reactions at extremely low loadings. Buchwald's catalysts S-PHOS (**134**) and X-PHOS (**135**) show precedent for 2,6-diisopropyl, dimethyl, di-*tert*-butyl substituted aryl bromides with phenyl boronic acids.[212, 213]

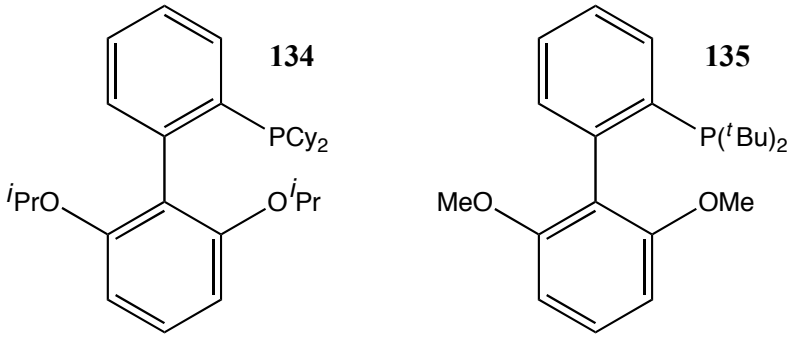

Figure 80 Buchwald's catalysts for Suzuki-Miyaura coupling reactions involving sterically hindered aryl halide substrates.

One inelegant aspect of using Suzuki methodology is the loss of a boronic acid moiety in the coupling process when an identical functionality is required in the final product. This may prove to complicate the synthesis, requiring protecting group strategy or chemoselective protocols. However, synthesis involving two different metallic coupling partners in the presence of a labile aryl halide may actually lead to a loss of synthetic control and require boronic acid protection anyway. These concerns, together with the low toxicity, relative ease of handling and synthesis of precursor substrates and depth of precedent combined to led us to initially utilise Suzuki-Miyaura chemistry.

3.2.3 Synthetic Considerations

General

Coupling reactions facilitated by traditional Suzuki catalysts, such as palladium tetrakis or Pd(dppf) are very low yielding or do not proceed at all with highly hindered aryl halide substrates. Also, deborylation or homocoupled products are common side reactions using these catalysts. Reactivity of the aryl halides vary according to the reactivity series I > Br ~ OTf > Cl. This hierarchy is due to the increasing ease of Pd insertion into the C-X bond down the group (bond energies of the carbon-halides: C-Cl = 330 $kJmol^{-1}$, C-Br = 288 $kJmol^{-1}$, C-I = 216 $kJmol^{-1}$). The substrates used to show catalytic scope in the literature are almost exclusively monoboronic acid and aryl halide, whereas our system required a double coupling reaction. A slight excess of boronic acid is typically utilised in Suzuki reactions, and often 2-4 equivalents of base are required to push a demanding substrate to complete conversion. Both these facts will have to be taken into account when attempting the crucial carbon-carbon bond forming step.

Route A

Working *via* this disconnection leads to a potentially shorter synthesis. If it is possible to mono protect a phenyldiboronic acid and subsequently react that with the bis arylhalide backbone then the need to synthesize potentially challenging boronic acid intermediates en route to the final bisboronic acid is avoided. It should be pointed out however, that a search of the literature reveals no Suzuki-Miyaura coupling reactions involving benzene diboronic acid. Simply accessing a 2,6-alkyl substituted aryl halide may pose problems but this issue is a feature of both syntheses.

Route B

Highly hindered boronic acids substrates are poorly represented in the literature.[214] Catalysts that have shown superior activity for hindered substrates are rarely relating to di-*ortho* substituted boronic acids. This shows these substrates are likely less available and likely more difficult to synthesize than the hindered aryl halide equivalent. Therefore the ability of the catalyst to function for this type of substrate is not well described. We considered that the steric bulk was vital in dictating the conformational change on binding so must be present in any useful molecular construct. The critical

carbon-carbon bond forming step would require either a protected halophenylboronic acid to prevent homocoupling or a dihalo substrate that is subsequently converted into the final bisboronic acid target. This route would also operate *via* a dihalo backbone which is the final coupling partner for route A, indicating a longer synthesis.

Route A was chosen virtue of it showing a shorter synthetic approach, and the interest in attempting a novel Suzuki coupling with a benzenediboronic acid. Accessing the highly hindered bisboronic acid was deemed a potentially challenging point in the longer B route. The literature is full of examples of sterically hindered aryl bromides but typically relatively unhindered phenylboronic acids are utilised.[213]

3.2.4 Target Molecule

The key intermediate was identified as the general structure **136** after consideration of the synthetic route. Even if Route A fails to proceed at the pivotal carbon-carbon bond formation step, conversion to the boronic acid and hence following Route B can be easily imagined.

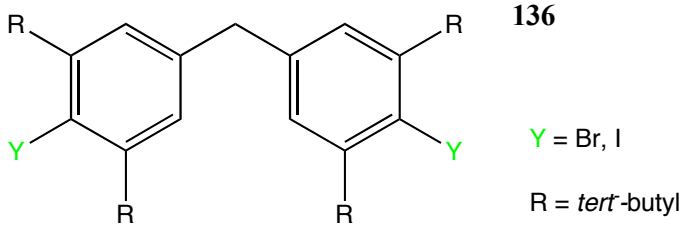

Figure 81 General key intermediate in the proposed synthesis.

In this key desired intermediate **136**, consideration was to be given to the nature of both the halogen and the bulky *ortho* groups. Although aryl iodides are the most reactive of the commonly available substrates for Suzuki-Miyaura couplings, the steric congestion involved appears extreme and very little precedent for these type of substrates was seen in the literature. Also, results for highly active catalysts such as X-PHOS and DuPHOS in reactions involving aryl iodides are not reported. Obviously this could allow for very mild reaction conditions but in light of the lack of precedent, unpredictable results could be foreseen. Aryl bromide activity is better described and seen as a compromise in terms of size and reactivity. Either bromide or iodides were seen as attractive substrates. Using *tert*-butyl groups maintains a direct comparison with the work on

sensors described in **R&D I** allowing a more disciplined approach to understanding any binding discovered as the basic motif is not altered. However, consideration was given to less demanding alkyl substituents.

3.2.5 Commercially Available Starting Materials

A detailed search of potential starting points with suitable steric hindrance yielded the group of reagents shown in Figure 82. Halogenated species were not available, restricting our starting materials to phenols and a limited selection of anilines, with no examples of *tert*-butyl substituents.

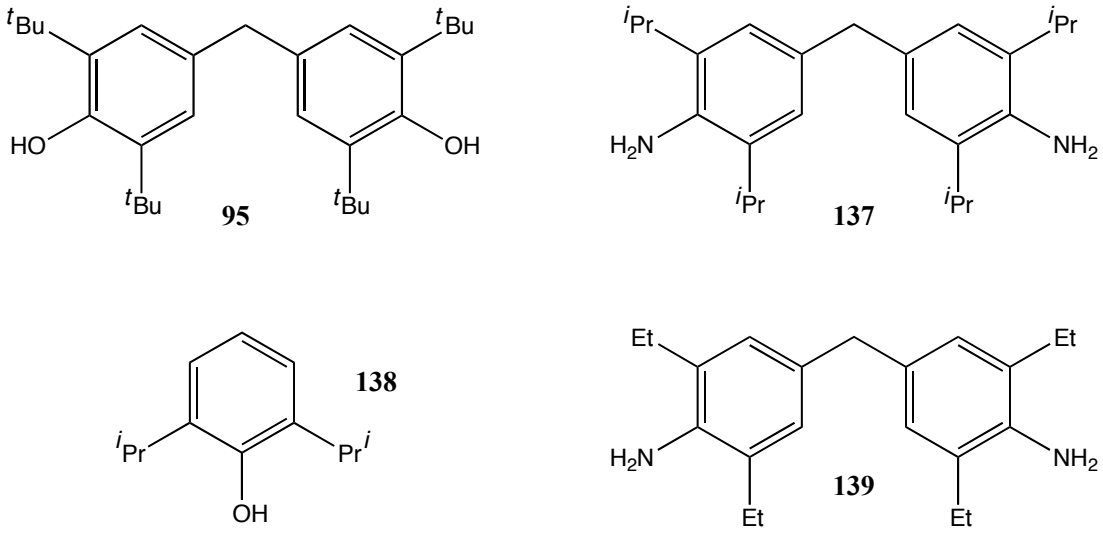

Figure 82 Some commercially available substrates.

3.3 Synthesis and Characterisation of Key Intermediate

3.3.1 Phenol starting material

Direct conversion from the phenol to the aryl halide was investigated. Formation of alkyl halides from the corresponding alcohols can proceed using phosphorous tribromide or thionyl chloride reagents. However, direct conversion of aryl substrates appears to be a lot more challenging, and highly hindered substrates are even more demanding.

Initially we attempted to convert bisphenol **95** into the bisarylbromide **140** using phosphine tribromide (PBr_3) in THF with 2,6-lutidine as base but this protocol led to no new products being observed. 2,6-lutidine is a fairly bulky base but switching to triethylamine and *N*-butyllithium resulted in no conversion to the desired product. Toluene and dichloromethane solvents prompted no improvement.

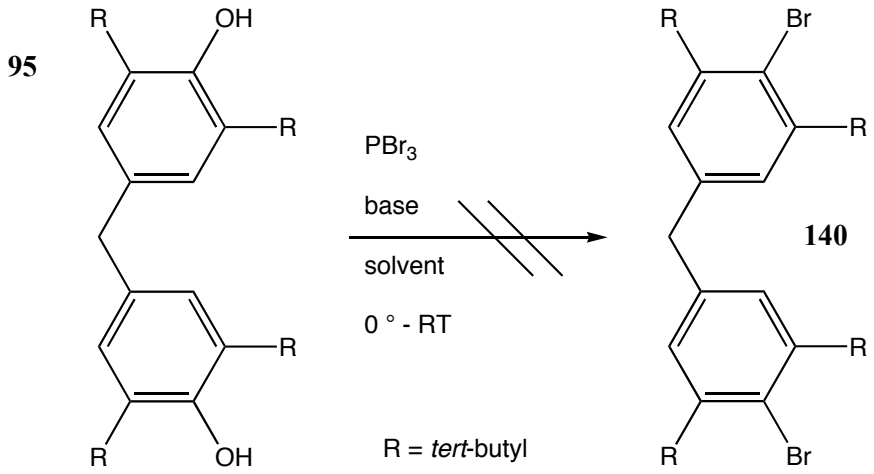

Scheme 38 Attempted conversion of phenol to aryl bromide directly was unsuccessful.

The most common method of obtaining aryl halides from phenolic substrates is *via* formation of the triflate species to create a better leaving group, and then forming a boronate ester which can be converted to the aryl halide using copper (I) bromide.

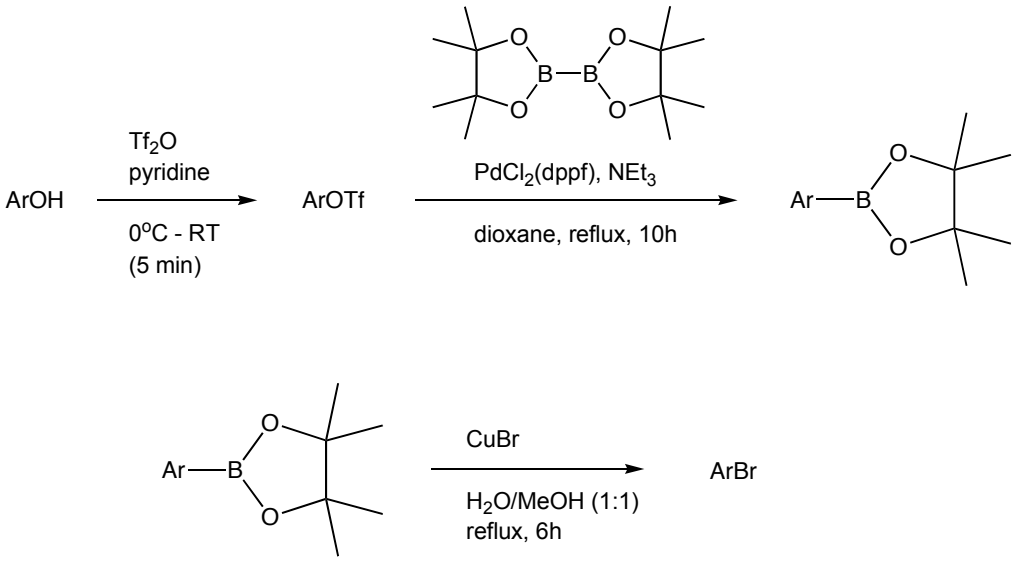

Scheme 39 The classic method of converting phenols to aryl bromides operates *via* a boronic acid derivative.

However, aryl triflates are often used as substrates in palladium catalysed cross-coupling reactions, with similar reactivity to aryl bromides so the aryl triflate itself is an appealing substrate. In addition, the procedure operates *via* another potential Suzuki coupling substrate, that is, a arylboronate species. Taking this into account, accessing a substrate suitable for attempting the critical bond forming reaction was immediately apparent.

4,4-methylenebis(2,6-*tert*-butylphenol) **95** was exposed to triflic anhydride in the presence of base in dichloromethane according to the preparation detailed in a publication by Thompson *et al.*[215] They showed several phenolic substrates to achieve excellent conversion after 5 minutes by TLC.

TLC analysis showed no new products were being formed and to confirm, ^{13}C NMR of the reaction mixture showed no characteristic signals of a triflate species and the OH proton of the starting phenol was still clearly visible at 5.0 ppm in the ^{1}H NMR spectrum of the crude after stirring for 5 minutes. No conversion was achieved with longer reaction times or with the use of triethylamine as base.

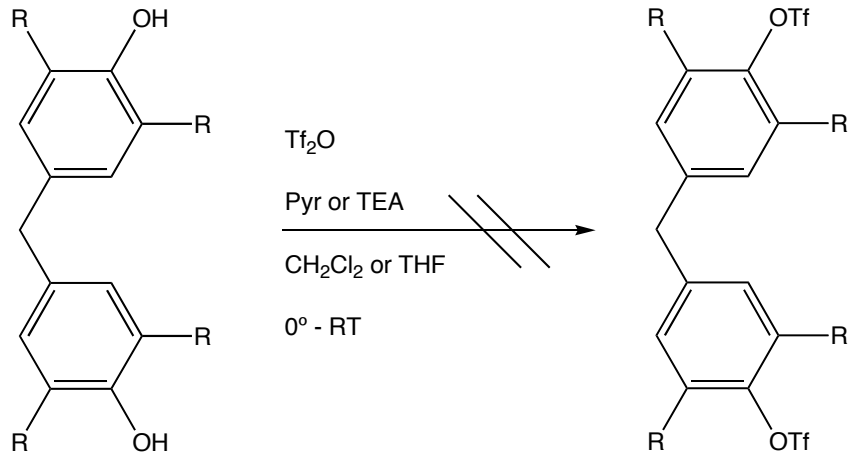

Scheme 40 Conversion to triflate unsuccessful. R group indicates *tert*-butyl group.

If the high degree of steric hindrance around the hydroxyl was causing the issue then reducing the bulk of the *ortho* substituents may have allowed the triflate to be formed but as zero conversion to product was observed, alternative starting materials were considered at this stage.

3.3.2 Aniline starting point

The range of commercially available methylenebis(anilines) compared to their analogous phenols is limited. 2,6-di-*tert*butylaniline and 4,4'methylenebis(2,6-*tert*butylaniline) are not commercially available. As these *tert*-butyl systems were not commercially available, and synthetically possibly too demanding given the lack of progress with bisphenol **95**, the available 2,6-di-*iso*propylaniline **141** was used as the starting material. Acros Organics supply 4,4'-methylenebis(2,6-di*iso*propylaniline) **137** but only at a "minimum 85%" grade purity, and although the ^{1}H NMR and TLC of Acros supplied material appeared to be of excellent purity and quality, we looked at preparing the compound in-house. A literature search showed a base catalysed reaction of 2,6-dimethylaniline in aqueous solution but gives no examples of more highly sterically hindered substrates.[216]

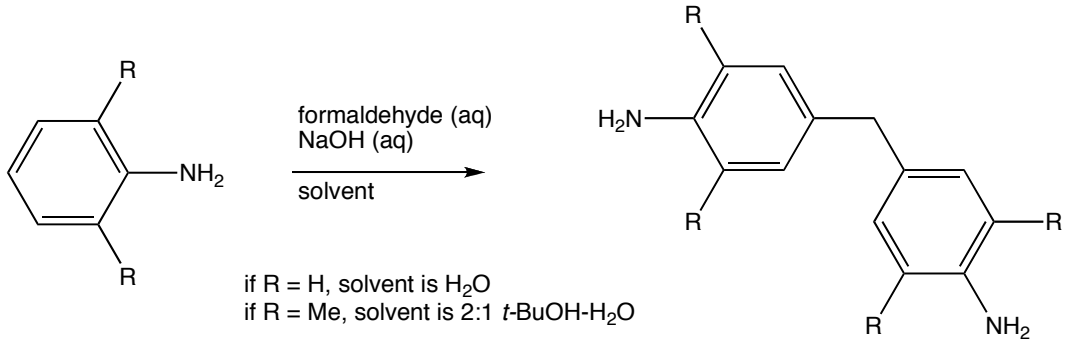

Scheme 41 Literature precedent of base catalysed bis aniline formation.

Solvent appears to play a key role in the success of this reaction, potentially due to the solubility of the starting anilines. Water, found to be the ideal solvent for most anilines, led to isolation of solely starting material in the dimethyl case. Any alkyl substituents increase the nonpolar character of the substrate, becoming poorly soluble in aqueous media. Use of a mixed *tert*-butanol/water solvent allowed for product formation, albeit in lower yield, with no mention of a change in work-up.

Mixed aqueous *tert*-butanol, methanol, ethanol and acetonitrile systems were all trialled but in fact the only solvent prompting reasonable conversions to product was *iso*propanol. In other solvents mostly starting 2,6-di*iso*propylaniline was isolated from the organic extracts. Column chromatography in pentane afforded the desired bisaniline **137** in 64 % isolated yield.

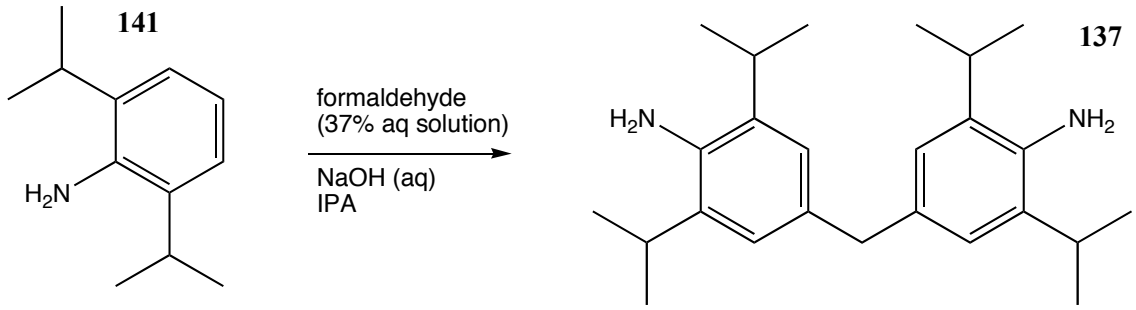

Scheme 42 Solvent optimisation prompted isolation of the desired bisaniline.

A publication by Hunter *et al.* provided precedent of a conversion of sterically hindered anilines to their corresponding iodides *via* the diazonium salt.[217]

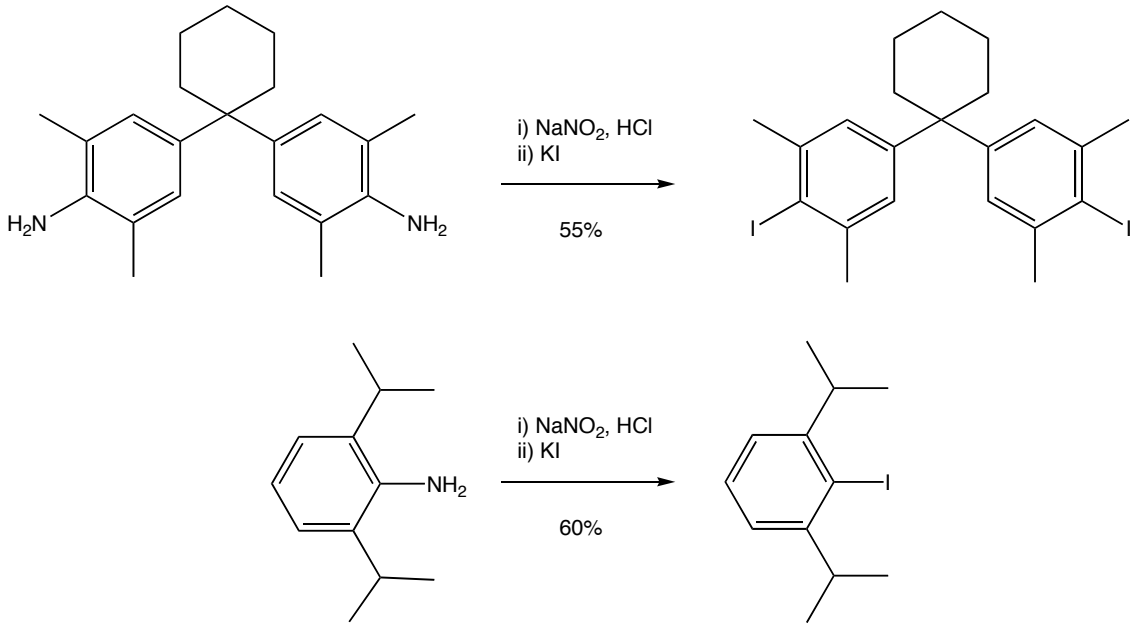

Scheme 43 Literature precedent for diazotisation and subsequent iodination of sterically hindered anilines.

The bisaniline **137** was treated with sodium nitrite under acidic conditions and then reacted with potassium iodide to afford bisaryliodide **142** in 63 % yield. Isolation of the diazonium salt intermediate formed *in situ* was not necessary but improved yields (93%) were achieved with the use of *p*-TSA as acid.

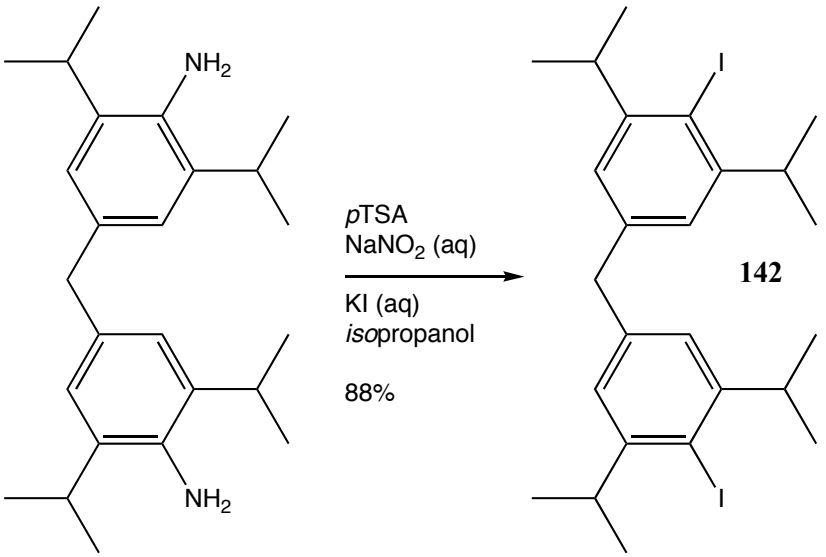

Scheme 44 Successful conversion of aniline **137** to aryl iodide **142**.

Upon obtaining the key intermediate **142**, in parallel to obtaining our principal target biaryl motif **133** we decided to investigate the synthesis of a novel compound with a triazole linker functionality.

3.4 Double Huisgen Cycloaddition Target

3.4.1 Background

The term 'click' chemistry was introduced by Sharpless to describe a class of robust reactions designed to accelerate the synthesis of drug molecules.[218] They have been applied to the sensor field only to a limited degree, although just recently several papers have highlighted its potential.[132] The principal characteristics of a 'click' protocol are highly stereospecific products in high yields, with environmentally friendly by-products, insensitivity to water and oxygen and high thermodynamic driving forces. One of the defining reactions under this term is the Huisgen 1,3-dipolar cycloaddition, first reported in 1961.[219] During the course of the reaction, a substituted triazole ring is formed from a terminal alkyne and an azide (as in Scheme 45 below).

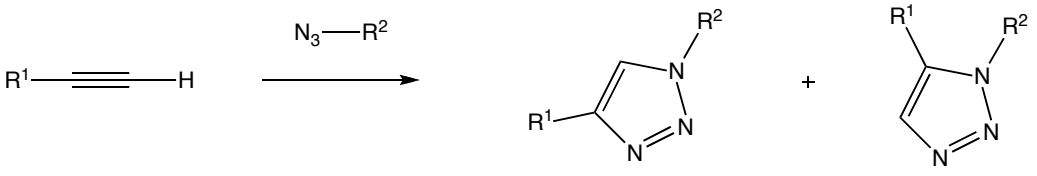

Scheme 45 Huisgen 1,3-dipolar cycloaddition reaction.

Concerns about the shock sensitivity and explosive nature of azides limited the attention this reaction received. Although compounds with adjacent olefinic, aromatic or carbonyl moieties and short chain azides are dangerous to work with, longer chain organic species and sodium azide are relatively safe to handle. Regioselective control was achieved in 2002 by Sharpless and co-workers, showing Cu(I) catalysed reaction generated only the 1,4-triazole species.[220] Copper (I) salts such as copper (I) iodide can be used directly, or alternatively, copper (II) salts such as $CuSO_4 \cdot 5H_2O$ can be reduced *in situ* by sodium ascorbate, allowing the formation of the 1,4-substituted 1,2,3-triazoles with high yields and less than a 2 mol% catalyst loading. The exact mechanism is not yet fully understood but has been proposed as proceeding in a stepwise fashion, initially with generation of a copper (I) acetylide (Scheme 46).

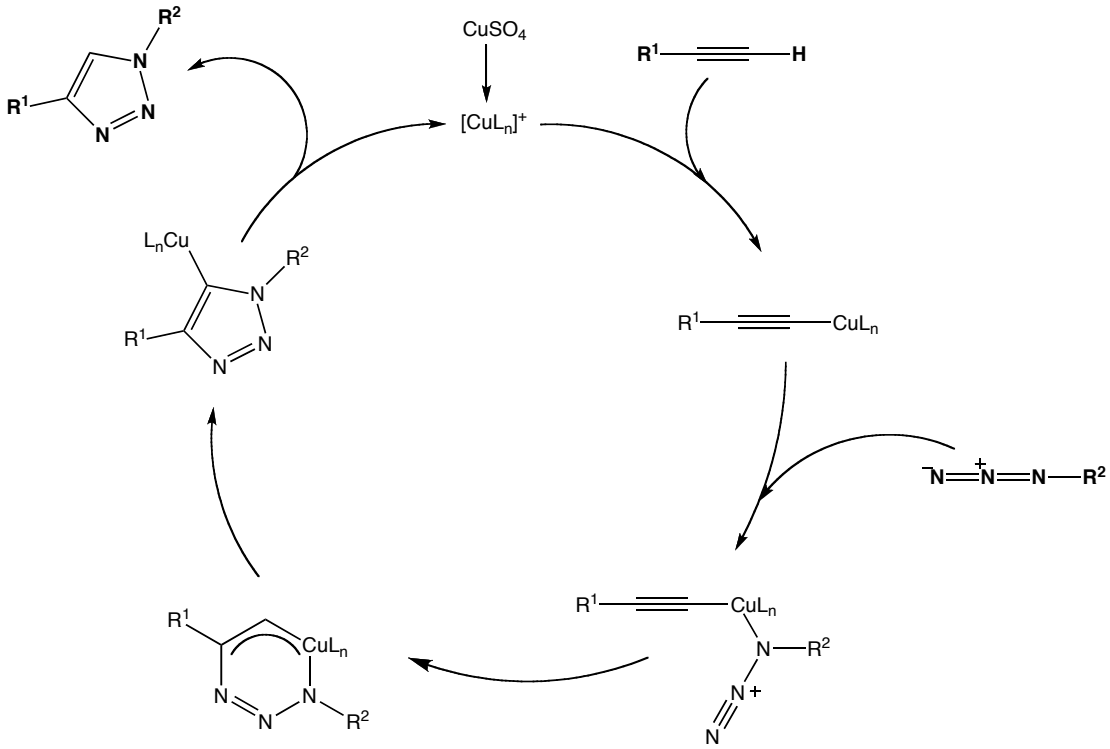

Scheme 46 The proposed catalytic cycle for the Huisgen 1,3-cycloaddition reaction.

The interesting aspect of the Huisgen 1,3-cycloaddition reaction for an optical sensor chemist is that a new optically active unit is formed in the reaction. The triazole ring has not yet been fully explored in this kind of application and the effect of highly sterically hindered substrates is not well described in the literature, providing an additional reason for attempting to access a novel molecule incorporating a triazole linker based on our biarylmethylene backbone.

3.4.2 Synthesis and Characterisation

Considering the two synthetic partners required, azide and alkyne, we chose to prepare the boronic acid derivative component with an alkynyl functionality and convert the bis(aniline) **137** into the corresponding bis(azide) **143**, because there is precedent for preparing alkynylphenylboronic acids.[221]

Synthesis of Azide Component

Possible conditions for isolating aryl azides include Zhu's protocol of CuI, NaN_3, *L*-proline and NaOH in DMSO[222]. However, previous success with diazotisation of highly hindered substrates discussed above meant we decided to use similar chemistry but using sodium azide in the place of potassium iodide.[217] Column chromatography (100% hexane) allowed isolation of pure bisaryl azide **143** in 78 % yield.

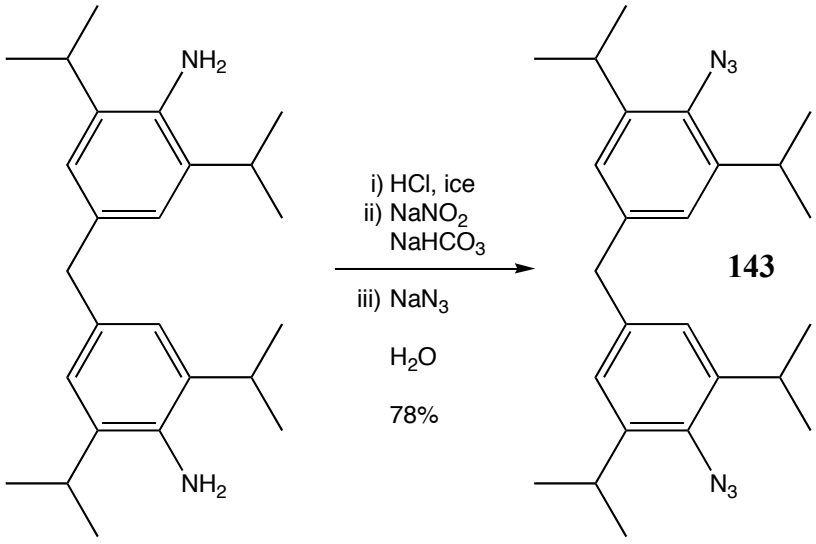

Scheme 47 Conversion of bisaniline **137** to bisarylazide **143**.

Synthesis of Alkynyl Boronic Acid Ester Component

Considering the formation of the desired alkynyl species involves forcing conditions (see below) and precedent for that step involves the use of pinacol protected derivates (pinacol is the most strongly binding diol protecting group), 3-bromophenylboronic acid was protected in the same way.

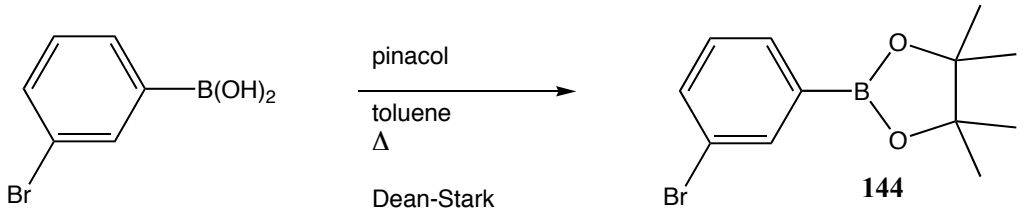

Scheme 48 Diol protection of 3-bromophenyl boronic acid.

Zheng disclosed the preparation of a range of alkynylphenylboronate esters using a mixed palladium-copper catalyst system and triphenylphosphine at high temperature in a sealed environment. They also demonstrated significantly shorter reaction times and higher yields using microwave irradiation but this methodology was not explored.

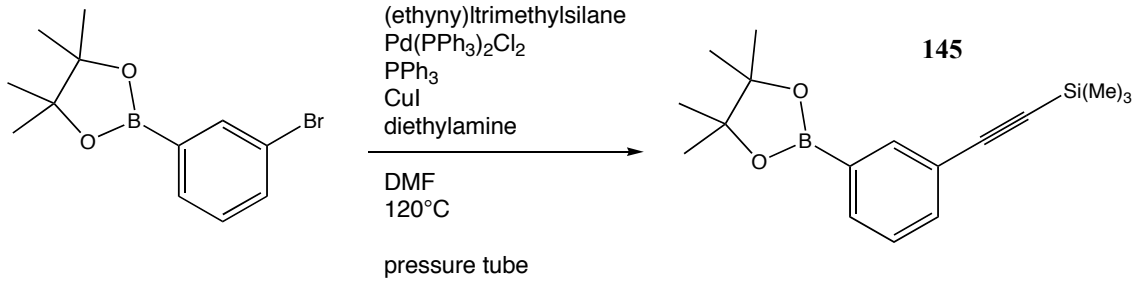

Scheme 49 Palladium/Copper catalysed preparation of alkyne **145**.

The trimethylsilyl group was removed by treatment with inorganic base in methanol at room temperature, liberating the pinacol ester **146** of 3-ethynylphenylboronate acid, also purified by column chromatography over silica gel.

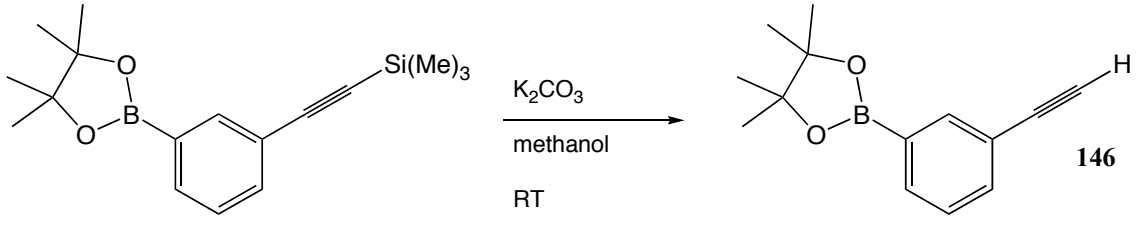

Scheme 50 Deprotection gave the desired intermediate **146**.

Click Reaction

Copper sulfate and sodium ascorbate aqueous systems often allow for improved yields in 1,3-Huisgen cycloadditions[223] but in this case our substrates are poorly soluble in aqueous media so Sharpless' protocol utilising DMSO as solvent was followed.[220]

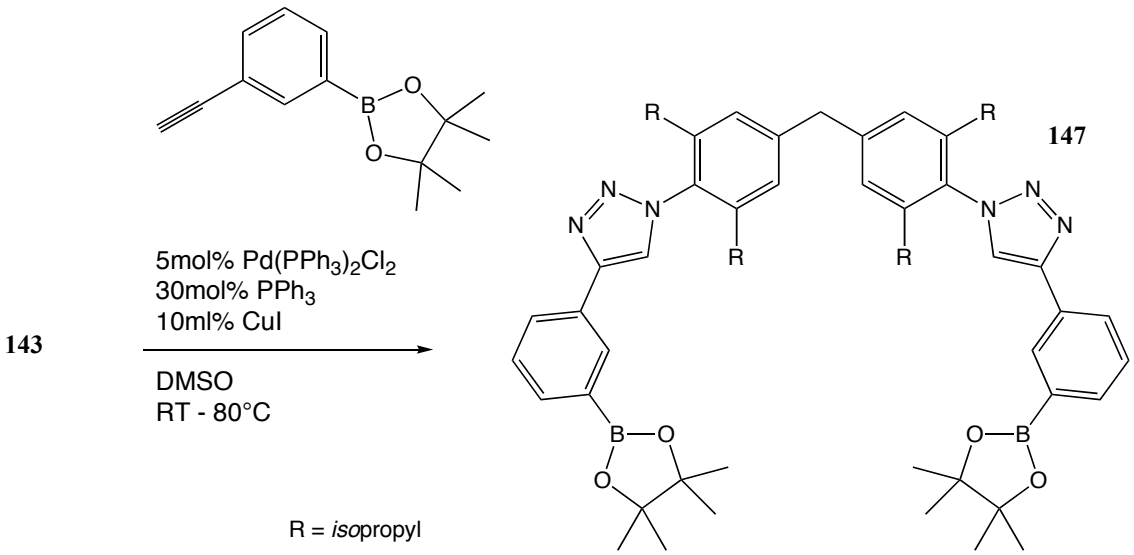

Scheme 51 Copper (I) catalysed Huisgen 1,3-cycloaddition.

The target compound **147** was isolated in a fairly poor yield (32 %) after column chromatography over silica gel in a gradient DCM-methanol eluent. However, as previously discussed, these cycloadditions are highly solvent dependant so this may be optimisable and the substrate is highly sterically hindered.

Binding studies were not performed with the isolated pinacol derivative, as steric hindrance between the two protected boron centres was thought to prevent fluoride bridging. The key outcome was the successful synthesis of a sterically hindered alkyne which undergoes 1,3-Huisgen cycloaddition with a protected phenylboronic acid species. The ability to tailor a sensor to a target analyte is extremely desirable and we have successfully shown the diversity and modular character of our backbone. We have introduced a new optically active unit and simultaneously changed the dimensions of the binding pocket. Our main focus however, was the original biaryl target motif **133**, the synthesis of which is now discussed.

3.5 Route to the Principal Biaryl

3.5.1 Boronic Acid Protecting Group Strategy

Our proposed general system **133** could now be refined to the *iso*propyl derivative **148** (Scheme 52). Following route A, the next step in the synthesis of the target species was to couple bisaryliodide **142** with a boronic acid *via* Suzuki chemistry. To the best of our knowledge, Suzuki coupling of an aryl halide with diboronic acid generating a product with a free boronic acid is unreported in the literature.

Ortho-diboronic acid benzene is not commercially available, and although the synthesis has been published, it involves several steps and involves highly toxic tin reagents and intermediates.[224] These considerations combined with the steric demands of reacting the *ortho* substrate with the bisaryl iodide **142** meant, temporarily at least, synthesis was postponed and the *meta* derivative targeted. Attempts to react **142** with *meta*-diboronic acid benzene **149** proved to be unsuccessful with no desired products detected or isolated from the reaction mixture (Scheme 52). Although a wide range of catalysts and ligands were not examined due to time limitations, neither palladium tetrakis (K_2CO_3, THF, reflux, 48 h) or the highly active S-PHOS ligand ($Pd(OAC)_2$, K_3PO_4, toluene, 100°C, 48 h), discussed later in this chapter, generated new products according to TLC or ^{1}H NMR analysis of the crude reaction mixture.

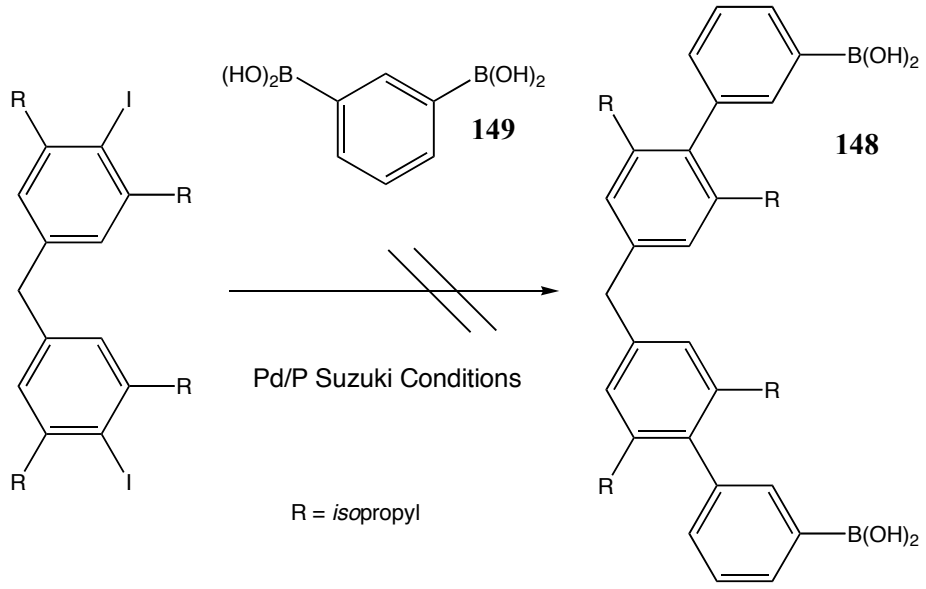

Scheme 52 No desired product was isolated from the crude mixture of the reaction with the bisboronic acid substrate.

Protecting Groups for Boronic Acids

Before departing from the planned route, we looked at mono protecting the *m*-diboronic acid benzene. Gillis and Burke used *N*-methyliminodiacetic acid (MIDA) group successfully to allow iterative Suzuki-Miyaura couplings.[225] Recently, the 1,8-diaminonaphthalene protecting group has been shown to perform well in a range of palladium catalysed reactions.[226]

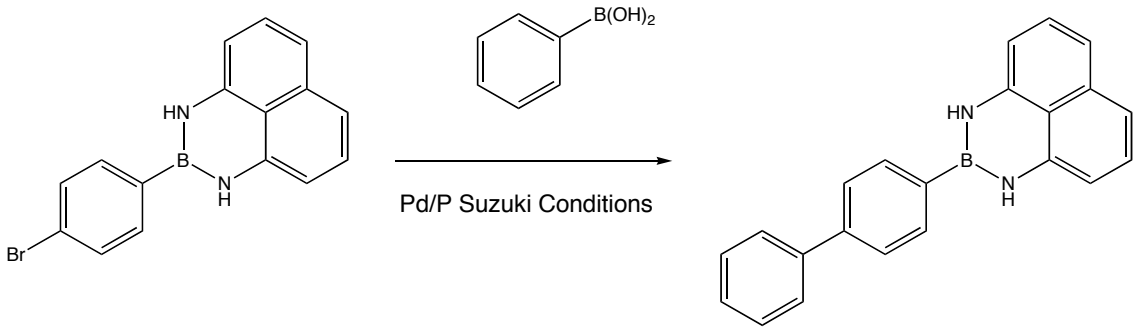

Scheme 53 Shows the platform that allows iterative Suzuki reactions facilitated by the use of 1,8-diaminonaphthalene protecting group.

These publications show no precedent for selective mono protection a diboronic acid, focusing on halogen substituted phenylboronic acids and thiophene examples. Protection of *meta*-diboronic acid was attempted by the 1,8-diaminonaphthalene masking methodology, due to the simple nature of the protection/deprotection synthetic protocols. However, azeotropic removal of water in a Dean-Stark apparatus proved unsuccessful in toluene, with only starting material recovery. The reaction may have been prevented by insolubility of the *meta*-diboronic acid in toluene, even at reflux temperatures. EtOH-benzene (95:5) can be used to facilitate the azeotropic removal of water from elimination/dehydration reactions by virtue of a low boiling point triple azeotrope. Although solubility was achieved and an expected black solid was obtained, the ^{1}H NMR was not encouraging.

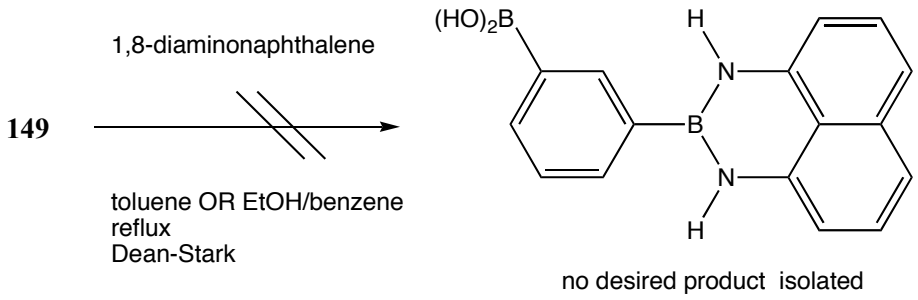

Scheme 54 Mono protection of *meta*-bisboronic acid **149** did not progress cleanly.

At this point we decided to investigate switching to Route B, since we had already obtained the bisaryl iodide material **142**.[227*] The two classical methods to synthesize boronic acids from aryl halides are lithiation or generating the Grignard reagent in coordinating solvent and subsequent quenching with a trialkoxyborate under an inert atmosphere. Finally, hydrolysis with aqueous acid liberates the desired boronic acid. Operating in THF in an inert atmosphere, the lithiation was performed at -78°C by dropwise addition of a 2.5 M solution of *n*BuLi in hexanes over a 10 minute period, after which the reaction mixture was transferred by cannula to a cooled flask charged with 4.0 equivalents of trimethoxyborate. After slow addition to an ice-cooled 10 % sulfuric acid solution the product was extracted with diethyl ether and evaporation afforded **150** as a dark brown oil (Scheme 55).

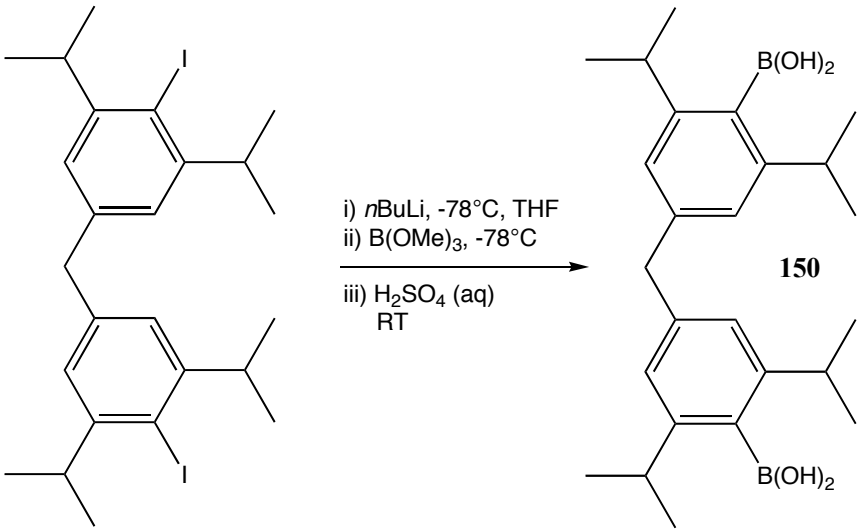

Scheme 55 Bisboronic acid synthesis.

[*] NB a later publication by Noguchi *et al.* details the differential protection of *meta*- and *ortho*-benzenediboronic acid but this methodology was not reported at the time.

^{11}B NMR analysis of **150** showed sp^3 boron was present in the product. ^{1}H NMR served to confirm there was only one species present but was not sufficient to prove transformation. ^{13}C NMR was used to determine product formation as the peak corresponding to the carbon at the reactive site (δ_C 106.3 ppm for C-I) disappeared with the substitution of the boronic acid functionality. Boron substituted carbons are poorly expressed in ^{13}C NMR experiments due to the quadrapolar relaxation caused by the spin 5/2 boron nucleus.

3.5.2 Carbon-Carbon Coupling Step

There are a wide variety of catalyst systems that facilitate the Suzuki coupling of two aryls, including palladium and nickel transition metals in various forms (metal source can affect activity) partnered with for example, phosphine[228], NHC (*N*-heterocyclic carbene)[229] and more recently, bishydrazone ligands.[230] Highly active phosphine ligands tend to be electron-rich and bulky, and although aryl iodides are active substrates, no examples of double Suzuki reactions of such highly hindered substrates have been reported to the best of our knowledge.

Buchwald and Fu have been amongst those at the forefront of ligand development over the past 10 years and Buchwald's commercially available S-PHOS ligand is a versatile phosphine capable of catalysing the most demanding substrates, including aryl chloride couplings at room temperature.[213] In a paper published in 2004, extremely demanding substrates are coupled, including 2,4,6-trimethylbromobenzene with 2,6-dimethylbenzene boronic acid. Several examples of successful couplings involving 2,6-di*iso*propylbromobenzene are presented. Aryl chlorides, less active substrates than aryl bromides are shown to react with a species with similarly congested sterics. 1-chloro-3,5-dimethoxybenzene and 2,4,6-tri*iso*propylphenyl-boronic acid are coupled in 99% yield. Although not precise precedent, impressive steric tolerance is displayed with this catalyst/ligand system (Scheme 56).

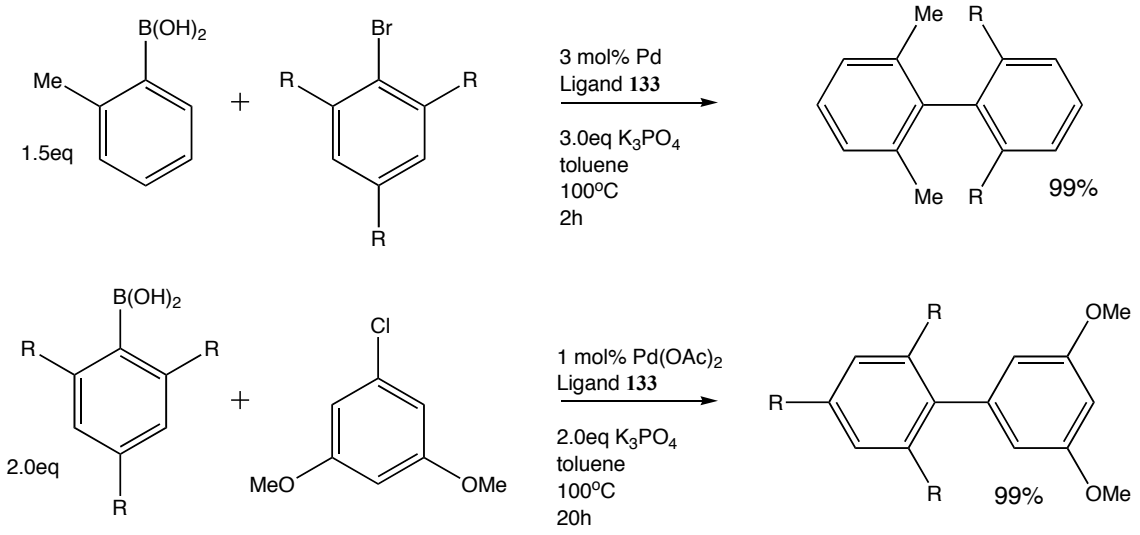

Scheme 56 Buchwald has shown precedent for successful conversion of highly sterically hindered substrates.

All of the examples discussed in the paper proceeded within 24 hours but as bisboronic acid **150** is required to react with two molecular equivalents of a suitable aryl bromide a longer reaction time was envisaged to ensure complete conversion. Another point to note is that in the more demanding examples, increased catalyst loadings and extra equivalents of both base and boronic acid substrate are used to drive the reactions to completion. At this stage we were not interested in optimising the synthesis, so extra-stoichiometric quantities would be employed in any attempted reactions.

Using unprotected 3-bromophenylboronic acid was likely to result in primarily the homocoupled product, despite the higher reactivity of an aryl iodide compared to an aryl bromide the unhindered bromide would react at a much faster rate. Utilising the same 1,8-diaminonaphthalene (dan) protecting group in an application similar to that detailed in Noguchi's original publication[226] (discussed above) appeared to be an attractive methodology.

The dan-protected form of 2- and 3-bromophenyl boronic acids were prepared by azeotropic removal of water from a refluxing toluene solution of the parent boronic acids. Purification by column chromatography (9:1 ethyl acetate/hexane) afforded **151** and **152** in 81 % and 91 % yields, respectively.

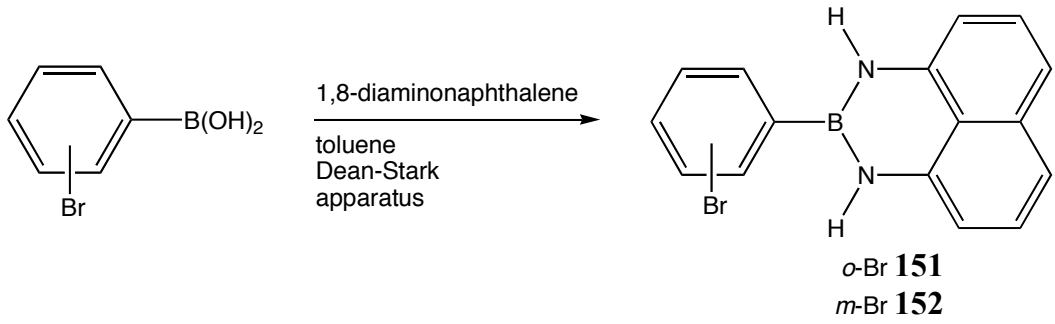

o-Br **151**
m-Br **152**

Scheme 57 Masking the boronic acid coupling partner.

Scheme 58 shows the protocol used to achieve the double Suzuki coupling with the *meta* derivative **152**. It should be noted this reaction was not optimised to minimise catalyst loading levels as obtaining the desired compound was the main objective, not achieving conversion with the most economic conditions. No coupling product was identified with similar forcing conditions using the extremely demanding *ortho* derivative **151**.

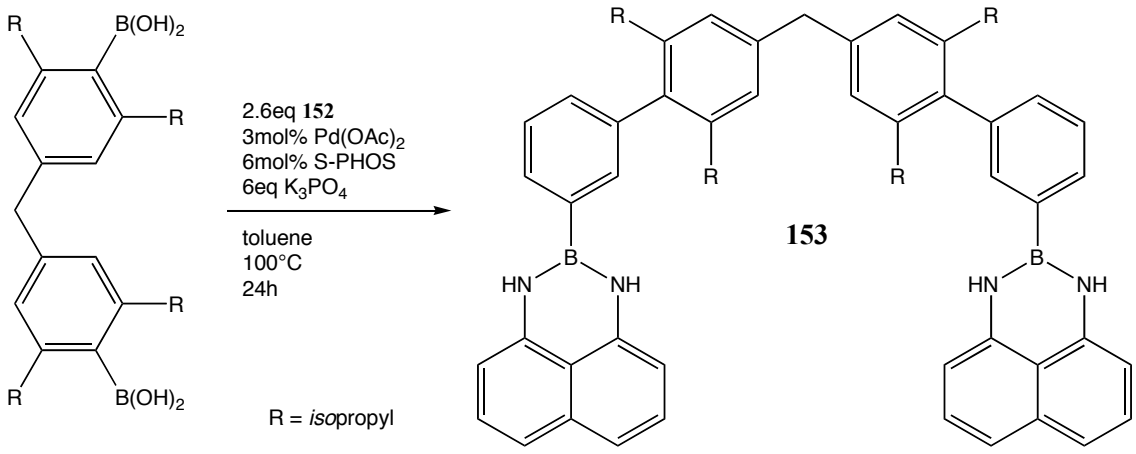

153

Scheme 58 Preparation of **153** *via* double Suzuki-Miyaura coupling.

Some compound **153**, although only an intermediate in the route to obtaining the bisboronic acid target, was retained to allow any anion binding properties to be investigated. The findings are discussed later in the Chapter.

Removal of the 1,8-diaminonaphthalene group proceeded as expected by treatment with concentrated sulfuric acid in methanol, affording the free boronic acid target species **148**.

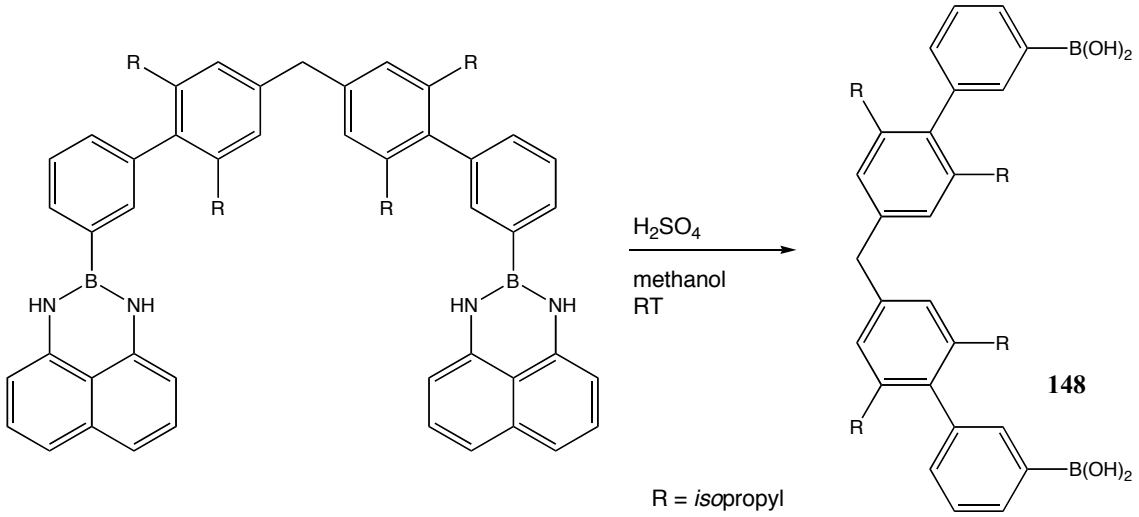

Scheme 59 Acid deprotection afforded the target molecule.

3.6 Binding Studies

3.6.1 Anion-Binding Behaviour of 148 and 153

Initially the fluorescence titration of **148** was performed. Disappointingly, no significant changes were observed in the presence of fluoride anion. There are several possibilities as to why no useful emission changes occurred. The fluoride is unlikely to undergo no interaction with the boron centres, as there is nothing to prevent the Lewis base - Lewis acid response. However, changing the electron density at the boron centres may not cause any dramatic changes to the emissive properties of the species. ^{11}B NMR confirmed the boronic acid became tetrahedral in the presence of excess fluoride anion. This result added credence to the idea that fluorescence changes of this type of framework are caused by conformational change.

The retained sample of bisboron compound **153** was also tested as a sensor in fluorescence studies. Surprisingly, significant changes were observed in the spectrum in the presence of fluoride, operating in dichloromethane solvent. Figure 83 shows the emission changes with increasing fluoride concentration.

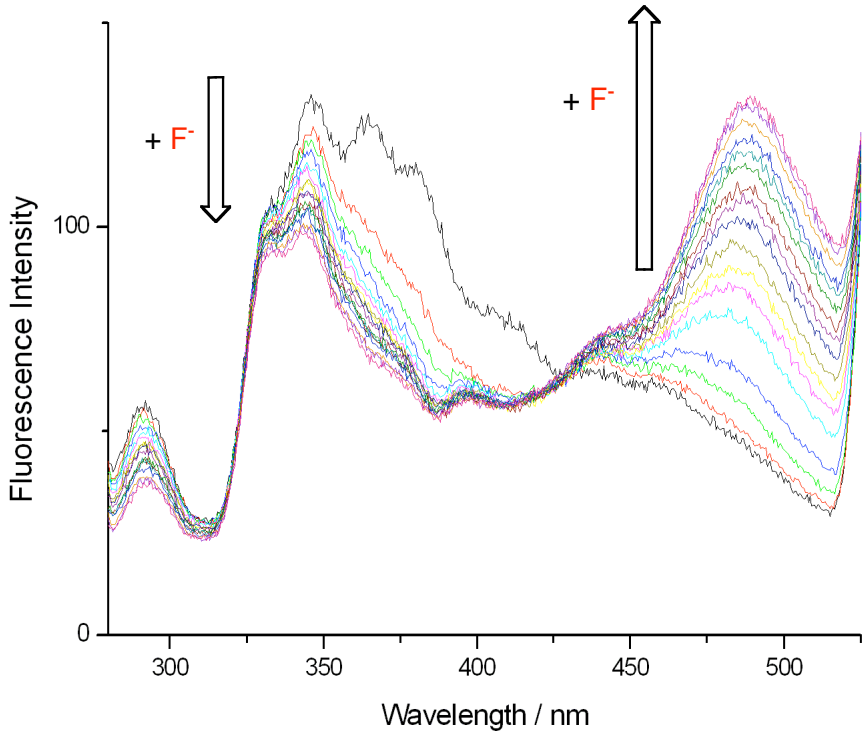

Figure 83 Overlaid fluorescence emission spectra of **153** titration with TBAF. (λ_{ex} = 275 nm, 0.1 mM **153** in dichloromethane. 0.0 – 1.5 mM TBAF.) Arrows indicate quenching or enhancement processes with increasing fluoride concentration.

The initial broad maxima at 345 nm were significantly quenched in the presence of just one equivalent of fluoride, and at concentrations greater than 0.2 mM fluoride (4 equivalents relative to 153) a new peak emerged at 490 nm, a large bathochromic shift. An isoemissive point can also be observed at 428 nm, indicating the presence of two emissive species in equilibrium, crucially, indicating the system is not acting as a chemodosimeter (as in species 96 in the presence of TBAF discussed in Chapter 2). Excimers between pyrenes typically result in a broad emission at similar wavelengths but this peak is sharper and not characteristic of an excimeric complex. One point to consider here however, is that compound **153** is unlikely to act in a bidentate fashion with a bridging fluoride anion, as the distance between the two boron centres is simply too large.

The ratiomeric changes were calculated and are shown in the plot below (Figure 84). The ratiomeric factor is the ratio of the emission changes at 491 and 348 nm. Ratiomeric changes like those observed, unlike single wavelength emissive

enhancements, are unaffected by probe concentration, offering a significant advantage over a single wavelength response. Also, once a ratiomeric response is calibrated, any background fluorescence can be accounted for.

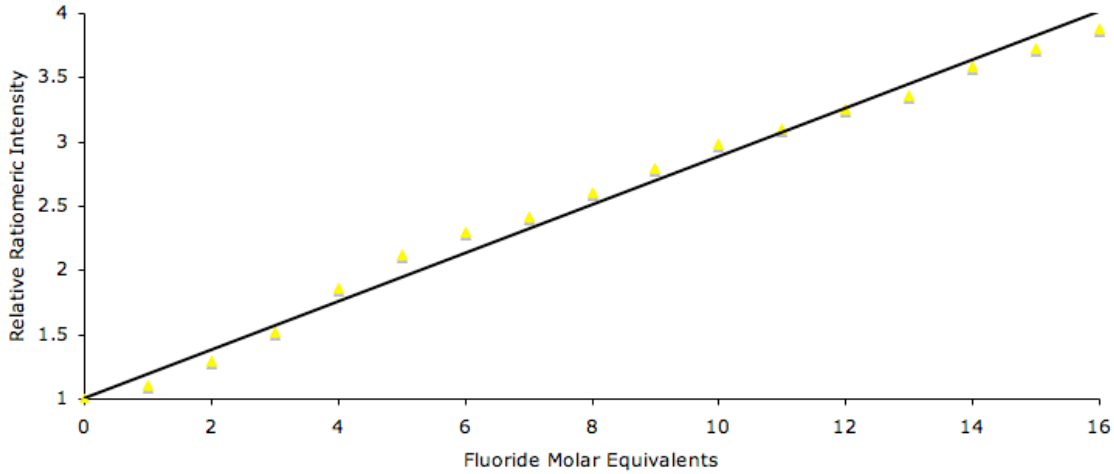

Figure 84 Ratiomeric emission response of **153**. Ratiomeric emission response factor calculated by I_{491}/I_{348}.

Other anions titrated (chloride, bromide, phosphate) resulted in negligible spectral changes, indicating excellent selectivity. The strongly Lewis basic acetate anion did initiate a slight quenching affect at the shorter wavelengths but gave no ratiomeric response. Unfortunately, when the TBAF titration experiment was repeated in methanol a similar ratiomeric response was not observed.

3.7 A Model Diazaborinine

3.7.1 Purpose

In an attempt to clarify the interaction of **153** and fluoride anion in solution a diazaborinine model compound was prepared *via* Noguchi's method.[226] The goal was to determine whether the fluoride interacts with the empty *p* orbital on the boron or the adjacent N-H groups, or a combination thereof.

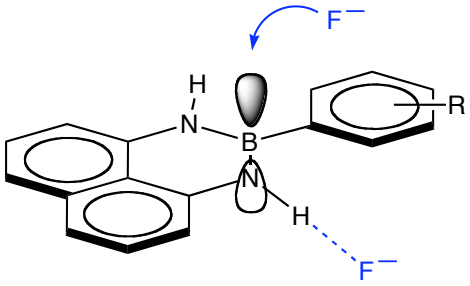

Figure 85 Diagram showing the two possible fluoride interactions.

3.7.2 Synthesis of a Model Compound

An extremely simple candidate for a model compound allowing us to determine the mode of binding was proposed. A mono receptor with an analogous Lewis acid centre would allow us to establish if the fluoride interacts with the boron centre and may provide information as to the nature of the species responsible for the long wave emission formed on binding. The boron centre may be more electron rich than a boronic acid moiety, as the lone pairs on the nitrogens, although conjugated across the naphthalene ring system, can potentially extend into the vacant *p* orbital on boron. The amount of electron density on boron influences the strength of the B-F interaction. That is, if the boron is less Lewis acidic, the Lewis basic fluoride will interact less strongly. If sensor **153** is unique in showing the unexpected bathochromic shift then although it may still be caused by a B-F interaction, it is possible it is due to conformational change, albeit unlikely to be in a similar fashion to that proposed for boron(phenolate) **90** (see Chapter 2) in the presence of chloride anions.

Using Noguchi's masking methodology described previously,[226] the model compound **154** was prepared from 4-tolylboronic acid successfully. The tolyl derivative was used, as the methyl group provides the useful analytical handle of a signal distinct from the aromatic region in the ^{1}H NMR spectrum of the compound.

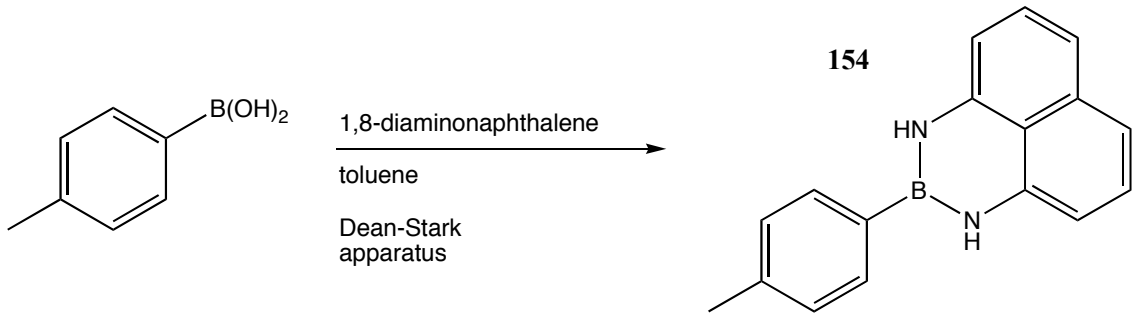

Scheme 60 Preparation of a model compound for binding studies.

Compound **154** was isolated as a white crystalline solid after column chromatography over silica gel (10:1 hexane-ethyl acetate).

3.7.3 Binding Studies of Diazaborinine 154

A range of analytical techniques were utilised in an attempt to elucidate what occurs at the binding site when interaction with fluoride anion occurs. As discussed in Chapter 1, sensors for fluoride often contain NH donors or trisubstituted planar boron centres but **153** and the model compound **154** can potentially interact in either manner. If fluoride anion does complex with the empty *p* orbital on boron, making the boron centre more electron rich, the lone pair on the nitrogen is likely to conjugate more strongly with the naphthyl ring system. If hydrogen bonding or deprotonation occurs, the resulting species could be capable of some unusual conjugation. Potentially both processes could occur simultaneously or systematically, causing more complicated changes in electron density.

3.7.4 ^{1}H NMR spectroscopy of Diazaborinine 154 with halide anions

*Titration of **155** (0.5 mM) against TBAC in $CDCl_3$*

At concentrations below 2 mM, significant changes in the spectrum of **154** are not observed. However, at 5 mM, chloride anions caused the resonance at 6.04 ppm due to the NH protons of **154** to shift to 6.21 ppm, potentially indicating NH···Cl^- hydrogen bonding may occur. The fact that no emission response was observed in the fluorescent spectroscopy shows that this event alone does not affect optical behaviour.

*Titration of **154** (0.5 mM) against TBAF in $CDCl_3$*

At equimolar concentration of **154** and TBAF, the integral of the signal corresponding to the NH protons in the ^{1}H NMR spectrum of **154** decreased from 2 protons to 0.7 proton with negligible shift. At higher fluoride concentrations (5.0 mM) the integral was further diminished to < 0.2 proton equivalents and shifted downfield to 6.21 ppm. All other signals showed small fluctuations (< 0.05 ppm) in chemical shift, indicating no dissociation was likely to have occurred. These findings appear to indicate compound **154** loses at least one proton in the presence of equimolar fluoride but at significantly higher concentrations of fluoride, although further deprotonated, it does not exist in a truly deprotonated form. The system is in an equilibrium, and the doubly deprotonated form of **154** is likely to be unstable or short-lived.

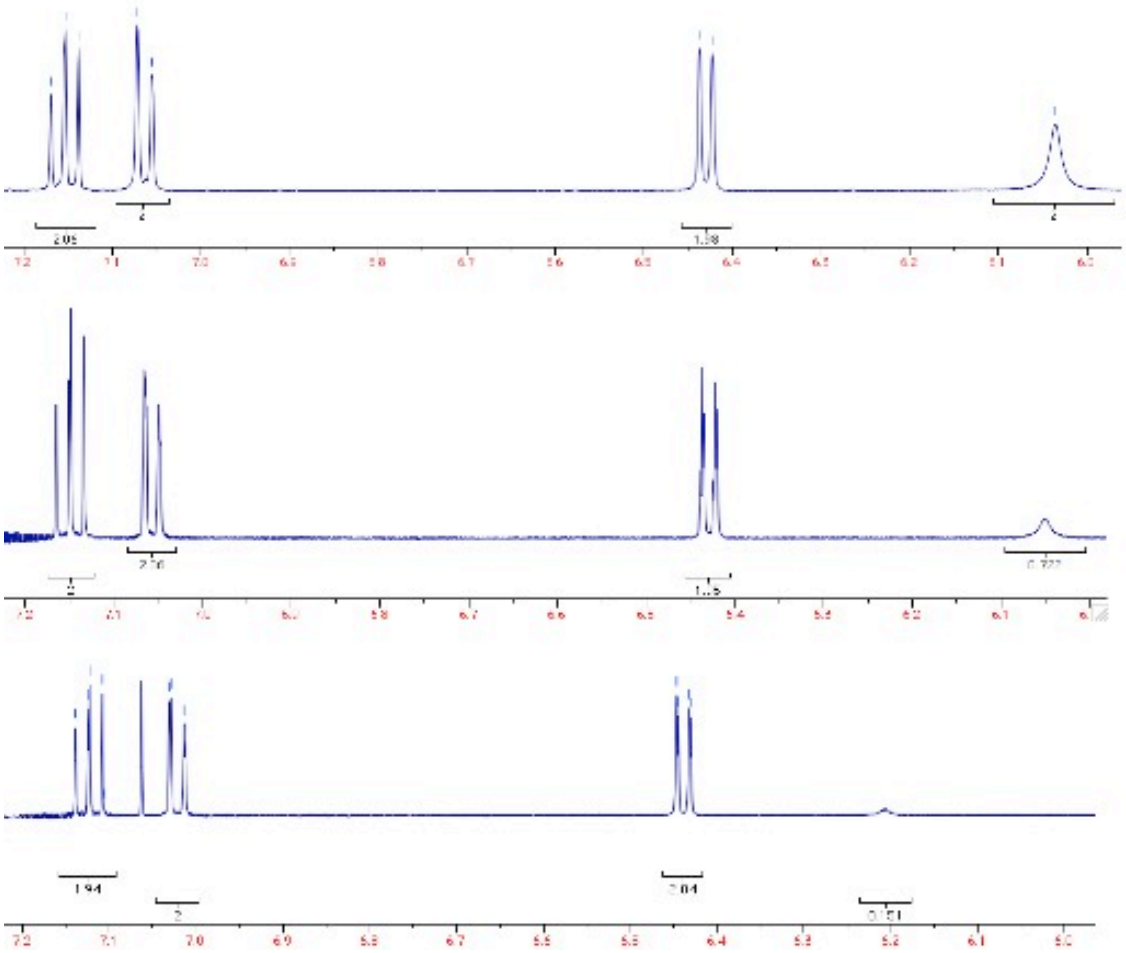

Figure 86 6.0-7.2 ppm region of the ^{1}H NMR spectra of 0.5 mM **154** in $CDCl_3$ without fluoride anion (upper spectrum) and in the presence of 0.5 mM TBAF (middle spectrum) and 5.0 mM TBAF (lower spectrum).

It should also be noted that addition of fluoride caused the aromatic signals to resolve, whereby the signals at 7.02 and 6.44 respectively both appear as a doublet of doublets but when free in solution these protons of compound **154** resolve as doublets. The formation of the bifluoride ion, HF_2^-, is thought to be a driving force for the deprotonation of NH-containing species.[231] Extremely deshielded, the ion appears as a triplet at approximately 16.3 ppm relative to a TMS standard in ^{1}H NMR spectra (d^6-DMSO). This peak is often difficult to resolve and few research groups manage to visualise it successfully and it was not visible in $CDCl_3$ solution in this case.

^{11}B NMR spectrum of **154** indicates the boron is sp^2 hybridised, trigonal planar and electron deficient in the same manner as a simple boronic acid. ^{11}B spectra were obtained of **154** in the presence of fluoride and showed the boron changed geometry from trigonal planar sp^2 (31.1 ppm) to tetrahedral sp^3 (0.8 ppm) but only after addition of more than one equivalent of TBAF. In fact at equimolar concentration two peaks are observed at 31.1 and 7.7 ppm showing the boron is interacting in equilibrium with the fluoride. When present in excess, the fluoride anion is proposed to complex to **154**, forming a diazafluoroboronate anion. In isolation, this change in geometry could be due to a chemodosimetric mode of action but this is unlikely due to the observation of an isoemissive point in the overlaid spectra of bisboron compound **153** and the lack of significant shift in the ^{1}H signals.

A ^{19}F NMR titration of **154** against TBAF initially revealed a broad singlet at -123 ppm typical of free fluoride in solution.[232] At > 2.0 equivalents of fluoride anion relative to **154** the naked fluoride peak is still visible but a new sharp singlet also appears at -118 ppm. At higher concentrations (10:1 TBAF-**154**), the broad fluoride peak remains visible at -123 ppm but the singlet at -118 ppm is almost absent. However, a new sharp singlet appears at -129 ppm. The characteristic doublet signal corresponding to HF_2^- (appears at -147 ppm in d^8-THF)[233] was not observed. These findings seem to indicate the presence of two new distinct fluoride environments. It is possible that the first signal corresponds to the BF adduct and then on further deprotonation the bound fluoride is then exposed to more electron density from the delocalised lone pair from the nitrogen, shifting the resonance further upfield.

3.7.5 Fluorescence of Diazaborinine 154

Compound **154** was titrated against TBAF in dichloromethane and the spectra recorded. Figure 87 shows the overlaid spectra.

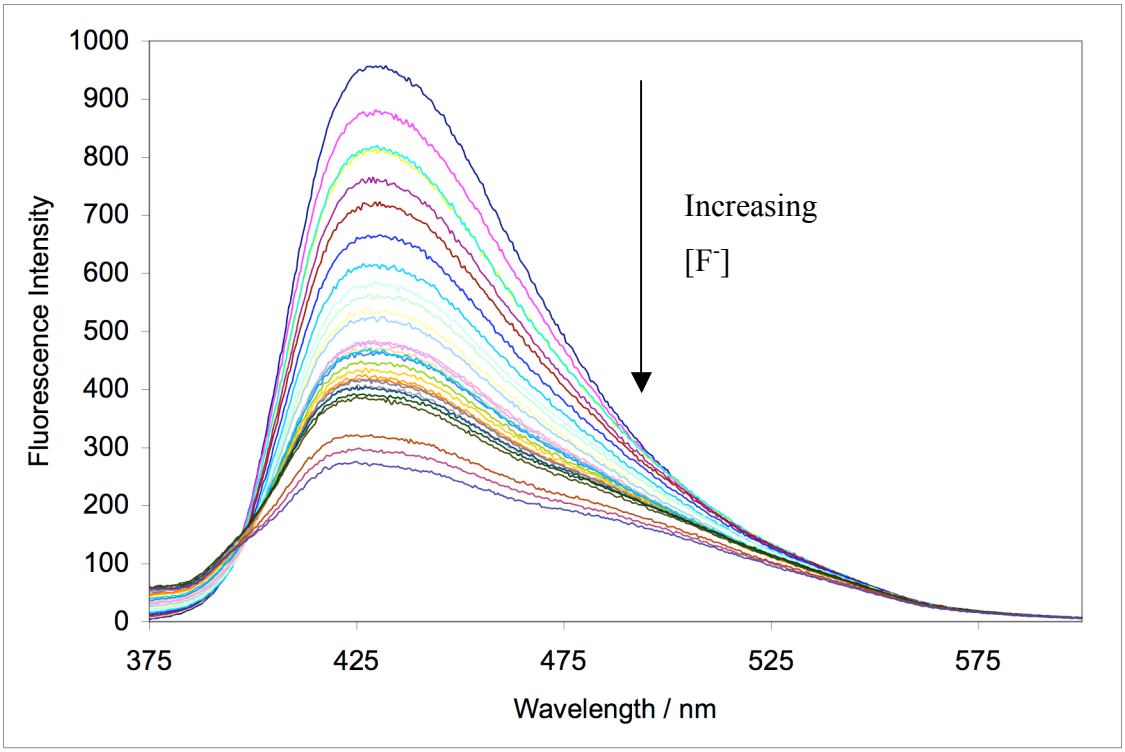

Figure 87 Overlaid emission spectra of **154** (arrows indicate emission changes with increasing fluoride concentration). λ_{ex} 305 nm. [**154**] 0.1 mM, [F^-] 0.1-8.6 mM in dichloromethane.

Exciting at 305 nm, compound **154** emits strongly with a maximum at 425-430 nm. Compound **154** shows a classic fluorescence quenching response to increasing concentrations of fluoride. Acetate, bromide, chloride and phosphate anions do not induce this quenching response. Interestingly, the simple model does not provide a ratiomeric response, which means the backbone of **153** must play a role in its optical response. Compound **148** did not show changes in emission behaviour in the presence of fluoride, so the ratiomeric character of **153** may still be due to a conformational change, although not as the model proposed. As the boron centre becomes the tetrahedral boronate species, with the bulky dan substituent attached, it is possible a change in the freedom of rotation occurs, or the molecule changes significantly structurally. The two 'arms', although not closing in a pincer mechanism, may be twisting relative to the backbone, or indeed forcing the boron centres further apart, changing the relative orientation of the two central aryl rings.

A proton NMR titration (performed in d^6-DMSO due the inadequate solubility of TBAF in $CDCl_3$ at higher concentrations) showed very small changes in chemical shift of any protons, including the NH. Above 3.0 equivalents of fluoride the NH peak was impossible to reliably resolve from the baseline possibly indicating deprotonation was occurring. Across this limited concentration range the change was linear which meant determining binding constants from the NMR resonance changes was likely to be inaccurate. A peak indicative of HF_2^- anion formation appeared (characteristic triplet at 16.13 ppm) after the addition of 1.0 equivalent of fluoride. This behaviour was not observed in D-chloroform. These findings meant the binding constant would have to be calculated from the fluorescence spectra. A Job plot was performed (operating in d^6-DMSO for solubility reasons) but a clear maximum was not identifiable (see Figure A-18 in Appendix). This may be due to the formation of HF_2^- at low concentration concentrations observed in the ^{1}H NMR titration, particularly as the points obtained at the higher ratios of fluoride:anion appeared misleading. However, it is possible to generate a Job plot from fluorescence data by measuring the degree of deviation from a linear regression between the maximum and minimum intensities.[234] In a similar fashion to a Job plot of the change in chemical shift by NMR spectroscopy, the mole fraction at which the maximum delta is observed indicates the value from which the stoichiometry may be obtained.

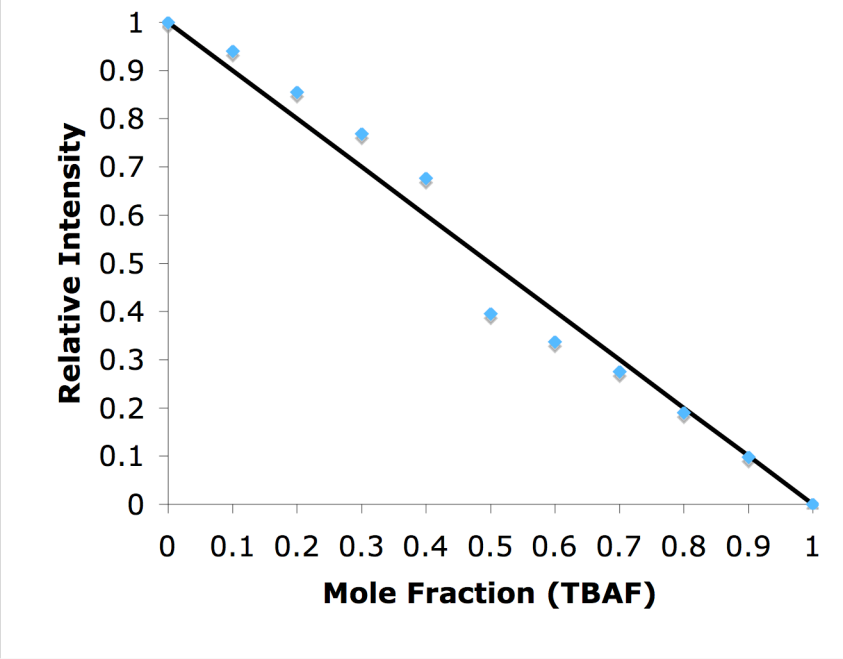

Figure 88 Plot of relative fluorescence intensity with increasing mole fraction of TBAF (points plotted in blue). The black line indicates a linear quenching response between I_{max} and I_{min}. Total concentration of [TBAF] + [**154**] kept constant at 3.3 μM in dichloromethane, λ_{ex} 305 nm, λ_{em} 425 nm.

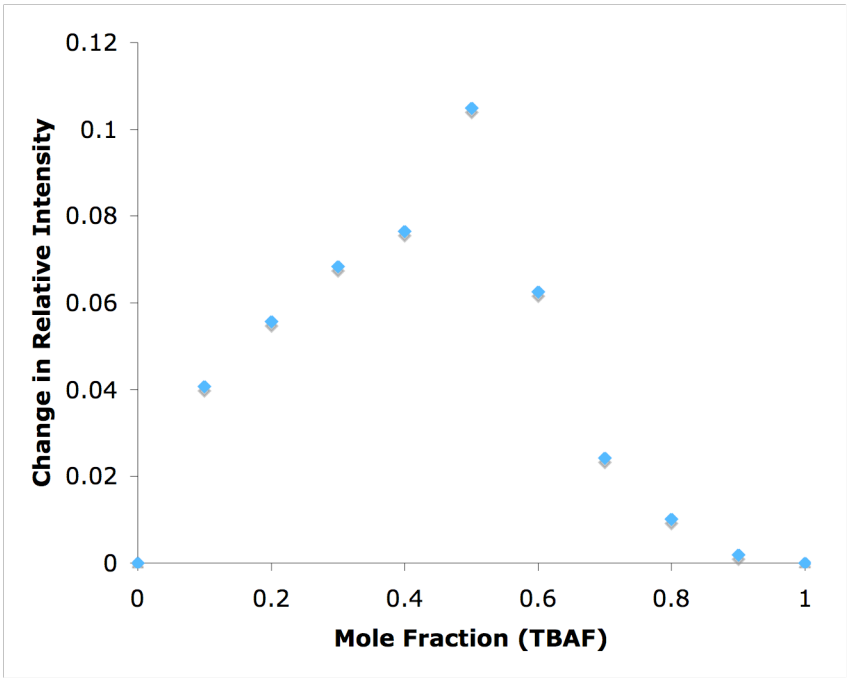

Figure 89 Job Plot for compound **154** showing clear maximum deviation from linear quenching at mole fraction of fluoride of 0.5 indicating a 1:1 associative stoichiometry.

Therefore, a plot of emission intensity at 430 nm against fluoride concentration allows a binding constant of 1371 M^{-1} to be calculated assuming a 1:1 **154**-fluoride interaction (see Figure A- 17 in Appendix). Fitting the curve to a 1:1 model produced an R^2 of 0.9958 and a 2:1 model fit poorly, confirming the Job Plot findings above. Fitting the binding curve (in 1:1 stoichiometry) for compound **153** gave a binding constant of 1270 M^{-1}, in excellent agreement with the mono compound.

The fluorescence quenching can be attributed to a classic ICT sensor mechanism as the fluorinated boron donates electron density to the naphthalene ring system *via* the conjugated nitrogens. This conjugation is thought to stabilise the dan group against dissociation and the addition of further fluoride anions - for example to generate a trifluoroboronate anion as with simple boronic acids. Crystals suitable for X-ray diffraction studies were not obtained. Several solvent combinations, **154**:TBAF ratios and crystallisation methods were trialled but the fluoride complex did not appear to be sufficiently crystalline.

3.8 Summary

The preparation of a sterically demanding bisdiazaborinine species **153** that displays a ratiomeric fluorescence response to fluoride selectively over competitive anions such as acetate and phosphate was completed. Although no novel methodology was employed, very demanding substrates were successfully converted through to the target species successfully after trialling a range of reaction conditions over 6 steps from commercially available molecules. A relatively long wavelength enhancement at 490nm is observed for sensor **153**. An isoemissive point at 428 nm was evident, indicating the binding is 1:1 receptor-analyte and that the binding is non-dissociative. Similar optical sensing phenomena were not observed in protic solvent. Although the conformational changes proposed in our model in Chapter 2 are unlikely to occur in the presence of the fluoride guest, the diphenylmethylene backbone is shown to create the ratiomeric sensing observed, possibly by an alternative structural modification when in the bound state. Due to the demanding steric constraints of the backbone during these early investigations only the *meta* derivative could be isolated. This meant bidentate binding to fluoride was thought not be achieved – likely due to the large intramolecular boron-boron distance.

A related species **147** was obtained by a 1,3-Huisgen cycloaddition reaction, using a Cu(I) catalyst allowed for regioselective control resulting in 1,4-triazole functionality. No successful examples of such highly hindered 1,3-Huisgen cycloadditions have been reported in the literature. This example was prepared to illustrate the synthetic flexibility of the sensor design but no binding studies were undertaken, partly due to time constraints and also because bidentate binding is highly unlikely to be achievable given the large intramolecular boron-boron distance. However, we have succeeded in demonstrating the ability to tune the size of the cavity which is crucial to any versatile sensor system.

Preparation of a model compound **154** allowed us to perform detailed binding studies of the unexplored diazaborinine moiety using various analytical methods. Fluorescence measurements, ^{1}H and ^{11}B NMR spectroscopy combined to allow us to propose that fluoride binds to the boron and the resultant negative charge induces fluorescence quenching *via* transfer to the conjugated naphthalene ring system in an ICT type sensor

mechanism. Although ^{1}H NMR studies in d^{6}-DMSO revealed that deprotonation can occur with subsequent formation of hydrogen bifluoride, a corresponding peak was not observed in $CDCl_3$. ^{11}B and ^{1}H NMR studies showed that hydrogen bonding between the NH groups of the diazaborinane and fluoride anions plays little or no role in the fluorescence quenching mechanism. This simple species showed no ratiomeric emission response, showing that the optically active diphenylmethylene unit had a favourable effect on the optical performance of sensor **153** despite the absence of bidentate binding. A 1:1 binding stoichiometry was ascertained *via* a Job plot based on fluorescence measurements and a binding constant of 1371 M^{-1} was calculated with an excellent fit. No other anions tested (chloride, bromide, phosphate or acetate) prompted significant fluorescence quenching. This work has opened up the use of a novel boron derivatised selective receptor site for anions which we can exploit further in future designed fluoride chemosensors for use in organic solvents. Diamine capped boronic acids could provide more versatile and robust binding sites for fluoride than non-derivatised boronic acids.

4 EXPERIMENTAL

4.1 General Procedures

Solvents and Reagents

Solvents and reagents were reagent grade unless stated otherwise and were purchased from Acros Organics, Avocado Research Chemicals Ltd, Fisher Scientific UK, Frontier Scientific Europe Ltd, Alfa Aesar, TCI, Lancaster Synthesis Ltd and Sigma-Aldrich Company Ltd and were used without further purification, unless stated otherwise. Anhydrous solvents were collected from the SPS system.

Chromatography

Thin layer chromatography was performed using commercially available Merck aluminium backed plates coated with a 0.20 mm layer of silica gel 60 with fluorescent indicator UV254. These plates were visualised using either ultraviolet light of 254 nm or 365 nm wavelength, or by staining the plates with PMA, DNP or Ninhydrin solutions. Silica gel column chromatography was carried out using Davisil LC 60A silica gel (35-70 μm).

Nuclear Magnetic Resonance Spectra

Nuclear magnetic resonance spectra were run in chloroform-D, methyl-D_3, dimethyl-D_6 sulfoxide or a combination thereof. ^{1}H, ^{11}B, ^{13}C and ^{31}P spectra were measured using a Bruker Avance 250 or Bruker AVANCE 300 spectrometer. ^{1}H spectra were recorded at 250.13 MHz or 300.22 MHz, ^{11}B spectra at 96.32 MHz and $\{^{1}H\}$-^{13}C at 69.5 or 75.5 MHz. Some titration experiments were recorded on a Bruker AVANCE 500 at 500.13 MHz. Chemical shifts (δ) are expressed in parts per million and are reported relative to the residual solvent peak or to tetramethylsilane as an internal standard in ^{1}H and $\{^{1}H\}$-^{13}C spectra, or boron trifluoride diethyl etherate as an external standard in ^{11}B spectra. The multiplicities and general assignments of the spectroscopic data are denoted as: singlet (s), doublet (d), triplet, (t), quartet (q), doublet of doublets (dd), doublet of triplets (dt), triplet of triplets (tt), unresolved multiplet (m), apparent (app), broad (br) and aryl (Ar). Coupling constants (*J*) are expressed in Hertz.

Mass Spectra

Some mass spectra were recorded by the EPSRC National Mass Spectrometry Service Centre, Swansea. Electron impact (EI) and chemical ionisation (CI) analyses were performed in positive ionisation mode. Low resolution EI and CI measurements were performed on a Micromass Quattro II triple quadrupole instrument, with ammonia as the CI reagent gas. Electrospray ionisation measurements were performed in both positive and negative ionisation modes (ESI^+ and ESI^- respectively). High resolution ESI^+ and ESI^- measurements were conducted on the micrOTOFQ electrospray time-of-flight (ESI-TOF) mass spectrometer (Bruker Daltonik GmbH) at the University of Bath. The micrOTOFQ spectrometer was coupled to an Agilent Technologies 1200 LC system. 10 μL of sample was directly injected into the mass spectrometer. The nebulising gas used was nitrogen, which was applied at a pressure of 1 bar. Nitrogen was also used as a drying gas, supplied at a flow rate of 8 L/min and a temperature of 110 °C.

Elemental Analyses

Elemental analyses were performed by the Department of Chemistry, University of Bath, using an Exeter Analytical Inc CE-440 Elemental Analyzer.

Melting Points

Capillary melting points were determined using a Büchi 535 melting point apparatus. The readings were taken from a mercury-in-glass thermometer and are reported uncorrected as the meniscus point (unless stated otherwise), rounded to the nearest 1 ºC with a heating ramp rate of 0.5 ºC min^{-1}. Where the sample changed colour or evolved gas during or after the melt, thermal decomposition (dec) is noted.

Fluorescence Measurements

Fluorescence measurements were performed on a Perkin-Elmer Luminescence Spectrophotometer LS 50B, utilising Starna Silica (quartz) cuvettes with 10 mm path lengths, four faces polished. Data was collected *via* the Perkin-Elmer FL Winlab software package. All pH measurements taken during fluorescence experiments were recorded on a Hanna Instruments HI 9321 Microprocessor pH meter which was routinely calibrated using Fisher Chemicals standard buffer solutions (pH 4.0 -

phthalate, 7.0 – phosphate, and 10.0 - borate). All solvents used in fluorescence measurements were HPLC or Fluorescence grade and the water was deionised.

4.2 Compounds – Protocols and Analysis

4,4'-methylenebis(2,6-di-*tert*-butyl-4,1-phenylene) bis(hydrogen phenylboronate)

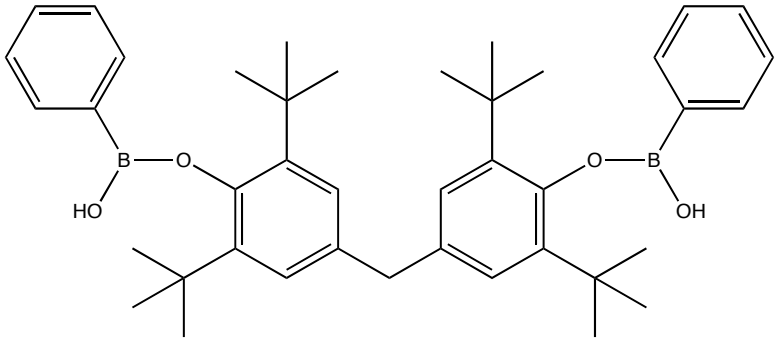

90

4,4'-methylenebis(2,6-di-*tert*-butylphenol) (1.00 g, 2.35 mmol) was dissolved in 40 mL dry toluene under nitrogen. During rapid stirring at 0°C, *N*-butyllithium (1.6 M in hexanes, 4.95 mmol, 3.09 mL) was added dropwise and the mixture stirred for 1 h. Maintaining the low temperature environment, dichlorophenylborane (680 μL, 5.18 mmol) was added and the reaction was allowed to return to room temperature and stirred for an additional 12 h. The resulting white suspension was washed three times with water (60 mL), dried over $MgSO_4$ and the solvent removed in *vacuo* to afford a yellow oil. Recrystallisation gave the title compound **90** as an off-white powder (1.250 g, 84%); mp 162-164ºC (dec); Found: C = 77.80%, H = 8.63%, $C_{41}H_{54}B_2O_4$ requires C = 77.86% H = 8.61%; δ_H (300 MHz, $CDCl_3$) 7.94 (4H, s, Ar*H*), 7.41 (6H, m, Ar*H*), 7.11 (4H, s, Ar*H*), 3.88 (2H, s, ArCH_2Ar`), 1.29 (36H, s, Ar(CH_3)$_3$); δ_C (75.5 MHz, $CDCl_3$) 148.9, 142.3, 136.1, 135.3, 131.9, 128.8, 127.1, 42.2, 35.9, 32.0; δ_B (96.4 MHz, $CDCl_3$) 28.3; *m/z* HRMS (ESI^+) found 650.4546 ($[M+NH_4]^+$ of $C_{41}H_{54}B_2O_4$ requires 650.4546).

2,6-di-*tert*-butylphenyl hydrogen phenylboronate

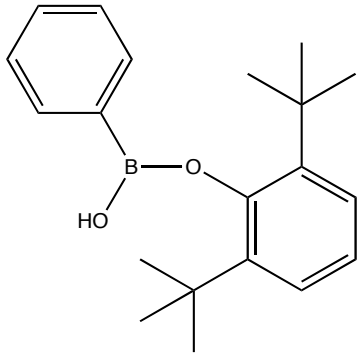

91

2,6-di-*tert*-butylphenol (1.00 g, 4.85 mmol) was dissolved in dry toluene (40 mL) and stirred in a nitrogen atmosphere. *N*-butyllithium (1.6 mM in hexanes, 3.33 mL, 5.33 mmol) was added dropwise by syringe and the mixture stirred for 1 h. Maintaining the low temperature environment, dichlorophenylborane (700 μL, 5.33mmol) was introduced and the mixture was allowed to return to room temperature and stirred for 18 h. The white precipitate dissolved in the subsequent thrice washing of the organic phase with water (3 x 60 mL) and after drying over $MgSO_4$ and subsequent evaporation, an off-white solid **91** was obtained (1.366 g, 91%); mp 114-116°C (dec); δ_H NMR (300 MHz, $CDCl_3$) 1.31 (s, 18H, C(C*H*$_3$)$_3$), 4.07 (bs, 1H, B-O*H*), 6.98 (1H, t, *J* 7.5, Ar-*H*), 7.28 (2H, d, *J* 7.9, Ar-*H*), 7.43 (3H, m, Ar-*H*), 7.95 (2H, dd, *J* 6.8, *J* 3.0, Ar-*H*); δ_C (75.5 MHz, $CDCl_3$,) 148.5, 142.2, 136.0, 135.6, 131.9, 128.2, 126.4, 36.0, 30.8; δ_B (96MHz, $CDCl_3$) 29.1; *m/z* HRMS (ESI^+) found 310.2031 ($[M-H]^-$ of $C_{20}H_{27}O_2B$ requires 310.2031);

4,4',4''-(2,4,6-trimethylbenzene-1,3,5-triyl)tris(methylene)tris(2,6-di-*tert*-butyl-benzene-4,1-diyl) tris(hydrogen phenylboronate)

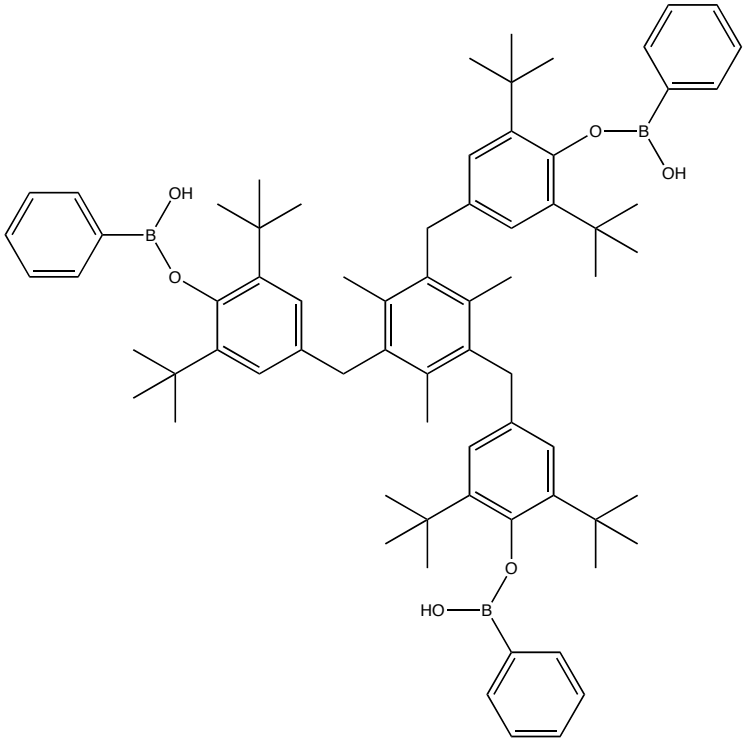

92

1,3,5-trimethyl-2,4,6-tris(3,5-di-*tert*-butyl-4-hydroxybenzyl)benzene (1.00 g, 1.29 mmol) was dissolved in 40 mL dry toluene under nitrogen. During rapid stirring at 0°C, *N*-butyllithium (1.6 M in hexanes, 2.42 mmol, 3.87 mL) was added dropwise and the mixture allowed to reach RT then stirred for 4 h. The solution was then cooled to 0°C in a ice/water bath and dichlorophenylborane (559 μL, 4.26 mmol) was added and then the solution was heated at 100°C for a further 12 h. Upon cooling, the resulting white suspension was washed three times with water (20 mL), dried over $MgSO_4$ and the solvent removed *in vacuo* to afford a white crystalline solid **92** (999 mg, 71%); mp 157-158ºC; δ_H (300 MHz, $CDCl_3$) 7.91 (6H, d, *J* 7.7, Ar-*H*), 7.32 (9H, m, Ar-*H*), 6.96 (6H, s, Ar-*H*), 4.04 (6H, s, Ar-CH_2-Ar`), 2.22 (9H, s, CH_3-Ar), 1.21 (54H, s, (CH_3)$_3$-Ar); δ_C (75.5 MHz, $CDCl_3$) 148.9, 142.3, 136.1, 135.3, 133.3, 131.9, 131.7, 128.8, 38.4, 35.9, 32.0, 20.1; δ_B (96.4 MHz, $CDCl_3$) 23.8; m/z HRMS (ESI^-) found 1085.7179 ($[M-H]^-$ of $C_{72}H_{93}B_3O_6$ requires 1085.7179).

(11*E*,23*E*)-3,15-dimethyl-6,18-*μ*-oxy-tetrabenzo[*c*,*g*,*k*,*o*][1,9,6,14,2,10]dioxadiazadiboracyclohexadecine

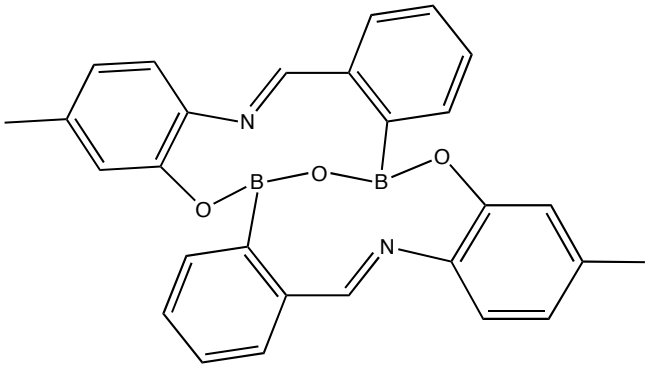

110

2-Hydroxy-5-methylaniline 6h (123 mg, 1.0 mmol) and 2-formyl-phenyl-boronic acid 1 (150 mg, 1.0 mmol) were dissolved in 95:5 ethanol–benzene (20 mL) in a round bottom flask fitted with a Dean–Stark condenser and stirred at reflux for 4 h. The reaction mixture was cooled and the solvent removed under reduced pressure. Washing with a little cold methanol afforded **110** as an orange powder (374 mg, 82%): mp 231–232 °C (dec.); δ_H (300 MHz, $CDCl_3$) 8.64 (2H, s, C*H*N), 7.42 (2H, m, Ar*H*), 7.36 (2H, s, Ar*H*), 7.29–7.16 (6H, m, Ar*H*), 7.11 (2H, d, *J* 8.4, Ar*H*), 6.85 (2H, d, *J* 8.4, Ar*H*), 2.35 (6H, s, CH_3); δ_C (75 MHz, $CDCl_3$) 158.2, 154.9, 148.8, 134.9, 134.1, 133.9, 132.9, 131.2, 128.2, 127.8, 115.3, 113.8, 21.5; δ_B (100 MHz, $CDCl_3$) 8.9; m/z HRMS (ESI^+) found 457.2011 ($[M+H]^+$ of $C_{28}H_{22}B_2N_2O_3$ requires 457.1889).

(11*E*, 23*E*)-6, 18-*μ*-oxy-tetrabenzo[*c*,*g*,*k*,*o*][1,9,6,14,2,10]dioxadiazadiboracyclohexadecine

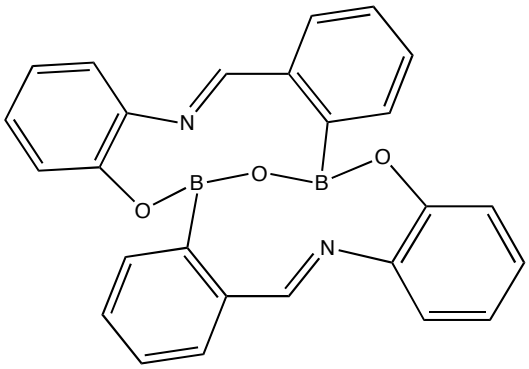

111

2-aminophenol (200mg, 1.83mmol) and 2-formylphenylboronic acid (275mg, 1.83mmol) were dissolved in 95:5 ethanol-benzene and the flask was fitted with a Dean-Stark apparatus to allow the azeotropic removal of water. The mixture was refluxed at 90°C overnight. Recrystallisation from hexane/chloroform and then trituration with a little cold methanol yields **111** as a vivid yellow powder (709mg, 90%); mp 182–183°C (dec.); δ_H (300 MHz, MeOD) 9.16 (1H, s, *CH*N), 7.73 (1H, dd, *J* 8.1, *J* 0.9, Ar*H*), 7.44 (1H, d, *J* 7.2, Ar*H*), 7.08 (3H, m, Ar*H*), 6.83 (1H, m, Ar*H*), 6.72 (1H, t, *J* 8.1, Ar*H*), 6.62 (1H, dt, *J* 8.3, *J* 1.1, Ar*H*); δ_C (75.5 MHz, MeOD) 160.9, 155.5, 135.1, 134.2, 134.13, 133.1, 132.9, 131.5, 127.9, 118.7, 115.8, 113.7; δ_B (96.3 MHz, MeOD) 9.6; m/z HRMS (ESI^+) found 429.1571 ($[M+H]^+$ of $C_{26}H_{18}B_2N_2O_3$ requires 429.1582).

(11*E*,23*E*)-6,18-*μ*-oxy-tetrabenzo[*c*,*g*,*k*,*o*][1,9,6,14,2,10]dioxadiazadiboracyclohexadecine-3,15-dicarboxylic acid

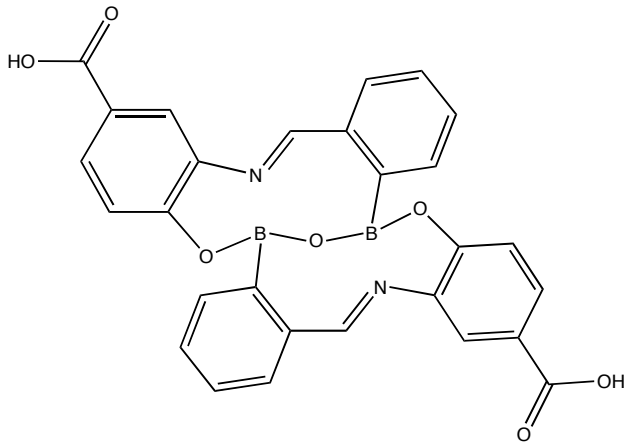

118

3-amino-4-hydroxybenzoic acid (184 mg, 1.20 mmol) and 2-formylphenylboronic acid (180 mg, 1.20 mmol) were dissolved in 95:5 ethanol-benzene and the flask was fitted with a Dean-Stark apparatus to allow the azeotropic removal of water. The mixture was refluxed at 90°C overnight. $CDCl_3$ added, solid product **118** collected by filtration as a bright yellow solid (167 mg, 54%); mp 178°C (dec); δ_H (300 MHz, MeOD) 9.98 (2H, br s, COO*H*), 9.07 (2H, s, C*H*N), 8.15 (2H, d, *J* 2.1, Ar*H*), 7.91 (2H, dd, *J* 8.7, *J* 2.1, Ar*H*), 7.77 (2H, d, *J* 7.8, Ar*H*), 7.57 (4H, m, Ar*H*), 7.46 (2H, td, *J* 7.3, *J* 1.8, Ar*H*), 7.02 (2H, d, *J* 8.7, Ar*H);* δ_B (96.4 MHz, MeOD) 17.7; *m/z* HRMS (ESI^-) found 515.1338 ($[M-H]^-$ of $C_{28}H_{18}B_2N_2O_7$ requires 515.1227).

(11*E*, 23*E*)-dimethyl-6,18-*μ*-oxy-tetrabenzo[*c*,*g*,*k*,*o*][1,9,6,14,2,10]dioxadiaza-diboracyclohexadecine-3,15-dicarboxylate

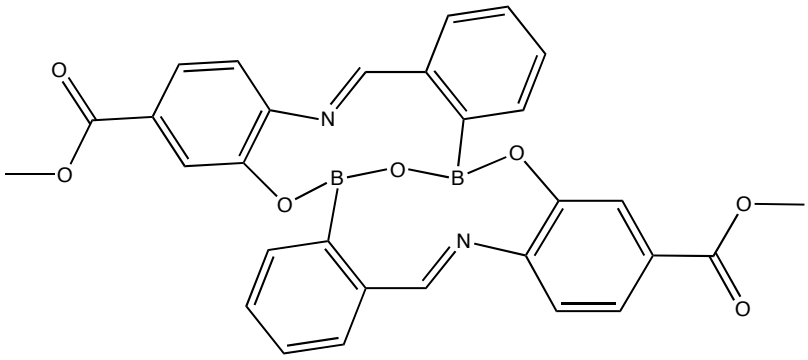

119

Methyl 4-amino-3-hydroxybenzoate (200 mg, 1.20 mmol) and 2-formylphenylboronic acid (180 mg, 1.20 mmol) were dissolved in 95:5 ethanol-benzene and the flask was fitted with a Dean-Stark apparatus to allow the azeotropic removal of water. The mixture was refluxed at 90°C overnight. $CDCl_3$ added, solid product **119** collected by filtration as a bright yellow solid (214 mg, 64%); mp 222-224°C (dec); δ_H NMR (300 MHz, d^6-DMSO) 9.56 (2H, s, ArC*H*NAr), 8.12 (2H, d, *J* 8.4, Ar*H*), 7.76 (2H, dd, *J* 6.3, *J* 1.8, Ar*H*), 7.60 (2H, dd, *J* 8.4, *J*, Ar*H*), 7.35 (2H, d, *J* 1.8, Ar*H*), 7.32 (4H, app t, Ar*H*), 7.08 (2H, dd, *J* 7.2, *J* 1.8, Ar*H*), 3.87 (6H, s, ArCOOCH_3); δ_C compound too poorly soluble to get resolution; δ_B (96.4 MHz, MeOD) 4.1; *m/z* HRMS (ESI^+) found 545.1664 ($[M+H]^+$ of $C_{30}H_{22}B_2N_2O_7$ requires 545.1686).

11*E*,23*E*)-6,18-*μ*-oxy-dinaphtho[*c*,*g*]dibenzo[*k*,*o*][1,9,6,14,2,10]-dioxadiazadiboracyclohexadecine

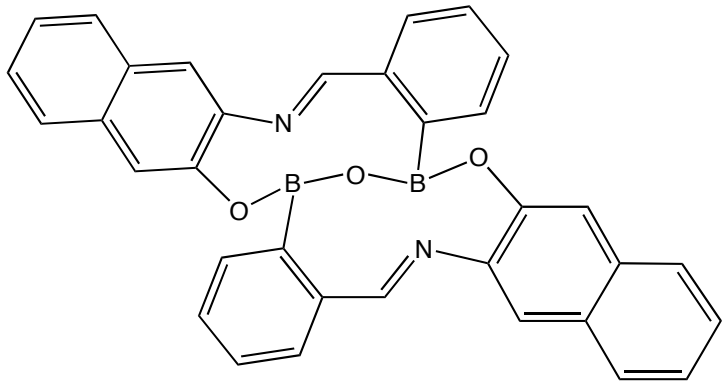

120

3-aminonaphthalen-2-ol (63.7 mg, 0.4 mmol) and 2-formylphenylboronic acid (60.0 mg, 0.4 mmol) were dissolved in 95:5 ethanol-benzene and the flask was fitted with a Dean-Stark apparatus to allow the azeotropic removal of water. The mixture was refluxed at 90°C overnight. $CDCl_3$ added, solid product **120** collected by filtration as a bright yellow solid (64.4mg, 61%); mp 190°C (dec); δ_H (300 MHz, d^6-DMSO) 9.71 (2H, s, N*H*), 8.59 (2H, s, Ar*H*), 7.90 (2H, d, *J* 8.1, Ar*H*), 7.81 (2H, d, *J* 7.8, Ar*H*), 7.76 (2H, d, *J* 8.4, Ar*H*), 7.47 (2H, td, *J* 7.5 *J* 1.2, Ar*H*), 7.36 (4H, app t, *J* 7.1, Ar*H*), 7.27 (2H, td, *J* 7.4 *J* 1.2, Ar*H*), 7.13 (2H, dd, *J* 7.5, *J* 1.2, Ar*H*); δ_C (75.5 MHz, d^6-DMSO) 160.8, 156.9, 136.7, 136.6, 136.5, 134.2, 133.8, 133.5, 129.0, 128.0, 127.3, 126.8, 124.2, 114.0, 107.1, C-B not observed due to quadrupolar relaxation effect of the boron nucleus; δ_B (96.3 MHz, d^6-DMSO) 5.8; m/z HRMS (ESI^+) found 529.1897 ($[M+H]^+$ of $C_{34}H_{22}B_2N_2O_3$ requires 529.1889).

(4*E*,16*E*)-1, 13-dimethoxy-9,21-*μ*-oxy-tetrabenzo[*c*,*g*,*k*,*o*][1,9,6,14,2,10]dioxadiazadiboracyclohexadecine

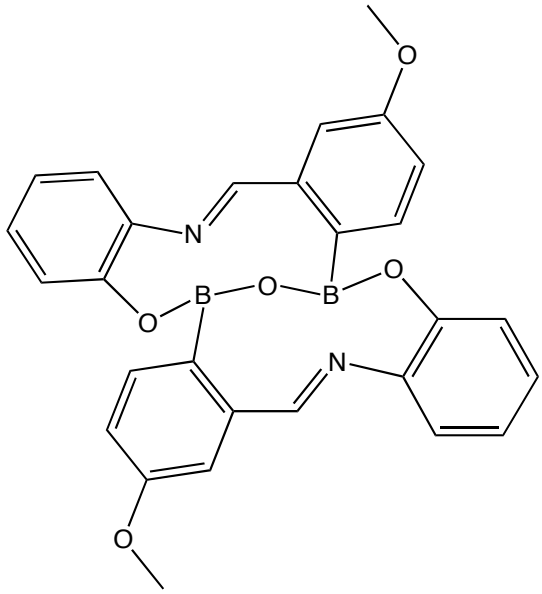

121

2-aminophenol (43.7 mg, 0.4 mmol) and 2-formyl-4-methoxyphenylboronic acid (72.0 mg, 0.4 mmol) were dissolved in 95:5 ethanol-benzene and the flask was fitted with a Dean-Stark apparatus to allow the azeotropic removal of water. The mixture was refluxed at 90°C overnight. $CDCl_3$ added, product **121** collected by filtration as a bright yellow solid (43.0 mg, 44%); mp 172°C (dec); δ_H (300MHz, d^6-DMSO) 9.33 (2H, s, C*H*N), 7.93 (2H, dd, *J* 8.0, *J* 1.2, Ar*H*), 7.34 (2H, td, *J* 8.1, *J* 1.2, Ar*H*), 7.27 (2H, d, *J* 2.4, Ar*H*), 6.95 (2H, td, *J* 8.4, *J* 1.2, Ar*H*), 6.92 (6H, m, Ar*H*), 3.66 (6H, s, OCH_3); δ_B (96.3 MHz, MeOD) 4.1ppm; m/z HRMS (ESI^+) found 488.1844 and 489.1805 ($C_{28}H_{22}B_2N_2O_5$ $[M]^+$ requires 488.1715, $[M+H]^+$ requires 489.1141).

(4*E*,15*E*)-15,17-*μ*-oxy-11,22-dibenzo[*g*,*o*]difuro[2,3*c*:2',3'*k*][1,9,6,14,2,10]dioxadiazadiboracyclohexadecine

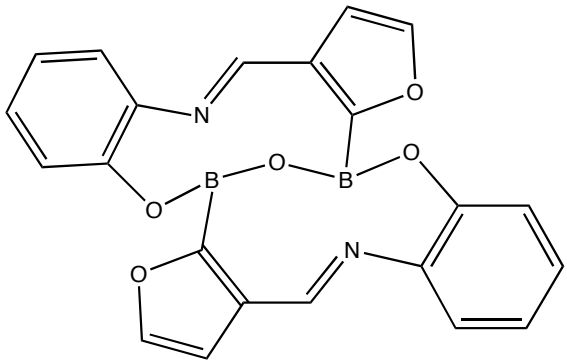

122

2-aminophenol (43.7 mg, 0.4 mmol) and 2-formylfuranboronic acid (62.4 mg, 0.4 mmol) were dissolved in 95:5 ethanol-benzene and the flask was fitted with a Dean-Stark apparatus to allow the azeotropic removal of water. The mixture was refluxed at 90°C overnight. After evaporation of the solvent under vacuum, a small volume of methanol was added, after which the bright yellow solid product **122** was collected by gravimetric filtration (57.9 mg, 71%); mp 208-210°C (dec); δ_H (300 MHz, DMSO) 9.25 (2H, s, C*H*N), 7.77 (2H, d, *J* 7.2, Ar*H*), 7.66 (2H, d, *J* 1.8, Ar*H*), 7.28 (2H, td, *J* 7.7, *J* 1.5, Ar*H*), 6.91 (4H, m, Ar*H*), 6.66 (2H, d, *J* 1.2, Ar*H*); δ_B (96.3 MHz, DMSO) 7.6; m/z HRMS (ESI^+) found 839.4754 ($C_{44}H_{28}B_4N_4O_{10}$ $[M_2Na]^+$ requires 839.2070).

5-((methylamino)methyl)-2-nitrophenol

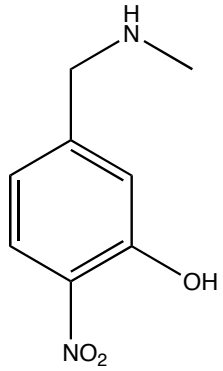

124

At RT under a nitrogen atmosphere, methylamine (1.5 mL as a 2M solution in methanol, 2.99 mmol) was added to a stirring solution of 3-hydroxy-4-nitrobenzaldehyde (500mg, 2.99 mmol) in anhydrous methanol. After 4h the solution was cooled to 0°C using an ice-water bath and under a flow of nitrogen gas sodium borohydride (181 mg, 4.79 mmol, 1.6eq) was added portion-wise. The solution was stirred for a further 2h, allowing the system to return to RT. 1M NaOH was added and extraction with ethyl acetate (3 x 20mL) was performed at pH = 8, as measured by a calibrated pH meter. Upon evaporation of the organic phase compound **124** was collected as an orange solid (441 mg, 81%); mp 146°C; δ_H (300 MHz, 20% DCl-D_2O,) 5.93 (1H, d, *J* 8.7, Ar*H*), 5.09 (1H, s, Ar*H*), 4.93 (1H, dd, *J* 8.7, *J* 1.8, Ar*H*), 2.06 (2H, s, ArCH_2), 0.53 (3H, s, NHCH_3); δ_C (75.5 MHz, 20% DCl-D_2O,) 152.0, 134.1, 139.9, 125.1, 123.6, 112.4, 56.8, 35.6; m/z HRMS (ESI^-) found 181.1693 ($[M-H]^-$ of $C_8H_9N_2O_3$ requires 181.1692).

2-amino-5-((methylamino)methyl)phenol

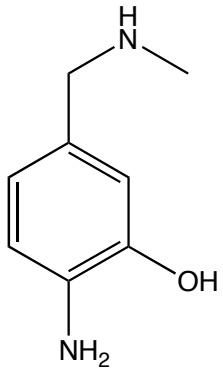

125

5-((methylamino)methyl)-2-nitrophenol **124** (190 mg, 1.04 mmol) and 10% palladium on carbon (60mg) was suspended in anhydrous methanol (15 mL) and the flask sealed with a rubber septum. Under a hydrogen gas atmosphere (balloon) the reaction mixture was stirred vigorously for 3h. After filtration over Celite, the methanol was removed under vacuum and then diethyl ether (15mL) and distilled water (15mL) were added. Extracting three times (10mL diethyl ether) at pH 7 - confirmed by calibrated pH meter – and subsequent drying over sodium sulfate and evaporation afforded the target compound **125** as a brown solid (119mg, 75%); mp 208°C; δ_H (300MHz, MeOD) 6.67 (1H, m, Ar*H*), 6.64 (2H, m, Ar*H*), 3.83 (2H, s, ArCH_2NH), 2.51 (3H, s, NHCH_3); δ_C (75.5MHz, MeOD) 144.2, 136.6, 128.0, 121.6, 116.8, 116.7, 57.5, 36.1; m/z HRMS (ESI^-) found 151.0873 ($[M-H]^-$ of $C_8H_{11}N_2O^-$ requires 151.0877)

(*R*,*E*)-2-((1-hydroxy-3-methylbutan-2-ylimino)methyl)phenyldiboronate

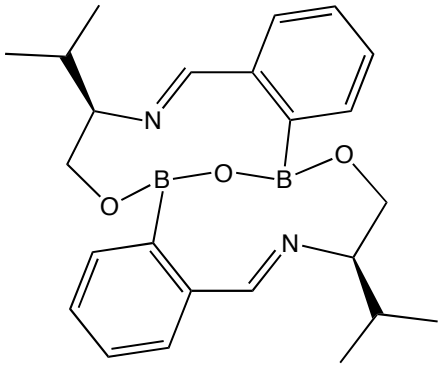

126

2-formylphenylboronic acid (60.0 mg, 0.40 mmol) and (*R*)-2-amino-3-methyl-1-butanol (45 μL, 0.40 mmol) were stirred in $CDCl_3$ (5 mL) for 5 min in the presence of 4 Å molecular sieves. The sieves were removed by gravimetric filtration and the solvent removed *in vacuo* to afford the title compound **126** as a yellow oil (81 mg, 98%), $[\alpha]_D^{20}$ +22.77 (*c* 1.520, CH_2Cl_2); ν_{max} (film)/cm^{-1} 1628 (C=N); δ_H (300 MHz, $CDCl_3$) 8.08 (2H, s, C*H*N), 7.51 (2H, d, *J* 7.4, Ar*H*), 7.35-7.27 (4H, m, Ar*H*), 7.11 (2H, dt, *J* 7.4, *J* 1.1, Ar*H*), 4.26 (2H, dd, *J* 12.2, *J* 1.3, CH_AH$_B$(O)), 3.98 (2H, dd, *J* 12.2, *J* 1.3, CH$_A$$H_B$(O)), 3.13 (2H, m, C*H*(iPr)(N)), 2.96-2.83 (2H, m, C*H*$(CH_3)_2$), 1.02 (6H, d, *J* 6.8, C(CH_3)(CH_3)), 0.88 (6H, d, *J* 6.8, C(CH_3)(CH_3)); δ_C (75.5 MHz, $CDCl_3$) 167.3, 136.8, 133.6, 129.4, 127.2, 127.0, 126.2, 76.0, 60.9, 27.0, 21.1, 19.4; δ_B (100 MHz, $CDCl_3$) 10.7; *m*/*z* HRMS (ESI^+) found 417.2521 ($[M+H]^+$ of $C_{24}H_{30}B_2N_2O_3$ requires 417.2518).

(8*S*,9*E*,18*S*,19*E*)-8,18-diphenyl-5,7,8,15,17,18-hexahydro-6,18-μ-oxy-dibenzo-[*c*,*k*][1,9,6,14,2,10]dioxadiazadiboracyclohexadecine

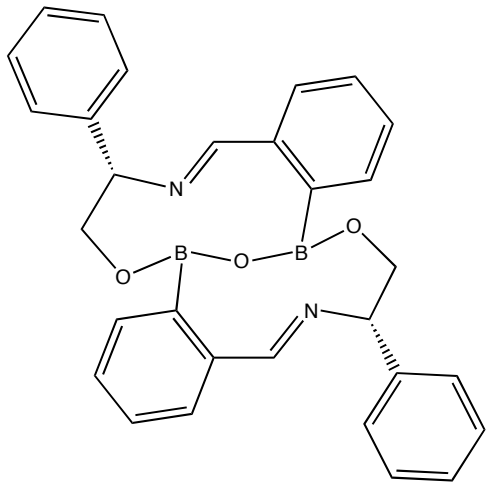

127

2-Formylphenylboronic acid 73 (60 mg, 0.4 mmol) and (*S*)-2-phenylglycinol (*S*)-150 (55 mg, 0.4 mmol) were stirred in $CDCl_3$ (5 mL) for 5 min in the presence of 4 Å molecular sieves at room temperature. The sieves were removed using gravity filtration and the solvent removed *in vacuo* to afford the title compound **127** as a yellow oil (92 mg, 95%); $[\alpha]^{20}D$ -21.10 (*c* 1.450, CH_2Cl_2); ν_{max} (film)/cm^{-1} 1627 (C=N); δ_H (300 MHz, $CDCl_3$) 7.65-7.63 (4H, m, C*H*N and Ar*H*), 7.43-7.30 (12H, m, Ar*H*), 7.20 (2H, br t, *J* 7.4, Ar*H*), 7.09 (2H, dt, *J* 7.4, *J* 0.8, Ar*H*), 5.25 (2H, m, $CH_AH_B(O)$), 4.65 (2H, dd, *J* 11.7, *J* 10.6, C*H*(Ph)(N)), 3.95 (2H, m, $CH_AH_B(O)$); δ_C (75 MHz, $CDCl_3$) 166.0, 137.0, 135.6, 133.9, 133.5, 132.3, 130.0, 129.9, 129.7, 129.4, 128.0, 127.3, 126.8, 71.3, 65.8; δ_B (100 MHz, $CDCl_3$) 10.8; *m*/*z* HRMS (ESI^+) found 485.2206 ($[M+H]^+$ of $C_{30}H_{26}B_2N_2O_3$ requires 485.2208).

4,4'-methylenebis(2,6-di-*tert*-butyl-4,1-phenylene) bis(phenylcarbamate)

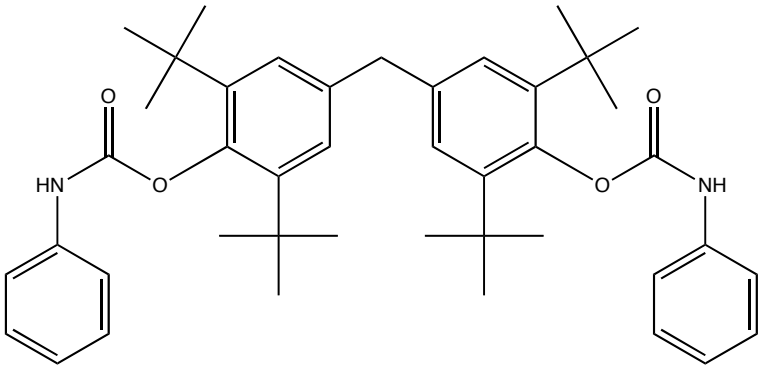

128

4,4'-methylenebis(3,5-di-t*ert*-butylphenol) **101** (0.47 mmol, 200 mg) was dissolved in anhydrous toluene (10mL) under a N_2 atmosphere. Dibutyl tin diacetate (0.05 mmol, 13 μL) and phenylisocyanate (1.00 mmol, 109 μL) were added and the mixture stirred at 100°C for 12 h. Upon cooling the reaction mixture was filtered through Celite and washed with water (3 x 10mL), the organic residues dried with Na_2SO_4 and evaporated to dryness under vacuum. Column Chromatography (100% Ethyl Acetate) afforded the desired compound **128** as a white powder. (243 mg, 78%); mp 220-221°C; δ_H (300 MHz, MeOD) 7.41 (4H, s, Ar*H*), 7.21 (4H, t, *J* 7.5, Ar*H*), 7.09 (4H, s, Ar*H*), 6.97 (2H, t, *J* 7.2, Ar*H*) 4.03 (2H, br s, N*H*), 3.86 (2H, s, ArCH_2Ar), 1.28 (36H, s, C(CH_3)$_3$); δ_C (75.5 MHz, $CDCl_3$-MeOD) 155.4, 147.8, 144.8, 140.2, 139.3, 130.6, 128.4, 125.1, 120.8, 43.5, 37.2, 33.0; m/z HRMS (ESI^+) found 680.4395 ($[M+NH_4]^+$ of $C_{43}H_{54}N_2O_4$ requires 680.4422).

2,6-di-*tert*-butyl-4-(3,5-di-*tert*-butyl-4-hydroxybenzyl)phenyl phenylcarbamate

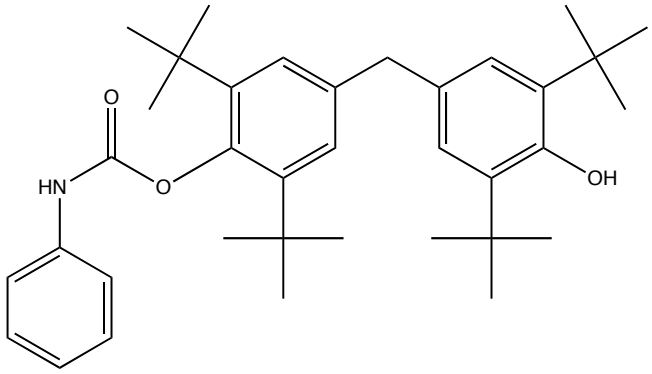

129

Compound **129** isolated from column of bis compound **128**, in 14% conversion (35.8 mg); mp 185-186°C; δ_H (300 MHz, $CDCl_3$) 7.39 (2H, d, *J* 7.8, Ar*H*), 7.24 (2H, t, *J* 7.5, Ar*H*), 7.07 (2H, s, Ar*H*), 7.00 (1H, t, *J* 7.5, Ar*H*), 6.96 (s, 2H, Ar*H*), 6.90 (1H, br s, N*H*), 4.99 (1H, s, ArO*H*), 3.82 (2H, s, ArCH_2Ar), 1.35 (18H, s, C(CH_3)$_3$), 1.27 (18H, s, C(CH_3)$_3$); δ_C (75.5 MHz, $CDCl_3$) 153.1, 152.6, 146.2, 143.2, 138.8, 138.2, 136.3, 131.7, 129.7, 127.3, 126.1, 124.2, 119.2, 42.1, 36.1, 34.9, 32.1, 31.1, 30.9; m/z HRMS (ESI^-) 542.3629 ($[M-H]^-$ of $C_{36}H_{49}NO_3$ requires 542.3640).

4,4'-methylenebis(2,6-diisopropylaniline)

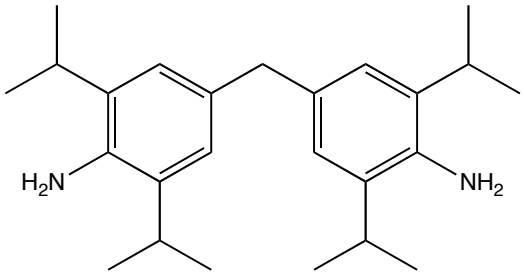

137

2,6-di*iso*propylaniline (500 μL, 2.65 mmol) and formaldehyde (215 μL, 2.65 mmol, as a 37% aq solution) were dissolved in 3.0 mL of *iso*propanol in a round bottomed flask fitted with a stirrer bar. Whilst stirring vigorously, NaOH (23% w/v aq solution, 3.98 mmol, 694 μL) was added dropwise and the mixture stirred for a further 4 hours. The solvent volume was reduced under vacuum to about 1 mL and diethyl ether (15mL) and water (5mL) added. The organic phase was extracted and evaporated to dryness under reduced pressure. Column chromatography (pentane/ether, 9:1) afforded the target compound **137** as an off-white solid (301 mg, 62%); mp 68-70°C; δ_H (300 MHz, $CDCl_3$) 6.89 (4H, s, Ar*H*), 3.87 (2H, s, ArCH_2Ar), 3.63 (4H, br s, NH_2), 2.94 (4H, septet, *J* 6.9, C*H*(CH_3)$_2$), 1.25 (24H, d, *J* 6.9, CH(CH_3)$_2$); δ_C (75.5 MH, $CDCl_3$,) 138.3, 133.0, 132.0, 123.7, 41.6, 28.4, 23.0; m/z HRMS (ESI^+) found 367.3096 ($[M+H]^+$ of $C_{25}H_{38}N_2$ requires 367.3108).

bis(4-iodo-3,5-di*iso*propylphenyl)methane

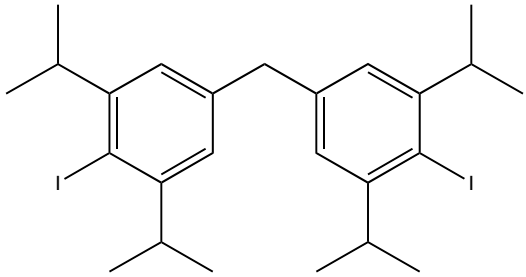

142

4,4'-methylenebis(3,5-di*iso*propylaniline) **137** (9.82 mmol, 3.60 g) was stirred vigorously in *iso*propanol (40 mL) and *p*-TSA (58.9 mmol, 11.2 g) was added. To the subsequent solution an aqueous solution (approx. 15mL) of $NaNO_2$ (39.28 mmol, 2.71 g) and KI (49.1 mmol, 8.15 g) was added dropwise. The resultant suspension was stirred for 4h. Saturated $NaHCO_3$ was added to neutrality and aqueous sodium thiosulfate (2M, 8 mL) was added affording an orange solution. The *iso*propanol was removed under vacuum and the residues were extracted with diethyl ether (3 x 20 mL). Column Chromatography (100% hexane) afforded the desire species **142** as a white solid (2.54 g, 88%); mp 91-92°C; δ_H (250 MHz, $CDCl_3$,) 6.97 (4H, s, Ar*H*), 3.99 (2H, s, ArCH_2Ar), 3.46 (4H, septet, *J* 7.0, Ar$CH(CH_3)_2$), 1.26 (24H, d, *J* 7.0, Ar$CH(CH_3)_2$); δ_C (75.4 MHz, $CDCl_3$) 151.1, 140.6, 124.5, 106.3, 41.0, 39.3, 23.5; m/z HRMS (EI^+) found 588.0738 ($[M]^+$ of $C_{25}H_{34}I_2$ requires 588.0744).

bis(4-azido-3,5-diisopropylphenyl)methane

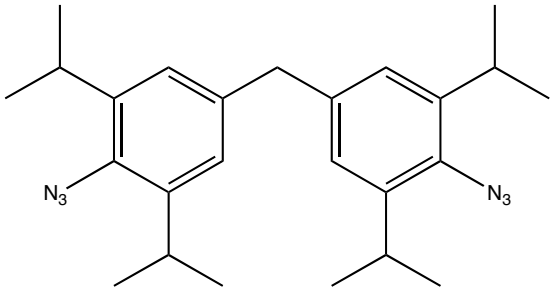

143

4,4'-methylenebis(3,5-di*iso*propylaniline) **137** (2.73 mmol, 1000 mg) was dissolved in HCl (33% v/v aq solution) with 10 g ice. $NaNO_2$ (423 mg, 6.13 mmol in 5mL H_2O) was added slowly over 5 minutes and left to stir for 40 min. $NaHCO_3$ (4.5 mL saturated aq solution) was added to the solution whilst maintaining a temperature of 0°C with an ice bath, then NaN_3, (6.35 mmol, 413 mg, in 4.5 mL H_2O) was slowly added. After 1 h stirring at 0°C, the solution was allowed to return to room temperature, then extracted with diethyl ether (3 x 20 ml). The organic extracts were combined, washed with sat. $NaHCO_3$ followed by H_2O and then dried over sodium sulfate, filtered and evaporated to dryness at reduced pressure. Column chromatography (100% hexane) afforded the desired compound **143** as a colourless gum. (891 mg, 78%); δ_H (250 MHz, $CDCl_3$) 6.99 (4H, s, Ar*H*), 3.98 (2H, s, ArCH_2Ar), 3.38 (4H, septet, *J* 6.8, C*H*$(CH_3)_2$), 1.30 (24H, d, *J* 6.8, CH(CH_3)$_2$); δ_C (75.4 MHz, $CDCl_3$) 148.2, 140.4, 124.3, 122.5, 41.1, 32.0, 21.6; *m/z* HRMS (ESI^+) found 393.2991 ($[M\text{-}N_2\text{+}3H]^{++}$ of $C_{25}H_{34}N_6$ requires 393.3013). Loss of nitrogen and subsequent protonation occurred in mass spectrometer as ^1H NMR indicates symmetrical species.

2-(3-bromophenyl)-4,4,5,5-tetramethyl-1,3,2-dioxaborolane

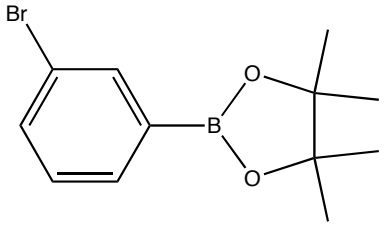

144

3-bromophenylboronic acid (800 mg, 3.98 mmol) and 2,3-dimethylbutane-2,3-diol (4.00 mmol, 472.7 mg) and calcium sulphate (3.00g) were mixed in toluene (40 mL) in a flask fitted with a Dean-Stark trap and condenser and heated at reflux for 4h. Whilst hot, the reaction mixture was filtered and the filter cake washed with further toluene (10 mL) and the filtrate was evaporated at reduced pressure yielding the desired compound **144** as a colourless oil. (1.103 g, 98%); δ_H (300 MHz, $CDCl_3$) 8.04 (1H, s, Ar*H*), 7.82 (1H, d, *J* 1.2, Ar*H*), 7.61 (1H, dt, *J* 7.2, *J* 0.8, Ar*H*), 7.28 (1H, app t, Ar*H*), 1.40 (12H, s, CH_3); δ_C (75.5 MHz, $CDCl_3$) 133.0, 134.6, 131.5, 129.9, 129.8, 123.3, 84.1, 25.6; δ_B (96.4 MHz, $CDCl_3$) 30.2; m/z HRMS (ESI^-) found 283.0501 ($[M+CH_3O]^-$ of $C_{13}H_{19}BBrO_3$ requires 283.0499).

trimethyl((3-(4,4,5,5-tetramethyl-1,3,2-dioxaborolan-2-yl)phenyl)ethynyl)silane

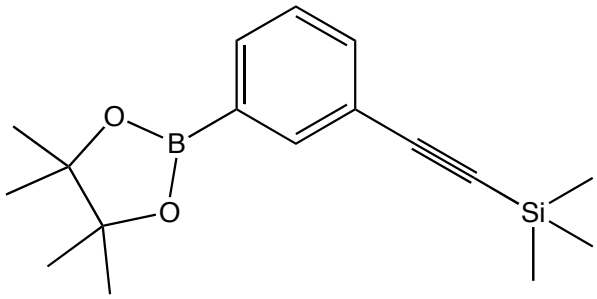

145

2-(3-bromophenyl)-4, 4, 5, 5-tetramethyl-1, 3, 2-dioxaborolane (1.41 mmol, 400 mg) , triphenylphosphine (0.28 mmol, mg), CuI (0.07 mmol, 13.3 mg), Pd[$(PPh_3)_2Cl_2$] (0.07 mmol, 49.1 mg), diethylamine (21.2 mmol, 2.19 mL) and DMF (4.0 mL) were added to a thick-walled glass pressure tube fitted with a stirrer. Trimethylsilylacetylene (1.55 mmol, 221 μL) was added and the teflon screw cap secured. The reaction mixture was stirred at 130°C for 12 h. Reaction mixture was cooled, filtered through Celite and washed with DCM (20mL). The combined organic extracts were evaporated at reduced pressure and subjected to column chromatography (hexane-EtOAc 10:1) to afford the desired compound **145** as a colourless gum. (411 mg, 97%); δ_H (250 MHz, $CDCl_3$) 7.95 (1H, s, Ar*H*), 7.74 (1H, dt, *J* 7.3, *J* 1.5, Ar*H*), 7.54 (1H, dt, *J* 7.8, *J* 1.5 Hz, Ar*H*), 7.31-7.30 (1H, m, Ar*H*), 1.33 (12H, s, OC($C H_3$)$_2$), 0.24 (9H, s, Si($C H_3$)$_3$); δ_C (62.9 MHz, $CDCl_3$) 138.5, 134.4, 133.9, 128.5, 127.6, 122.7, 105.1, 94.0, 77.1, 24.9, 0.0; δ_B (96.3 MHz, $CDCl_3$) 30.0; m/z HRMS (ESI^-) found 321.0216 ($[M-H]^-$ for $C_{16}H_{12}BBr_2N_2$ requires 321.0204).

2-(3-ethynylphenyl)-4, 4, 5, 5-tetramethyl-1, 3, 2-dioxaborolane

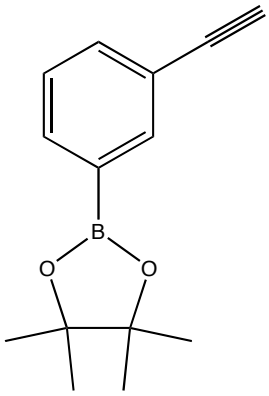

146

trimethyl((3-(4,4,5,5-tetramethyl-1,3,2-dioxaborolan-2-yl)phenyl)ethynyl)silane **145**, (1.0 mmol, 300 mg) was dissolved in methanol (8 mL) and potassium carbonate (5.0 mmol, 373 mg) added. The mixture was stirred for 4 h at RT and filtered. Column chromatography (hexane-EtOAc 9:1) afforded the target alkyne **146** as a white solid. (164 mg, 72%); mp 109°C; δ_H (300 MHz, $CDCl_3$,) 8.03 (1H, s, Ar*H*), 7.82 (1H, dt, *J* 7.5, *J* 1.2, Ar*H*), 7.63 (1H, dt, *J* 7.8, *J* 1.5, Ar*H*), 7.38 (1H, t, *J* 7.5, Ar*H*), 3.11 (1H, s, ArC≡C*H*), 1.40 (12H, s, CH_3); δ_C (75.5 MHz, $CDCl_3$) 138.9, 135.1, 132.0, 128.7, 128.1, 122.1, 89.8, 84.4, 84.0, 25.3; δ_B (96.4 MHz, $CDCl_3$,) 30.0; m/z HRMS (ESI^-) found 259.1510 ($[M+CH_3O]^-$ of $C_{15}H_{20}BO_3$ is 259.1506).

bis(3,5-diisopropyl-4-(4-(3-(4,4,5,5-tetramethyl-1,3,2-dioxaborolan-2-yl)-phenyl)1*H*-1,2,3-triazol-1-yl)phenyl)methane

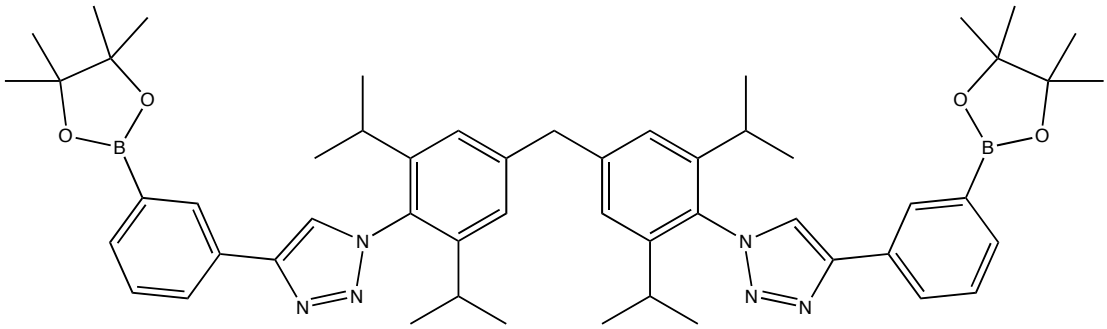

147

Bisazide **143** (0.12 mmol, 50 mg), 2-(3-ethynylphenyl)-4, 4, 5, 5-tetramethyl-1, 3, 2-dioxaborolane **146** (0.48 mmol, 110 mg) and Copper (I) Iodide (0.03 mmol, 6.0 mg) were charged to a Schlenk tube and exposed to 3 x N_2/purge cycle. Fresh anhydrous DMSO was added (8 mL) under N_2 and the reaction was stirred at 70°C for 12 h. Column chromatography (DCM-MeOH, 99:1) afforded the desired diboronic acid ester **147** as a brown solid. (65.1 mg, 62%); mp 198-200 °C (dec); δ_H (300MHz, $CDCl_3$) 8.18, (2H, s, C*H*N), 8.12 (2H, dt, *J* 7.5, *J* 1.7, Ar*H*), 7.89 (2H, s, Ar*H*), 7.74 (2H, dt, *J* 7.5, *J* 1.2, Ar*H*), 7.43 (2H, t, *J* 7.5, Ar*H*), 7.08 (4H, s, Ar*H*), 4.08 (2H, ArCH_2Ar), 2.27 (4H, septet, *J* 6.9, C*H*$(CH_3)_2$), 1.29 (24H, s, ArCH(CH_3)$_2$), 1.08 (24H, dd, *J* 6.3, *J* 1.2 ArCH(CH_3)$_2$); δ_B (96.3 MHz, $CDCl_3$) 29.8;

4',4''-methylenebis(2',6'-diisopropylbiphenyl-4',3-diyl)diboronic acid

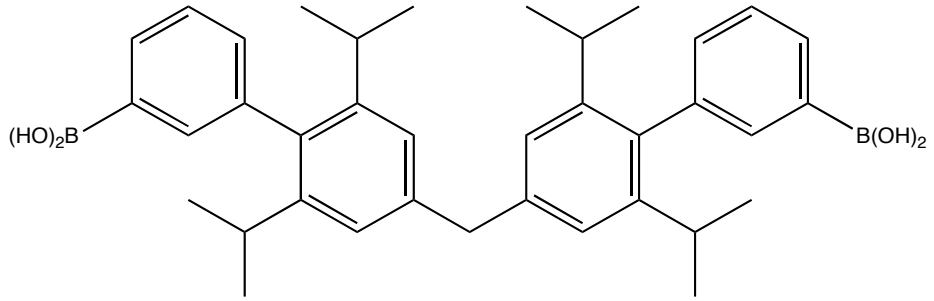

148

Compound **153** (0.19 mmol, 112 mg) was dissolved in MeOH (8 mL) and conc. H_2SO_4 (500 μl) was added. This mixture was stirred at RT for 2 hr, after which the product was extracted with diethyl ether (3 x 10 mL portions). The organic phase were evaporated to dryness *in vacuo* to afford the desired compound **148** as a brown solid (89.8 mg, 82%); mp 248-249°C; δ_H (300 MHz, $CDCl_3$) 6.92-6.83 (6H, m, Ar*H*), 6.82 (4H, s, Ar-*H*), 3.88 (2H, ArCH_2Ar), 2.77 (4H, *J* 6.9, $CH(CH_3)_2$), 1.15 (24H, *J* 6.9, $CH(CH_3)_2$); δ_C (75.5 MHz, $CDCl_3$) 148.2, 141.1, 136.7, 134.8, 130.4, 128.1, 125.0, 122.7, 42.6, 31.6, 23.4; δ_B (96.3 MHz, $CDCl_3$) 30.8; m/z HRMS (ESI^-) found 607.3781 ($[M+MeO]^-$ of $C_{37}H_{46}B_2O_4$ requires 607.3772).

4,4'-methylenebis(2,6-diisopropyl-4,1-phenylene)diboronic acid

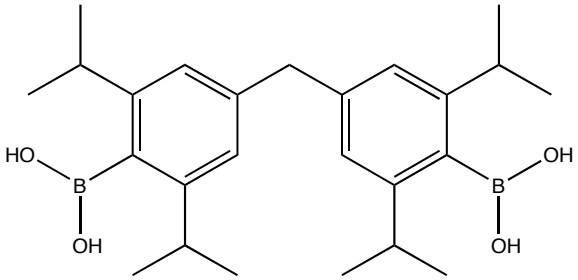

150

bis(3,5-di-*tert*-butyl-4-iodophenyl)methane **142** (0.51 mmol, 300 mg) was dissolved in anhydrous tetrahydrofuran (20 mL) in a sealed round bottom flask under nitrogen gas atmosphere and stirred at -78°C. Dropwise addition of *n*BuLi (1.122 mmol, 0.45mL of a 2.5M in hexanes) *via* syringe was completed and stirring continued at low temperature for 45 min. Trimethyl borate (3.06 mmol, 340 μL) was added to a separate reaction vessel cooled to -78°C under N_2 in 10 mL THF. The lithiated species was transferred to this second cooled flask by cannula under N_2 pressure and the reaction was allowed to return to room temperature overnight. The mixture was added to 50 ml of a 10% aqueous sulphuric acid solution with stirring. After 1h, the mixture was extracted with diethyl ether (3 x 20 mL). The combined organic extracts were dried over Na_2SO_4, filtered and evaporated under vacuum. The desired bisboronic acid species **150** was afforded as a yellow solid without need for further purification. (151 mg, 70%); mp 198-199 °C; δ_H (250 MHz, MeOD-$CDCl_3$) δ 6.55 (4H, s, Ar*H*), 4.02 (2H, s, ArCH_2Ar), 3.48 (4H, septet, *J* 7.0, $CH(CH_3)_2$), 0.84 (24H, d, *J* 7.0, $CH(CH_3)_2$); δ_C (62.9 MHz, MeOD-$CDCl_3$,) 148.7, 141.0, 124.3, 122.0, 42.0, 34.1, 23.7; δ_B (96.3 MHz, MeOD-$CDCl_3$) 30.0; *m/z* HRMS (ESI^+) found 455.3152 ($[M+MeO]^-$ of $C_{25}H_{38}B_2O_4$ requires 455.2233).

2-(2-bromophenyl)-2,3-dihydro-1*H*-naphtho[1,8-*de*][1,3,2]diazaborinine

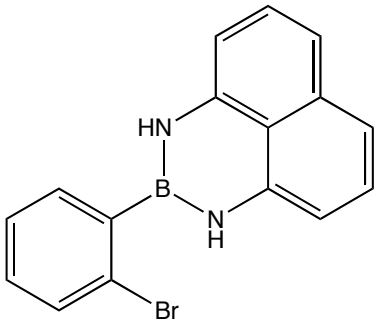

151

2-bromophenyl boronic acid (1.49 mmol, 300 mg) and 1,8-naphthalene (1.50 mmol, 237.3 mg) were dissolved in toluene (30 mL) and refluxed in apparatus fitted with a Dean-Stark trap for 3 h. Upon cooling the solvent was evaporated at reduced pressure and the crude mixture was subjected to silica gel column chromatography (hexane-EtOAc 10:1) affording the desired compound **151** (462 mg, 96%); mp 156°C (dec); δ_H (300 MHz, $CDCl_3$) 7.49 (1H, dd, *J* 7.8, *J* 1.2, Ar*H*), (1H, dd, *J* 7.5, *J* 1.8, Ar*H*), 7.25 (1H, dt, *J* 7.2, *J* 1.2, Ar*H*), 7.20-7.14 (1H, m, Ar*H*), 7.10-6.95 (6H, m, Ar*H*), 6.27 (2H, dd, *J* 7.2, *J* 1.2, Ar*H*), 5.88 (2H, br s, N*H*); δ_C (75.5 MHz, $CDCl_3$) 139.8, 135.3, 133.1, 131.2, 130.0, 128.0, 127.2, 126.6, 125.9, 117.0, 105.9 C-B not visible due to quadrupolar relaxation effect of boron nucleus; δ_B (96.3 MHz, $CDCl_3$) 29.2; m/z HRMS $(ESI)^-$ found 321.0266 ($[M-H]^-$ for $C_{16}H_{12}BBrN_2$ requires 321.0204).

2-(3-bromophenyl)-2, 3-dihydro-1*H*-naphtho[1,8-*de*][1,3,2]diazaborinine

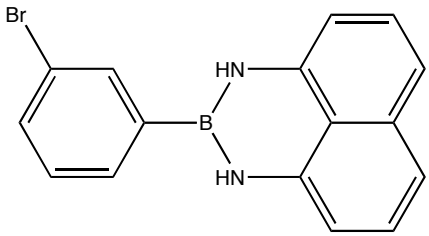

152

3-bromophenyl boronic acid (2.49 mmol, 500 mg) and 1,8-diaminonaphthalene (2.49 mmol, 394 mg) were dissolved in toluene (35 mL) and refluxed in a round-bottomed flask fitted with a Dean-Stark trap and condenser for 3h. Upon cooling the solvent was evaporated at reduced pressure and column chromatography (hexane:EtOAc 9:1) afforded the desired compound **152** (756 mg, 94%); mp 181°C (dec); δ_H (250 MHz, $CDCl_3$) 7.67 (1H. s, Ar*H*), 7.48 (2H, m, Ar*H*), 7.20 (2H, m, Ar*H*), 7.03 (4H, m, Ar*H*), 6.32 (2H, dd, *J* 8.4, *J* 1.5, Ar*H*), 5.87 (2H, br s, N*H*); δ_C ($CDCl_3$, 62.9 MHz) 140.5, 136.1, 134.4, 133.2, 130.0, 129.9, 127.6, 123.0, 119.9, 118.3, 106.4, C-B not visible due to quadrupolar relaxation effect of boron nucleus; δ_B (96.4 MHz, $CDCl_3$) 29.9; m/z HRMS $(ESI)^-$ found 321.0256 ($[M-H]^-$ of $C_{16}H_{12}BBrN_2$ requires 321.0204);

bis(2,6-diisopropyl-3'-(1*H*-naphtho[1,8-*de*][1,3,2]diazaborinin-2(3*H*)-yl)biphenyl-4-yl)methane

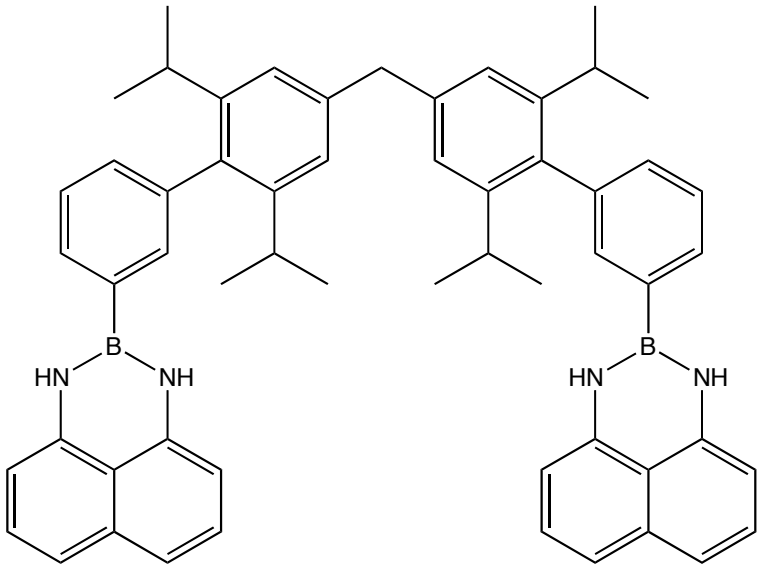

153

Boronic acid **150** (200 mg, 0.47 mmol), aryl bromide **152** (396 mg, 1.23 mmol), finely ground K_3PO_4 (596 mg, 2.82 mmol), Pd_2dba_3 (25.8 mg, 0.03 mmol) and S-PHOS (13.2 mg, 0.03 mmol) were dissolved in anhydrous toluene (10mL) under nitrogen in a Schlenk tube fitted with a magnetic stirrer. The mixture was stirred vigorously at 100°C for 24 h. Upon cooling the reaction mixture was diluted with ethyl acetate (10mL) and passed through Celite and washed with additional ethyl acetate (20mL). The organic washings were evaporated *in vacuo*. DCM-MeOH (98:2) column chromatography of the crude product allowed isolation of the title compound **153** as a brown solid. (235 mg, 61%); mp 188°C (dec); δ_H (300 MHz, $CDCl_3$) 7.64 (2H, t, *J* 1.5, Ar*H*), 7.48 (2H, dq, *J* 7.8, *J* 1.5, Ar*H*), 7.41 (2H, dt, *J* 7.5, *J* 1.1, Ar*H*), 7.18 (2H, t, *J* 7.5, Ar*H*), 7.06-6.95 (10H, m, Ar*H*), 6.83-6.80 (2H, m, Ar*H*), 6.29 (4H, dd, *J* 7.1, *J* 1.1, Ar*H*), 5.83 (4H, br s, N*H*), 3.85 (2H, s, ArCH_2Ar), 2.76 (4H, septet, *J* 6.9 Hz, $CH(CH_3)_2$), 1.14 (24H, d, *J* 6.9 Hz, $CH(CH_3)_2$); δ_C (75.5 MHz, $CDCl_3$) 149.2, 141.4, 141.1, 136.7, 134.8, 133.6, 130.4, 128.1, 125.0, 123.5, 122.7, 120.3, 118.6, 106.7, 42.6, 34.6, 24.5; δ_B (96.3 MHz, $CDCl_3$) 29.2; m/z HRMS (ESI^-) found 695.2048 and 695.2032 (implies loss of 1 or 2 dan groups in MS environment - $[C_{47}H_{49}B_2N_2O_2^{3-}]$ requires 695.3997, $[C_{43}H_{60}B_2O_6^{2-}]$ requires 695.4660).

2-*p*-tolyl-2,3-dihydro-1*H*-naphtho[1,8-*de*][1,3,2]diazaborinine

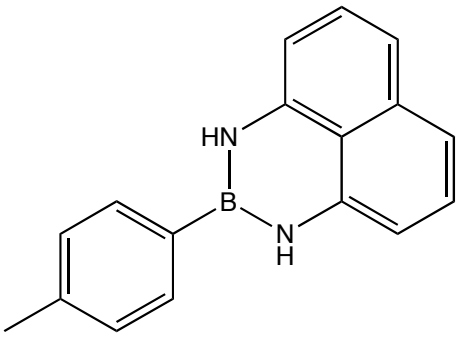

154

4-tolylboronic acid (3.68 mmol, 500 mg) and 1,8-diaminonaphthalene (3.68 mmol, 581.8 mg) were dissolved in toluene and refluxed in apparatus fitted with a Dean-Stark trap for 3h. Upon cooling the solvent was evaporated at reduced pressure. The resulting dark brown solid was purified by column chromatography (DCM/methanol 9:1) and the product **154** was obtained as a white crystalline solid. (873 mg, 92%); mp 172°C (dec); δ_H (300 MHz, $CDCl_3$) 7.47 (2H, d, *J* 7.8, Ar*H*), 7.21 (2H, d, *J* 7.0, Ar*H*), 7.06 (2H, t, *J* 8.0, Ar*H*), 6.98 (2H, d, *J* 8.5, Ar*H*), 6.33 (2H, d, *J* 7.5, Ar*H*), 5.94 (2H, br s, N*H*), 2.32 (3H, s, ArCH_3); δ_C (75.5 MHz, $CDCl_3$) 141.6, 140.8, 136.8, 131.8, 129.5, 128.0, 120.2, 118.1, 106.4, 22.0, C-B not visible due to quadrupolar relaxation effect of boron nucleus; δ_B (96.3 MHz, $CDCl_3$) 30.1; m/z HRMS (ESI^-) found 257.1231 ($[M-H]^-$ of $C_{17}H_{15}BN_2$ requires 257.1256).

5-((dimethylamino)methyl)nitrophenol

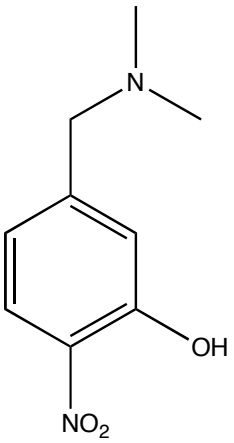

155

At RT under a nitrogen atmosphere, dimethylamine (1.5 mL as a 2M solution in THF, 2.99 mmol) was added to a stirring solution of 3-hydroxy-4-nitrobenzaldehyde (500mg, 2.99 mmol) in anhydrous methanol. After 4h the solution was cooled to 0°C using an ice-water bath and under a flow of nitrogen gas sodium borohydride (181 mg, 4.79 mmol, 1.6 eq) was added portion-wise. The solution was stirred for a further 2h, allowing the system to return to RT. 1M NaOH was added and extraction with ethyl acetate (3 x 20mL) was performed at pH 8, as measured by a calibrated pH meter. Upon evaporation of the organic phase compound **156** was collected as an orange solid (456 mg, 78%); mp 144°C; ^{1}H NMR (MeOD, 300 MHz) δ 6.71 (3H, m, Ar*H*), 3.79 (2H, s, CH_2), 2.42 (6H, s, N(CH_3)$_2$); ^{13}C NMR (MeOD, 75.5 MHz) 146.5, 135.4, 128.2, 123.2, 118.0, 115.3, 66.7, 45.1; m/z HRMS (ESI$^-$) found 1065.1034 ([M-H]$^-$ of $C_9H_{13}N_2$ requires 165.1033).

2-amino-5-((dimethylamino)methyl)phenol

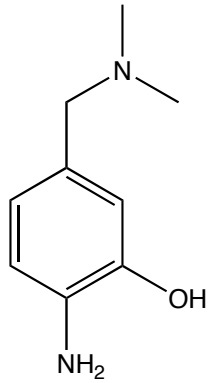

156

5-((dimethylamino)methyl)nitrophenol **156** (210 mg, 1.07 mmol) and 10% palladium on carbon (65 mg) were suspended in anhydrous methanol (15 mL) and the flask sealed with a rubber septum. Under a hydrogen gas atmosphere (balloon) the reaction mixture as stirred vigorously for 3h. After filtration over Celite, the methanol was removed under vacuum and then diethyl ether (15mL) and distilled water (15mL) were added. Extracting three times (10mL diethyl ether) at pH 7 - confirmed by calibrated pH meter – and subsequent drying over sodium sulfate and evaporation afforded the target compound **157** as a brown solid (117mg, 66%)**;** mp 201°C; ^{1}H NMR (MeOD, 300 MHz) δ 6.80-6.74 (3H, m, Ar*H*), 3.77 (2H, s, CH_2), 2.40 (6H, s, N(CH_3)$_2$); ^{13}C NMR (MeOD, 75.5 MHz) 146.5, 135.4, 128.2, 123.2, 118.0, 115.3, 66.7, 45.1; m/z HRMS (ESI$^-$) found 165.1034 ([M-H]$^-$ of $C_9H_{13}N_2$ requires 165.1033).

4,4'-methylenebis(2,6-di*iso*propylphenol)

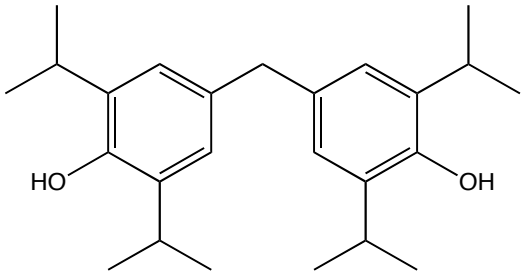

157

2,6-di*iso*propylphenol (993 mg, 5.24 mmol) and formaldehyde (0.93 mL as a 37% aq solution) were dissolved in 5.0 mL of ethanol in a round bottomed flask fitted with a stirrer bar. Whilst stirring vigorously, NaOH (23% w/v aq solution, 7.86 mmol, 1.37 mL) was added dropwise over 30 min period and the mixture stirred for a further 4 h at RT. The solvent volume was reduced under vacuum to about 1 mL and diethyl ether (15mL) and water (5mL) added. The organic phase was extracted and evaporated to dryness under reduced pressure. Column chromatography over silica gel (hexane/ethyl acetate, 95:5) afforded the target compound **157** as an off-white solid (686 mg, 71%); mp 82-84°C; δ_H (300 MHz, $CDCl_3$) 6.79 (4H, s, Ar*H*), 4.60 (2H, s, OH), 3.78 (2H, s, ArCH_2Ar), 3.04 (4H, septet, *J* 3.1, $CH(CH_3)_2$), 1.14 (24H, d, *J* 6.9, $CH(CH_3)_2$); δ_C (75.5 MHz, $CDCl_3$) 148.4, 133.9, 133.7, 124.2, 41.5, 27.6, 23.2; m/z HRMS (ESI^+) 367.2652 ($[M-H]^-$ of $C_{25}H_{36}O_2$ requires 367.2643).

(*E*)-2-((4-hydroxyphenylimino)methyl)phenylboronic acid

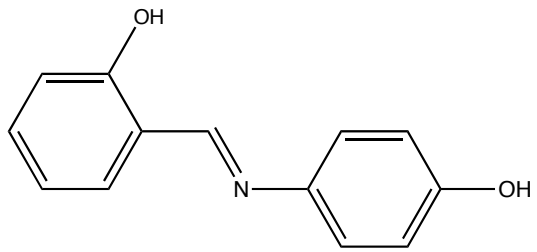

158

2-hydroxybenzaldehyde (73.3 mg, 0.6 mmol) and 4-aminophenol (65.5 mg, 0.6 mmol) were dissolved in 95:5 ethanol-benzene (10 mL) under a nitrogen gas atmosphere and trimethoxyborate (68.6 mg, 0.66 mmol) was added *via* syringe to the stirring solution. After stirring at reflux for 4h, the mixture was filtered, affording imine **158**, with no desired boron adduct detected (117.7mg, 92%); mp 136-138 °C; δ_H (300 MHz, MeOD) 8.46 (1H, s, C*H*N), 7.79 (2H, m, Ar*H*), 7.38 (2H, m, Ar*H*), 7.09 (2H, d, *J* 9.0, Ar*H*), 6.73 (2H, d, *J* 9.0, Ar*H*); δ_C (75.5 MHz, MeOD) 160.9, 157.9, 145.1, 137.8, 132.9, 130.4, 130.2, 123.9, 119.2, 117.5; m/z HRMS (ESI^-) found 212.0916 ($[M-H]^-$ of $C_{13}H_{10}NO_2$ requires 212.0717).

(*E*)-2-(2-hydroxybenzylideneamino)phenol

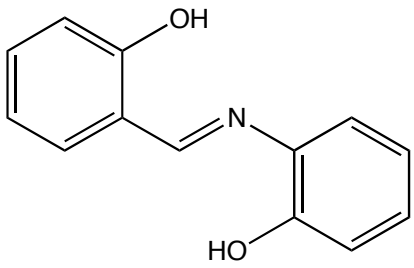

159

2-hydroxybenzaldehyde (73.3 mg, 0.6 mmol) and 2-aminophenol (65.5 mg, 0.6 mmol) were dissolved in 95:5 ethanol-benzene under a nitrogen gas atmosphere and trimethoxyborate (68.6 mg, 0.66 mmol) was added via syringe to the stirring solution. After stirring at reflux for 4h, the mixture was filtered, affording imine **159**, with no desired boron adduct detected. (115.1 mg, 90 %); mp 185-187°C; δ_H (300 MHz, MeOD) 8.79 (1H, s, C*H*N), 7.39 (1H, m, Ar*H*), 7.24 (2H, m, Ar*H*), 7.02 (1H, m, Ar*H*), 6.82 (4H, m, Ar*H*); δ_C (75.5 MHz, MeOD) 161.9, 161.1, 153.0, 140.8, 132.2, 132.0, 128.6, 124.1, 123.9, 121.7, 119.9, 117.4, 115.5; m/z HRMS (ESI^-) 212.0719. ($[M-H]^-$ of $C_{13}H_{11}NO_2$ requires 212.0717).

5 BIBLIOGRAPHY

1. A. Hulanicki, S. Glab and F. Ingman, *Pure Appl. Chem.*, 1991, **63**, 1247-1250.
2. M. Melaimi and F. P. Gabbai, *J. Am. Chem. Soc.*, 2005, **127**, 9680-9681.
3. M. H. Jouvin, M. C. De Vernejoul and P. Druet, *American Journal of Kidney Disease*, 1987, **10**, 136-139.
4. J. Fawell, K. Bailey, J. Chilton and E. Dahi, *Fluoride in Drinking-water*, World Health Organisation, 2006.
5. K. Heard, R. E. Hill, C. B. Cairns and R. C. Dart, *Journal of Toxicology-Clinical Toxicology*, 2001, **39**, 349-353.
6. M. P. Anderson, R. J. Gregory, S. Thompson, D. W. Souza, S. Paul, R. C. Mulligan, A. E. Smith and M. J. Welsh, *Science*, 1991, **253**, 202-205.
7. D. B. Simon, R. S. Bindra, T. A. Mansfield, C. NelsonWilliams, E. Mendonca, R. Stone, S. Schurman, A. Nayir, H. Alpay, A. Bakkaloglu, J. RodriguezSoriano, J. M. Morales, S. A. Sanjad, C. M. Taylor, D. Pilz, A. Brem, H. Trachtman, W. Griswold, G. A. Richard, E. John and R. P. Lifton, *Nat. Gen.*, 1997, **17**, 171-178.
8. O. Devuyst, P. T. Christie, P. J. Courtoy, R. Beauwens and R. V. Thakker, *Hum. Molec. Gen.*, 1999, **8**, 247-257.
9. S. C. Koch, M. Fitzgerald and G. J. Hathway, *Anesthesiology*, 2008, **108**, 122-129.
10. D. A. Scott, R. Wang, T. M. Kreman, V. C. Sheffield and L. P. Karniski, *Nat. Gen.*, 1999, **21**, 440-443.
11. A. Yoshida, S. Taniguchi, I. Hisatome, I. E. Royaux, E. D. Green, L. D. Kohn and K. Suzuki, *J. Clin. Endocrinol. Metab.*, 2002, **87**, 3356-3361.
12. U. Kornak, D. Kasper, M. R. Bosl, E. Kaiser, M. Schweizer, A. Schulz, W. Friedrich, G. Delling and T. J. Jentsch, *Cell*, 2001, **104**, 205-215.
13. B. Alberts, D. Bray, J. Lewis, M. Raff, K. Roberts and J. D. Watson, *Molecular Biology of the Cell*, Garland Science, New York, 1994.
14. K. H. G. Verschueren, S. M. Franken, H. J. Rozeboom, K. H. Kalk and B. W. Dijkstra, *J. Mol. Biol.*, 1993, **232**, 856-872.
15. K. H. G. Verschueren, F. Seljee, H. J. Rozeboom, K. H. Kalk and B. W. Dijkstra, *Nature*, 1993, **363**, 693-698.
16. P. Burkhard, C. H. Tai, J. N. Jansonius and P. F. Cook, *J. Mol. Biol.*, 2000, **303**, 279-286.
17. A. S. Eustáquio, F. Pojer, J. P. Noel and B. S. Moore, *Nature Chemical Biology*, 2007, **4**, 69-74.
18. R. Dutzler, E. B. Campbell, M. Cadene, B. T. Chait and R. MacKinnon, *Nature*, 2002, **415**, 287-294.
19. R. Dutzler, E. B. Campbell and R. MacKinnon, *Science*, 2003, **300**, 108-112.
20. T. J. Cheng, T. M. Chen, C. H. Chen and Y. K. Lai, *J. Cell. Biochem.*, 1998, **69**, 221-231.
21. A. J. Murphy and R. J. Coll, *The Journal of Biological Chemistry*, 1992, **267**, 5229-5235.
22. R. D. Shannon, *Acta Crystallogr., Sect. A: Found. Crystallogr.*, 1976, **32**, 751-767.
23. S. Alunni, A. Pero and G. Reichenbach, *Journal of the Chemical Society-Perkin Transactions 2*, 1998, 1747-1750.
24. F. Hofmeister, *Arch. Exp. Pathol. Pharmacol.*, 1888, **24**.

25. R. A. Bissell, A. P. Desilva, H. Q. N. Gunaratne, P. L. M. Lynch, G. E. M. Maguire and K. Sandanayake, *Chem. Soc. Rev*, 1992, **21**, 187-195.
26. C. Joo, H. Balci, Y. Ishitsuka, C. Buranachai and T. Ha, *Annu. Rev. Biochem*, 2008, **77**, 51-76.
27. M. Böhmer and J. Enderlein, *Chemphyschem*, 2003, **4**, 793-808.
28. W. E. Moerner and D. P. Fromm, *Rev. Sci. Instrum.*, 2003, **74**, 3597-3619.
29. W. P. Ambrose, P. M. Goodwin, J. H. Jett, A. Van Orden, J. H. Werner and R. A. Keller, *Chem. Rev*, 1999, **99**, 2929-2956.
30. M. Sauer, *Angew. Chem. Int. Ed.*, 2003, **42**, 1790-1793.
31. S. W. Thomas III, G. D. Joly and T. M. Swager, *Chem. Rev*, 2007, **107**, 1339-1386.
32. Z. Gitai, *Current Opinion in Microbiology*, 2009, **12**, 341.
33. L. E. Edgington, A. B. Berger, G. Blum, V. E. Albrow, M. G. Paulick, N. Lineberry and M. Bogyo, *Nature Medicine*, 2009, **15**, 967-973.
34. P. Cekan, *Nucleic Acids Res.*, 2009, **37**, 3990-3995.
35. C. R. Cooper, N. Spencer and T. D. James, *Chem. Commun.*, 1998, 1365-1366.
36. J. R. Lakowicz, *Principles of Fluorescence Spectroscopy*, Plenum, New York, 1999.
37. A. Siemiarczuk, Z. R. Grabowski, A. Krowczynski, M. Asher and M. Ottolenghi, *Chem. Phys. Lett.*, 1977, **51**, 315-320.
38. A. P. de Silva, H. Q. N. Gunaratne, T. Gunnlaugsson, A. J. M. Huxley, C. P. McCoy, J. T. Rademacher and T. E. Rice, *Chem. Rev*, 1997, **97**, 1515-1566.
39. V. Balzani and F. Scandola, *Supramolecular Photochemistry*, Ellis Horwood Limited, Chichester, 1991.
40. M. D. Ward, *Chem. Soc. Rev*, 1997, **26**, 365-376.
41. C. M. G. Dos Santos, M. Glynn, T. McCabe, J. S. Seixas de Melo, H. D. Burrows and T. Gunnlaugsson, *Supramol. Chem.*, 2007, **20**, 407-418.
42. A. Juris, V. Balzani, F. Barigelletti, S. Campagna, P. Belser and A. Vonzelewsky, *Coord. Chem. Rev*, 1988, **84**, 85-277.
43. T. J. Meyer, *Acc. Chem. Res*, 1989, **22**, 163-170.
44. C. Creutz, M. Chou, T. L. Netzel, M. Okumura and N. Sutin, *J. Am. Chem. Soc.*, 1980, **102**, 1309-1319.
45. C. Tanford, *J. Am. Chem. Soc.*, 1954, **76**.
46. D. F. Shriver and M. J. Biallas, *J. Am. Chem. Soc.*, 1967, **89**.
47. X. Yang, C. B. Knobler and M. F. Hawthorne, *Angew. Chem. Int. Ed. Engl.*, 1991, **30**, 1507-1508.
48. X. G. Yang, C. B. Knobler and M. F. Hawthorne, *J. Am. Chem. Soc.*, 1992, **114**, 380-382.
49. Z. P. Zheng, X. G. Yang, C. B. Knobler and M. F. Hawthorne, *J. Am. Chem. Soc.*, 1993, **115**, 5320-5321.
50. Y. Azuma and M. Newcomb, *Organomet.*, 1984, **3**, 9-14.
51. M. Newcomb and M. T. Blanda, *Tet. Lett.*, 1988, **29**, 4261-4264.
52. M. Newcomb, M. T. Blanda, Y. Azuma and T. J. Delord, *J. Chem. Soc.-Chem. Commun.*, 1984, 1159-1160.
53. M. Newcomb, J. H. Horner and M. T. Blanda, *J. Am. Chem. Soc.*, 1987, **109**, 7878-7879.
54. M. Newcomb, J. H. Horner, M. T. Blanda and P. J. Squattrito, *J. Am. Chem. Soc.*, 1989, **111**, 6294-6301.
55. M. Newcomb, A. M. Madonik, M. T. Blanda and J. K. Judice, *Organomet.*, 1987, **6**, 145-150.

56. K. Ogawa, S. Aoyagi and Y. Takeuchi, *J. Chem. Soc.-Perkin Trans. 2*, 1993, 2389-2392.
57. S. Aoyagi, K. Tanaka and Y. Takeuchi, *J. Chem. Soc.-Perkin Trans. 2*, 1994, 1549-1553.
58. S. Aoyagi, K. Tanaka, I. Zicmane and Y. Takeuchi, *J. Chem. Soc.-Perkin Trans. 2*, 1992, 2217-2220.
59. K. Tamao, T. Hayashi and Y. Ito, *J. Organomet. Chem.*, 1996, **506**, 85-91.
60. R. A. Bell, G. G. Christoph, F. R. Fronczek and R. E. Marsh, *Science*, 1975, **190**, 151-152.
61. E. Graf and J. M. Lehn, *J. Am. Chem. Soc.*, 1975, **97**, 5022-5024.
62. E. Graf and J. M. Lehn, *J. Am. Chem. Soc.*, 1976, **98**, 6403-6405.
63. B. Metz, J. M. Rosalky and R. Weiss, *J. Chem. Soc.-Chem. Commun.*, 1976, 533-534.
64. F. P. Schmidtchen and M. Berger, *Chem. Rev*, 1997, **97**, 1609-1646.
65. K. Worm and F. P. Schmidtchen, *Angew. Chem. Int. Ed. Engl.*, 1995, **34**, 65-66.
66. K. Worm, F. P. Schmidtchen, A. Schier, A. Schafer and M. Hesse, *Angew. Chem. Int. Ed. Engl.*, 1994, **33**, 327-329.
67. R. A. Pascal, J. Spergel and D. Vanengen, *Tet. Lett.*, 1986, **27**, 4099-4102.
68. H. E. Katz, *J. Org. Chem.*, 1985, **50**, 5027-5032.
69. H. E. Katz, *J. Am. Chem. Soc.*, 1986, **108**, 7640-7645.
70. V. J. Bauer, D. L. J. Clive, D. Dolphin, J. B. Paine III and F. L. Harris, *J. Am. Chem. Soc.*, 1983, **105**, 6429-6436.
71. M. Shionoya, H. Furuta, V. Lynch, A. Harriman and J. L. Sessler, *J. Am. Chem. Soc.*, 1992, **114**, 5714-5722.
72. J. L. Sessler, M. Cyr, H. Furuta, V. Kral, T. Mody, T. Morishima, M. Shionoya and S. Weghorn, *Pure Appl. Chem.*, 1993, **65**, 393-398.
73. P. Konieczka, B. Zygmunt and J. Namiesnik, *Bulletin of Environmental Contamination and Toxicology*, 2000, **64**, 794-803.
74. K. Itai and H. Tsunoda, *Clin. Chim. Acta*, 2001, **308**, 163-171.
75. M. S. Frant and J. W. Ross, *Science*, 1966, **154**, 1553.
76. J. P. Lorand and J. O. Edwards, *J. Org. Chem.*, 1959, **24**, 769-774.
77. L. Babcock and R. Pizer, *Inorg. Chem.*, 1980, **19**, 56-61.
78. M. F. Lappert, *Chem. Rev*, 1956, **56**, 959-1064.
79. M. I. Wolfrom and J. Solms, *J. Org. Chem.*, 1956, **21**, 815-816.
80. N. DiCesare and J. R. Lakowicz, *Anal. Biochem.*, 2001, **294**, 154-160.
81. S. Friedman and R. Pizer, *J. Am. Chem. Soc.*, 1975, **97**, 6059-6062.
82. L. Babcock and R. Pizer, *Inorg. Chem.*, 1980, **19**, 56-61.
83. H. C. Brown, J. Prasad and S. H. Zee, *J. Org. Chem.*, 1986, **51**, 439-445.
84. S. Itsuno, M. Nakano, K. Miyazaki, H. Masuda, K. Ito, A. Hirao and S. Nakahama, *Journal of the Chemical Society-Perkin Transactions 1*, 1985, 2039-2044.
85. A. Pelter, R. M. Rosser and S. Mills, *Journal of the Chemical Society-Perkin Transactions 1*, 1984, 717-720.
86. A. Pelter, K. Smith and H. C. Brown, *Borane Reagents*, Academic Press Limited, 1988.
87. E. Frankland, *Liebigs Annalen*, 1862, **124**, 129.
88. H. E. Dunn, J. C. Catlin and H. R. Snyder, *J. Org. Chem.*, 1968, **33**, 4483-&.
89. S. Toyota and M. Oki, *Bull. Chem. Soc. Jpn.*, 1992, **65**, 1832-1840.
90. H. Hopfl, *J. Organomet. Chem.*, 1999, **581**, 129-149.
91. M. T. Reetz, C. M. Niemeyer and K. Harms, *Angew. Chem. Int. Ed. Engl.*, 1991, **30**, 1472-1474.

92. S. Jacobson and R. Pizer, *J. Am. Chem. Soc.*, 1993, **115**, 11216-11221.
93. C. Dusemund, K. Sandanayake and S. Shinkai, *J. Chem. Soc.-Chem. Commun.*, 1995, 333-334.
94. H. Yamamoto, A. Ori, K. Ueda, C. Dusemund and S. Shinkai, *Chem. Commun.*, 1996, 407-408.
95. S. Yamaguchi, S. Akiyama and K. Tamao, *J. Am. Chem. Soc.*, 2001, **123**, 11372-11375.
96. Y. Kubo, M. Yamamoto, M. Ikeda, M. Takeuchi, S. Shinkai, S. Yamaguchi and K. Tamao, *Angew. Chem. Int. Ed.*, 2003, **42**, 2036-2040.
97. M. J. Crossley and A. Johnston, *Chem. Commun.*, 2002, 1122-1123.
98. J. Ren, Q. Wang, D. Qu, X. Zhao and H. Tian, *Chem. Lett*, 2004, **33**, 974-975.
99. G. Xu and M. A. Tarr, *Chem. Commun.*, 2004, 1050-1051.
100. J. Raker and T. E. Glass, *J. Org. Chem.*, 2002, **67**, 6113-6116.
101. H. Fu, B. H. Loo, D. Xiao, R. Xie, X. Ji, J. Yao, B. Zhang and L. Zhang, *Angew. Chem. Int. Ed.*, 2002, **41**, 962-965.
102. G. J. Mohr, I. Klimant, U. E. Spochiger-Keller and O. S. Wolfbeis, *Anal. Chem.*, 2001, **73**, 1053-1056.
103. J. V. Mello and N. S. Finney, *Angew. Chem. Int. Ed.*, 2001, **40**, 1536-1538.
104. S. Sole and F. P. Gabbai, *Chem. Commun.*, 2004, 1284-1285.
105. Y. Kubo, A. Kobayashi, T. Ishida, Y. Misawa and T. D. James, *Chem. Commun.*, 2005, 2846-2848.
106. Z. Q. Liu, M. Shi, F. Y. Li, Q. Fang, Z. H. Chen, T. Yi and C. H. Huang, *Org. Lett.*, 2005, **7**, 5481-5484.
107. X. Y. Liu, D. R. Bai and S. N. Wang, *Angew. Chem. Int. Ed.*, 2006, **45**, 5475-5478.
108. Y. Kim and F. P. Gabbai, *J. Am. Chem. Soc.*, 2009, **131**, 3363-3369.
109. M. H. Lee, T. Agou, J. Kobayashi, T. Kawashima and F. P. Gabbai, *Chem. Commun.*, 2007, 1133-1135.
110. M. H. Lee and F. P. Gabbai, *Inorg. Chem.*, 2007, **46**, 8132-8138.
111. C. W. Chiu and F. P. Gabbai, *J. Am. Chem. Soc.*, 2006, **128**, 14248-14249.
112. A. Kawachi, A. Tani, J. P. Shimada and Y. Yamamoto, *J. Am. Chem. Soc.*, 2008, **130**, 4222.
113. Z. C. Xu, S. K. Kim, S. J. Han, C. Lee, G. I. Kociok-Kohn, T. D. James and J. Yoon, *Eur. J. Org. Chem.*, 2009, **18**, 3058-3065.
114. P. A. Gale, J. L. Sessler, V. Kral and V. Lynch, *J. Am. Chem. Soc.*, 1996, **118**, 5140-5141.
115. A. Andrievsky, F. Ahuis, J. L. Sessler, F. Vogtle, D. Gudat and M. Moini, *J. Am. Chem. Soc.*, 1998, **120**, 9712-9713.
116. M. Scherer, J. L. Sessler, A. Gebauer and V. Lynch, *Chem. Commun.*, 1998, 85-86.
117. C. B. Black, B. Andrioletti, A. C. Try, C. Ruiperez and J. L. Sessler, *J. Am. Chem. Soc.*, 1999, **121**, 10438-10439.
118. T. Mizuno, W. H. Wei, L. R. Eller and J. L. Sessler, *J. Am. Chem. Soc.*, 2002, **124**, 1134-1135.
119. P. A. Gale, L. J. Twyman, C. I. Handlin and J. L. Sessler, *Chem. Commun.*, 1999, 1851-1852.
120. P. Anzenbacher, K. Jursikova and J. L. Sessler, *J. Am. Chem. Soc.*, 2000, **122**, 9350-9351.
121. H. Miyaji and J. L. Sessler, *Angew. Chem. Int. Ed.*, 2001, **40**, 154-157.
122. S. Camiolo and P. A. Gale, *Chem. Commun.*, 2000, 1129-1130.

123. C. J. Woods, S. Camiolo, M. E. Light, S. J. Coles, M. B. Hursthouse, M. A. King, P. A. Gale and J. W. Essex, *J. Am. Chem. Soc.*, 2002, **124**, 8644-8652.
124. J. Yoo, M. S. Kim, S. J. Hong, J. L. Sessler and C. H. Lee, *J. Org. Chem.*, 2009, **74**, 1065-1069.
125. S. K. Kim and J. Yoon, *Chem. Commun.*, 2002, 770-771.
126. E. J. Cho, B. J. Ryu, Y. J. Lee and K. C. Nam, *Org. Lett.*, 2005, **7**, 2607-2609.
127. D. Curiel, A. Cowley and P. D. Beer, *Chem. Commun.*, 2005, 236-238.
128. X. J. Peng, Y. K. Wu, J. L. Fan, M. Z. Tian and K. L. Han, *J. Org. Chem.*, 2005, **70**, 10524-10531.
129. J. Shao, X. Yu, H. Lin and H. Lin, *Journal of Molecular Recognition*, 2008, **21**, 425-430.
130. J. Shao, Y. Qiao, H. Lin and H. Lin, *J. Fluoresc.*, 2009, **19**, 183-188.
131. B. Schazmann, N. Alhashimy and D. Diamond, *J. Am. Chem. Soc.*, 2006, **128**, 8607-8614.
132. Y. Li and A. H. Flood, *Angew. Chem. Int. Ed.*, 2008, **47**, 2649-2652.
133. Y. Li and A. H. Flood, *J. Am. Chem. Soc.*, 2008, **130**, 12111-12122.
134. I. Bandyopadhyay, K. Raghavachari and A. H. Flood, *Chemphyschem*, 2009, **10**, 2535-2540.
135. C. Caltagirone, A. Mulas, F. Isaia, V. Lippolis, P. A. Gale and M. E. Light, *Chem. Commun.*, 2009, 6279-6281.
136. M. Arunachalam and P. Ghosh, *Chem. Commun.*, 2009, 5389-5391.
137. P. D. Beer and A. D. Keefe, *J. Organomet. Chem.*, 1989, **375**, C40-C42.
138. P. D. Beer, J. W. Wheeler, A. Grieve, C. Moore and T. Wear, *J. Chem. Soc.-Chem. Commun.*, 1992, 1225-1227.
139. P. D. Beer, Z. Chen, A. J. Goulden, A. Graydon, S. E. Stokes and T. Wear, *J. Chem. Soc.-Chem. Commun.*, 1993, 1834-1836.
140. P. D. Beer and F. Szemes, *J. Chem. Soc.-Chem. Commun.*, 1995, 2245-2247.
141. F. Szemes, D. Hesek, Z. Chen, S. W. Dent, M. G. B. Drew, A. J. Goulden, A. R. Graydon, A. Grieve, R. J. Mortimer, T. Wear, J. S. Weightman and P. D. Beer, *Inorg. Chem.*, 1996, **35**, 5868-5879.
142. S. Y. Kim and J. I. Hong, *Org. Lett.*, 2007, **9**, 3109-3112.
143. S. Xu, K. C. Chen and H. Tian, *J. Mater. Chem.*, 2005, **15**, 2676-2680.
144. M. Mascal, I. Yakovlev, E. B. Nikitin and J. C. Fettinger, *Angew. Chem. Int. Ed.*, 2007, **46**, 8782-8784.
145. F. Oton, A. Tarraga, M. D. Velasco, A. Espinosa and P. Molina, *Chem. Commun.*, 2004, 1658-1659.
146. F. Oton, A. Tarraga, A. Espinosa, M. D. Velasco and P. Molina, *J. Org. Chem.*, 2006, **71**, 4590-4598.
147. S. Yamaguchi, S. Akiyama and K. Tamao, *J. Am. Chem. Soc.*, 2000, **122**, 6793-6794.
148. J. F. Callan, R. C. Mulrooney, S. Kamila and B. McCaughan, *J. Fluoresc.*, 2008, **18**, 527-532.
149. C. Bazzicalupi, A. Bencini, S. Biagini, E. Faggi, S. Meini, C. Giorgi, A. Spepi and B. Valtancoli, *J. Org. Chem.*, 2009, **74**, 7349-7363.
150. Q. Zhou and T. M. Swager, *J. Am. Chem. Soc.*, 1995, **117**, 12593-12602.
151. J.-S. Yang and T. M. Swager, *J. Am. Chem. Soc.*, 1998, **120**, 5321-5322.
152. D. T. McQuade, A. E. Pullen and T. M. Swager, *Chem. Rev*, 2000, **100**, 2537-2574.
153. T. M. Swager, *Acc. Chem. Res*, 1998, **31**, 201-207.
154. I. H. A. Badr and M. E. Meyerhoff, *J. Am. Chem. Soc.*, 2005, **127**, 5318-5319.

155. I. Szymanska, H. Radecka, J. Radecki, P. A. Gale and C. N. Warriner, *J. Electroanal. Chem.*, 2006, **591**, 223-228.
156. K. P. Xiao, P. Bhlmann and Y. Umezawa, *Anal. Chem.*, 1999, **71**, 1183-1187.
157. M. Nicolas, B. Fabre and J. Simonet, *Chem. Commun.*, 1999, 1881-1882.
158. M. M. G. Antonisse and D. N. Reinhoudt, *Chem. Commun.*, 1998, 443-448.
159. P. D. Beer, *Acc. Chem. Res*, 1998, **31**, 71-80.
160. A. C. Ion, J. C. Moutet, A. Pailleret, A. Popescu, E. St Aman, E. Siebert and E. M. Ungureanu, *J. Electroanal. Chem.*, 1999, **464**, 24-30.
161. M. Buda, A. Ion, J. C. Moutet, E. Saint-Aman and R. Ziessel, *J. Electroanal. Chem.*, 1999, **469**, 132-138.
162. T. H. Kim and T. M. Swager, *Angew. Chem. Int. Ed.*, 2003, **42**, 4803-4806.
163. R. B. Coapes, F. E. S. Souza, R. L. Thomas, J. J. Hall and T. B. Marder, *Chem. Commun.*, 2003, 614-615.
164. X. M. He and J. F. Hartwig, *J. Am. Chem. Soc.*, 1996, **118**, 1696-1702.
165. S. Das, V. L. Alexeev, A. C. Sharma, S. J. Geib and S. A. Asher, *Tet. Lett.*, 2003, **44**, 7719-7722.
166. T. Ishiyama, M. Murata and N. Miyaura, *J. Org. Chem.*, 1995, **60**, 7508-7510.
167. T. Ishiyama, K. Ishida and N. Miyaura, *Tetrahedron*, 2001, **57**, 9813-9816.
168. M. J. Sharp and V. Snieckus, *Tet. Lett.*, 1985, **26**, 5997-6000.
169. W. Haubold, J. Herdtle, W. Gollinger and W. Einholz, *J. Organomet. Chem.*, 1986, **315**, 1-8.
170. D. G. Hall, *Boronic Acids*, Wiley-VCH, 2005.
171. M. Melaimi, S. Sole, C. W. Chiu, H. D. Wang and P. Gabbai, *Inorg. Chem.*, 2006, **45**, 8136-8143.
172. Y. Yamamoto, M. Takizawa, X.-Q. Yu and M. Miyaura, *Angew. Chem. Int. Ed.*, 2008, **47**, 928-931.
173. M. Yamashita, Y. Yamamoto, K. Akiba and S. Nagase, *Angew. Chem. Int. Ed.*, 2000, **39**, 4055-4058.
174. S. J. M. Koskela, T. M. Fyles and T. D. James, *Chem. Commun.*, 2005, 945-947.
175. S. Arimori, M. G. Davidson, T. M. Fyles, T. G. Hibbert, T. D. James and G. I. Kociok-Kohn, *Chem. Commun.*, 2004, 1640-1641.
176. D. J. Cram, *Angew. Chem. Int. Ed. Engl.*, 1988, **27**, 1009-1020.
177. C. Bresner, J. K. Day, N. D. Coombs, I. A. Fallis, S. Aldridge, S. J. Coles and M. B. Hursthouse, *Dalton Transactions*, 2006, 3660-3667.
178. M. D. Philips, *unpublished work*, University of Bath, 2005.
179. H. N. Lee, Z. C. Xu, S. K. Kim, K. M. K. Swamy, Y. Kim, S. J. Kim and J. Yoon, *J. Am. Chem. Soc.*, 2007, **129**, 3828.
180. S. K. Kim, J. H. Bok, R. A. Bartsch, J. Y. Lee and J. S. Kim, *Org. Lett.*, 2005, **7**, 4839-4842.
181. J. S. Martin and F. Y. Fujiwara, *Can. J. Chem.*, 1971, **49**, 3071.
182. M. A. Khan, A. W. McCulloch and A. G. McInnes, *Can. J. Chem., Rev. Can.*, 1985, **63**, 2119-2122.
183. M. A. Khan, *J. Mol. Struct.*, 1986, **145**, 203-218.
184. D. H. Lee, H. Y. Lee, K. H. Lee and J. I. Hong, *Chem. Commun.*, 2001, 1188-1189.
185. K. H. Lee, H. Y. Lee, D. H. Lee and J. I. Hong, *Tet. Lett.*, 2001, **42**, 5447-5449.
186. C. Lee, D. H. Lee and J. I. Hong, *Tet. Lett.*, 2001, **42**, 8665-8668.
187. K. J. Winstanley, A. M. Sayer and D. K. Smith, *Org. Biomolec. Chem.*, 2006, **4**, 1760-1767.
188. M. N. Berberan-Santos, *Physchemcomm*, 2000, art. no.-5.

189. W. Lin, Y. Lin, X. Cao, B. Chen and Y. Feng, *Sensors and Actuators, B: Chemistry*, 2009, **138**, 637-641.
190. D. D. Ebbing, *General Chemistry*, Houghton Mifflin, 1990.
191. K. J. Winstanley and D. K. Smith, *J. Org. Chem.*, 2007, **72**, 2803-2815.
192. M. S. J. Briggs, J. S. Fossey, C. J. Richards, B. Scott and J. Whateley, *Tet. Lett.*, 2002, **43**, 5169-5171.
193. M. Demuth, P. Ritterskamp, E. Weigt and K. Schaffner, *J. Am. Chem. Soc.*, 1986, **108**, 4149-4154.
194. A. Horeau and J. P. Guette, *Tetrahedron*, 1974, **30**, 1923-1931.
195. J. A. Dale, D. L. Dull and H. S. Mosher, *J. Org. Chem.*, 1969, **34**, 2543.
196. J. A. Dale and H. S. Mosher, *J. Am. Chem. Soc.*, 1973, **95**, 512-519.
197. Y. Perez-Fuertes, A. M. Kelly, A. L. Johnson, S. Arimori, S. D. Bull and T. D. James, *Org. Lett.*, 2006, **8**, 609-612.
198. A. M. Kelly, Y. Perez-Fuertes, S. Arimori, S. D. Bull and T. D. James, *Org. Lett.*, 2006, **8**, 1971-1974.
199. M. E. Powell, A. M. Kelly, S. D. Bull and T. D. James, *Tet. Lett.*, 2009, **50**, 876-879.
200. D. W. Norman, J. P. Edwards, C. M. Vogels, A. Decken and S. A. Westcott, *Can. J. Chem., Rev. Can.*, 2002, **80**.
201. V. Barba, E. Gallegos, R. Santillan and N. Farfan, *J. Organomet. Chem.*, 2001, **622**, 259-264.
202. E. Galbraith, A. M. Kelly, J. S. Fossey, G. I. Kociok-Kohn, M. G. Davidson, S. D. Bull and T. D. James, *New J. Chem.*, 2009, **33**, 181-185.
203. D. W. Norman, J. P. Edwards, C. M. Vogels, A. Decken and S. A. Westcott, *Can. J. Chem., Rev. Can.*, 2002, **80**, 31-40.
204. B. Loev, *J. Org. Chem.*, 1963, **28**, 3421-&.
205. C. Sanmartin, M. Echeverria, B. Mendivil, L. Cordeu, E. Cubedo, J. Garcia-Foncillas, M. Font and J. A. Palop, *Biorg. Med. Chem.*, 2005, **13**, 2031-2044.
206. L. D. S. Yadav and R. Kapoor, *Synlett*, 2005, 3055-3058.
207. W. J. Bailey and J. R. Griffith, *J. Org. Chem.*, 1978, **43**, 2690-2692.
208. R. A. Altman, A. Shafir, A. Choi, P. A. Lichtor and S. L. Buchwald, *J. Org. Chem.*, 2008, **73**, 284-286.
209. H. J. Cristau, P. P. Cellier, S. Hamada, J. F. Spindler and M. Taillefer, *Org. Lett.*, 2004, **6**, 913-916.
210. A. Aranyos, D. W. Old, A. Kiyomori, J. P. Wolfe, J. P. Sadighi and S. L. Buchwald, *J. Am. Chem. Soc.*, 1999, **121**, 4369-4378.
211. R. Martin and S. L. Buchwald, *Acc. Chem. Res*, 2008, **41**, 1461-1473.
212. H. N. Nguyen, X. H. Huang and S. L. Buchwald, *J. Am. Chem. Soc.*, 2003, **125**, 11818-11819.
213. S. D. Walker, T. E. Barder, J. R. Martinelli and S. L. Buchwald, *Angew. Chem. Int. Ed.*, 2004, **43**, 1871-1876.
214. H. Fang, G. Kaur, J. Yan and B. Wang, *Tet. Lett.*, 2005, **46**, 1671-1674.
215. A. L. S. Thompson, G. W. Kabalka, M. R. Akula and J. W. Huffman, *Synthesis-Stuttgart*, 2005, 547-550.
216. D. Bahulayan, R. Sukumar, K. R. Sabu and M. Lalithambika, *Green Chemistry*, 1999, **1**, 191-193.
217. C. A. Hunter, P. S. Jones, P. M. N. Tiger and S. Tomas, *Chem. Commun.*, 2003, 1642-1643.
218. H. C. Kolb, M. G. Finn and K. B. Sharpless, *Angew. Chem. Int. Ed.*, 2001, **40**, 2004.
219. R. Huisgen, *Proceedings of the Chemical Society of London*, 1961, 357-&.

220. V. V. Rostovtsev, L. G. Green, V. V. Fokin and K. B. Sharpless, *Angew. Chem. Int. Ed.*, 2002, **41**, 2596.
221. S. L. Zheng, S. Reid, N. Lin and B. H. Wang, *Tet. Lett.*, 2006, **47**, 2331-2335.
222. W. Zhu and D. W. Ma, *Chem. Commun.*, 2004, 888-889.
223. B. Y. Lee, S. R. Park, H. B. Jeon and K. S. Kim, *Tet. Lett.*, 2006, **47**, 5105-5109.
224. J. J. Eisch and B. W. Kotowicz, *Eur. J. Inorg. Chem.*, 1998, 761-769.
225. E. P. Gillis and M. D. Burke, *J. Am. Chem. Soc.*, 2007, **129**, 6716.
226. H. Noguchi, K. Hojo and M. Suginome, *J. Am. Chem. Soc.*, 2007, **129**, 758-759.
227. H. Noguchi, T. Shioda, C. M. Chou and M. Suginome, *Org. Lett.*, 2008, **10**, 377-380.
228. K. Billingsley and S. L. Buchwald, *J. Am. Chem. Soc.*, 2007, **129**, 3358-3366.
229. Z. X. Xi, X. M. Zhang, W. Z. Chen, S. Z. Fu and D. Q. Wang, *Organomet.*, 2007, **26**, 6636-6642.
230. A. Bermejo, A. Ros, R. Fernandez and J. M. Lassaletta, *J. Am. Chem. Soc.*, 2008, **130**, 15798.
231. B. G. Zhang, J. Xu, Y. G. Zhao, C. Y. Duan, X. Cao and Q. J. Meng, *Dalton Trans.*, 2006, 1271-1276.
232. M. A. Fox, W. R. Gill, P. L. Herbertson, J. A. H. MacBride, K. Wade and H. M. Colquhoun, *Polyhedron*, 1996, **15**, 565-571.
233. H. R. Sun and S. G. DiMagno, *J. Am. Chem. Soc.*, 2005, **127**, 2050-2051.
234. A. Facchiano and R. Ragone, *Anal. Biochem.*, 2003, **313**, 170-172.

6 APPENDIX

6.1 Selected NMR Spectra

Compound **90** ^{1}H NMR

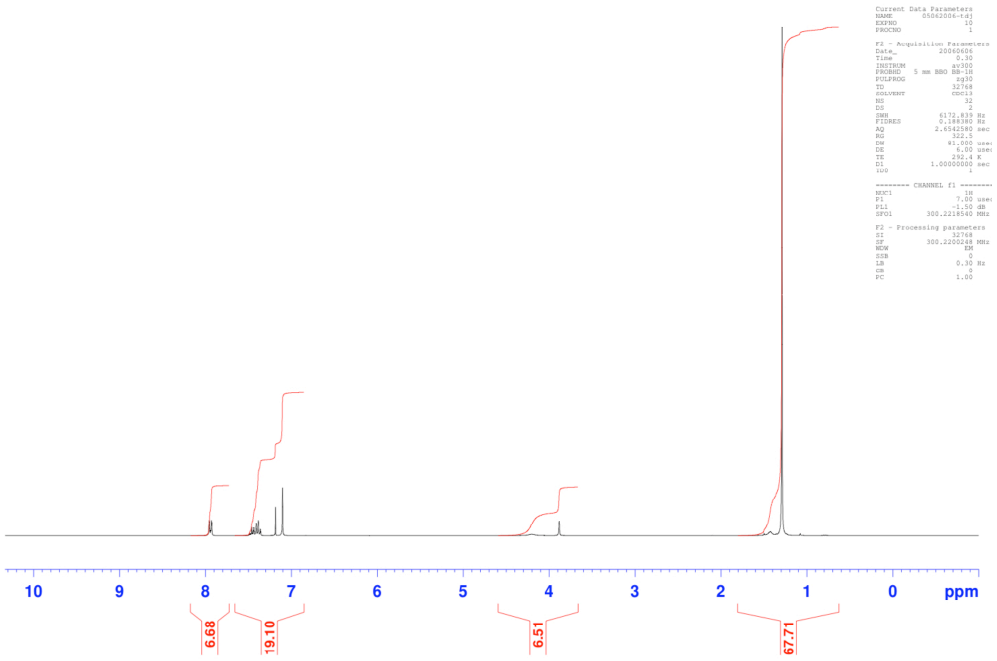

Compound **90** ^{13}C NMR

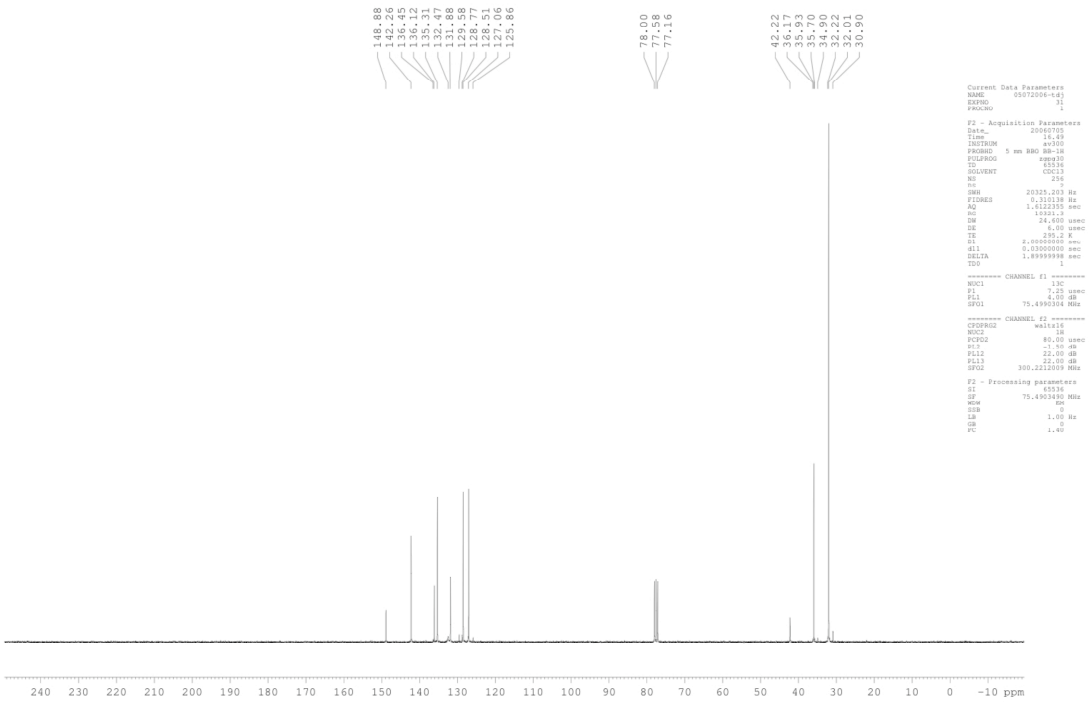

Compound **119** ^{1}H NMR spectrum in d^{6}-DMSO.

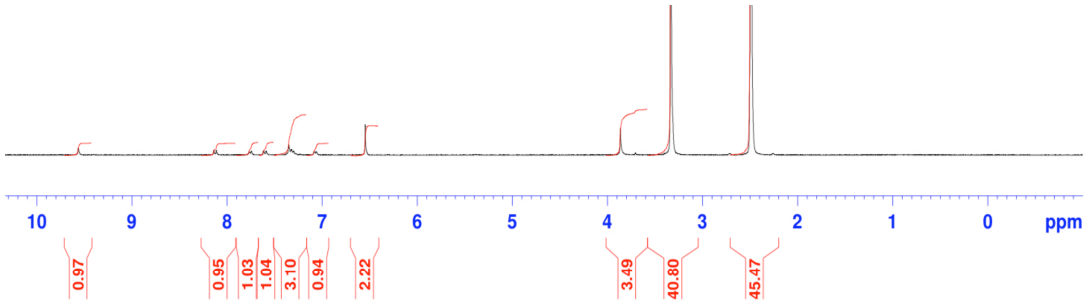

Compound **142** ^{13}C NMR

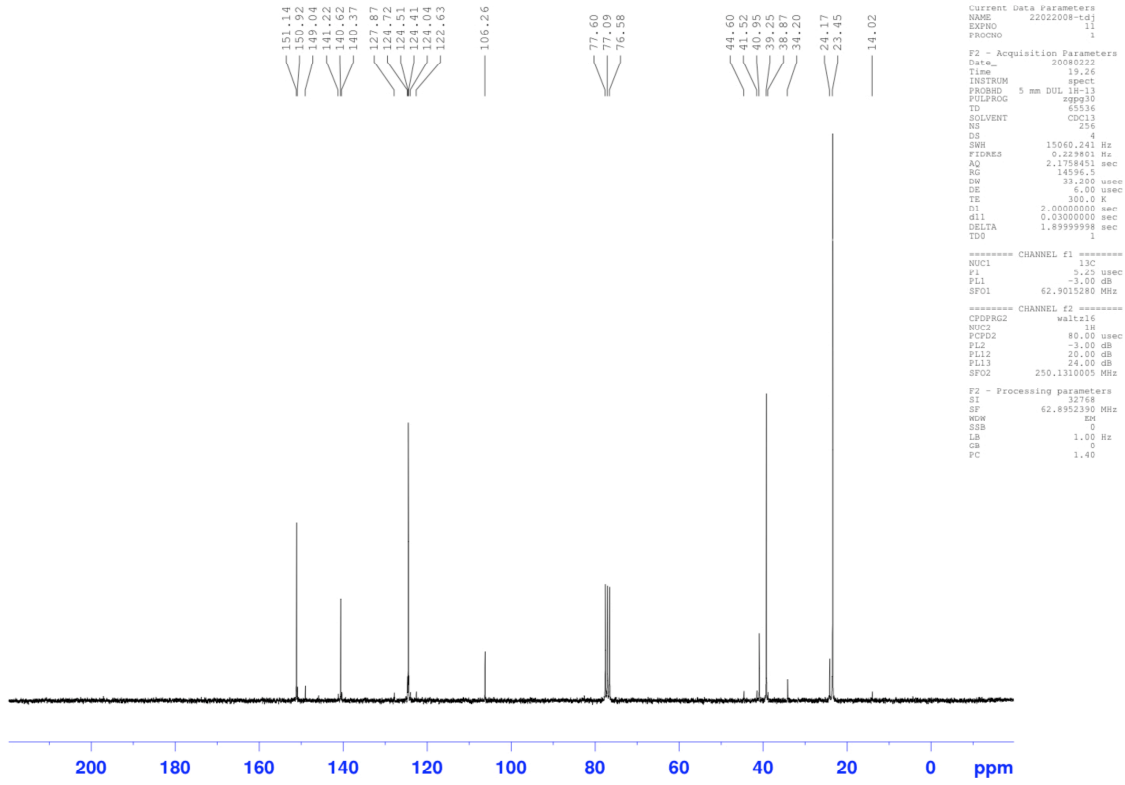

Compound **147** ^{1}H NMR

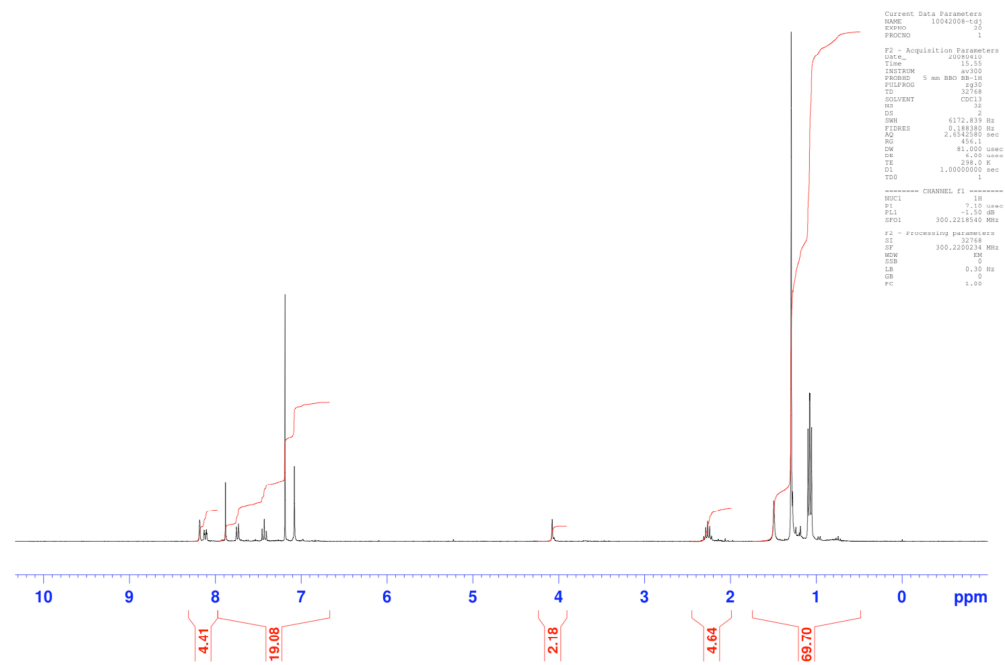

Compound **150** ^{13}C NMR

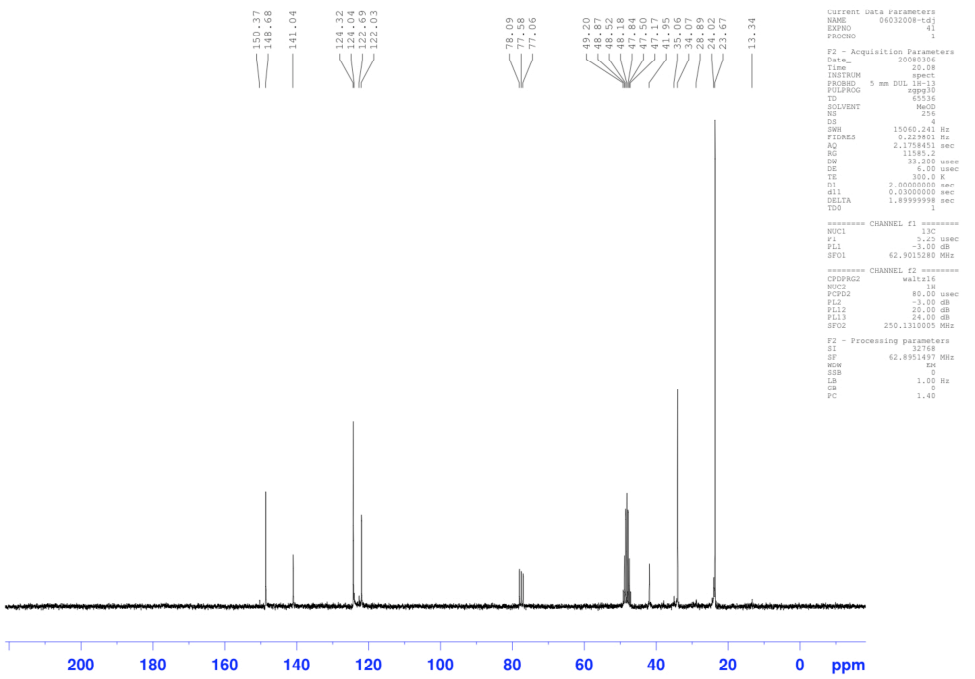

Compound **153** ^{1}H NMR

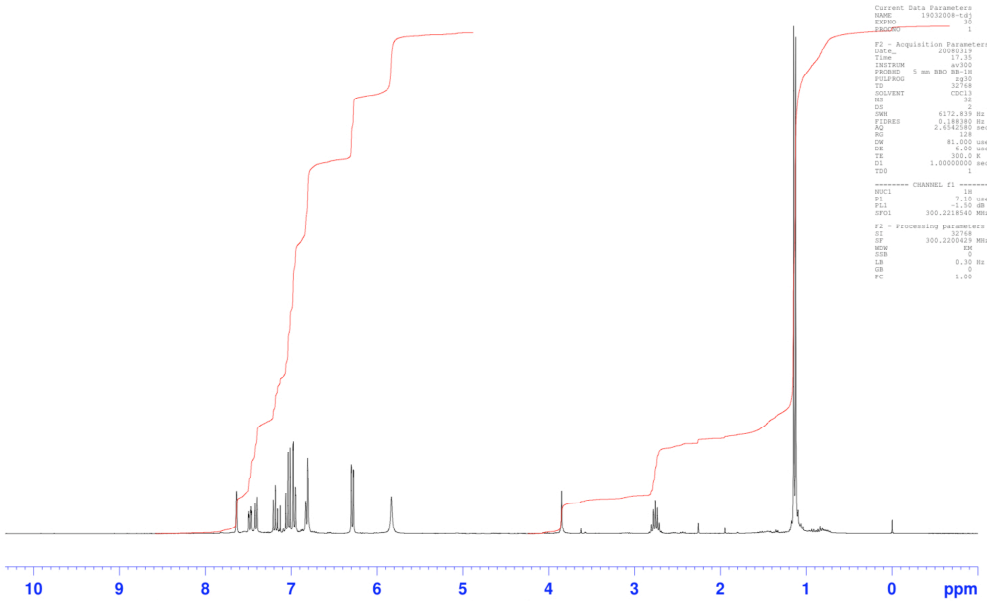

Compound **153** ^{13}C NMR

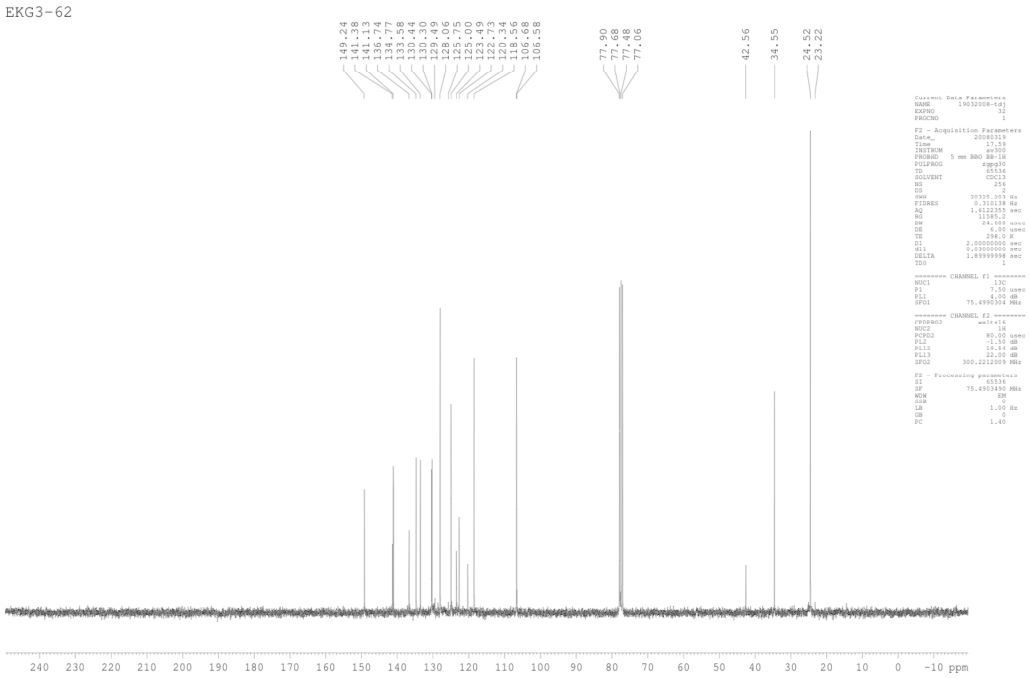

Compound **153** ^{11}B NMR

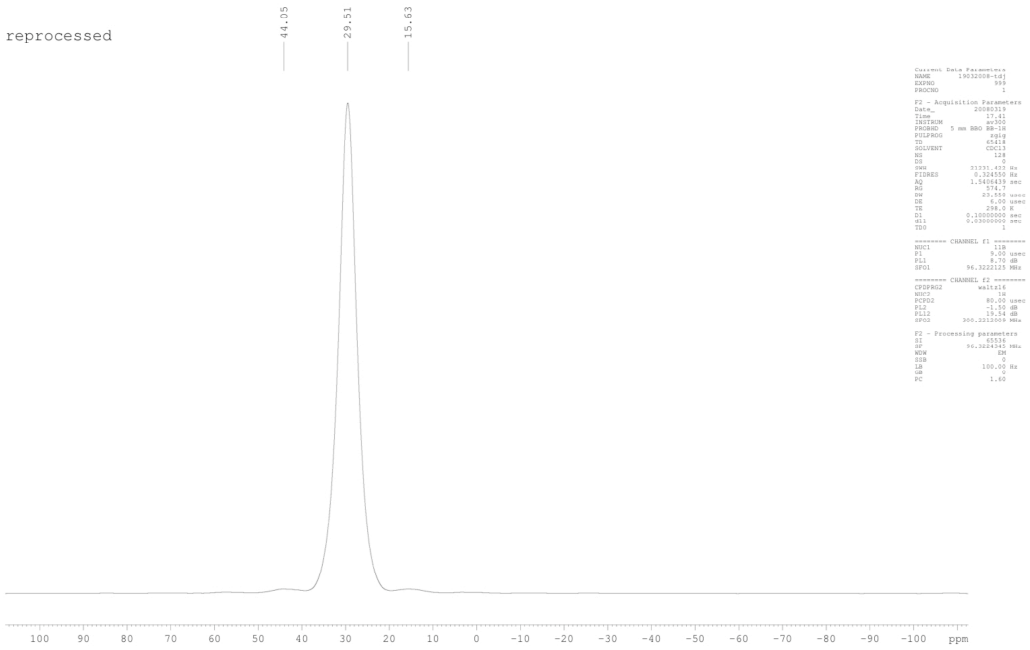

Compound **154** ^{1}H NMR spectrum in $CDCl_3$.

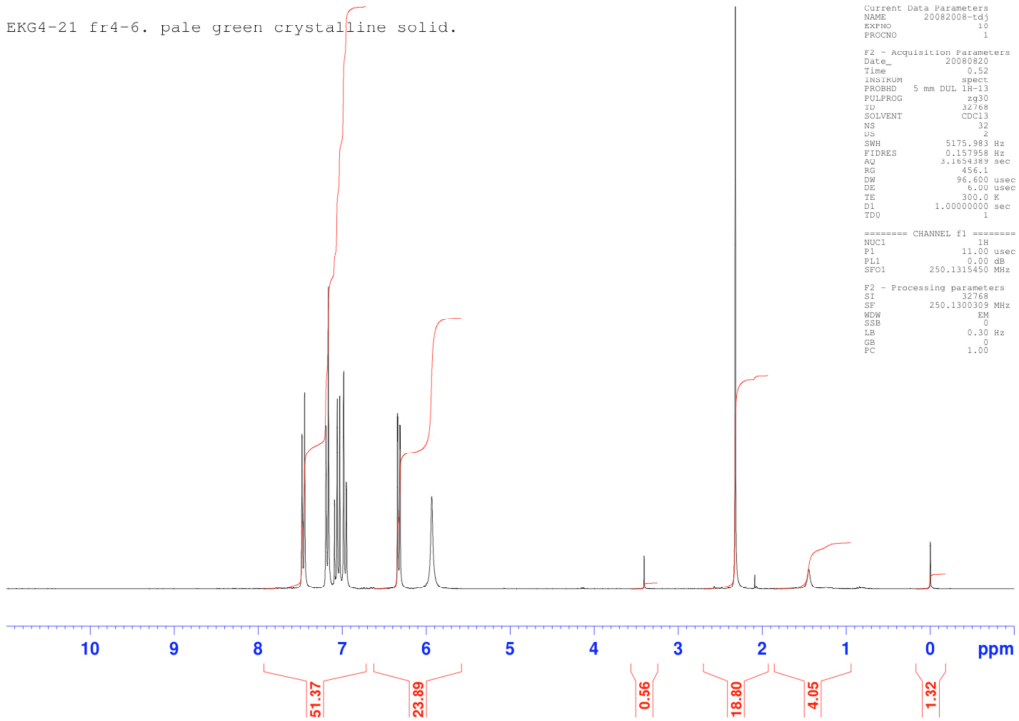

6.2 Selected NMR Spectra from Anion Titrations

6.2.1 Compound 128

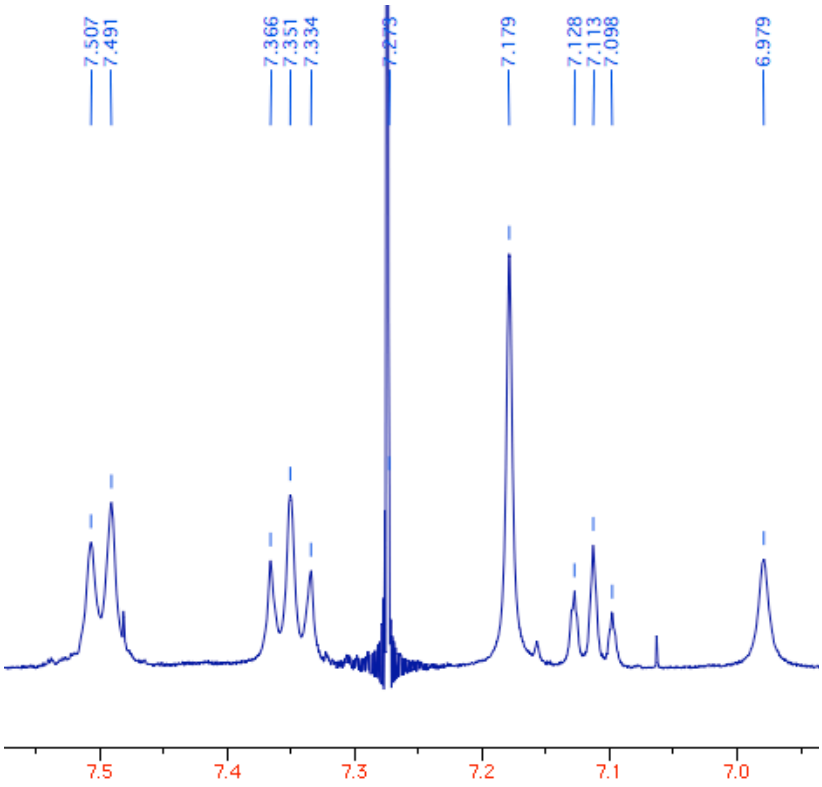

Figure A- 1 ^{1}H NMR spectrum of compound **128** (2.5mM in $CDCl_3$ at 298K).

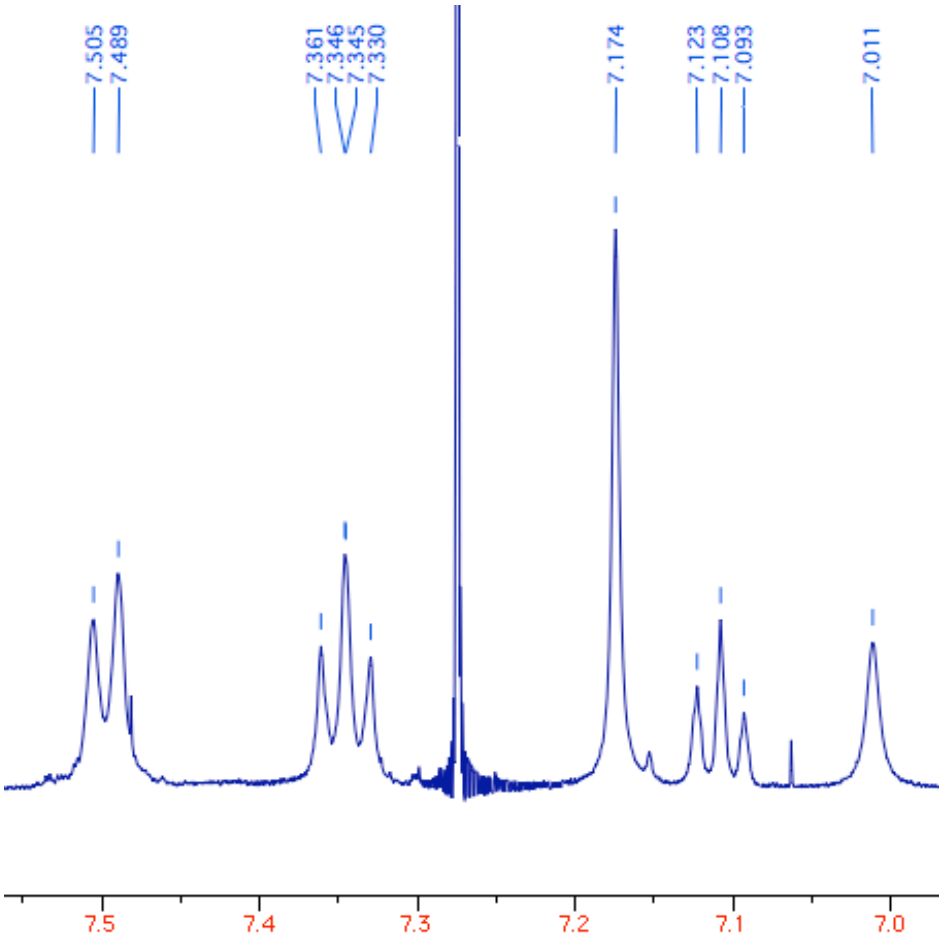

Figure A- 2 ^{1}H NMR spectrum of **128** + TBAC (1:1)

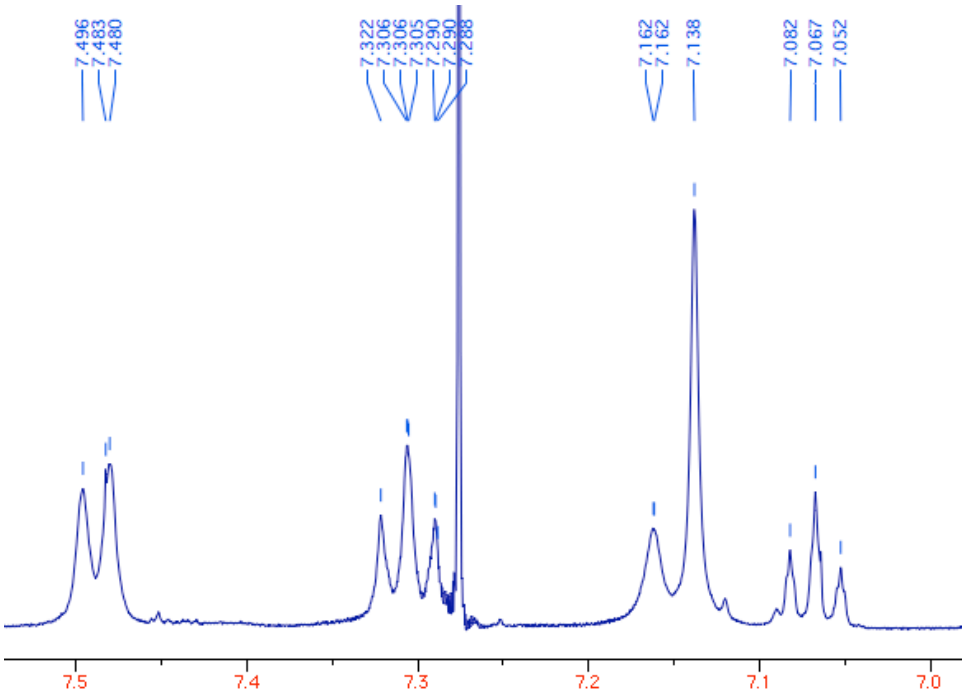

Figure A- 3 ^{1}H NMR spectrum of **128** + TBAC (1:10)

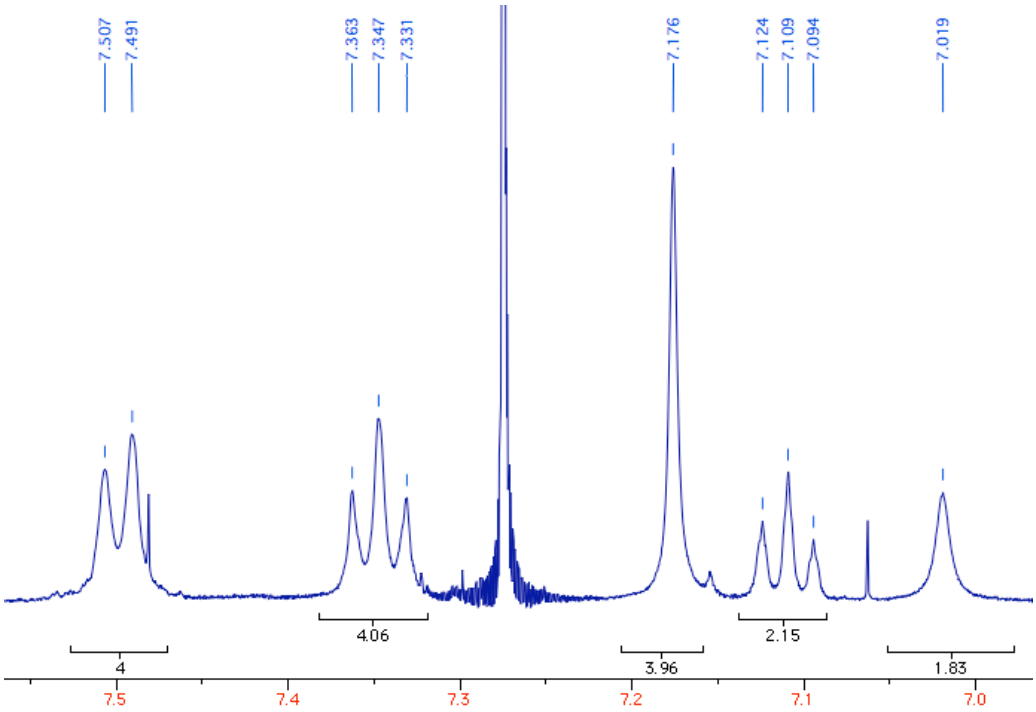

Figure A- 4 ^{1}H NMR spectrum of **128** + TBAF (1:1)

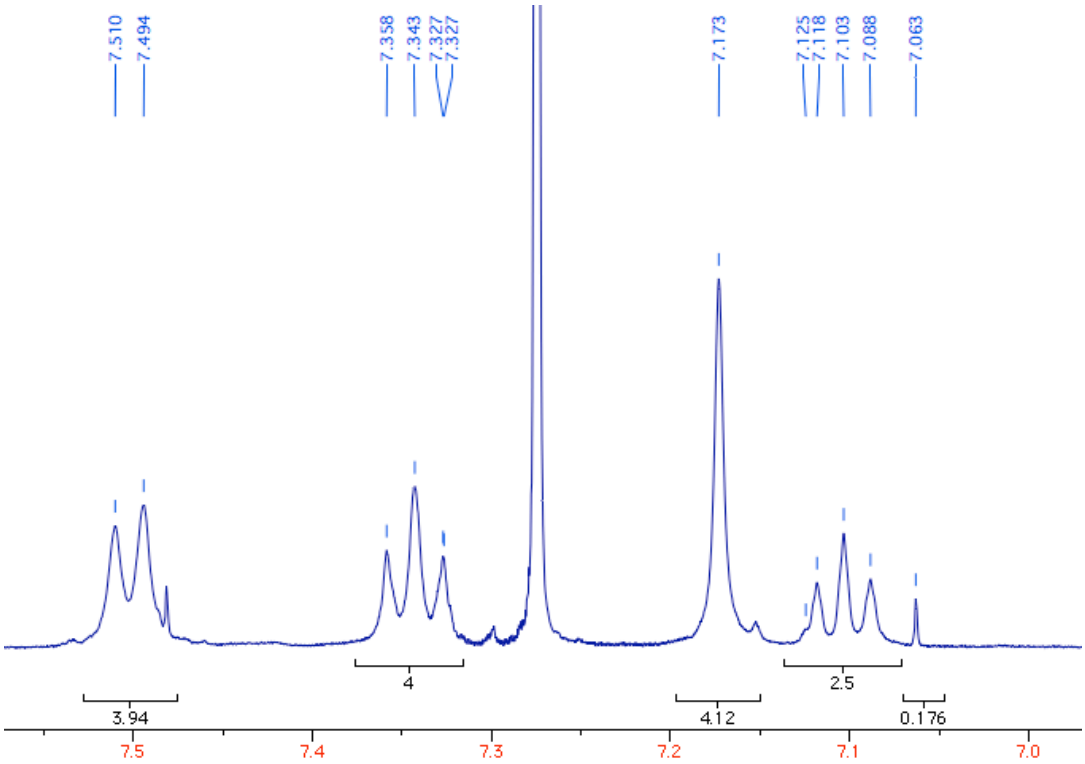

Figure A- 5 ^{1}H NMR spectrum of **128** + TBAF (1:2)

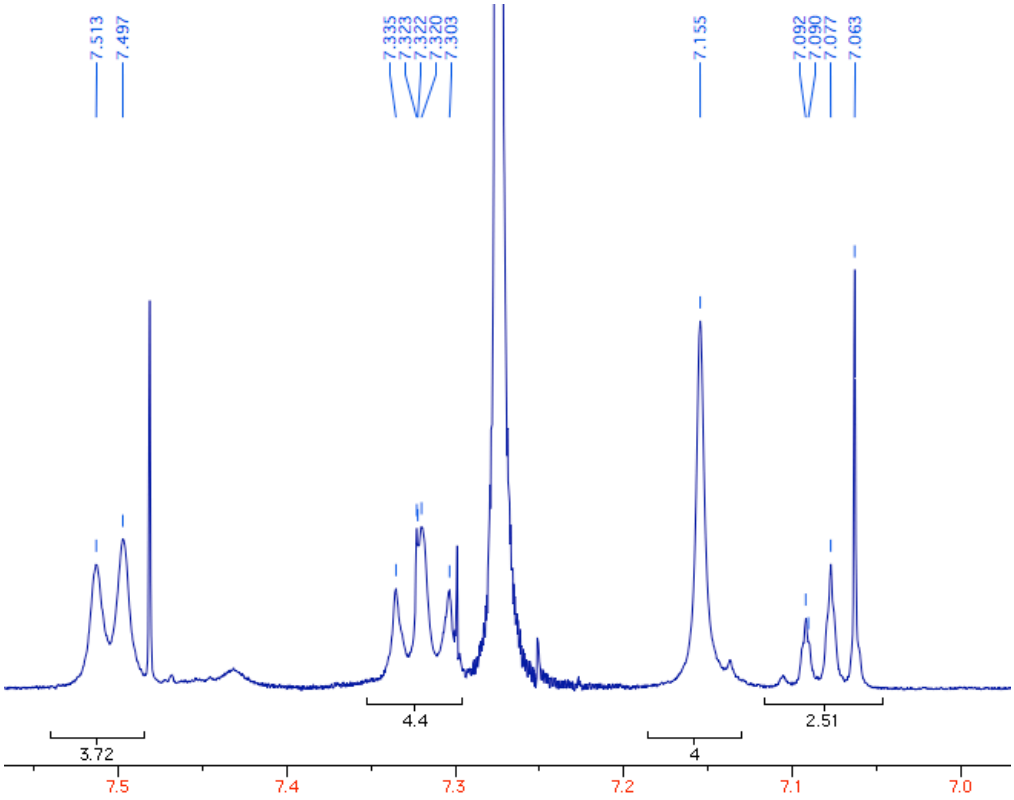

Figure A- 6 ^{1}H NMR spectrum of **128** + TBAF (1:10)

6.2.2 Compound 154

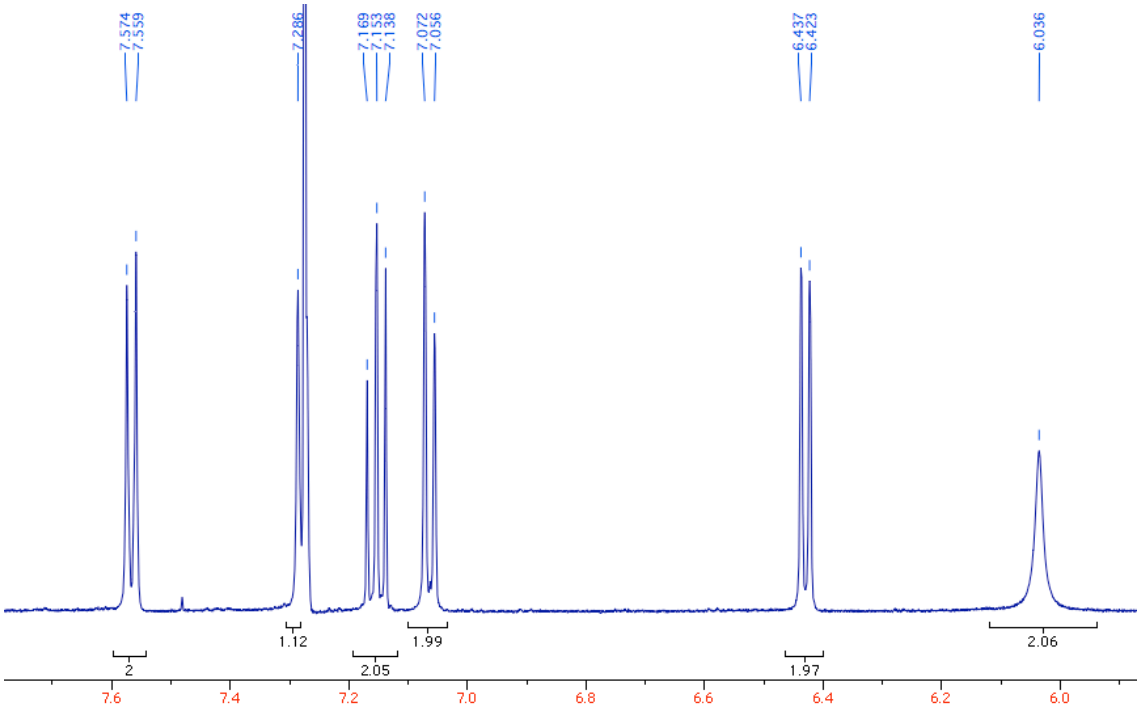

Figure A- 7 ^{1}H NMR spectrum of compound **154** (2.5 M in $CDCl_3$ at 298 K)

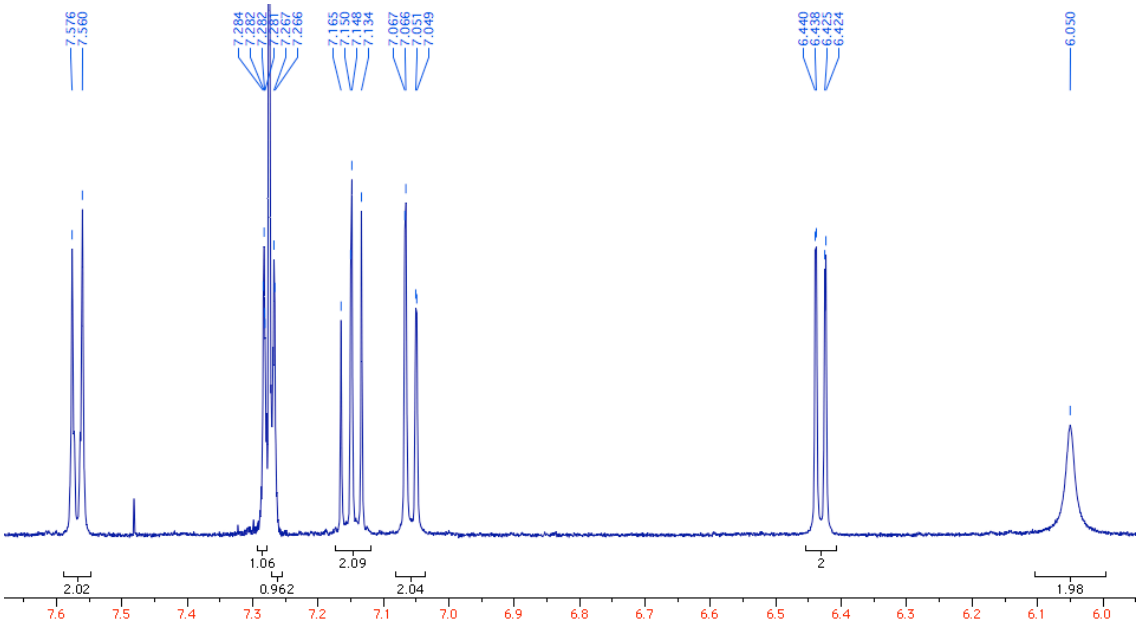

Figure A- 8 ^{1}H NMR spectrum of **154** + TBAC (1:1)

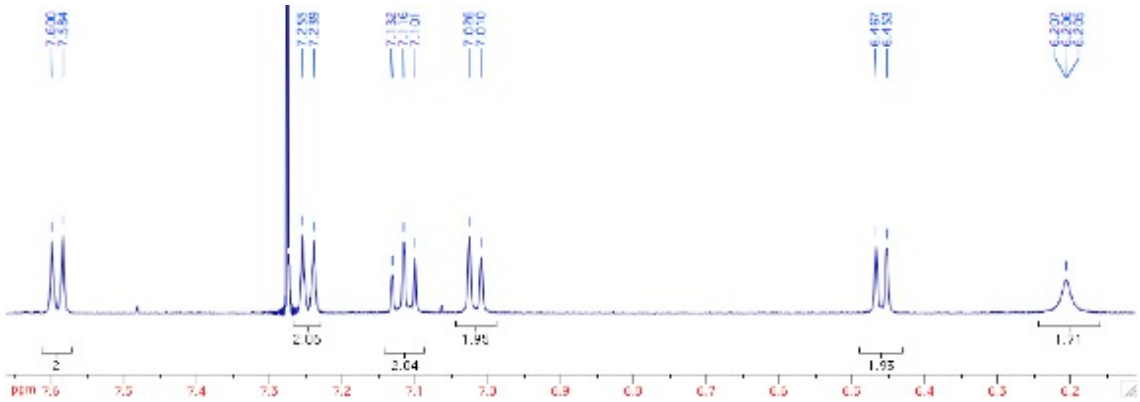

Figure A- 9 ^{1}H NMR spectrum of **154** + TBAC (1:10)

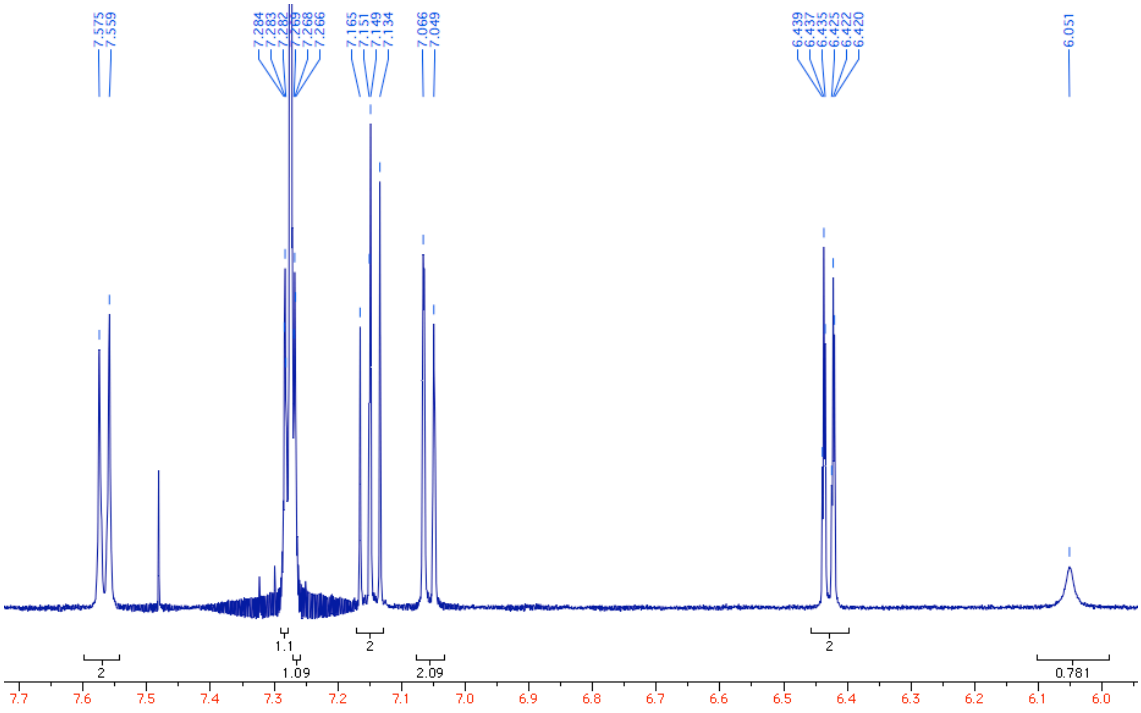

Figure A- 10 ^{1}H NMR spectrum of **154** + TBAF (1:1)

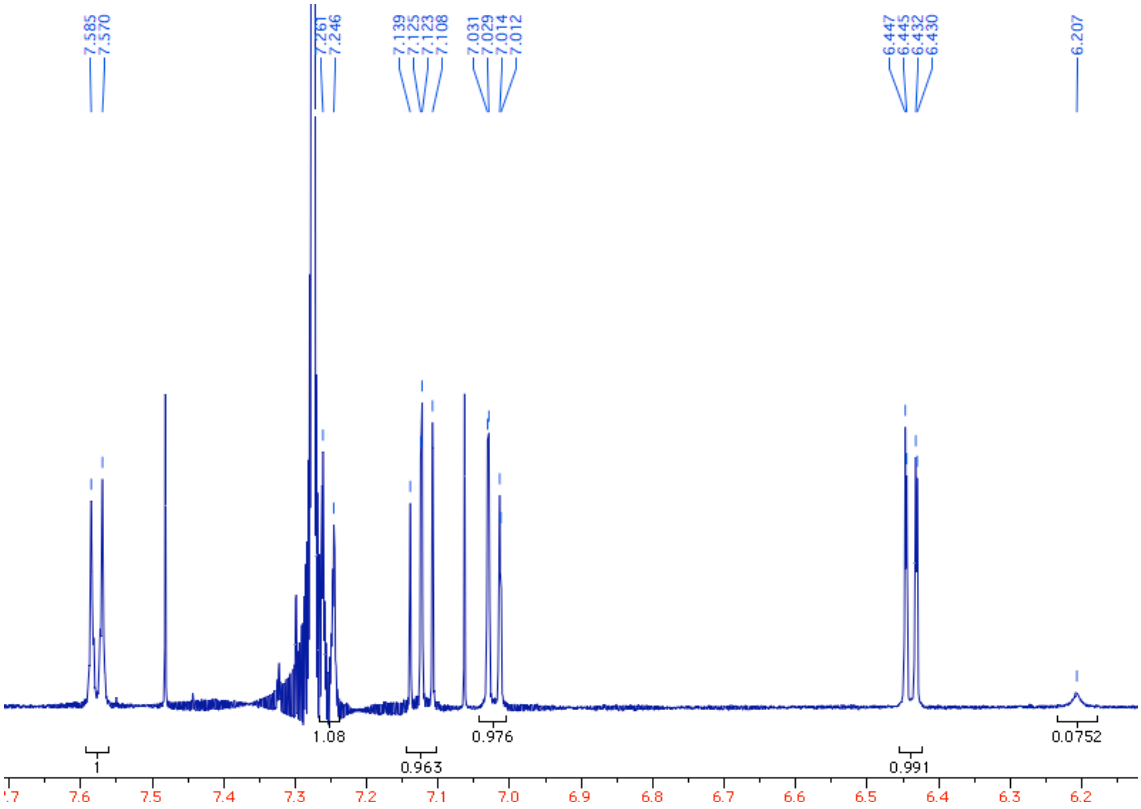

Figure A- 11 ^{1}H NMR spectrum of **154** + TBAF (1:10)

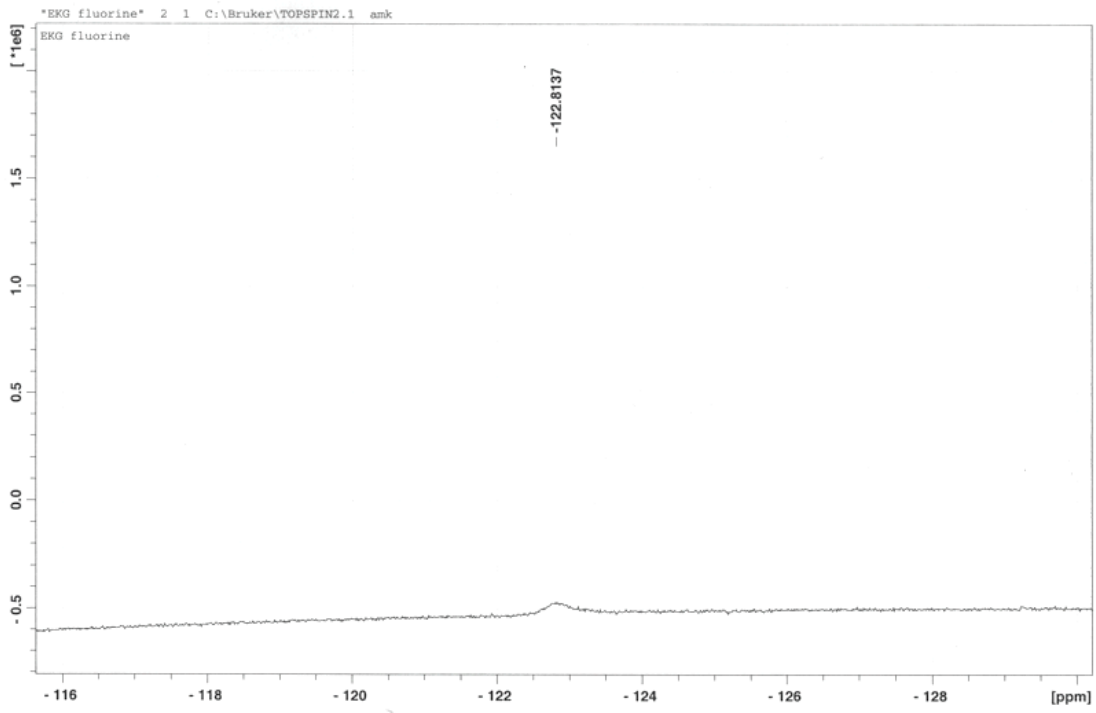

Figure A- 12 ^{19}F NMR spectrum of **154** + TBAF (2:1 sensor-anion, 2.5 M in $CDCl_3$ at 298 K).

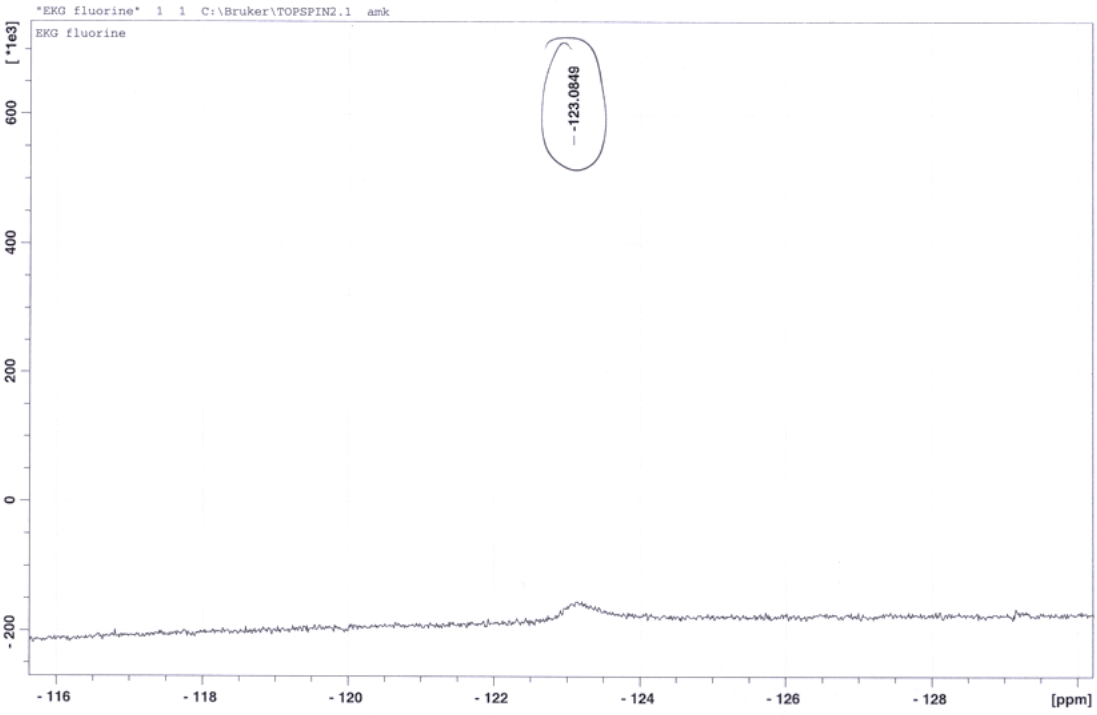

Figure A- 13 ^{19}F NMR spectrum of **154** + TBAF (1:1)

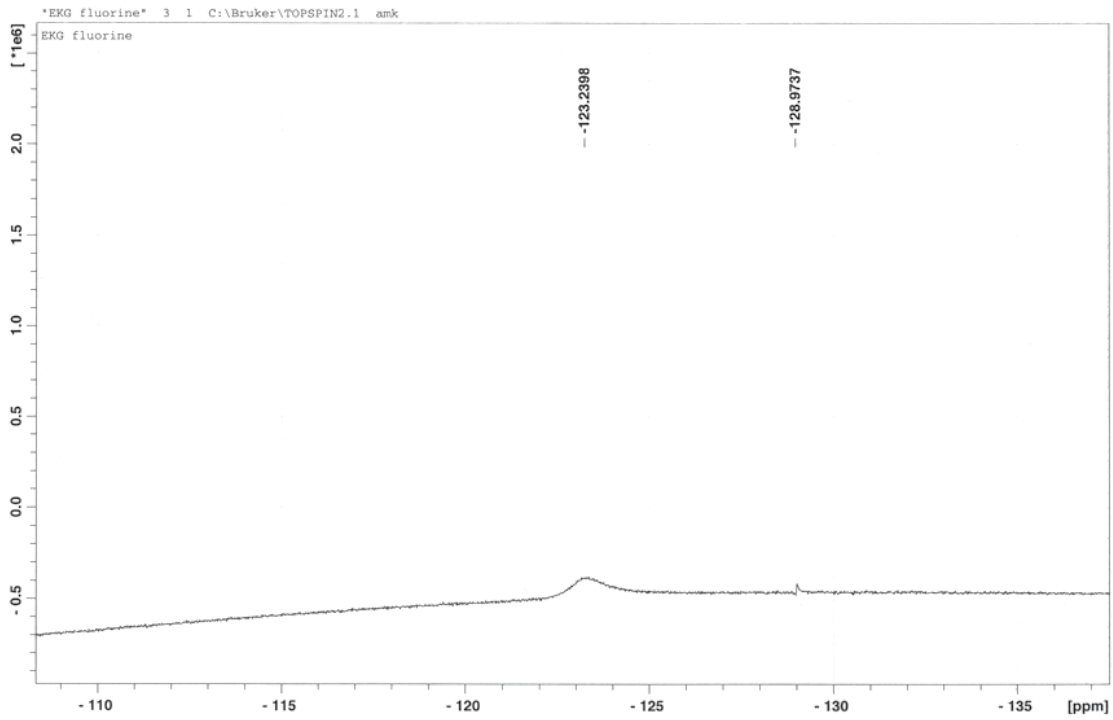

Figure A- 14 ^{19}F NMR of **154** + TBAF (1:2 sensor-anion)

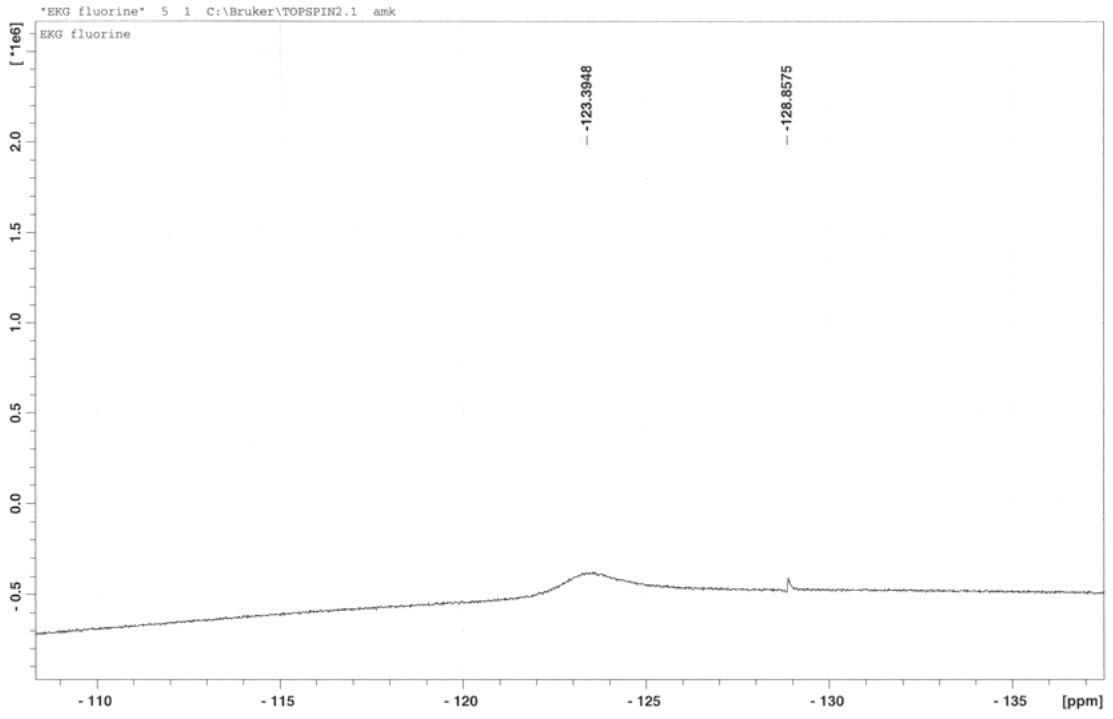

Figure A- 15 ^{19}F NMR spectrum of **154** + TBAF (1:5)

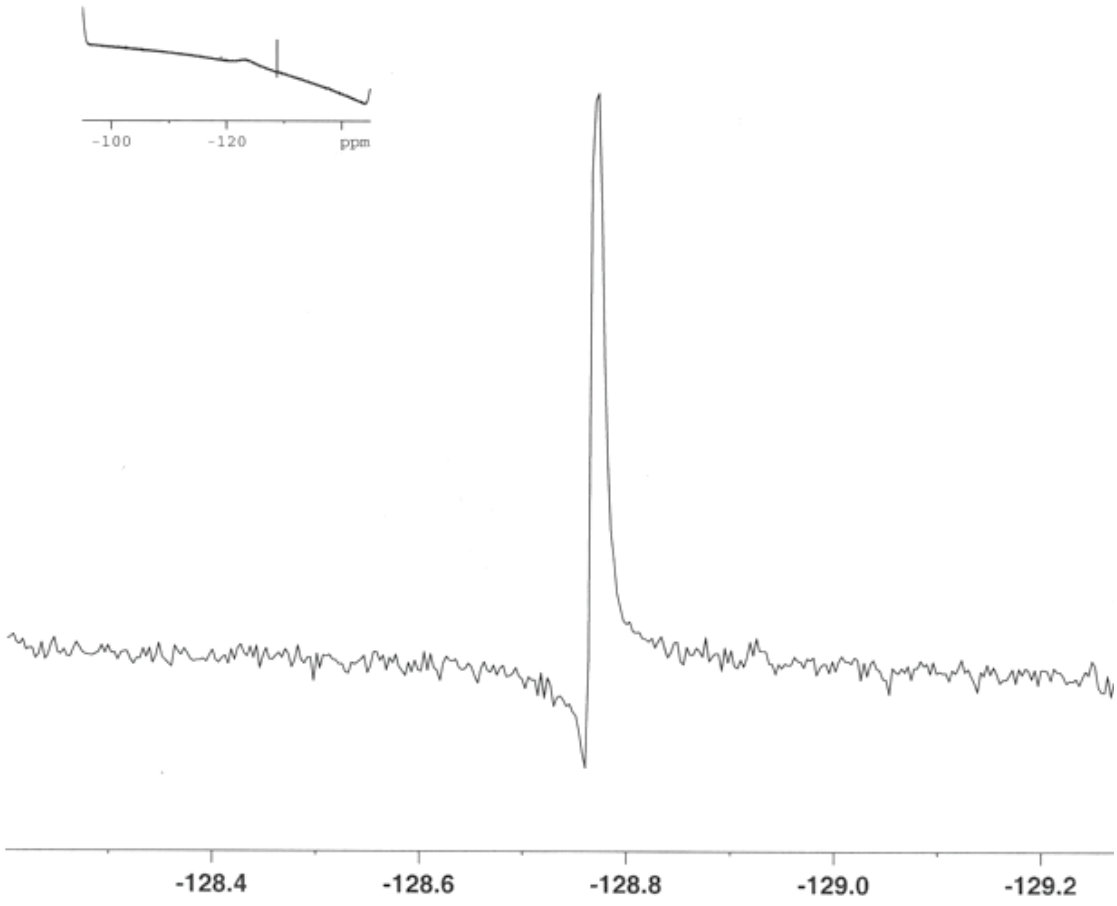

Figure A- 16 ^{19}F NMR spectrum of **154** + TBAF (1:10)

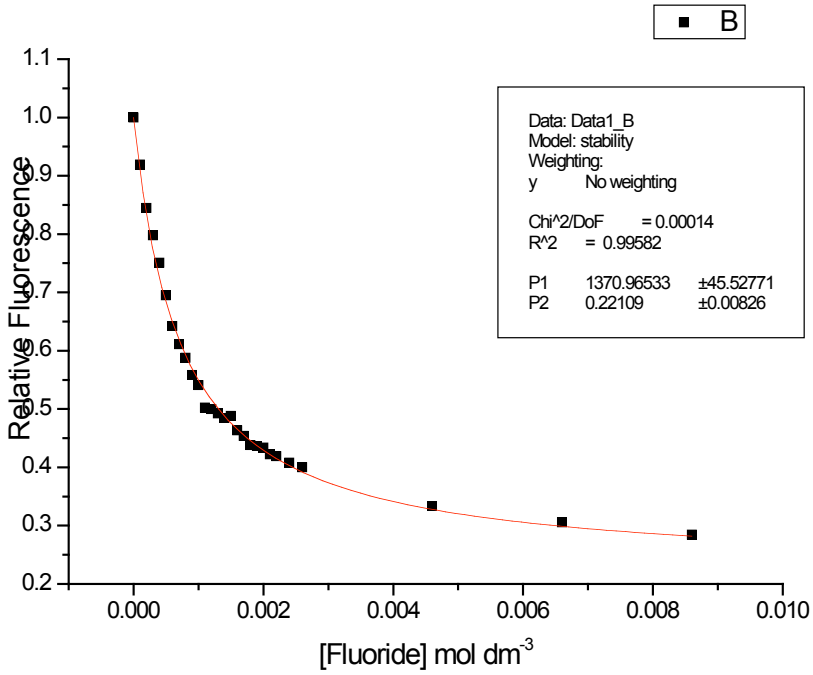

Figure A- 17 Plot of Fluorescence Emission Intensity at 430 nm (λ_{ex} = 305 nm) in dichloromethane at 1.0 x 10^{-4} M **154**. Curve analysis with R^2 = 0.99582 and P1 = binding constant, 1371 ± 46 M^{-1}.

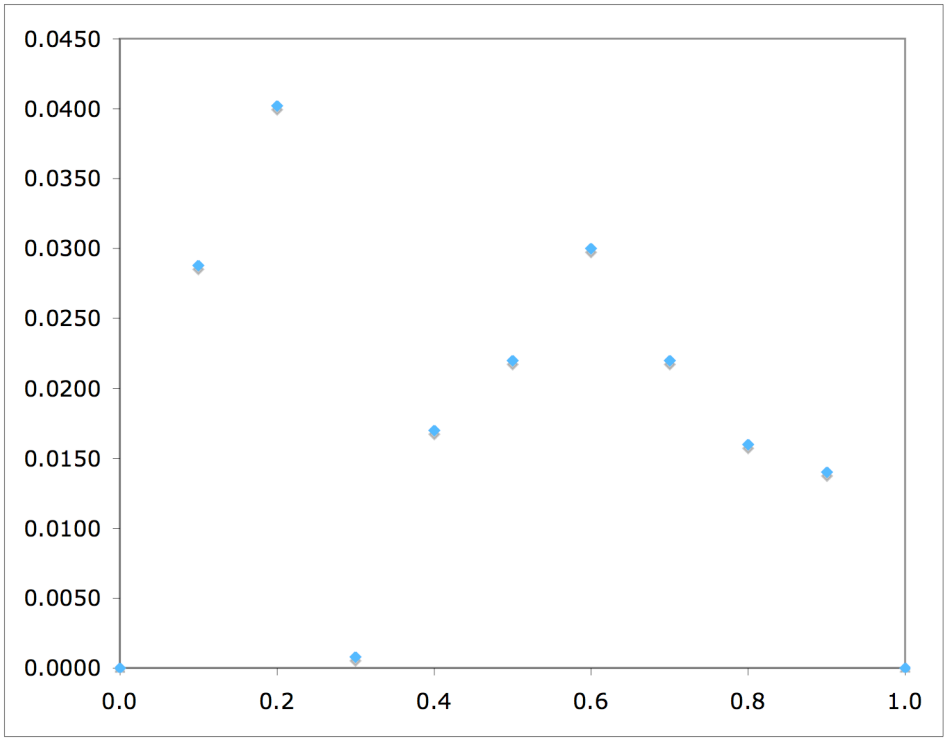

Figure A- 18 Attempted Job Plot for Compound **154** based on ^{1}H NMR data. Total Concentration of **154** + TBAF = 4.528 mM in $CDCl_3$. 500 MHz Bruker Avance Spectrometer.

6.3 X-ray Diffraction Data

6.3.1 Data for compound $[90]_2 \cdot 2H_2O$

Table 1. Crystal data and structure refinement

Identification code	d:rayd~15xsta~1mgd36mgd36	
Empirical formula	C41 H56 B2 N0 O5	
Formula weight	650.48	
Temperature	150(2) K	
Wavelength	0.71073 Å	
Crystal system	Monoclinic	
Space group	C2/c	
Unit cell dimensions	a = 19.1590(3) Å	a= 90.0000(10)°.
	b = 21.4040(3) Å	b= 90.6740(10)°.
	c = 19.1280(6) Å	g = 90.000(2)°.
Volume	7843.5(3) $Å^3$	
Z	8	
Density (calculated)	1.102 Mg/m^3	
Absorption coefficient	0.070 mm^{-1}	
F(000)	2816	
Crystal size	0.10 x 0.10 x 0.05 mm^3	
Theta range for data collection	3.51 to 26.37°.	
Index ranges	-21<=h<=19, -26<=k<=20, -14<=l<=23	
Reflections collected	17122	
Independent reflections	7574 [R(int) = 0.0635]	
Completeness to theta = 26.37°	94.7 %	
Max. and min. transmission	0.9965 and 0.9931	
Refinement method	Full-matrix least-squares on F^2	
Data / restraints / parameters	7574 / 0 / 447	
Goodness-of-fit on F^2	1.014	
Final R indices [I>2sigma(I)]	R1 = 0.0613, wR2 = 0.1319	
R indices (all data)	R1 = 0.1201, wR2 = 0.1607	
Extinction coefficient	0.0009(2)	
Largest diff. peak and hole	0.442 and -0.259 $e.Å^{-3}$	

Table 2. Atomic coordinates (x 10^4) and equivalent isotropic displacement parameters ($Å^2$x 10^3)
for k05mgd36. U(eq) is defined as one third of the trace of the orthogonalized U^{ij} tensor.

	x	y	z	U(eq)
O(1)	3677(1)	2785(1)	2881(1)	51(1)
O(2)	4595(1)	2420(1)	1101(1)	58(1)
O(10)	4650(2)	1845(2)	2650(3)	82(1)
O(20)	4874	3356	2142	71
O(3)	2908(1)	3621(1)	3166(1)	34(1)
O(4)	4342(1)	1557(1)	347(1)	37(1)
C(11)	2418(1)	2551(1)	3251(1)	48(1)
C(12)	2468(2)	1904(1)	3184(1)	62(1)
C(13)	1894(2)	1521(2)	3299(2)	81(1)
C(14)	1268(2)	1777(2)	3485(2)	88(1)
C(15)	1201(2)	2412(2)	3560(2)	82(1)
C(16)	1773(1)	2795(2)	3442(1)	63(1)
C(21)	4249(1)	2614(1)	-183(2)	49(1)
C(22)	4117(1)	2346(1)	-836(2)	62(1)
C(23)	4012(2)	2711(2)	-1435(2)	72(1)
C(24)	4036(1)	3353(2)	-1373(2)	72(1)
C(25)	4149(1)	3627(1)	-739(2)	75(1)
C(26)	4255(1)	3259(1)	-144(2)	62(1)
C(31)	3394(1)	4086(1)	3016(1)	31(1)
C(32)	3391(1)	4341(1)	2342(1)	34(1)
C(33)	3910(1)	4783(1)	2206(1)	38(1)
C(34)	4391(1)	4972(1)	2702(1)	39(1)
C(35)	4337(1)	4738(1)	3374(1)	37(1)
C(36)	3834(1)	4296(1)	3561(1)	31(1)
C(37)	5000	5387(2)	2500	48(1)
C(38)	3762(1)	4086(1)	4329(1)	35(1)
C(39)	4278(1)	4429(1)	4813(1)	50(1)
C(40)	3029(1)	4240(1)	4585(1)	47(1)
C(41)	3905(1)	3382(1)	4426(1)	45(1)

C(42)	2846(1)	4172(1)	1768(1)	42(1)
C(43)	2949(2)	4567(1)	1110(1)	64(1)
C(44)	2111(1)	4312(1)	2032(1)	60(1)
C(45)	2894(1)	3485(1)	1540(1)	54(1)
C(51)	4492(1)	1107(1)	852(1)	31(1)
C(52)	3950(1)	893(1)	1277(1)	31(1)
C(53)	4135(1)	465(1)	1795(1)	35(1)
C(54)	4807(1)	244(1)	1882(1)	34(1)
C(55)	5310(1)	438(1)	1421(1)	36(1)
C(56)	5173(1)	861(1)	883(1)	34(1)
C(57)	5000	-168(2)	2500	42(1)
C(58)	3181(1)	1096(1)	1173(1)	36(1)
C(59)	2940(1)	954(1)	426(1)	47(1)
C(60)	3064(1)	1793(1)	1328(1)	48(1)
C(61)	2698(1)	723(1)	1658(1)	49(1)
C(62)	5741(1)	1018(1)	346(1)	45(1)
C(63)	5477(2)	860(1)	-391(1)	66(1)
C(64)	5973(1)	1703(1)	376(2)	56(1)
C(65)	6397(1)	625(1)	485(2)	77(1)
B(1)	3045(1)	2994(1)	3089(1)	38(1)
B(2)	4402(1)	2188(1)	465(2)	42(1)

Table 3. Bond lengths [Å] and angles [°] for k05mgd36.

O(1)-B(1)	1.355(3)	C(25)-H(25)	0.9500
O(1)-H(1)	0.9500	C(26)-H(26)	0.9500
O(1)-H(1')	0.9500	C(31)-C(32)	1.401(3)
O(2)-B(2)	1.361(3)	C(31)-C(36)	1.405(3)
O(2)-H(2)	0.9500	C(32)-C(33)	1.398(3)
O(2)-H(2')	0.9500	C(32)-C(42)	1.550(3)
O(10)-O(10)#1	1.464(8)	C(33)-C(34)	1.374(3)
O(10)-H(100)	0.8302	C(33)-H(33)	0.9500
O(10)-H(101)	0.8938	C(34)-C(35)	1.385(3)
O(20)-O(20)#1	1.4449	C(34)-C(37)	1.521(3)
O(20)-H(200)	0.8258	C(35)-C(36)	1.400(3)
O(20)-H(201)	0.8508	C(35)-H(35)	0.9500
O(3)-B(1)	1.377(3)	C(36)-C(38)	1.545(3)
O(3)-C(31)	1.395(2)	C(37)-C(34)#1	1.521(3)
O(4)-B(2)	1.375(3)	C(37)-H(37A)	0.9900
O(4)-C(51)	1.391(2)	C(37)-H(37B)	0.9900
C(11)-C(16)	1.394(4)	C(38)-C(40)	1.530(3)
C(11)-C(12)	1.395(4)	C(38)-C(39)	1.534(3)
C(11)-B(1)	1.565(4)	C(38)-C(41)	1.542(3)
C(12)-C(13)	1.390(4)	C(39)-H(39A)	0.9800
C(12)-H(12)	0.9500	C(39)-H(39B)	0.9800
C(13)-C(14)	1.369(5)	C(39)-H(39C)	0.9800
C(13)-H(13)	0.9500	C(40)-H(40A)	0.9800
C(14)-C(15)	1.372(5)	C(40)-H(40B)	0.9800
C(14)-H(14)	0.9500	C(40)-H(40C)	0.9800
C(15)-C(16)	1.389(4)	C(41)-H(41A)	0.9800
C(15)-H(15)	0.9500	C(41)-H(41B)	0.9800
C(16)-H(16)	0.9500	C(41)-H(41C)	0.9800
C(21)-C(26)	1.383(4)	C(42)-C(43)	1.530(3)
C(21)-C(22)	1.394(4)	C(42)-C(44)	1.533(3)
C(21)-B(2)	1.564(4)	C(42)-C(45)	1.537(3)
C(22)-C(23)	1.400(4)	C(43)-H(43A)	0.9800
C(22)-H(22)	0.9500	C(43)-H(43B)	0.9800
C(23)-C(24)	1.379(4)	C(43)-H(43C)	0.9800
C(23)-H(23)	0.9500	C(44)-H(44A)	0.9800
C(24)-C(25)	1.362(5)	C(44)-H(44B)	0.9800
C(24)-H(24)	0.9500	C(44)-H(44C)	0.9800
C(25)-C(26)	1.396(4)	C(45)-H(45A)	0.9800

C(45)-H(45B)	0.9800	C(65)-H(65B)	0.9800
C(45)-H(45C)	0.9800	C(65)-H(65C)	0.9800
C(51)-C(52)	1.403(3)		
C(51)-C(56)	1.407(3)	B(1)-O(1)-H(1)	120.0
C(52)-C(53)	1.394(3)	B(1)-O(1)-H(1')	120.0
C(52)-C(58)	1.545(3)	H(1)-O(1)-H(1')	120.0
C(53)-C(54)	1.379(3)	B(2)-O(2)-H(2)	120.0
C(53)-H(53)	0.9500	B(2)-O(2)-H(2')	120.0
C(54)-C(55)	1.378(3)	H(2)-O(2)-H(2')	120.0
C(54)-C(57)	1.517(3)	O(10)#1-O(10)-H(100)	88.9
C(55)-C(56)	1.393(3)	O(10)#1-O(10)-H(101)	20.1
C(55)-H(55)	0.9500	H(100)-O(10)-H(101)	107.7
C(56)-C(62)	1.542(3)	O(20)#1-O(20)-H(200)	44.8
C(57)-C(54)#1	1.517(3)	O(20)#1-O(20)-H(201)	89.0
C(57)-H(57A)	0.9900	H(200)-O(20)-H(201)	99.2
C(57)-H(57B)	0.9900	B(1)-O(3)-C(31)	123.08(17)
C(58)-C(59)	1.527(3)	B(2)-O(4)-C(51)	123.47(19)
C(58)-C(60)	1.539(3)	C(16)-C(11)-C(12)	117.3(2)
C(58)-C(61)	1.540(3)	C(16)-C(11)-B(1)	120.7(2)
C(59)-H(59A)	0.9800	C(12)-C(11)-B(1)	122.0(2)
C(59)-H(59B)	0.9800	C(13)-C(12)-C(11)	121.1(3)
C(59)-H(59C)	0.9800	C(13)-C(12)-H(12)	119.5
C(60)-H(60A)	0.9800	C(11)-C(12)-H(12)	119.5
C(60)-H(60B)	0.9800	C(14)-C(13)-C(12)	120.0(3)
C(60)-H(60C)	0.9800	C(14)-C(13)-H(13)	120.0
C(61)-H(61A)	0.9800	C(12)-C(13)-H(13)	120.0
C(61)-H(61B)	0.9800	C(13)-C(14)-C(15)	120.6(3)
C(61)-H(61C)	0.9800	C(13)-C(14)-H(14)	119.7
C(62)-C(63)	1.530(4)	C(15)-C(14)-H(14)	119.7
C(62)-C(64)	1.533(3)	C(14)-C(15)-C(16)	119.5(3)
C(62)-C(65)	1.533(4)	C(14)-C(15)-H(15)	120.3
C(63)-H(63A)	0.9800	C(16)-C(15)-H(15)	120.3
C(63)-H(63B)	0.9800	C(15)-C(16)-C(11)	121.6(3)
C(63)-H(63C)	0.9800	C(15)-C(16)-H(16)	119.2
C(64)-H(64A)	0.9800	C(11)-C(16)-H(16)	119.2
C(64)-H(64B)	0.9800	C(26)-C(21)-C(22)	117.4(3)
C(64)-H(64C)	0.9800	C(26)-C(21)-B(2)	122.5(3)
C(65)-H(65A)	0.9800	C(22)-C(21)-B(2)	120.1(2)

C(21)-C(22)-C(23)	121.7(3)	H(37A)-C(37)-H(37B)	108.4
C(21)-C(22)-H(22)	119.1	C(40)-C(38)-C(39)	106.87(18)
C(23)-C(22)-H(22)	119.1	C(40)-C(38)-C(41)	109.51(19)
C(24)-C(23)-C(22)	118.8(3)	C(39)-C(38)-C(41)	106.50(18)
C(24)-C(23)-H(23)	120.6	C(40)-C(38)-C(36)	109.52(17)
C(22)-C(23)-H(23)	120.6	C(39)-C(38)-C(36)	111.79(18)
C(25)-C(24)-C(23)	120.6(3)	C(41)-C(38)-C(36)	112.46(17)
C(25)-C(24)-H(24)	119.7	C(38)-C(39)-H(39A)	109.5
C(23)-C(24)-H(24)	119.7	C(38)-C(39)-H(39B)	109.5
C(24)-C(25)-C(26)	120.3(3)	H(39A)-C(39)-H(39B)	109.5
C(24)-C(25)-H(25)	119.9	C(38)-C(39)-H(39C)	109.5
C(26)-C(25)-H(25)	119.9	H(39A)-C(39)-H(39C)	109.5
C(21)-C(26)-C(25)	121.1(3)	H(39B)-C(39)-H(39C)	109.5
C(21)-C(26)-H(26)	119.4	C(38)-C(40)-H(40A)	109.5
C(25)-C(26)-H(26)	119.4	C(38)-C(40)-H(40B)	109.5
O(3)-C(31)-C(32)	118.10(18)	H(40A)-C(40)-H(40B)	109.5
O(3)-C(31)-C(36)	118.18(18)	C(38)-C(40)-H(40C)	109.5
C(32)-C(31)-C(36)	123.63(19)	H(40A)-C(40)-H(40C)	109.5
C(33)-C(32)-C(31)	116.1(2)	H(40B)-C(40)-H(40C)	109.5
C(33)-C(32)-C(42)	120.0(2)	C(38)-C(41)-H(41A)	109.5
C(31)-C(32)-C(42)	123.87(19)	C(38)-C(41)-H(41B)	109.5
C(34)-C(33)-C(32)	122.8(2)	H(41A)-C(41)-H(41B)	109.5
C(34)-C(33)-H(33)	118.6	C(38)-C(41)-H(41C)	109.5
C(32)-C(33)-H(33)	118.6	H(41A)-C(41)-H(41C)	109.5
C(33)-C(34)-C(35)	118.6(2)	H(41B)-C(41)-H(41C)	109.5
C(33)-C(34)-C(37)	120.46(19)	C(43)-C(42)-C(44)	106.9(2)
C(35)-C(34)-C(37)	120.77(19)	C(43)-C(42)-C(45)	106.7(2)
C(34)-C(35)-C(36)	122.6(2)	C(44)-C(42)-C(45)	109.8(2)
C(34)-C(35)-H(35)	118.7	C(43)-C(42)-C(32)	111.2(2)
C(36)-C(35)-H(35)	118.7	C(44)-C(42)-C(32)	109.57(18)
C(35)-C(36)-C(31)	115.9(2)	C(45)-C(42)-C(32)	112.48(19)
C(35)-C(36)-C(38)	120.53(19)	C(42)-C(43)-H(43A)	109.5
C(31)-C(36)-C(38)	123.55(18)	C(42)-C(43)-H(43B)	109.5
C(34)-C(37)-C(34)#1	108.5(2)	H(43A)-C(43)-H(43B)	109.5
C(34)-C(37)-H(37A)	110.0	C(42)-C(43)-H(43C)	109.5
C(34)#1-C(37)-H(37A)	110.0	H(43A)-C(43)-H(43C)	109.5
C(34)-C(37)-H(37B)	110.0	H(43B)-C(43)-H(43C)	109.5
C(34)#1-C(37)-H(37B)	110.0	C(42)-C(44)-H(44A)	109.5

C(42)-C(44)-H(44B)	109.5	C(59)-C(58)-C(52)	109.99(18)
H(44A)-C(44)-H(44B)	109.5	C(60)-C(58)-C(52)	112.84(17)
C(42)-C(44)-H(44C)	109.5	C(61)-C(58)-C(52)	110.85(18)
H(44A)-C(44)-H(44C)	109.5	C(58)-C(59)-H(59A)	109.5
H(44B)-C(44)-H(44C)	109.5	C(58)-C(59)-H(59B)	109.5
C(42)-C(45)-H(45A)	109.5	H(59A)-C(59)-H(59B)	109.5
C(42)-C(45)-H(45B)	109.5	C(58)-C(59)-H(59C)	109.5
H(45A)-C(45)-H(45B)	109.5	H(59A)-C(59)-H(59C)	109.5
C(42)-C(45)-H(45C)	109.5	H(59B)-C(59)-H(59C)	109.5
H(45A)-C(45)-H(45C)	109.5	C(58)-C(60)-H(60A)	109.5
H(45B)-C(45)-H(45C)	109.5	C(58)-C(60)-H(60B)	109.5
O(4)-C(51)-C(52)	118.62(18)	H(60A)-C(60)-H(60B)	109.5
O(4)-C(51)-C(56)	118.15(18)	C(58)-C(60)-H(60C)	109.5
C(52)-C(51)-C(56)	123.12(19)	H(60A)-C(60)-H(60C)	109.5
C(53)-C(52)-C(51)	116.18(19)	H(60B)-C(60)-H(60C)	109.5
C(53)-C(52)-C(58)	120.71(19)	C(58)-C(61)-H(61A)	109.5
C(51)-C(52)-C(58)	123.08(19)	C(58)-C(61)-H(61B)	109.5
C(54)-C(53)-C(52)	122.8(2)	H(61A)-C(61)-H(61B)	109.5
C(54)-C(53)-H(53)	118.6	C(58)-C(61)-H(61C)	109.5
C(52)-C(53)-H(53)	118.6	H(61A)-C(61)-H(61C)	109.5
C(55)-C(54)-C(53)	118.6(2)	H(61B)-C(61)-H(61C)	109.5
C(55)-C(54)-C(57)	120.50(17)	C(63)-C(62)-C(64)	109.8(2)
C(53)-C(54)-C(57)	120.75(18)	C(63)-C(62)-C(65)	107.4(2)
C(54)-C(55)-C(56)	122.7(2)	C(64)-C(62)-C(65)	106.4(2)
C(54)-C(55)-H(55)	118.6	C(63)-C(62)-C(56)	109.76(19)
C(56)-C(55)-H(55)	118.6	C(64)-C(62)-C(56)	112.94(19)
C(55)-C(56)-C(51)	116.21(19)	C(65)-C(62)-C(56)	110.4(2)
C(55)-C(56)-C(62)	120.28(19)	C(62)-C(63)-H(63A)	109.5
C(51)-C(56)-C(62)	123.5(2)	C(62)-C(63)-H(63B)	109.5
C(54)-C(57)-C(54)#1	109.0(2)	H(63A)-C(63)-H(63B)	109.5
C(54)-C(57)-H(57A)	109.9	C(62)-C(63)-H(63C)	109.5
C(54)#1-C(57)-H(57A)	109.9	H(63A)-C(63)-H(63C)	109.5
C(54)-C(57)-H(57B)	109.9	H(63B)-C(63)-H(63C)	109.5
C(54)#1-C(57)-H(57B)	109.9	C(62)-C(64)-H(64A)	109.5
H(57A)-C(57)-H(57B)	108.3	C(62)-C(64)-H(64B)	109.5
C(59)-C(58)-C(60)	109.20(19)	H(64A)-C(64)-H(64B)	109.5
C(59)-C(58)-C(61)	106.47(18)	C(62)-C(64)-H(64C)	109.5
C(60)-C(58)-C(61)	107.25(18)	H(64A)-C(64)-H(64C)	109.5

H(64B)-C(64)-H(64C)	109.5
C(62)-C(65)-H(65A)	109.5
C(62)-C(65)-H(65B)	109.5
H(65A)-C(65)-H(65B)	109.5
C(62)-C(65)-H(65C)	109.5
H(65A)-C(65)-H(65C)	109.5
H(65B)-C(65)-H(65C)	109.5
O(1)-B(1)-O(3)	121.7(2)
O(1)-B(1)-C(11)	123.3(2)
O(3)-B(1)-C(11)	115.0(2)
O(2)-B(2)-O(4)	121.7(2)
O(2)-B(2)-C(21)	122.9(2)
O(4)-B(2)-C(21)	115.4(2)

Symmetry transformations used to generate equivalent atoms:
#1 -x+1,y,-z+1/2

Table 4. Anisotropic displacement parameters ($Å^2 x\ 10^3$)for k05mgd36. The anisotropic
displacement factor exponent takes the form: $-2p^2[\ h^2a^{*2}U^{11} + ... + 2\ h\ k\ a^*\ b^*\ U^{12}\ ]$

	U^{11}	U^{22}	U^{33}	U^{23}	U^{13}	U^{12}
O(1)	65(1)	43(1)	45(1)	-5(1)	1(1)	18(1)
O(2)	49(1)	43(1)	80(1)	-20(1)	-4(1)	-6(1)
O(10)	77(3)	26(2)	142(4)	4(2)	-28(3)	7(2)
O(20)	73	41	99	-3	18	-4
O(3)	35(1)	33(1)	35(1)	-4(1)	2(1)	-4(1)
O(4)	42(1)	31(1)	39(1)	3(1)	-1(1)	-4(1)
C(11)	71(2)	45(2)	29(1)	-2(1)	2(1)	-17(1)
C(12)	99(2)	46(2)	40(2)	2(1)	3(1)	-24(2)
C(13)	133(3)	55(2)	54(2)	0(2)	11(2)	-43(2)
C(14)	119(3)	96(3)	50(2)	-10(2)	17(2)	-69(2)
C(15)	77(2)	103(3)	66(2)	-19(2)	18(2)	-45(2)
C(16)	63(2)	71(2)	56(2)	-15(2)	12(1)	-25(2)
C(21)	34(1)	41(2)	73(2)	14(1)	-2(1)	-4(1)
C(22)	67(2)	55(2)	66(2)	21(2)	2(2)	2(1)
C(23)	65(2)	80(2)	70(2)	24(2)	-3(2)	3(2)
C(24)	44(2)	74(2)	99(3)	47(2)	-6(2)	-4(1)
C(25)	57(2)	48(2)	119(3)	30(2)	-24(2)	-6(1)
C(26)	45(2)	43(2)	97(2)	18(2)	-16(1)	-5(1)
C(31)	29(1)	26(1)	37(1)	-3(1)	4(1)	0(1)
C(32)	37(1)	30(1)	35(1)	-4(1)	4(1)	6(1)
C(33)	47(1)	29(1)	39(1)	3(1)	12(1)	8(1)
C(34)	35(1)	26(1)	56(2)	-2(1)	9(1)	4(1)
C(35)	33(1)	30(1)	50(2)	-9(1)	0(1)	4(1)
C(36)	29(1)	27(1)	38(1)	-3(1)	1(1)	6(1)
C(37)	43(2)	31(2)	69(3)	0	18(2)	0
C(38)	35(1)	32(1)	38(1)	-4(1)	-4(1)	3(1)
C(39)	57(2)	45(2)	49(2)	-4(1)	-18(1)	-1(1)
C(40)	48(1)	56(2)	36(1)	-6(1)	1(1)	12(1)
C(41)	53(2)	36(1)	45(2)	2(1)	-7(1)	3(1)
C(42)	57(2)	35(1)	36(1)	-7(1)	-4(1)	5(1)

C(43)	102(2)	46(2)	44(2)	3(1)	-16(2)	-1(2)
C(44)	52(2)	69(2)	58(2)	-14(2)	-18(1)	12(1)
C(45)	77(2)	42(2)	42(2)	-8(1)	-9(1)	3(1)
C(51)	38(1)	26(1)	28(1)	-2(1)	-4(1)	-3(1)
C(52)	36(1)	27(1)	31(1)	-7(1)	-2(1)	-3(1)
C(53)	39(1)	35(1)	30(1)	-4(1)	1(1)	-4(1)
C(54)	41(1)	29(1)	32(1)	-5(1)	-7(1)	-1(1)
C(55)	34(1)	32(1)	41(1)	-7(1)	-7(1)	-2(1)
C(56)	37(1)	26(1)	38(1)	-5(1)	1(1)	-6(1)
C(57)	50(2)	35(2)	40(2)	0	-8(2)	0
C(58)	33(1)	37(1)	38(1)	-2(1)	1(1)	-2(1)
C(59)	39(1)	52(2)	48(2)	-2(1)	-8(1)	-4(1)
C(60)	44(1)	40(1)	60(2)	-5(1)	5(1)	5(1)
C(61)	38(1)	50(2)	60(2)	2(1)	5(1)	-1(1)
C(62)	39(1)	40(1)	56(2)	1(1)	10(1)	-3(1)
C(63)	78(2)	66(2)	54(2)	-11(2)	28(2)	-20(2)
C(64)	46(2)	50(2)	71(2)	4(1)	7(1)	-13(1)
C(65)	56(2)	63(2)	114(3)	20(2)	36(2)	12(1)
B(1)	50(2)	36(2)	27(1)	-5(1)	-1(1)	-1(1)
B(2)	34(1)	37(2)	57(2)	-1(1)	2(1)	-4(1)

Table 5. Hydrogen coordinates (x 10^4) and isotropic displacement parameters (Å^{2}x 10^3) for k05mgd36.

	x	y	z	U(eq)
H(1)	4040	3073	2784	77
H(1')	3758	2349	2832	77
H(2)	4692	2144	1478	86
H(2')	4632	2859	1167	86
H(100)	4676	1459	2688	123
H(101)	5023	1974	2414	123
H(200)	4696	3299	2528	106
H(201)	4891	3753	2145	106
H(12)	2900	1721	3058	74
H(13)	1936	1081	3249	97
H(14)	878	1514	3563	106
H(15)	767	2588	3692	98
H(16)	1723	3234	3494	76
H(22)	4099	1904	-875	75
H(23)	3925	2521	-1876	86
H(24)	3973	3607	-1777	86
H(25)	4155	4069	-701	90
H(26)	4333	3456	295	74
H(33)	3931	4961	1752	46
H(35)	4654	4884	3723	45
H(37A)	5136	5658	2899	57
H(37B)	4864	5658	2101	57
H(39A)	4210	4292	5296	75
H(39B)	4197	4880	4781	75
H(39C)	4757	4335	4672	75
H(40A)	2683	4022	4293	70
H(40B)	2951	4692	4555	70
H(40C)	2983	4104	5072	70
H(41A)	3972	3290	4925	67
H(41B)	4326	3266	4172	67

H(41C)	3506	3142	4245	67
H(43A)	3405	4473	909	96
H(43B)	2927	5011	1233	96
H(43C)	2580	4470	768	96
H(44A)	1767	4211	1665	90
H(44B)	2075	4756	2152	90
H(44C)	2019	4059	2448	90
H(45A)	3384	3374	1464	80
H(45B)	2628	3425	1105	80
H(45C)	2702	3217	1906	80
H(53)	3785	320	2102	42
H(55)	5770	277	1472	43
H(57A)	5400	-438	2379	50
H(57B)	4600	-438	2621	50
H(59A)	2996	507	332	70
H(59B)	3222	1195	98	70
H(59C)	2448	1070	370	70
H(60A)	3255	2045	948	72
H(60B)	3299	1904	1769	72
H(60C)	2562	1875	1366	72
H(61A)	2211	834	1557	74
H(61B)	2811	822	2146	74
H(61C)	2765	274	1578	74
H(63A)	5364	414	-418	99
H(63B)	5841	958	-730	99
H(63C)	5059	1107	-498	99
H(64A)	5601	1969	183	83
H(64B)	6397	1756	102	83
H(64C)	6067	1821	863	83
H(65A)	6593	730	945	116
H(65B)	6743	712	124	116
H(65C)	6275	180	473	116

6.3.2 Data for compound 90 (anhydrous).

Table 1. Crystal data and structure refinement.

Identification code	c:~1~1.chpmgd11mgd11	
Empirical formula	C48 H62 B2 O4	
Formula weight	724.60	
Temperature	150(2) K	
Wavelength	0.71073 Å	
Crystal system	Monoclinic	
Space group	C2/c	
Unit cell dimensions	a = 26.7710(6) Å	a= 90°.
	b = 8.6100(2) Å	b= 95.4120(10)°.
	c = 18.6130(5) Å	g = 90°.
Volume	4271.14(18) $Å^3$	
Z	4	
Density (calculated)	1.127 Mg/m^3	
Absorption coefficient	0.069 mm^{-1}	
F(000)	1568	
Crystal size	0.25 x 0.13 x 0.13 mm^3	
Theta range for data collection	3.84 to 27.48°.	
Index ranges	-34<=h<=34, -11<=k<=11, -24<=l<=24	
Reflections collected	40948	
Independent reflections	4872 [R(int) = 0.0581]	
Completeness to theta = 27.48°	99.6 %	
Max. and min. transmission	0.9911 and 0.9830	
Refinement method	Full-matrix least-squares on F^2	
Data / restraints / parameters	4872 / 0 / 272	
Goodness-of-fit on F^2	1.044	
Final R indices [I>2sigma(I)]	R1 = 0.0570, wR2 = 0.1501	
R indices (all data)	R1 = 0.0874, wR2 = 0.1723	
Largest diff. peak and hole	0.550 and -0.439e	

Table 2. Atomic coordinates (x 10^4) and equivalent isotropic displacement parameters ($Å^2$x 10^3) for h06mgd11. U(eq) is defined as one third of the trace of the orthogonalized U^{ij} tensor.

	x	y	z	U(eq)
O(1)	3230(1)	175(1)	1589(1)	30(1)
B(1)	2777(1)	350(2)	1870(1)	30(1)
O(2)	2686(1)	1344(2)	2404(1)	42(1)
C(11)	3660(1)	1017(2)	1821(1)	27(1)
C(12)	3994(1)	385(2)	2373(1)	28(1)
C(13)	4422(1)	1252(2)	2591(1)	29(1)
C(14)	4531(1)	2645(2)	2262(1)	27(1)
C(15)	4200(1)	3185(2)	1703(1)	29(1)
C(16)	3759(1)	2401(2)	1457(1)	29(1)
C(17)	3923(1)	-1252(2)	2696(1)	34(1)
C(18)	5000	3572(3)	2500	33(1)
C(19)	3427(1)	3014(2)	792(1)	38(1)
C(21)	2332(1)	-679(2)	1536(1)	29(1)
C(22)	1857(1)	-533(2)	1785(1)	35(1)
C(23)	1457(1)	-1452(2)	1512(1)	42(1)
C(24)	1529(1)	-2546(2)	990(1)	44(1)
C(25)	1995(1)	-2725(2)	741(1)	42(1)
C(26)	2393(1)	-1798(2)	1009(1)	36(1)
C(27)	3929(1)	-2468(2)	2096(1)	45(1)
C(28)	3432(1)	-1397(2)	3069(1)	40(1)
C(29)	4353(1)	-1646(2)	3276(1)	53(1)
C(30)	3351(1)	1750(2)	210(1)	53(1)
C(31)	2917(1)	3594(3)	999(1)	56(1)
C(32)	3674(1)	4391(3)	439(1)	56(1)
C(41)	5195(2)	973(4)	-132(2)	74(2)
C(42)	5249(1)	-425(5)	-490(2)	53(2)
C(43)	4976(2)	-1720(4)	-314(3)	73(2)
C(44)	4648(2)	-1616(6)	221(3)	99(3)
C(45)	4594(2)	-218(7)	580(2)	91(3)
C(46)	4868(2)	1076(5)	403(2)	73(3)

C(47)	5398(2)	2512(5)	-341(3)	123(3)

Table 3. Bond lengths [Å] and angles [°] for h06mgd11.

O(1)-B(1)	1.372(2)	C(27)-H(27A)	0.9800
O(1)-C(11)	1.3949(17)	C(27)-H(27B)	0.9800
B(1)-O(2)	1.351(2)	C(27)-H(27C)	0.9800
B(1)-C(21)	1.567(2)	C(28)-H(28A)	0.9800
O(2)-H(1)	0.96(3)	C(28)-H(28B)	0.9800
C(11)-C(12)	1.407(2)	C(28)-H(28C)	0.9800
C(11)-C(16)	1.408(2)	C(29)-H(29A)	0.9800
C(12)-C(13)	1.394(2)	C(29)-H(29B)	0.9800
C(12)-C(17)	1.551(2)	C(29)-H(29C)	0.9800
C(13)-C(14)	1.389(2)	C(30)-H(30A)	0.9800
C(13)-H(13)	0.9500	C(30)-H(30B)	0.9800
C(14)-C(15)	1.383(2)	C(30)-H(30C)	0.9800
C(14)-C(18)	1.5187(18)	C(31)-H(31A)	0.9800
C(15)-C(16)	1.398(2)	C(31)-H(31B)	0.9800
C(15)-H(15)	0.9500	C(31)-H(31C)	0.9800
C(16)-C(19)	1.548(2)	C(32)-H(32A)	0.9800
C(17)-C(27)	1.533(3)	C(32)-H(32B)	0.9800
C(17)-C(29)	1.539(3)	C(32)-H(32C)	0.9800
C(17)-C(28)	1.546(2)	C(41)-C(42)	1.3900
C(18)-C(14)#1	1.5187(18)	C(41)-C(46)	1.3900
C(18)-H(18A)	0.9900	C(41)-C(47)	1.4973
C(18)-H(18B)	0.9900	C(42)-C(43)	1.3900
C(19)-C(30)	1.535(3)	C(42)-H(42)	0.9500
C(19)-C(32)	1.536(3)	C(43)-C(44)	1.3900
C(19)-C(31)	1.536(3)	C(43)-H(43)	0.9500
C(21)-C(26)	1.395(2)	C(44)-C(45)	1.3900
C(21)-C(22)	1.400(2)	C(44)-H(44)	0.9500
C(22)-C(23)	1.389(2)	C(45)-C(46)	1.3900
C(22)-H(22)	0.9500	C(45)-H(45)	0.9500
C(23)-C(24)	1.380(3)	C(46)-H(46)	0.9500
C(23)-H(23)	0.9500	C(47)-H(47A)	0.9800
C(24)-C(25)	1.378(3)	C(47)-H(47B)	0.9800
C(24)-H(24)	0.9500	C(47)-H(47C)	0.9800
C(25)-C(26)	1.385(2)		
C(25)-H(25)	0.9500	B(1)-O(1)-C(11)	123.88(12)
C(26)-H(26)	0.9500	O(2)-B(1)-O(1)	125.27(15)

O(2)-B(1)-C(21)	117.86(14)	C(31)-C(19)-C(16)	111.58(15)
O(1)-B(1)-C(21)	116.88(14)	C(26)-C(21)-C(22)	117.72(15)
B(1)-O(2)-H(1)	115.2(16)	C(26)-C(21)-B(1)	122.36(14)
O(1)-C(11)-C(12)	118.32(13)	C(22)-C(21)-B(1)	119.87(15)
O(1)-C(11)-C(16)	118.58(13)	C(23)-C(22)-C(21)	121.36(17)
C(12)-C(11)-C(16)	122.93(13)	C(23)-C(22)-H(22)	119.3
C(13)-C(12)-C(11)	116.90(14)	C(21)-C(22)-H(22)	119.3
C(13)-C(12)-C(17)	120.14(14)	C(24)-C(23)-C(22)	119.49(16)
C(11)-C(12)-C(17)	122.80(14)	C(24)-C(23)-H(23)	120.3
C(14)-C(13)-C(12)	122.39(15)	C(22)-C(23)-H(23)	120.3
C(14)-C(13)-H(13)	118.8	C(25)-C(24)-C(23)	120.23(16)
C(12)-C(13)-H(13)	118.8	C(25)-C(24)-H(24)	119.9
C(15)-C(14)-C(13)	118.34(14)	C(23)-C(24)-H(24)	119.9
C(15)-C(14)-C(18)	119.77(14)	C(24)-C(25)-C(26)	120.29(18)
C(13)-C(14)-C(18)	121.88(14)	C(24)-C(25)-H(25)	119.9
C(14)-C(15)-C(16)	123.08(14)	C(26)-C(25)-H(25)	119.9
C(14)-C(15)-H(15)	118.5	C(25)-C(26)-C(21)	120.91(16)
C(16)-C(15)-H(15)	118.5	C(25)-C(26)-H(26)	119.5
C(15)-C(16)-C(11)	116.22(14)	C(21)-C(26)-H(26)	119.5
C(15)-C(16)-C(19)	120.08(14)	C(17)-C(27)-H(27A)	109.5
C(11)-C(16)-C(19)	123.60(14)	C(17)-C(27)-H(27B)	109.5
C(27)-C(17)-C(29)	107.60(15)	H(27A)-C(27)-H(27B)	109.5
C(27)-C(17)-C(28)	109.86(14)	C(17)-C(27)-H(27C)	109.5
C(29)-C(17)-C(28)	106.16(15)	H(27A)-C(27)-H(27C)	109.5
C(27)-C(17)-C(12)	109.13(14)	H(27B)-C(27)-H(27C)	109.5
C(29)-C(17)-C(12)	111.11(13)	C(17)-C(28)-H(28A)	109.5
C(28)-C(17)-C(12)	112.83(13)	C(17)-C(28)-H(28B)	109.5
C(14)#1-C(18)-C(14)	116.57(18)	H(28A)-C(28)-H(28B)	109.5
C(14)#1-C(18)-H(18A)	108.1	C(17)-C(28)-H(28C)	109.5
C(14)-C(18)-H(18A)	108.1	H(28A)-C(28)-H(28C)	109.5
C(14)#1-C(18)-H(18B)	108.1	H(28B)-C(28)-H(28C)	109.5
C(14)-C(18)-H(18B)	108.1	C(17)-C(29)-H(29A)	109.5
H(18A)-C(18)-H(18B)	107.3	C(17)-C(29)-H(29B)	109.5
C(30)-C(19)-C(32)	106.23(17)	H(29A)-C(29)-H(29B)	109.5
C(30)-C(19)-C(31)	110.23(17)	C(17)-C(29)-H(29C)	109.5
C(32)-C(19)-C(31)	106.61(16)	H(29A)-C(29)-H(29C)	109.5
C(30)-C(19)-C(16)	110.51(15)	H(29B)-C(29)-H(29C)	109.5
C(32)-C(19)-C(16)	111.49(14)	C(19)-C(30)-H(30A)	109.5

C(19)-C(30)-H(30B)	109.5	C(46)-C(41)-C(47)	113.4
H(30A)-C(30)-H(30B)	109.5	C(41)-C(42)-C(43)	120.0
C(19)-C(30)-H(30C)	109.5	C(41)-C(42)-H(42)	120.0
H(30A)-C(30)-H(30C)	109.5	C(43)-C(42)-H(42)	120.0
H(30B)-C(30)-H(30C)	109.5	C(44)-C(43)-C(42)	120.0
C(19)-C(31)-H(31A)	109.5	C(44)-C(43)-H(43)	120.0
C(19)-C(31)-H(31B)	109.5	C(42)-C(43)-H(43)	120.0
H(31A)-C(31)-H(31B)	109.5	C(43)-C(44)-C(45)	120.0
C(19)-C(31)-H(31C)	109.5	C(43)-C(44)-H(44)	120.0
H(31A)-C(31)-H(31C)	109.5	C(45)-C(44)-H(44)	120.0
H(31B)-C(31)-H(31C)	109.5	C(46)-C(45)-C(44)	120.0
C(19)-C(32)-H(32A)	109.5	C(46)-C(45)-H(45)	120.0
C(19)-C(32)-H(32B)	109.5	C(44)-C(45)-H(45)	120.0
H(32A)-C(32)-H(32B)	109.5	C(45)-C(46)-C(41)	120.0
C(19)-C(32)-H(32C)	109.5	C(45)-C(46)-H(46)	120.0
H(32A)-C(32)-H(32C)	109.5	C(41)-C(46)-H(46)	120.0
H(32B)-C(32)-H(32C)	109.5		
C(42)-C(41)-C(46)	120.0		
C(42)-C(41)-C(47)	125.8		

Symmetry transformations used to generate equivalent atoms:
#1 -x+1,y,-z+1/2

Table 4. Anisotropic displacement parameters ($Å^2 x\ 10^3$)for h06mgd11. The anisotropic
displacement factor exponent takes the form: $-2p^2[\ h^2 a^{*2} U^{11} + ... + 2\ h\ k\ a^*\ b^*\ U^{12}\ ]$

	U^{11}	U^{22}	U^{33}	U^{23}	U^{13}	U^{12}
O(1)	23(1)	33(1)	35(1)	-5(1)	0(1)	-4(1)
B(1)	27(1)	31(1)	32(1)	-1(1)	0(1)	0(1)
O(2)	31(1)	45(1)	48(1)	-16(1)	2(1)	-1(1)
C(11)	21(1)	29(1)	32(1)	-6(1)	2(1)	-2(1)
C(12)	24(1)	28(1)	32(1)	0(1)	4(1)	1(1)
C(13)	22(1)	30(1)	34(1)	0(1)	1(1)	3(1)
C(14)	20(1)	28(1)	34(1)	-3(1)	2(1)	2(1)
C(15)	25(1)	28(1)	32(1)	0(1)	1(1)	0(1)
C(16)	25(1)	32(1)	30(1)	-2(1)	-1(1)	1(1)
C(17)	30(1)	30(1)	42(1)	4(1)	3(1)	-1(1)
C(18)	23(1)	29(1)	47(1)	0	-6(1)	0
C(19)	35(1)	39(1)	39(1)	5(1)	-9(1)	-4(1)
C(21)	26(1)	30(1)	31(1)	4(1)	0(1)	-1(1)
C(22)	29(1)	33(1)	42(1)	6(1)	4(1)	2(1)
C(23)	25(1)	43(1)	57(1)	14(1)	1(1)	-2(1)
C(24)	37(1)	41(1)	51(1)	13(1)	-12(1)	-14(1)
C(25)	51(1)	37(1)	37(1)	-3(1)	-4(1)	-12(1)
C(26)	33(1)	39(1)	34(1)	-1(1)	3(1)	-5(1)
C(27)	47(1)	31(1)	58(1)	-1(1)	16(1)	2(1)
C(28)	41(1)	35(1)	44(1)	1(1)	12(1)	-5(1)
C(29)	43(1)	44(1)	68(1)	23(1)	-9(1)	-5(1)
C(30)	63(1)	57(1)	35(1)	1(1)	-13(1)	-12(1)
C(31)	39(1)	65(1)	62(1)	13(1)	-12(1)	12(1)
C(32)	56(1)	56(1)	51(1)	20(1)	-20(1)	-15(1)
C(41)	72(4)	95(5)	50(4)	26(3)	-22(3)	-18(3)
C(42)	32(3)	92(6)	37(3)	-19(3)	14(2)	7(3)
C(43)	78(4)	75(5)	61(4)	-10(3)	-20(3)	13(3)
C(44)	69(5)	151(10)	72(4)	69(6)	-20(4)	-8(5)
C(45)	49(4)	138(8)	90(5)	33(5)	24(3)	32(5)
C(46)	103(7)	71(6)	43(3)	-14(4)	-6(4)	25(5)

C(47)	105(6)	169(9)	87(6)	45(6)	-26(5)	-17(6)

Table 5. Hydrogen coordinates (x 10^4) and isotropic displacement parameters (Å^{2}x 10^3)
for h06mgd11.

	x	y	z	U(eq)
H(1)	2966(11)	1970(30)	2585(15)	74(8)
H(13)	4647	877	2977	35
H(15)	4275	4133	1476	34
H(18A)	5075	4254	2095	40
H(18B)	4925	4254	2905	40
H(22)	1807	211	2149	42
H(23)	1136	-1329	1683	50
H(24)	1257	-3179	801	53
H(25)	2043	-3486	385	51
H(26)	2711	-1926	831	43
H(27A)	4243	-2384	1868	67
H(27B)	3645	-2287	1733	67
H(27C)	3902	-3509	2301	67
H(28A)	3148	-1540	2703	60
H(28B)	3382	-451	3345	60
H(28C)	3456	-2293	3395	60
H(29A)	4306	-2699	3457	79
H(29B)	4352	-903	3675	79
H(29C)	4674	-1585	3064	79
H(30A)	3678	1395	81	79
H(30B)	3157	2175	-218	79
H(30C)	3169	873	397	79
H(31A)	2737	4115	583	84
H(31B)	2970	4327	1401	84
H(31C)	2719	2710	1143	84
H(32A)	4002	4071	296	84
H(32B)	3719	5250	785	84

H(32C)	3460	4730	12	84
H(42)	5473	-496	-856	64
H(43)	5013	-2675	-558	88
H(44)	4461	-2501	342	119
H(45)	4371	-147	945	109
H(46)	4831	2032	648	87
H(47A)	5749	2391	-441	184
H(47B)	5378	3252	56	184
H(47C)	5200	2900	-773	184

6.3.3 Data for compound 91.

Table 1. Crystal data and structure refinement.

Identification code	k06mgd05	
Empirical formula	C20 H27 B O2	
Formula weight	310.23	
Temperature	150(2) K	
Wavelength	0.71073 Å	
Crystal system	Monoclinic	
Space group	$P2_1/a$	
Unit cell dimensions	a = 12.01200(10) Å	a= 90°.
	b = 14.42000(10) Å	b= 105.1010(10)°.
	c = 21.9640(2) Å	g = 90°.
Volume	3673.08(5) $Å^3$	
Z	8	
Density (calculated)	1.122 Mg/m^3	
Absorption coefficient	0.069 mm^{-1}	
F(000)	1344	
Crystal size	0.20 x 0.20 x 0.10 mm^3	
Theta range for data collection	2.98 to 26.02°.	
Index ranges	-14<=h<=14, -17<=k<=17, -26<=l<=26	
Reflections collected	53331	
Independent reflections	7217 [R(int) = 0.0440]	
Completeness to theta = 26.02°	99.6 %	
Max. and min. transmission	0.9931 and 0.9863	
Refinement method	Full-matrix least-squares on F^2	
Data / restraints / parameters	7217 / 0 / 451	
Goodness-of-fit on F^2	1.037	
Final R indices [I>2sigma(I)]	R1 = 0.0474, wR2 = 0.1096	
R indices (all data)	R1 = 0.0602, wR2 = 0.1182	
Largest diff. peak and hole	0.249 and -0.267 $e.Å^{-3}$	

Table 2. Atomic coordinates (x 10^4) and equivalent isotropic displacement parameters ($Å^2$x 10^3) for k06mgd05. U(eq) is defined as one third of the trace of the orthogonalized U^{ij} tensor.

	x	y	z	U(eq)
O(1)	7973(1)	5228(1)	2937(1)	32(1)
O(2)	9484(1)	5095(1)	3900(1)	24(1)
O(3)	5678(1)	5118(1)	2135(1)	41(1)
O(4)	5949(1)	5046(1)	1089(1)	23(1)
C(11)	7454(1)	4824(1)	3955(1)	24(1)
C(12)	6268(1)	4781(1)	3672(1)	31(1)
C(13)	5497(1)	4545(1)	4020(1)	35(1)
C(14)	5886(1)	4350(1)	4654(1)	34(1)
C(15)	7048(1)	4402(1)	4946(1)	36(1)
C(16)	7823(1)	4634(1)	4600(1)	32(1)
C(21)	3947(1)	4854(1)	1229(1)	25(1)
C(22)	3439(1)	4788(1)	582(1)	30(1)
C(23)	2261(1)	4643(1)	349(1)	36(1)
C(24)	1571(1)	4559(1)	763(1)	38(1)
C(25)	2056(1)	4616(1)	1405(1)	35(1)
C(26)	3231(1)	4765(1)	1637(1)	31(1)
C(31)	10382(1)	5292(1)	3624(1)	22(1)
C(32)	10669(1)	6222(1)	3543(1)	23(1)
C(33)	11583(1)	6358(1)	3263(1)	27(1)
C(34)	12168(1)	5632(1)	3084(1)	30(1)
C(35)	11889(1)	4730(1)	3196(1)	30(1)
C(36)	11002(1)	4527(1)	3477(1)	26(1)
C(37)	10153(1)	7113(1)	3757(1)	26(1)
C(38)	11076(1)	7564(1)	4290(1)	46(1)
C(39)	9824(2)	7799(1)	3205(1)	56(1)
C(40)	9081(1)	7000(1)	4001(1)	44(1)
C(42)	10937(2)	3413(1)	4354(1)	47(1)
C(41)	10780(1)	3515(1)	3640(1)	34(1)
C(43)	11637(2)	2848(1)	3463(1)	65(1)
C(44)	9561(2)	3185(1)	3292(1)	47(1)

C(51)	7133(1)	5200(1)	1302(1)	21(1)
C(52)	7540(1)	6117(1)	1388(1)	22(1)
C(53)	8722(1)	6225(1)	1660(1)	27(1)
C(54)	9452(1)	5478(1)	1813(1)	29(1)
C(55)	9035(1)	4589(1)	1674(1)	27(1)
C(56)	7865(1)	4416(1)	1410(1)	22(1)
C(57)	6805(1)	7005(1)	1211(1)	28(1)
C(58)	5940(4)	6925(2)	586(2)	70(1)
C(59)	6212(4)	7204(2)	1735(2)	69(1)
C(60)	7575(2)	7839(2)	1184(2)	59(1)
C(58')	5500(5)	6892(4)	861(3)	40(1)
C(59')	6809(5)	7585(4)	1787(2)	36(1)
C(60')	7304(5)	7583(4)	750(3)	39(1)
C(61)	7441(1)	3413(1)	1254(1)	26(1)
C(62)	8456(1)	2747(1)	1290(1)	38(1)
C(63)	6661(2)	3334(1)	582(1)	43(1)
C(64)	6787(1)	3066(1)	1726(1)	39(1)
B(1)	8346(1)	5064(1)	3572(1)	25(1)
B(2)	5271(1)	5017(1)	1505(1)	25(1)

Table 3. Bond lengths [Å] and angles [°] for k06mgd05.

O(1)-B(1)	1.3694(18)	C(13)-H(13)	0.9500
O(1)-H(1)	0.84(2)	C(14)-C(15)	1.378(2)
O(2)-B(1)	1.3700(18)	C(14)-H(14)	0.9500
O(2)-C(31)	1.3967(15)	C(15)-C(16)	1.387(2)
O(3)-B(2)	1.3486(19)	C(15)-H(15)	0.9500
O(3)-H(3)	0.86(3)	C(16)-H(16)	0.9500
O(4)-B(2)	1.3743(18)	C(21)-C(22)	1.396(2)
O(4)-C(51)	1.3944(15)	C(21)-C(26)	1.3998(19)
C(11)-C(16)	1.3967(19)	C(21)-B(2)	1.565(2)
C(11)-C(12)	1.399(2)	C(22)-C(23)	1.389(2)
C(11)-B(1)	1.564(2)	C(22)-H(22)	0.9500
C(12)-C(13)	1.388(2)	C(23)-C(24)	1.387(2)
C(12)-H(12)	0.9500	C(23)-H(23)	0.9500
C(13)-C(14)	1.378(2)	C(24)-C(25)	1.381(2)

C(24)-H(24)	0.9500	C(44)-H(44C)	0.9800
C(25)-C(26)	1.387(2)	C(51)-C(52)	1.4047(18)
C(25)-H(25)	0.9500	C(51)-C(56)	1.4138(18)
C(26)-H(26)	0.9500	C(52)-C(53)	1.3982(18)
C(31)-C(32)	1.4075(19)	C(52)-C(57)	1.5467(19)
C(31)-C(36)	1.4152(19)	C(53)-C(54)	1.375(2)
C(32)-C(33)	1.4042(18)	C(53)-H(53)	0.9500
C(32)-C(37)	1.5526(19)	C(54)-C(55)	1.382(2)
C(33)-C(34)	1.374(2)	C(54)-H(54)	0.9500
C(33)-H(33)	0.9500	C(55)-C(56)	1.3956(19)
C(34)-C(35)	1.380(2)	C(55)-H(55)	0.9500
C(34)-H(34)	0.9500	C(56)-C(61)	1.5422(18)
C(35)-C(36)	1.393(2)	C(57)-C(58)	1.496(3)
C(35)-H(35)	0.9500	C(57)-C(59')	1.516(5)
C(36)-C(41)	1.542(2)	C(57)-C(60)	1.528(3)
C(37)-C(40)	1.527(2)	C(57)-C(59)	1.529(3)
C(37)-C(38)	1.533(2)	C(57)-C(60')	1.548(5)
C(37)-C(39)	1.534(2)	C(57)-C(58')	1.564(6)
C(38)-H(38A)	0.9800	C(58)-H(58A)	0.9800
C(38)-H(38B)	0.9800	C(58)-H(58B)	0.9800
C(38)-H(38C)	0.9800	C(58)-H(58C)	0.9800
C(39)-H(39A)	0.9800	C(59)-H(59A)	0.9800
C(39)-H(39B)	0.9800	C(59)-H(59B)	0.9800
C(39)-H(39C)	0.9800	C(59)-H(59C)	0.9800
C(40)-H(40A)	0.9800	C(60)-H(60A)	0.9800
C(40)-H(40B)	0.9800	C(60)-H(60B)	0.9800
C(40)-H(40C)	0.9800	C(60)-H(60C)	0.9800
C(42)-C(41)	1.537(2)	C(58')-H(58D)	0.9800
C(42)-H(42A)	0.9800	C(58')-H(58E)	0.9800
C(42)-H(42B)	0.9800	C(58')-H(58F)	0.9800
C(42)-H(42C)	0.9800	C(59')-H(59D)	0.9800
C(41)-C(43)	1.531(2)	C(59')-H(59E)	0.9800
C(41)-C(44)	1.539(2)	C(59')-H(59F)	0.9800
C(43)-H(43A)	0.9800	C(60')-H(60D)	0.9800
C(43)-H(43B)	0.9800	C(60')-H(60E)	0.9800
C(43)-H(43C)	0.9800	C(60')-H(60F)	0.9800
C(44)-H(44A)	0.9800	C(61)-C(63)	1.533(2)
C(44)-H(44B)	0.9800	C(61)-C(62)	1.538(2)

C(61)-C(64)	1.538(2)	C(21)-C(22)-H(22)	119.4
C(62)-H(62A)	0.9800	C(24)-C(23)-C(22)	119.85(14)
C(62)-H(62B)	0.9800	C(24)-C(23)-H(23)	120.1
C(62)-H(62C)	0.9800	C(22)-C(23)-H(23)	120.1
C(63)-H(63A)	0.9800	C(25)-C(24)-C(23)	120.00(13)
C(63)-H(63B)	0.9800	C(25)-C(24)-H(24)	120.0
C(63)-H(63C)	0.9800	C(23)-C(24)-H(24)	120.0
C(64)-H(64A)	0.9800	C(24)-C(25)-C(26)	120.07(14)
C(64)-H(64B)	0.9800	C(24)-C(25)-H(25)	120.0
C(64)-H(64C)	0.9800	C(26)-C(25)-H(25)	120.0
		C(25)-C(26)-C(21)	121.10(14)
B(1)-O(1)-H(1)	116.1(15)	C(25)-C(26)-H(26)	119.4
B(1)-O(2)-C(31)	123.83(10)	C(21)-C(26)-H(26)	119.4
B(2)-O(3)-H(3)	118.9(17)	O(2)-C(31)-C(32)	119.44(11)
B(2)-O(4)-C(51)	120.78(10)	O(2)-C(31)-C(36)	116.92(12)
C(16)-C(11)-C(12)	117.35(12)	C(32)-C(31)-C(36)	123.53(12)
C(16)-C(11)-B(1)	120.53(12)	C(33)-C(32)-C(31)	115.73(12)
C(12)-C(11)-B(1)	122.11(12)	C(33)-C(32)-C(37)	115.86(12)
C(13)-C(12)-C(11)	120.97(13)	C(31)-C(32)-C(37)	128.31(11)
C(13)-C(12)-H(12)	119.5	C(34)-C(33)-C(32)	122.33(13)
C(11)-C(12)-H(12)	119.5	C(34)-C(33)-H(33)	118.8
C(14)-C(13)-C(12)	120.44(14)	C(32)-C(33)-H(33)	118.8
C(14)-C(13)-H(13)	119.8	C(33)-C(34)-C(35)	120.05(13)
C(12)-C(13)-H(13)	119.8	C(33)-C(34)-H(34)	120.0
C(13)-C(14)-C(15)	119.73(13)	C(35)-C(34)-H(34)	120.0
C(13)-C(14)-H(14)	120.1	C(34)-C(35)-C(36)	121.72(13)
C(15)-C(14)-H(14)	120.1	C(34)-C(35)-H(35)	119.1
C(14)-C(15)-C(16)	120.01(14)	C(36)-C(35)-H(35)	119.1
C(14)-C(15)-H(15)	120.0	C(35)-C(36)-C(31)	116.48(13)
C(16)-C(15)-H(15)	120.0	C(35)-C(36)-C(41)	120.06(12)
C(15)-C(16)-C(11)	121.49(13)	C(31)-C(36)-C(41)	123.39(12)
C(15)-C(16)-H(16)	119.3	C(40)-C(37)-C(38)	106.53(13)
C(11)-C(16)-H(16)	119.3	C(40)-C(37)-C(39)	106.22(13)
C(22)-C(21)-C(26)	117.83(13)	C(38)-C(37)-C(39)	108.49(14)
C(22)-C(21)-B(2)	122.36(12)	C(40)-C(37)-C(32)	117.25(12)
C(26)-C(21)-B(2)	119.81(12)	C(38)-C(37)-C(32)	108.42(11)
C(23)-C(22)-C(21)	121.16(14)	C(39)-C(37)-C(32)	109.62(12)
C(23)-C(22)-H(22)	119.4	C(37)-C(38)-H(38A)	109.5

C(37)-C(38)-H(38B)	109.5	C(41)-C(44)-H(44C)	109.5
H(38A)-C(38)-H(38B)	109.5	H(44A)-C(44)-H(44C)	109.5
C(37)-C(38)-H(38C)	109.5	H(44B)-C(44)-H(44C)	109.5
H(38A)-C(38)-H(38C)	109.5	O(4)-C(51)-C(52)	118.91(11)
H(38B)-C(38)-H(38C)	109.5	O(4)-C(51)-C(56)	117.68(11)
C(37)-C(39)-H(39A)	109.5	C(52)-C(51)-C(56)	123.40(11)
C(37)-C(39)-H(39B)	109.5	C(53)-C(52)-C(51)	116.20(12)
H(39A)-C(39)-H(39B)	109.5	C(53)-C(52)-C(57)	117.67(12)
C(37)-C(39)-H(39C)	109.5	C(51)-C(52)-C(57)	126.13(11)
H(39A)-C(39)-H(39C)	109.5	C(54)-C(53)-C(52)	121.94(13)
H(39B)-C(39)-H(39C)	109.5	C(54)-C(53)-H(53)	119.0
C(37)-C(40)-H(40A)	109.5	C(52)-C(53)-H(53)	119.0
C(37)-C(40)-H(40B)	109.5	C(53)-C(54)-C(55)	120.10(12)
H(40A)-C(40)-H(40B)	109.5	C(53)-C(54)-H(54)	120.0
C(37)-C(40)-H(40C)	109.5	C(55)-C(54)-H(54)	120.0
H(40A)-C(40)-H(40C)	109.5	C(54)-C(55)-C(56)	121.69(13)
H(40B)-C(40)-H(40C)	109.5	C(54)-C(55)-H(55)	119.2
C(41)-C(42)-H(42A)	109.5	C(56)-C(55)-H(55)	119.2
C(41)-C(42)-H(42B)	109.5	C(55)-C(56)-C(51)	116.23(12)
H(42A)-C(42)-H(42B)	109.5	C(55)-C(56)-C(61)	119.90(12)
C(41)-C(42)-H(42C)	109.5	C(51)-C(56)-C(61)	123.86(11)
H(42A)-C(42)-H(42C)	109.5	C(58)-C(57)-C(59')	131.3(3)
H(42B)-C(42)-H(42C)	109.5	C(58)-C(57)-C(60)	107.9(2)
C(43)-C(41)-C(42)	106.64(15)	C(59')-C(57)-C(60)	74.2(3)
C(43)-C(41)-C(44)	107.15(15)	C(58)-C(57)-C(59)	110.9(3)
C(42)-C(41)-C(44)	108.98(14)	C(59')-C(57)-C(59)	33.9(2)
C(43)-C(41)-C(36)	111.48(13)	C(60)-C(57)-C(59)	106.7(2)
C(42)-C(41)-C(36)	110.24(12)	C(58)-C(57)-C(52)	112.39(15)
C(44)-C(41)-C(36)	112.14(12)	C(59')-C(57)-C(52)	111.7(2)
C(41)-C(43)-H(43A)	109.5	C(60)-C(57)-C(52)	110.45(14)
C(41)-C(43)-H(43B)	109.5	C(59)-C(57)-C(52)	108.31(15)
H(43A)-C(43)-H(43B)	109.5	C(58)-C(57)-C(60')	74.6(3)
C(41)-C(43)-H(43C)	109.5	C(59')-C(57)-C(60')	109.3(3)
H(43A)-C(43)-H(43C)	109.5	C(60)-C(57)-C(60')	37.7(2)
H(43B)-C(43)-H(43C)	109.5	C(59)-C(57)-C(60')	136.6(3)
C(41)-C(44)-H(44A)	109.5	C(52)-C(57)-C(60')	108.5(2)
C(41)-C(44)-H(44B)	109.5	C(58)-C(57)-C(58')	34.2(2)
H(44A)-C(44)-H(44B)	109.5	C(59')-C(57)-C(58')	104.7(3)

C(60)-C(57)-C(58')	127.0(3)	C(61)-C(62)-H(62B)	109.5
C(59)-C(57)-C(58')	77.7(3)	H(62A)-C(62)-H(62B)	109.5
C(52)-C(57)-C(58')	118.1(2)	C(61)-C(62)-H(62C)	109.5
C(60')-C(57)-C(58')	104.1(3)	H(62A)-C(62)-H(62C)	109.5
C(57)-C(58)-H(58A)	109.5	H(62B)-C(62)-H(62C)	109.5
C(57)-C(58)-H(58B)	109.5	C(61)-C(63)-H(63A)	109.5
C(57)-C(58)-H(58C)	109.5	C(61)-C(63)-H(63B)	109.5
C(57)-C(59)-H(59A)	109.5	H(63A)-C(63)-H(63B)	109.5
C(57)-C(59)-H(59B)	109.5	C(61)-C(63)-H(63C)	109.5
C(57)-C(59)-H(59C)	109.5	H(63A)-C(63)-H(63C)	109.5
C(57)-C(60)-H(60A)	109.5	H(63B)-C(63)-H(63C)	109.5
C(57)-C(60)-H(60B)	109.5	C(61)-C(64)-H(64A)	109.5
C(57)-C(60)-H(60C)	109.5	C(61)-C(64)-H(64B)	109.5
C(57)-C(58')-H(58D)	109.5	H(64A)-C(64)-H(64B)	109.5
C(57)-C(58')-H(58E)	109.5	C(61)-C(64)-H(64C)	109.5
H(58D)-C(58')-H(58E)	109.5	H(64A)-C(64)-H(64C)	109.5
C(57)-C(58')-H(58F)	109.5	H(64B)-C(64)-H(64C)	109.5
H(58D)-C(58')-H(58F)	109.5	O(1)-B(1)-O(2)	123.11(12)
H(58E)-C(58')-H(58F)	109.5	O(1)-B(1)-C(11)	119.86(12)
C(57)-C(59')-H(59D)	109.5	O(2)-B(1)-C(11)	117.03(12)
C(57)-C(59')-H(59E)	109.5	O(3)-B(2)-O(4)	123.98(13)
H(59D)-C(59')-H(59E)	109.5	O(3)-B(2)-C(21)	118.32(12)
C(57)-C(59')-H(59F)	109.5	O(4)-B(2)-C(21)	117.71(12)
H(59D)-C(59')-H(59F)	109.5		
H(59E)-C(59')-H(59F)	109.5		
C(57)-C(60')-H(60D)	109.5		
C(57)-C(60')-H(60E)	109.5		
H(60D)-C(60')-H(60E)	109.5		
C(57)-C(60')-H(60F)	109.5		
H(60D)-C(60')-H(60F)	109.5		
H(60E)-C(60')-H(60F)	109.5		
C(63)-C(61)-C(62)	106.27(12)		
C(63)-C(61)-C(64)	109.51(13)		
C(62)-C(61)-C(64)	107.37(12)		
C(63)-C(61)-C(56)	111.57(11)		
C(62)-C(61)-C(56)	111.22(11)		
C(64)-C(61)-C(56)	110.73(11)		
C(61)-C(62)-H(62A)	109.5		

Table 4. Anisotropic displacement parameters ($Å^2 x\ 10^3$)for k06mgd05. The anisotropic displacement factor exponent takes the form: $-2p^2[\ h^2a^{*2}U^{11} + ... + 2\ h\ k\ a^*\ b^*\ U^{12}\ ]$

	U^{11}	U^{22}	U^{33}	U^{23}	U^{13}	U^{12}
O(1)	23(1)	51(1)	24(1)	2(1)	7(1)	-5(1)
O(2)	20(1)	29(1)	24(1)	2(1)	8(1)	-1(1)
O(3)	24(1)	74(1)	27(1)	-7(1)	7(1)	-8(1)
O(4)	17(1)	28(1)	25(1)	0(1)	4(1)	-1(1)
C(11)	25(1)	22(1)	27(1)	-2(1)	9(1)	-1(1)
C(12)	26(1)	38(1)	29(1)	3(1)	8(1)	-1(1)
C(13)	24(1)	40(1)	43(1)	4(1)	12(1)	0(1)
C(14)	36(1)	32(1)	41(1)	4(1)	23(1)	2(1)
C(15)	40(1)	44(1)	28(1)	5(1)	14(1)	2(1)
C(16)	28(1)	39(1)	29(1)	1(1)	8(1)	-2(1)
C(21)	23(1)	21(1)	32(1)	-1(1)	8(1)	0(1)
C(22)	24(1)	30(1)	35(1)	3(1)	7(1)	-1(1)
C(23)	27(1)	37(1)	37(1)	2(1)	-1(1)	-2(1)
C(24)	20(1)	33(1)	59(1)	-2(1)	6(1)	-1(1)
C(25)	25(1)	34(1)	51(1)	-5(1)	18(1)	-2(1)
C(26)	27(1)	31(1)	35(1)	-4(1)	11(1)	0(1)
C(31)	17(1)	31(1)	19(1)	1(1)	4(1)	-1(1)
C(32)	19(1)	29(1)	21(1)	0(1)	3(1)	0(1)
C(33)	24(1)	31(1)	26(1)	-1(1)	6(1)	-6(1)
C(34)	21(1)	40(1)	30(1)	-4(1)	9(1)	-3(1)
C(35)	24(1)	35(1)	31(1)	-5(1)	8(1)	3(1)
C(36)	24(1)	28(1)	26(1)	-2(1)	4(1)	0(1)
C(37)	24(1)	27(1)	28(1)	0(1)	7(1)	1(1)
C(38)	35(1)	46(1)	55(1)	-21(1)	7(1)	2(1)
C(39)	81(1)	45(1)	48(1)	13(1)	25(1)	28(1)
C(40)	37(1)	35(1)	68(1)	-11(1)	27(1)	1(1)
C(42)	61(1)	34(1)	42(1)	10(1)	6(1)	6(1)
C(41)	37(1)	27(1)	39(1)	0(1)	12(1)	2(1)
C(43)	76(1)	30(1)	105(2)	-1(1)	52(1)	9(1)
C(44)	55(1)	35(1)	49(1)	-1(1)	8(1)	-14(1)
C(51)	16(1)	28(1)	18(1)	-1(1)	5(1)	-2(1)

C(52)	24(1)	24(1)	20(1)	-2(1)	8(1)	1(1)
C(53)	25(1)	26(1)	31(1)	-4(1)	9(1)	-5(1)
C(54)	19(1)	34(1)	34(1)	-2(1)	5(1)	-4(1)
C(55)	22(1)	28(1)	31(1)	1(1)	7(1)	3(1)
C(56)	22(1)	25(1)	20(1)	0(1)	7(1)	0(1)
C(57)	26(1)	23(1)	34(1)	-3(1)	6(1)	1(1)
C(58)	89(3)	28(1)	61(2)	2(1)	-39(2)	10(2)
C(59)	83(3)	47(2)	92(3)	7(2)	54(2)	33(2)
C(60)	39(2)	28(1)	103(3)	17(2)	8(2)	2(1)
C(61)	27(1)	22(1)	29(1)	1(1)	5(1)	0(1)
C(62)	37(1)	24(1)	54(1)	-2(1)	12(1)	3(1)
C(63)	56(1)	28(1)	37(1)	-7(1)	-5(1)	1(1)
C(64)	40(1)	29(1)	49(1)	4(1)	17(1)	-6(1)
B(1)	24(1)	25(1)	25(1)	-1(1)	6(1)	-1(1)
B(2)	24(1)	25(1)	27(1)	-1(1)	8(1)	-1(1)

Table 5. Hydrogen coordinates (x 10^4) and isotropic displacement parameters ($Å^2$x 10^3) for k06mgd05.

	x	y	z	U(eq)
H(12)	5987	4915	3235	37
H(13)	4695	4518	3819	42
H(14)	5356	4180	4889	40
H(15)	7319	4279	5385	43
H(16)	8622	4663	4806	38
H(22)	3908	4842	295	36
H(23)	1929	4603	-93	43
H(24)	765	4461	605	45
H(25)	1583	4554	1689	42
H(26)	3556	4806	2079	37
H(33)	11804	6974	3195	33
H(34)	12765	5750	2883	36
H(35)	12312	4235	3079	36
H(38A)	10790	8159	4404	69
H(38B)	11776	7668	4150	69
H(38C)	11253	7154	4659	69
H(39A)	9248	7514	2855	84
H(39B)	10511	7958	3065	84
H(39C)	9502	8363	3342	84
H(40A)	8858	7605	4136	67
H(40B)	9249	6572	4359	67
H(40C)	8448	6753	3664	67
H(42A)	10807	2765	4453	71
H(42B)	10382	3812	4486	71
H(42C)	11722	3596	4578	71
H(43A)	12425	3038	3677	97
H(43B)	11534	2862	3006	97
H(43C)	11500	2218	3594	97
H(44A)	9403	3351	2845	71
H(44B)	8993	3484	3477	71
H(44C)	9513	2511	3333	71

H(53)	9029	6833	1743	32
H(54)	10245	5573	2015	35
H(55)	9558	4082	1760	32
H(58A)	5512	7508	488	105
H(58B)	5402	6419	600	105
H(58C)	6338	6794	258	105
H(59A)	5848	7817	1668	103
H(59B)	6785	7192	2144	103
H(59C)	5623	6731	1728	103
H(60A)	8036	7712	885	88
H(60B)	8089	7951	1603	88
H(60C)	7094	8387	1046	88
H(58D)	5174	7499	711	60
H(58E)	5085	6632	1151	60
H(58F)	5423	6473	501	60
H(59D)	6333	8139	1658	54
H(59E)	7601	7772	1995	54
H(59F)	6496	7220	2081	54
H(60D)	7204	7242	354	58
H(60E)	8126	7695	938	58
H(60F)	6897	8177	667	58
H(62A)	8159	2129	1149	57
H(62B)	8929	2712	1727	57
H(62C)	8926	2976	1019	57
H(63A)	5965	3707	544	65
H(63B)	6444	2683	490	65
H(63C)	7076	3559	281	65
H(64A)	6063	3410	1665	58
H(64B)	7262	3163	2157	58
H(64C)	6620	2403	1657	58
H(1)	8489(19)	5319(14)	2749(10)	60(6)
H(3)	6410(20)	5180(17)	2293(12)	87(8)

Hydrogen bonds with H..A < r(A) + 2.000 Angstroms and <DHA > 110 deg.

D-H	d(D-H)	d(H..A)	<DHA	d(D..A)	A
O3-H3	0.863	2.036	160.46	2.864	O1

O-H…pi (pi = centroid of C51-C56)

O…pi	3.191
O-H	0.840
H…pi	2.602
O.-H…pi	128.3

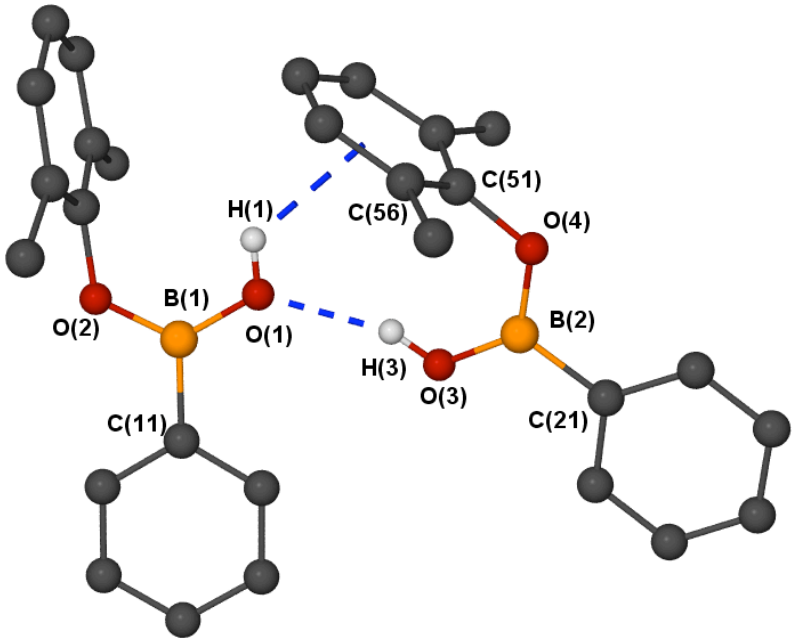

6.3.4 Data for Compound 110

Table 1. Crystal data and structure refinement for k07tdj2.

Identification code	k07tdj2
Empirical formula	C30 H24 B2 Cl6 N2 O3
Formula weight	694.83
Temperature	150(2) K
Wavelength	0.71073 A
Crystal system	triclinic
Space group	P $\bar{1}$
Unit cell dimensions	a = 9.90300(10) A alpha = 78.8420(10) deg.
	b = 12.1380(2) A beta = 72.3620(10) deg.
	c = 13.9070(2) A gamma = 83.1790(10) deg.
Volume	1559.72(4) A^3
Z, Calculated density	2, 1.479 Mg/m^3
Absorption coefficient	0.587 mm^-1
F(000)	708
Crystal size	0.50 x 0.25 x 0.25 mm
Theta range for data collection	3.01 to 30.11 deg.
Limiting indices	-13<=h<=13, -16<=k<=17, -19<=l<=19
Reflections collected / unique	37035 / 9137 [R(int) = 0.0450]
Completeness to theta = 30.11	99.5 %
Max. and min. transmission	0.8671 and 0.7579
Refinement method	Full-matrix least-squares on F^2
Data / restraints / parameters	9137 / 0 / 480
Goodness-of-fit on F^2	1.026
Final R indices [I>2sigma(I)]	R1 = 0.0504, wR2 = 0.1244
R indices (all data)	R1 = 0.0829, wR2 = 0.1427
Largest diff. peak and hole	0.623 and -0.445 e.A^-3

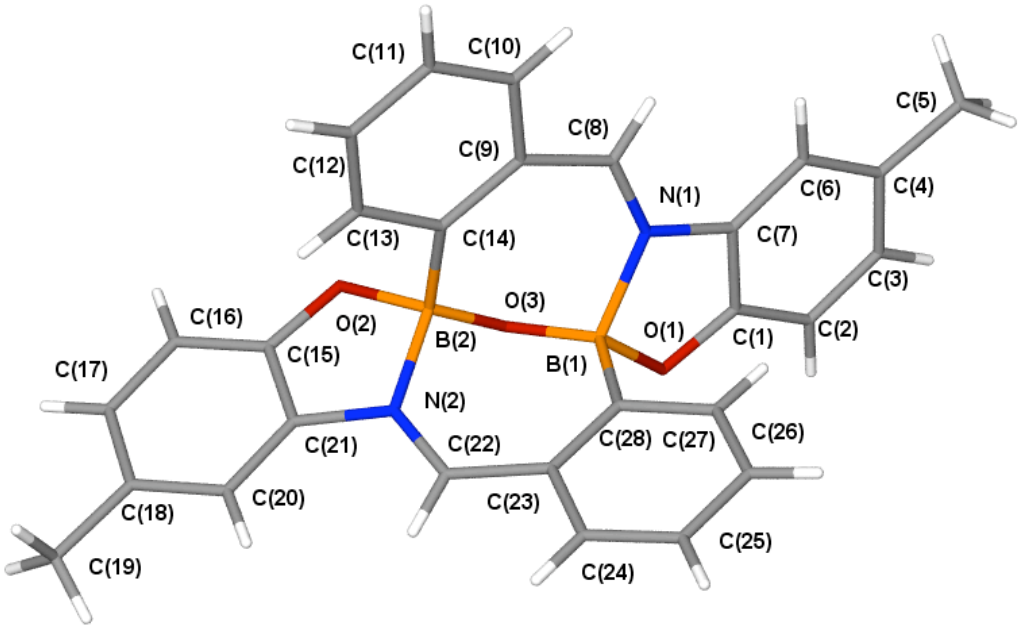
C(11)
C(10)
C(5)
C(8)
C(9)
C(12)
N(1)
C(6)
C(4)
C(13)
C(14)
C(7)
C(3)
O(3)
C(16)
O(2)
O(1)
C(1)
C(2)
B(2)
C(15)
B(1)
C(17)
N(2)
C(21)
C(22)
C(28)
C(27)
C(26)
C(18)
C(20)
C(23)
C(25)
C(19)
C(24)

Table 2. Atomic coordinates (x 10^4) and equivalent isotropic displacement parameters (A^2 x 10^3) for k07tdj2.
U(eq) is defined as one third of the trace of the orthogonalized Uij tensor.

	x	y	z	U(eq)
B(1)	6379(2)	1813(1)	2820(1)	24(1)
B(2)	6456(2)	2183(1)	4458(1)	24(1)
N(1)	5189(1)	877(1)	3171(1)	24(1)
N(2)	6652(1)	3546(1)	4206(1)	24(1)
O(1)	7355(1)	1398(1)	1889(1)	28(1)
O(2)	7306(1)	1842(1)	5212(1)	27(1)
O(3)	7092(1)	1715(1)	3571(1)	24(1)
C(1)	6765(2)	573(1)	1660(1)	27(1)
C(2)	7325(2)	51(2)	806(1)	35(1)
C(3)	6543(2)	-755(2)	674(1)	38(1)
C(4)	5235(2)	-1063(1)	1358(1)	33(1)
C(5)	4408(2)	-1905(2)	1142(2)	44(1)
C(6)	4708(2)	-561(1)	2228(1)	29(1)
C(7)	5482(2)	245(1)	2365(1)	26(1)
C(8)	4195(2)	686(1)	4019(1)	25(1)
C(9)	3871(2)	1291(1)	4879(1)	24(1)
C(10)	2525(2)	1083(1)	5580(1)	30(1)
C(11)	2021(2)	1597(2)	6436(1)	34(1)
C(12)	2876(2)	2305(2)	6621(1)	33(1)
C(13)	4223(2)	2484(1)	5953(1)	29(1)
C(14)	4780(2)	1994(1)	5066(1)	24(1)
C(15)	7680(2)	2762(1)	5458(1)	25(1)
C(16)	8359(2)	2767(2)	6196(1)	31(1)
C(17)	8630(2)	3800(2)	6366(1)	33(1)
C(18)	8247(2)	4831(1)	5831(1)	29(1)
C(19)	8514(2)	5932(2)	6065(1)	36(1)
C(20)	7589(2)	4816(1)	5077(1)	27(1)
C(21)	7316(2)	3786(1)	4905(1)	24(1)
C(22)	6324(2)	4277(1)	3494(1)	26(1)
C(23)	5666(2)	4079(1)	2743(1)	25(1)
C(24)	5076(2)	5072(1)	2267(1)	32(1)
C(25)	4365(2)	5043(1)	1560(1)	34(1)
C(26)	4242(2)	4016(1)	1310(1)	32(1)
C(27)	4855(2)	3041(1)	1755(1)	30(1)
C(28)	5589(2)	3024(1)	2476(1)	24(1)
C(30)	10244(2)	1224(2)	2614(1)	42(1)
Cl(1)	10888(6)	163(5)	1760(3)	50(1)
Cl(2)	10812(2)	1109(2)	3695(2)	63(1)
Cl(3)	10698(8)	2682(4)	1937(4)	82(1)
Cl(1A)	10903(8)	352(6)	1808(4)	77(2)

Cl(2A)	10757(2)	534(2)	3730(1)	58(1)
Cl(3A)	10940(8)	2428(5)	2048(5)	94(2)
C(40)	9622(6)	3113(5)	-275(4)	54(1)
Cl(4)	9600(9)	2249(8)	-1130(5)	52(1)
Cl(5)	11204(5)	3780(5)	-709(5)	74(2)
Cl(6)	8274(4)	4219(4)	-28(3)	67(1)
Cl(4A)	9306(10)	2367(9)	-1104(7)	90(3)
Cl(5A)	11422(7)	3575(6)	-723(4)	90(2)
Cl(6A)	8405(12)	4228(10)	-459(9)	224(6)
C(50)	9741(9)	3588(6)	-559(5)	46(2)
Cl(7)	10217(6)	2241(3)	-867(3)	150(2)
Cl(8)	10167(2)	4658(1)	-1644(1)	70(1)
Cl(9)	7948(3)	3726(3)	42(2)	56(1)

Table 3. Bond lengths [A]for k07tdj2.

B(1)-O(3)	1.408(2)
B(1)-O(1)	1.497(2)
B(1)-N(1)	1.636(2)
B(1)-C(28)	1.637(2)
B(2)-O(3)	1.399(2)
B(2)-O(2)	1.505(2)
B(2)-C(14)	1.639(2)
B(2)-N(2)	1.646(2)
N(1)-C(8)	1.288(2)
N(1)-C(7)	1.418(2)
N(2)-C(22)	1.288(2)
N(2)-C(21)	1.4157(19)
O(1)-C(1)	1.3494(19)
O(2)-C(15)	1.3503(19)
C(1)-C(2)	1.388(2)
C(1)-C(7)	1.396(2)
C(2)-C(3)	1.388(3)
C(3)-C(4)	1.397(3)
C(4)-C(6)	1.391(2)
C(4)-C(5)	1.507(3)
C(6)-C(7)	1.386(2)
C(8)-C(9)	1.457(2)
C(9)-C(10)	1.410(2)
C(9)-C(14)	1.421(2)
C(10)-C(11)	1.382(2)
C(11)-C(12)	1.383(3)
C(12)-C(13)	1.389(2)
C(13)-C(14)	1.404(2)
C(15)-C(16)	1.388(2)

C(15)-C(21)	1.399(2)
C(16)-C(17)	1.390(2)
C(17)-C(18)	1.401(2)
C(18)-C(20)	1.395(2)
C(18)-C(19)	1.505(2)
C(20)-C(21)	1.390(2)
C(22)-C(23)	1.456(2)
C(23)-C(24)	1.410(2)
C(23)-C(28)	1.417(2)
C(24)-C(25)	1.379(2)
C(25)-C(26)	1.386(2)
C(26)-C(27)	1.387(2)
C(27)-C(28)	1.403(2)
C(30)-Cl(1A)	1.628(7)
C(30)-Cl(3A)	1.641(6)
C(30)-Cl(2)	1.736(3)
C(30)-Cl(2A)	1.801(3)
C(30)-Cl(1)	1.847(7)
C(30)-Cl(3)	1.872(6)
C(40)-Cl(4A)	1.713(11)
C(40)-Cl(5)	1.736(7)
C(40)-Cl(6A)	1.737(9)
C(40)-Cl(4)	1.737(9)
C(40)-Cl(6)	1.782(7)
C(40)-Cl(5A)	1.819(9)
Cl(5)-Cl(8)	1.973(7)
Cl(5)-Cl(7)	2.284(8)
Cl(6)-Cl(8)	2.463(5)
Cl(4A)-Cl(7)	1.036(13)
Cl(5A)-Cl(7)	2.195(9)
Cl(5A)-Cl(8)	2.200(6)
Cl(6A)-Cl(8)	2.043(14)
C(50)-Cl(9)	1.722(8)
C(50)-Cl(7)	1.745(9)
C(50)-Cl(8)	1.767(7)

Table 4. Bond angles [deg] for k07tdj2.

O(3)-B(1)-O(1)	109.65(12)
O(3)-B(1)-N(1)	109.65(12)
O(1)-B(1)-N(1)	99.75(12)
O(3)-B(1)-C(28)	119.47(13)
O(1)-B(1)-C(28)	109.52(12)
N(1)-B(1)-C(28)	106.97(11)
O(3)-B(2)-O(2)	110.80(12)
O(3)-B(2)-C(14)	119.25(13)
O(2)-B(2)-C(14)	108.50(12)

O(3)-B(2)-N(2)	109.55(12)
O(2)-B(2)-N(2)	99.21(11)
C(14)-B(2)-N(2)	107.62(11)
C(8)-N(1)-C(7)	124.54(13)
C(8)-N(1)-B(1)	128.67(13)
C(7)-N(1)-B(1)	106.73(12)
C(22)-N(2)-C(21)	124.83(13)
C(22)-N(2)-B(2)	128.08(13)
C(21)-N(2)-B(2)	107.06(11)
C(1)-O(1)-B(1)	110.01(12)
C(15)-O(2)-B(2)	110.32(11)
B(2)-O(3)-B(1)	119.98(12)
O(1)-C(1)-C(2)	125.72(15)
O(1)-C(1)-C(7)	114.80(14)
C(2)-C(1)-C(7)	119.48(15)
C(3)-C(2)-C(1)	117.78(16)
C(2)-C(3)-C(4)	123.15(16)
C(6)-C(4)-C(3)	118.56(16)
C(6)-C(4)-C(5)	121.05(17)
C(3)-C(4)-C(5)	120.39(16)
C(7)-C(6)-C(4)	118.60(15)
C(6)-C(7)-C(1)	122.37(15)
C(6)-C(7)-N(1)	129.91(14)
C(1)-C(7)-N(1)	107.72(13)
N(1)-C(8)-C(9)	126.72(14)
C(10)-C(9)-C(14)	120.43(14)
C(10)-C(9)-C(8)	113.03(14)
C(14)-C(9)-C(8)	126.49(13)
C(11)-C(10)-C(9)	121.42(16)
C(10)-C(11)-C(12)	119.01(15)
C(11)-C(12)-C(13)	119.94(16)
C(12)-C(13)-C(14)	123.35(15)
C(13)-C(14)-C(9)	115.77(14)
C(13)-C(14)-B(2)	115.76(13)
C(9)-C(14)-B(2)	128.02(14)
O(2)-C(15)-C(16)	126.02(14)
O(2)-C(15)-C(21)	114.75(13)
C(16)-C(15)-C(21)	119.23(14)
C(15)-C(16)-C(17)	118.18(15)
C(16)-C(17)-C(18)	123.11(15)
C(20)-C(18)-C(17)	118.25(15)
C(20)-C(18)-C(19)	120.34(15)
C(17)-C(18)-C(19)	121.40(15)
C(21)-C(20)-C(18)	118.81(15)
C(20)-C(21)-C(15)	122.39(14)
C(20)-C(21)-N(2)	129.75(14)
C(15)-C(21)-N(2)	107.86(13)
N(2)-C(22)-C(23)	127.39(14)
C(24)-C(23)-C(28)	120.57(14)
C(24)-C(23)-C(22)	113.22(14)
C(28)-C(23)-C(22)	126.20(13)

C(25)-C(24)-C(23)	121.38(15)
C(24)-C(25)-C(26)	118.94(15)
C(25)-C(26)-C(27)	119.90(15)
C(26)-C(27)-C(28)	123.37(15)
C(27)-C(28)-C(23)	115.78(14)
C(27)-C(28)-B(1)	115.95(14)
C(23)-C(28)-B(1)	127.97(13)
Cl(1A)-C(30)-Cl(3A)	105.9(3)
Cl(1A)-C(30)-Cl(2)	120.2(3)
Cl(3A)-C(30)-Cl(2)	95.8(2)
Cl(1A)-C(30)-Cl(2A)	102.8(3)
Cl(3A)-C(30)-Cl(2A)	116.2(2)
Cl(2)-C(30)-Cl(2A)	22.68(7)
Cl(1A)-C(30)-Cl(1)	4.3(4)
Cl(3A)-C(30)-Cl(1)	110.1(3)
Cl(2)-C(30)-Cl(1)	119.9(2)
Cl(2A)-C(30)-Cl(1)	101.4(2)
Cl(1A)-C(30)-Cl(3)	108.6(3)
Cl(3A)-C(30)-Cl(3)	10.8(4)
Cl(2)-C(30)-Cl(3)	102.67(18)
Cl(2A)-C(30)-Cl(3)	124.32(18)
Cl(1)-C(30)-Cl(3)	112.5(3)
Cl(4A)-C(40)-Cl(5)	115.7(5)
Cl(4A)-C(40)-Cl(6A)	95.5(6)
Cl(5)-C(40)-Cl(6A)	101.5(6)
Cl(4A)-C(40)-Cl(4)	10.1(6)
Cl(5)-C(40)-Cl(4)	109.1(4)
Cl(6A)-C(40)-Cl(4)	104.7(5)
Cl(4A)-C(40)-Cl(6)	109.6(5)
Cl(5)-C(40)-Cl(6)	104.7(4)
Cl(6A)-C(40)-Cl(6)	18.6(4)
Cl(4)-C(40)-Cl(6)	119.5(5)
Cl(4A)-C(40)-Cl(5A)	111.4(5)
Cl(5)-C(40)-Cl(5A)	9.6(4)
Cl(6A)-C(40)-Cl(5A)	110.9(6)
Cl(4)-C(40)-Cl(5A)	103.7(4)
Cl(6)-C(40)-Cl(5A)	114.3(4)
Cl(7)-Cl(4)-C(40)	54.4(5)
C(40)-Cl(5)-Cl(8)	79.6(3)
C(40)-Cl(5)-Cl(7)	38.7(2)
Cl(8)-Cl(5)-Cl(7)	86.4(2)
Cl(9)-Cl(6)-C(40)	71.8(5)
Cl(9)-Cl(6)-Cl(8)	116.3(5)
C(40)-Cl(6)-Cl(8)	66.0(2)
Cl(7)-Cl(4A)-C(40)	56.3(5)
C(40)-Cl(5A)-Cl(7)	40.3(2)
C(40)-Cl(5A)-Cl(8)	71.9(3)
Cl(7)-Cl(5A)-Cl(8)	83.4(2)
Cl(9)-Cl(6A)-C(40)	72.8(6)
Cl(9)-Cl(6A)-Cl(8)	149.8(8)
C(40)-Cl(6A)-Cl(8)	77.6(4)

Cl(9)-C(50)-Cl(7)	110.3(5)
Cl(9)-C(50)-Cl(8)	108.8(4)
Cl(7)-C(50)-Cl(8)	112.7(4)
Cl(4)-Cl(7)-Cl(4A)	12.1(9)
Cl(4)-Cl(7)-C(50)	94.7(7)
Cl(4A)-Cl(7)-C(50)	84.0(6)
Cl(4)-Cl(7)-Cl(5A)	132.5(7)
Cl(4A)-Cl(7)-Cl(5A)	125.4(7)
C(50)-Cl(7)-Cl(5A)	46.5(4)
Cl(4)-Cl(7)-Cl(5)	126.0(7)
Cl(4A)-Cl(7)-Cl(5)	118.3(7)
C(50)-Cl(7)-Cl(5)	39.1(3)
Cl(5A)-Cl(7)-Cl(5)	7.6(3)
C(50)-Cl(8)-Cl(5)	44.9(3)
C(50)-Cl(8)-Cl(6A)	43.5(4)
Cl(5)-Cl(8)-Cl(6A)	84.1(3)
C(50)-Cl(8)-Cl(5A)	46.3(3)
Cl(5)-Cl(8)-Cl(5A)	5.8(3)
Cl(6A)-Cl(8)-Cl(5A)	87.2(3)
C(50)-Cl(8)-Cl(6)	40.3(3)
Cl(5)-Cl(8)-Cl(6)	77.0(2)
Cl(6A)-Cl(8)-Cl(6)	9.9(3)
Cl(5A)-Cl(8)-Cl(6)	80.7(2)
Cl(6)-Cl(9)-Cl(6A)	40.5(8)
Cl(6)-Cl(9)-C(50)	67.9(5)
Cl(6A)-Cl(9)-C(50)	56.3(6)

Table 5. Anisotropic displacement parameters (A^2 x 10^3) for k07tdj2.
The anisotropic displacement factor exponent takes the form:
-2 pi^2 [h^2 a*^2 U11 + ... + 2 h k a* b* U12]

	U11	U22	U33	U23	U13	U12
B(1)	24(1)	21(1)	28(1)	-5(1)	-7(1)	-2(1)
B(2)	25(1)	18(1)	27(1)	-1(1)	-9(1)	-2(1)
N(1)	26(1)	19(1)	28(1)	-3(1)	-11(1)	0(1)
N(2)	26(1)	22(1)	26(1)	-3(1)	-9(1)	-3(1)
O(1)	28(1)	25(1)	32(1)	-8(1)	-5(1)	-4(1)
O(2)	30(1)	21(1)	33(1)	-1(1)	-16(1)	-4(1)
O(3)	23(1)	21(1)	30(1)	-4(1)	-9(1)	-1(1)
C(1)	33(1)	20(1)	31(1)	-2(1)	-11(1)	-1(1)
C(2)	42(1)	30(1)	30(1)	-7(1)	-6(1)	-4(1)
C(3)	56(1)	27(1)	31(1)	-9(1)	-11(1)	-4(1)
C(4)	50(1)	21(1)	32(1)	-3(1)	-17(1)	-3(1)
C(5)	67(1)	30(1)	42(1)	-7(1)	-23(1)	-12(1)
C(6)	35(1)	21(1)	32(1)	-1(1)	-15(1)	-3(1)
C(7)	32(1)	18(1)	28(1)	-3(1)	-11(1)	0(1)
C(8)	25(1)	20(1)	31(1)	-1(1)	-12(1)	-2(1)
C(9)	26(1)	22(1)	26(1)	1(1)	-10(1)	0(1)
C(10)	27(1)	32(1)	30(1)	1(1)	-9(1)	-5(1)
C(11)	27(1)	41(1)	29(1)	-1(1)	-5(1)	-3(1)
C(12)	34(1)	36(1)	27(1)	-5(1)	-7(1)	2(1)
C(13)	32(1)	28(1)	29(1)	-5(1)	-11(1)	-1(1)
C(14)	26(1)	20(1)	25(1)	1(1)	-10(1)	0(1)
C(15)	24(1)	24(1)	28(1)	-2(1)	-8(1)	-4(1)
C(16)	31(1)	32(1)	32(1)	-1(1)	-14(1)	-3(1)
C(17)	32(1)	39(1)	32(1)	-7(1)	-14(1)	-7(1)
C(18)	28(1)	32(1)	29(1)	-9(1)	-6(1)	-6(1)
C(19)	41(1)	37(1)	36(1)	-13(1)	-11(1)	-9(1)
C(20)	29(1)	26(1)	27(1)	-5(1)	-7(1)	-4(1)
C(21)	25(1)	24(1)	25(1)	-3(1)	-9(1)	-4(1)
C(22)	32(1)	19(1)	29(1)	-2(1)	-10(1)	-3(1)
C(23)	30(1)	21(1)	25(1)	-1(1)	-9(1)	-3(1)
C(24)	44(1)	20(1)	33(1)	-1(1)	-17(1)	-2(1)
C(25)	46(1)	24(1)	35(1)	1(1)	-20(1)	-1(1)
C(26)	40(1)	29(1)	33(1)	-4(1)	-19(1)	-3(1)
C(27)	36(1)	24(1)	31(1)	-4(1)	-14(1)	-2(1)
C(28)	25(1)	22(1)	25(1)	-2(1)	-7(1)	-3(1)
C(30)	30(1)	65(1)	34(1)	-12(1)	-7(1)	-7(1)
Cl(1)	59(1)	43(1)	37(1)	-16(1)	11(1)	-8(1)

Cl(2)	62(1)	89(1)	46(1)	-10(1)	-27(1)	1(1)
Cl(3)	127(3)	71(3)	68(1)	-2(2)	-47(2)	-50(2)
Cl(1A)	75(2)	70(3)	74(2)	-39(1)	10(1)	1(2)
Cl(2A)	36(1)	101(1)	36(1)	-4(1)	-16(1)	-3(1)
Cl(3A)	120(3)	49(2)	110(3)	-16(2)	-11(2)	-43(2)
C(40)	55(2)	61(3)	51(3)	-8(2)	-23(2)	-2(3)
Cl(4)	66(2)	57(2)	31(2)	-10(2)	-1(1)	-21(2)
Cl(5)	38(1)	72(2)	116(3)	-52(2)	-3(2)	-11(1)
Cl(6)	47(1)	68(2)	90(2)	-23(2)	-18(1)	-14(1)
Cl(4A)	130(7)	82(5)	72(4)	8(3)	-41(3)	-59(4)
Cl(5A)	85(3)	127(4)	71(3)	-16(2)	-42(2)	-10(3)
Cl(6A)	222(10)	189(9)	347(13)	-135(10)	-210(11)	141(8)
C(50)	53(3)	52(4)	35(3)	-6(3)	-16(3)	0(3)
Cl(7)	209(4)	73(2)	75(2)	14(1)	50(2)	69(2)
Cl(8)	97(1)	59(1)	48(1)	-1(1)	-9(1)	-29(1)
Cl(9)	39(1)	72(2)	48(1)	-5(1)	-6(1)	7(1)

Table 6. Hydrogen coordinates (x 10^4) and isotropic displacement parameters (A^2 x 10^3) for k07tdj2.

	x	y	z	U(eq)
H(2)	8214	238	329	41
H(3)	6914	-1114	90	45
H(5A)	3779	-1510	744	66
H(5B)	3840	-2314	1790	66
H(5C)	5068	-2438	752	66
H(6)	3835	-767	2719	34
H(8)	3614	88	4092	30
H(10)	1952	579	5461	36
H(11)	1100	1467	6891	40
H(12)	2544	2668	7204	40
H(13)	4797	2963	6103	35
H(16)	8632	2083	6574	37
H(17)	9097	3807	6869	39
H(19A)	8573	6518	5462	55
H(19B)	9409	5854	6243	55
H(19C)	7733	6141	6641	55
H(20)	7333	5499	4689	33
H(22)	6536	5030	3454	32
H(24)	5171	5775	2437	38
H(25)	3965	5718	1250	41
H(26)	3740	3979	835	39
H(27)	4773	2349	1560	36

H(30)	9184	1223	2851	51
H(40)	9603	2621	394	65
H(50)	10265	3698	-77	56

6.3.5 Date for Compound 128

Table 1. Crystal data and structure refinement for k07tdj8.

Identification code	k07tdj8
Empirical formula	C44 H55 Cl3 N2 O4
Formula weight	782.25
Temperature	150(2) K
Wavelength	0.71073 A
Crystal system	monoclinic
Space group	P 2_1/n
Unit cell dimensions	a = 13.7671(2) A alpha = 90 deg.
	b = 17.6382(3) A beta = 110.1640(10) deg.
	c = 18.4870(2) A gamma = 90 deg.
Volume	4214.00(10) A^3
Z, Calculated density	4, 1.233 Mg/m^3
Absorption coefficient	0.260 mm^-1
F(000)	1664
Crystal size	0.50 x 0.25 x 0.18 mm
Theta range for data collection	4.46 to 27.51 deg.
Limiting indices	-17<=h<=16, -22<=k<=22, -24<=l<=24
Reflections collected / unique	60662 / 9598 [R(int) = 0.0667]
Completeness to theta = 27.51	99.0 %
Max. and min. transmission	0.9546 and 0.8808
Refinement method	Full-matrix least-squares on F^2
Data / restraints / parameters	9598 / 2 / 528
Goodness-of-fit on F^2	1.033
Final R indices [I>2sigma(I)]	R1 = 0.0484, wR2 = 0.1080
R indices (all data)	R1 = 0.0725, wR2 = 0.1232

Largest diff. peak and hole 0.351 and -0.642 e.A^-3

Table 2. Atomic coordinates (x 10^4) and equivalent isotropic displacement parameters (A^2 x 10^3) for k07tdj8.
U(eq) is defined as one third of the trace of the orthogonalized Uij tensor.

	x	y	z	U(eq)
N(1)	2221(1)	2554(1)	1771(1)	25(1)
N(2)	11881(1)	5432(1)	1989(1)	26(1)
O(1)	3574(1)	1711(1)	2054(1)	29(1)
O(2)	3822(1)	2988(1)	2071(1)	23(1)
O(3)	11489(1)	4174(1)	1702(1)	30(1)
O(4)	10604(1)	4923(1)	2267(1)	25(1)
C(1)	1352(1)	2062(1)	1507(1)	25(1)
C(2)	1423(2)	1307(1)	1323(1)	33(1)
C(3)	531(2)	870(1)	1055(1)	43(1)
C(4)	-428(2)	1180(1)	959(1)	48(1)
C(5)	-493(2)	1934(1)	1134(1)	47(1)
C(6)	392(1)	2377(1)	1411(1)	35(1)
C(7)	3227(1)	2349(1)	1969(1)	23(1)
C(8)	4884(1)	2872(1)	2185(1)	22(1)
C(9)	5182(1)	2782(1)	1536(1)	22(1)
C(10)	4461(1)	2778(1)	679(1)	26(1)
C(11)	5026(2)	3137(2)	178(1)	44(1)
C(12)	3447(2)	3225(1)	498(1)	36(1)
C(13)	4204(2)	1952(1)	422(1)	36(1)
C(14)	6234(1)	2642(1)	1689(1)	25(1)
C(15)	6960(1)	2626(1)	2427(1)	23(1)
C(16)	6625(1)	2761(1)	3044(1)	24(1)
C(17)	5586(1)	2886(1)	2948(1)	23(1)
C(18)	5267(1)	3062(1)	3653(1)	27(1)
C(19)	6192(2)	3005(2)	4407(1)	51(1)
C(20)	4449(2)	2508(1)	3741(1)	36(1)
C(21)	4854(2)	3873(1)	3592(1)	35(1)
C(22)	8089(1)	2461(1)	2564(1)	26(1)
C(23)	8731(1)	3139(1)	2488(1)	23(1)
C(24)	9623(1)	3337(1)	3093(1)	23(1)
C(25)	10269(1)	3930(1)	3040(1)	23(1)
C(26)	11238(1)	4137(1)	3741(1)	26(1)
C(27)	12237(2)	3974(2)	3579(1)	45(1)
C(28)	11283(2)	3682(1)	4455(1)	36(1)
C(29)	11210(2)	4978(1)	3957(1)	40(1)
C(30)	9974(1)	4318(1)	2332(1)	23(1)
C(31)	9046(1)	4179(1)	1718(1)	28(1)

C(32)	8643(2)	4637(1)	958(1)	44(1)
C(33)	7494(15)	4682(12)	722(9)	77(5)
C(34)	9128(4)	5391(3)	930(3)	44(1)
C(35)	8896(6)	4113(4)	335(3)	62(2)
C(33A)	7479(15)	4551(13)	523(9)	58(3)
C(34A)	8632(6)	5515(3)	1186(5)	92(3)
C(35A)	9242(6)	4559(7)	460(5)	107(4)
C(36)	8452(1)	3569(1)	1820(1)	28(1)
C(37)	11353(1)	4781(1)	1958(1)	24(1)
C(38)	12773(1)	5537(1)	1782(1)	23(1)
C(39)	13381(1)	4943(1)	1697(1)	28(1)
C(40)	14270(2)	5099(1)	1529(1)	34(1)
C(41)	14555(2)	5834(1)	1448(1)	37(1)
C(42)	13943(2)	6426(1)	1532(1)	39(1)
C(43)	13052(2)	6281(1)	1695(1)	33(1)
C(50)	8022(2)	4913(1)	3132(1)	36(1)
Cl(1)	6689(1)	4923(1)	2647(1)	73(1)
Cl(2)	8306(1)	4612(1)	4084(1)	68(1)
Cl(3)	8545(1)	5801(1)	3087(1)	85(1)

Table 3. Bond lengths [A] for k07tdj8.

N(1)-C(7)	1.354(2)
N(1)-C(1)	1.421(2)
N(1)-H(1)	0.81(2)
N(2)-C(37)	1.350(2)
N(2)-C(38)	1.419(2)
N(2)-H(2)	0.86(2)
O(1)-C(7)	1.212(2)
O(2)-C(7)	1.367(2)
O(2)-C(8)	1.4174(19)
O(3)-C(37)	1.211(2)
O(4)-C(37)	1.364(2)
O(4)-C(30)	1.4056(19)
C(1)-C(2)	1.387(3)
C(1)-C(6)	1.387(3)
C(2)-C(3)	1.388(3)
C(3)-C(4)	1.382(3)
C(4)-C(5)	1.379(3)
C(5)-C(6)	1.388(3)
C(8)-C(9)	1.404(2)
C(8)-C(17)	1.409(2)
C(9)-C(14)	1.399(2)
C(9)-C(10)	1.553(2)
C(10)-C(13)	1.535(3)
C(10)-C(11)	1.537(3)
C(10)-C(12)	1.537(3)
C(14)-C(15)	1.386(2)
C(15)-C(16)	1.390(2)
C(15)-C(22)	1.514(2)
C(16)-C(17)	1.397(2)
C(17)-C(18)	1.544(2)
C(18)-C(21)	1.530(3)
C(18)-C(19)	1.533(3)
C(18)-C(20)	1.541(3)
C(22)-C(23)	1.521(2)
C(23)-C(36)	1.388(2)
C(23)-C(24)	1.391(2)
C(24)-C(25)	1.398(2)
C(25)-C(30)	1.405(2)
C(25)-C(26)	1.550(2)
C(26)-C(28)	1.528(2)
C(26)-C(27)	1.532(3)
C(26)-C(29)	1.540(3)
C(30)-C(31)	1.409(2)
C(31)-C(36)	1.402(2)
C(31)-C(32)	1.549(3)
C(32)-C(35A)	1.439(8)
C(32)-C(33)	1.49(2)

C(32)-C(34)	1.497(5)
C(32)-C(33A)	1.531(19)
C(32)-C(35)	1.605(6)
C(32)-C(34A)	1.607(7)
C(38)-C(39)	1.384(2)
C(38)-C(43)	1.393(2)
C(39)-C(40)	1.390(3)
C(40)-C(41)	1.379(3)
C(41)-C(42)	1.383(3)
C(42)-C(43)	1.384(3)
C(50)-Cl(3)	1.739(2)
C(50)-Cl(1)	1.744(2)
C(50)-Cl(2)	1.749(2)

Table 4. Bond angles [deg] for k07tdj8.

C(7)-N(1)-C(1)	126.28(16)
C(7)-N(1)-H(1)	116.1(14)
C(1)-N(1)-H(1)	117.2(14)
C(37)-N(2)-C(38)	127.05(15)
C(37)-N(2)-H(2)	116.1(14)
C(38)-N(2)-H(2)	116.5(14)
C(7)-O(2)-C(8)	116.10(12)
C(37)-O(4)-C(30)	118.38(13)
C(2)-C(1)-C(6)	119.91(17)
C(2)-C(1)-N(1)	123.25(16)
C(6)-C(1)-N(1)	116.81(17)
C(1)-C(2)-C(3)	119.43(19)
C(4)-C(3)-C(2)	121.0(2)
C(5)-C(4)-C(3)	119.09(19)
C(4)-C(5)-C(6)	120.7(2)
C(1)-C(6)-C(5)	119.8(2)
O(1)-C(7)-N(1)	127.13(16)
O(1)-C(7)-O(2)	123.82(15)
N(1)-C(7)-O(2)	109.04(14)
C(9)-C(8)-C(17)	123.71(15)
C(9)-C(8)-O(2)	118.64(14)
C(17)-C(8)-O(2)	117.59(14)
C(14)-C(9)-C(8)	115.78(15)
C(14)-C(9)-C(10)	117.27(15)
C(8)-C(9)-C(10)	126.86(15)
C(13)-C(10)-C(11)	108.34(16)
C(13)-C(10)-C(12)	108.88(15)
C(11)-C(10)-C(12)	105.52(16)
C(13)-C(10)-C(9)	108.59(14)
C(11)-C(10)-C(9)	109.57(14)
C(12)-C(10)-C(9)	115.71(14)
C(15)-C(14)-C(9)	123.20(15)
C(14)-C(15)-C(16)	118.27(15)
C(14)-C(15)-C(22)	121.23(15)
C(16)-C(15)-C(22)	120.50(15)
C(15)-C(16)-C(17)	122.49(16)
C(16)-C(17)-C(8)	116.38(15)
C(16)-C(17)-C(18)	120.05(15)
C(8)-C(17)-C(18)	123.52(14)
C(21)-C(18)-C(19)	107.43(17)
C(21)-C(18)-C(20)	109.48(15)
C(19)-C(18)-C(20)	105.77(17)
C(21)-C(18)-C(17)	109.44(14)
C(19)-C(18)-C(17)	111.44(15)
C(20)-C(18)-C(17)	113.07(15)
C(15)-C(22)-C(23)	115.34(14)
C(36)-C(23)-C(24)	118.32(16)

C(36)-C(23)-C(22)	121.40(15)
C(24)-C(23)-C(22)	120.28(15)
C(23)-C(24)-C(25)	122.59(16)
C(24)-C(25)-C(30)	116.30(15)
C(24)-C(25)-C(26)	120.15(15)
C(30)-C(25)-C(26)	123.54(15)
C(28)-C(26)-C(27)	107.38(16)
C(28)-C(26)-C(29)	106.19(15)
C(27)-C(26)-C(29)	109.67(17)
C(28)-C(26)-C(25)	111.43(14)
C(27)-C(26)-C(25)	111.36(15)
C(29)-C(26)-C(25)	110.64(15)
C(25)-C(30)-O(4)	117.42(14)
C(25)-C(30)-C(31)	123.79(15)
O(4)-C(30)-C(31)	118.55(15)
C(36)-C(31)-C(30)	115.73(15)
C(36)-C(31)-C(32)	118.61(16)
C(30)-C(31)-C(32)	125.66(16)
C(35A)-C(32)-C(33)	127.1(7)
C(35A)-C(32)-C(34)	72.7(6)
C(33)-C(32)-C(34)	112.5(8)
C(35A)-C(32)-C(33A)	112.5(7)
C(33)-C(32)-C(33A)	16.2(13)
C(34)-C(32)-C(33A)	117.9(8)
C(35A)-C(32)-C(31)	115.2(4)
C(33)-C(32)-C(31)	107.8(6)
C(34)-C(32)-C(31)	118.0(2)
C(33A)-C(32)-C(31)	114.0(7)
C(35A)-C(32)-C(35)	34.2(5)
C(33)-C(32)-C(35)	107.0(8)
C(34)-C(32)-C(35)	106.1(4)
C(33A)-C(32)-C(35)	90.8(8)
C(31)-C(32)-C(35)	104.6(3)
C(35A)-C(32)-C(34A)	108.6(7)
C(33)-C(32)-C(34A)	85.4(9)
C(34)-C(32)-C(34A)	36.6(3)
C(33A)-C(32)-C(34A)	97.5(9)
C(31)-C(32)-C(34A)	107.3(3)
C(35)-C(32)-C(34A)	140.1(4)
C(23)-C(36)-C(31)	123.00(16)
O(3)-C(37)-N(2)	127.99(16)
O(3)-C(37)-O(4)	124.53(15)
N(2)-C(37)-O(4)	107.47(14)
C(39)-C(38)-C(43)	119.96(16)
C(39)-C(38)-N(2)	123.10(15)
C(43)-C(38)-N(2)	116.88(16)
C(38)-C(39)-C(40)	119.26(17)
C(41)-C(40)-C(39)	121.13(18)
C(40)-C(41)-C(42)	119.33(17)
C(41)-C(42)-C(43)	120.38(18)
C(42)-C(43)-C(38)	119.93(18)

Cl(3)-C(50)-Cl(1)	110.24(11)
Cl(3)-C(50)-Cl(2)	111.65(12)
Cl(1)-C(50)-Cl(2)	110.56(12)

Table 5. Anisotropic displacement parameters (A^2 x 10^3) for k07tdj8.
The anisotropic displacement factor exponent takes the form:
-2 pi^2 [h^2 a*^2 U11 + ... + 2 h k a* b* U12]

	U11	U22	U33	U23	U13	U12
N(1)	20(1)	20(1)	36(1)	0(1)	10(1)	-1(1)
N(2)	27(1)	21(1)	36(1)	-4(1)	18(1)	-4(1)
O(1)	26(1)	22(1)	39(1)	1(1)	13(1)	1(1)
O(2)	17(1)	21(1)	29(1)	1(1)	8(1)	-1(1)
O(3)	30(1)	23(1)	42(1)	-5(1)	18(1)	-6(1)
O(4)	24(1)	24(1)	31(1)	1(1)	14(1)	-3(1)
C(1)	22(1)	30(1)	24(1)	1(1)	8(1)	-6(1)
C(2)	31(1)	27(1)	38(1)	2(1)	7(1)	-3(1)
C(3)	45(1)	30(1)	47(1)	1(1)	6(1)	-12(1)
C(4)	36(1)	54(1)	51(1)	-6(1)	12(1)	-23(1)
C(5)	25(1)	60(2)	57(1)	-15(1)	17(1)	-11(1)
C(6)	26(1)	41(1)	41(1)	-11(1)	14(1)	-5(1)
C(7)	23(1)	22(1)	25(1)	0(1)	10(1)	-2(1)
C(8)	17(1)	19(1)	29(1)	0(1)	8(1)	0(1)
C(9)	22(1)	19(1)	26(1)	-1(1)	8(1)	-3(1)
C(10)	25(1)	27(1)	24(1)	-1(1)	8(1)	-3(1)
C(11)	36(1)	65(2)	29(1)	8(1)	9(1)	-12(1)
C(12)	34(1)	40(1)	28(1)	-1(1)	4(1)	6(1)
C(13)	40(1)	33(1)	32(1)	-8(1)	7(1)	-3(1)
C(14)	25(1)	22(1)	30(1)	-2(1)	14(1)	-3(1)
C(15)	20(1)	16(1)	33(1)	1(1)	11(1)	-2(1)
C(16)	20(1)	23(1)	27(1)	0(1)	6(1)	-1(1)
C(17)	22(1)	21(1)	27(1)	1(1)	9(1)	2(1)
C(18)	23(1)	34(1)	25(1)	-1(1)	9(1)	4(1)
C(19)	34(1)	91(2)	25(1)	-5(1)	7(1)	14(1)
C(20)	46(1)	34(1)	35(1)	3(1)	23(1)	1(1)
C(21)	39(1)	31(1)	40(1)	-7(1)	20(1)	-1(1)
C(22)	21(1)	23(1)	36(1)	0(1)	12(1)	0(1)
C(23)	19(1)	23(1)	31(1)	0(1)	12(1)	1(1)
C(24)	20(1)	22(1)	28(1)	2(1)	10(1)	4(1)
C(25)	19(1)	22(1)	28(1)	-1(1)	10(1)	2(1)
C(26)	21(1)	31(1)	26(1)	1(1)	6(1)	-2(1)
C(27)	22(1)	72(2)	39(1)	4(1)	7(1)	6(1)
C(28)	36(1)	40(1)	29(1)	4(1)	5(1)	-7(1)
C(29)	46(1)	34(1)	33(1)	-4(1)	7(1)	-10(1)
C(30)	21(1)	21(1)	31(1)	0(1)	12(1)	-2(1)
C(31)	24(1)	32(1)	27(1)	4(1)	8(1)	-1(1)

C(32)	30(1)	57(1)	34(1)	20(1)	0(1)	-10(1)
C(33)	35(4)	108(11)	71(10)	72(9)	-4(6)	3(6)
C(34)	36(3)	48(3)	44(3)	25(2)	8(2)	-6(2)
C(35)	94(6)	63(4)	24(2)	6(2)	15(3)	-2(3)
C(33A)	29(3)	100(7)	34(5)	30(4)	-3(3)	-18(4)
C(34A)	77(5)	54(4)	96(6)	39(4)	-34(4)	-14(4)
C(35A)	56(4)	215(12)	60(5)	75(7)	32(4)	26(6)
C(36)	20(1)	32(1)	30(1)	1(1)	6(1)	-2(1)
C(37)	23(1)	24(1)	26(1)	1(1)	10(1)	-2(1)
C(38)	23(1)	26(1)	21(1)	0(1)	8(1)	-4(1)
C(39)	25(1)	25(1)	33(1)	-1(1)	10(1)	-4(1)
C(40)	26(1)	37(1)	41(1)	-3(1)	14(1)	-1(1)
C(41)	27(1)	45(1)	42(1)	6(1)	17(1)	-7(1)
C(42)	36(1)	30(1)	55(1)	9(1)	21(1)	-7(1)
C(43)	32(1)	25(1)	43(1)	3(1)	17(1)	-2(1)
C(50)	34(1)	29(1)	44(1)	2(1)	14(1)	3(1)
Cl(1)	33(1)	101(1)	77(1)	28(1)	8(1)	-2(1)
Cl(2)	80(1)	83(1)	39(1)	5(1)	19(1)	19(1)
Cl(3)	60(1)	31(1)	147(1)	16(1)	12(1)	-6(1)

Table 6. Hydrogen coordinates (x 10^4) and isotropic displacement parameters (A^2 x 10^3) for k07tdj8.

	x	y	z	U(eq)
H(1)	2107(15)	3004(12)	1760(11)	22(5)
H(2)	11693(15)	5812(12)	2199(12)	27(5)
H(2A)	2077	1090	1379	40
H(3)	580	351	935	52
H(4)	-1035	877	775	57
H(5)	-1150	2152	1064	56
H(6)	340	2895	1535	42
H(14A)	5637	2833	215	66
H(14B)	5241	3653	359	66
H(14C)	4560	3153	-359	66
H(12A)	3595	3729	732	53
H(12B)	2980	2954	706	53
H(12C)	3117	3276	-62	53
H(13A)	3795	1939	-129	54
H(13B)	3806	1723	715	54
H(13C)	4847	1667	517	54
H(15)	6462	2554	1267	29
H(17)	7122	2768	3550	29
H(22A)	6725	3369	4397	76
H(22B)	6478	2490	4462	76
H(22C)	5965	3118	4842	76
H(20A)	4377	2582	4245	54
H(20B)	4666	1986	3699	54
H(20C)	3783	2605	3333	54
H(21A)	4230	3919	3134	52
H(21B)	5382	4226	3552	52
H(21C)	4684	3994	4053	52
H(23A)	8127	2067	2193	31
H(23B)	8405	2247	3088	31
H(25)	9800	3059	3561	28
H(27A)	12829	4001	4061	68
H(27B)	12321	4350	3215	68
H(27C)	12199	3466	3356	68
H(28A)	11348	3141	4359	55
H(28B)	10648	3767	4570	55
H(28C)	11881	3845	4894	55
H(29A)	10617	5067	4124	60
H(29B)	11145	5296	3508	60
H(29C)	11851	5107	4377	60
H(33A)	7214	4930	218	115
H(33B)	7308	4977	1104	115
H(33C)	7207	4170	688	115

H(34A)	9845	5317	959	66
H(34B)	9115	5701	1367	66
H(34C)	8740	5648	447	66
H(35A)	8665	4368	-166	93
H(35B)	8535	3627	291	93
H(35C)	9644	4023	501	93
H(33D)	7255	4929	110	88
H(33E)	7103	4628	880	88
H(33F)	7336	4041	301	88
H(34D)	9334	5674	1496	138
H(34E)	8171	5584	1484	138
H(34F)	8383	5823	716	138
H(35D)	8923	4858	-9	161
H(35E)	9266	4024	324	161
H(35F)	9947	4743	727	161
H(36)	7831	3445	1412	34
H(39)	13194	4433	1753	33
H(40)	14687	4692	1468	41
H(41)	15167	5934	1337	44
H(42)	14135	6934	1477	47
H(43)	12632	6689	1749	39
H(50)	8336	4542	2867	43